Santa Clara Valley
Water District

FINAL
Santa Clara Plain Groundwater Flow Model Development and Calibration

Indirect Potable Reuse Groundwater Studies

December 2017

Prepared for:
Santa Clara Valley Water District

Prepared By:

TODD
GROUNDWATER

2490 Mariner Square Loop, Suite 215
Alameda, CA 94501
510 747 6920
toddgroundwater.com

SIGNATURE PAGE

CERTIFIED HYDROGEOLOGIST
SALLY McCRAVEN
No. 356
Exp. 12/31/18
STATE OF CALIFORNIA

Sally McCraven

Sally McCraven, PG, CHg, CEG
Principal Hydrogeologist

REGISTERED GEOLOGIST
EUGENE B. GUS YATES
PG 7178
CHG 740
EXP. 01/18
STATE OF CALIFORNIA

Gus Yates

Gus Yates, PG, CHg
Senior Hydrogeologist

CERTIFIED HYDROGEOLOGIST
CHAD N. TAYLOR
No.915
STATE OF CALIFORNIA

Chad Taylor, PG, CHg
Senior Hydrogeologist

Table of Contents

Page

Executive Summary ES-1

1 Introduction 1
- 1.1 Purpose and Goals of Model 1
- 1.2 Description of Model Area 1
- 1.3 Previous Groundwater Modeling Investigations 2

2 Hydrogeologic Conceptual Model 3
- 2.1 Subbasin Boundaries 3
- 2.2 Basin Fill Materials and Layering 4
  - 2.2.1 Hydrogeologic Conceptual Model Geometry Refinement 5
    - 2.2.1.1 Available Data and Information 5
    - 2.2.1.2 Cross Section Construction and Hydrostratigraphic Evaluation 6
    - 2.2.1.3 Geophysical Log Review 8
    - 2.2.1.4 Depth Discrete Groundwater Elevation Monitoring 8
- 2.3 Aquifer Hydraulic Characteristics 9
  - 2.3.1 Hydraulic Conductivity 9
  - 2.3.2 Storativity and Specific Yield 10
- 2.4 Groundwater Levels and Flow 11
- 2.5 Sources of Inflow and Outflow 12
- 2.6 Subsidence 13

3 Numerical Model Development 14
- 3.1 Software Used for Modeling 14
- 3.2 Model Grid and Active Flow Area 14
- 3.3 Model Layers 15
  - 3.3.1 Top of Layer 1 15
  - 3.3.2 Bottom of Layer 1 15
  - 3.3.3 Bottom of Layer 2 16
  - 3.3.4 Bottom of Layer 3 16
  - 3.3.5 Bottom of Layers 4 through 6 16
- 3.4 Aquifer Characteristics 16
- 3.5 Simulation Period and Time Increments 17
- 3.6 Initial Water Levels 17
- 3.7 Inflows 18
  - 3.7.1 Dispersed Recharge 18
    - 3.7.1.1 Rainfall and Interception 19
    - 3.7.1.2 Runoff and Infiltration 20
    - 3.7.1.3 Root Zone Depth and Moisture Content 21
    - 3.7.1.4 Evapotranspiration 22
    - 3.7.1.5 Irrigation 22

3.7.1.6 Deep Percolation from Root Zone to Shallow Groundwater 24
3.7.1.7 Pipe Leaks 24
3.7.1.8 Movement of Shallow Groundwater to Deep Recharge and Stream Base Flow 25
3.7.2 Managed Aquifer Recharge 26
3.7.3 Percolation from Streams 26
3.7.4 Subsurface Inflow across Inland Subbasin Boundaries 28
3.7.5 Inflow from San Francisco Bay 29
3.8 Outflows 29
3.8.1 Groundwater Pumping 29
3.8.2 Seepage into Streams 30
3.8.3 Evapotranspiration by Riparian Vegetation 31
3.8.4 Outflow to San Francisco Bay 32
3.9 Water Balance Summary and Change in Storage 33
4 Numerical Model Calibration 35
4.1.1 Objectives 35
4.1.2 Method 36
4.1.3 Water Level Results 37
4.1.3.1 Hydrographs 37
4.1.3.2 Contours 41
4.1.3.3 Flooded Cells 42
4.1.4 Stream Flow Results 42
4.1.5 Residuals Statistics 43
4.1.6 Discussion of Calibrated Parameters 44
4.1.7 Model Advantages and Limitations 46
5 References 48

List of Tables

3-1 Recharge Zone Parameters
3-2 Monthly Crop Coefficients for Vegetation Types Simulated by the Recharge Program
3-3 Sources of Stream Flow Data for Tributary Watersheds
3-4 Annual Groundwater Balances 1985-2014
4-1 Wells Responsible for Most of the 100 Largest Residuals in Each Layer

List of Figures

1-1 Location of Santa Clara Plain Portion of Santa Clara Groundwater Subbasin
2-1 Basin and Model Boundaries
2-2 Geologic Map
2-3 All Well Locations in Santa Clara County
2-4 Wells with Lithology Records
2-5 Wells with Construction Records
2-6 Wells with Lithology and Construction Records
2-7 Local Hydrogeologic Conceptual Model Refinement Areas
2-8 Cross Section Locations and Orientations
2-9 Wells with Lithology and Construction Records near Sections
2-10 Example Cross Sections with Lithology and Screens
2-11 Example Cross Sections with Lithology and GMOD and XMOD Model Layers
2-12 Example Cross Sections Showing Wentworth Interpretations and Lithology
2-13 Example Cross Sections Showing All Data
2-14 Wells with Geophysical Logs Near Section Locations
2-15 Multi-Completion Well Locations Near Section Locations
2-16 Frequency Distribution of Horizontal Hydraulic Conductivity Estimated from Well Tests
2-17 Water-Level Hydrograph at a Well near Downtown San Jose, 1915-1995
2-18 Contours of Measured Groundwater Elevations in June 1989
2-19 Contours of Measured Groundwater Elevations in March-April 2012
2-20 Hydrographs of Measured Water Levels at Multiple-Depth Monitoring Well Clusters
3-1 Aquifer Characteristics in Model Layer 1
3-2 Aquifer Characteristics in Model Layer 2
3-3 Aquifer Characteristics in Model Layer 3
3-4 Aquifer Characteristics in Model Layer 4
3-5 Aquifer Characteristics in Model Layer 5
3-6 Aquifer Characteristics in Model Layer 6
3-7 Estimated December 1984 Water Levels
3-8 Recharge Zones
3-9 Cumulative Departure of Annual Precipitation
3-10 Map of Mean Annual Precipitation and Watersheds
3-11 Generalized Relationship of Daily Infiltration to Rainfall
3-12 Locations of Managed Aquifer Recharge Facilities
3-13 MAR Pond Percolation 1985-2014
3-14 Stream Segments in Model
3-15 Stream Channel Depth and Width Functions
3-16 Annual Groundwater Production 1985-2014
3-17 Groundwater Production Locations
3-18 Annual Groundwater Balances 1985-2014
3-19 Water Balance Comparison with GMOD and XMOD
4-1 Hydrographs of Measured and Simulated Groundwater Levels, Northeast Subbasin Margin

4-2 Hydrographs of Measured and Simulated Groundwater Levels, Southeast Subbasin Margin
4-3a-b Hydrographs of Measured and Simulated Groundwater Levels, Northwest Subbasin Margin
4-4a-i Hydrographs of Measured and Simulated Groundwater Levels, Southwest Subbasin Margin
4-5a-b Hydrographs of Measured and Simulated Groundwater Levels, Santa Teresa Area
4-6a-j Hydrographs of Measured and Simulated Groundwater Levels, Southeast-Central Area
4-7a-i Hydrographs of Measured and Simulated Groundwater Levels, Central Low-K Zone
4-8a-c Hydrographs of Measured and Simulated Groundwater Levels, San Francisco Bay Margin
4-9 Simulated and Measured Groundwater Levels, March 2012, Layer 1
4-10 Simulated and Measured Groundwater Levels, March 2012, Layer 2
4-11 Simulated and Measured Groundwater Levels, March 2012, Layer 3
4-12 Simulated and Measured Groundwater Levels, March 2012, Layer 4
4-13 Simulated and Measured Groundwater Levels, March 2012, Layer 5
4-14 Simulated and Measured Groundwater Levels, March 2012, Layer 6
4-15 Simulated and Measured Extent of Shallow Groundwater
4-16a-h Simulated and Measured Stream Flow Hydrographs
4-17 Scatterplot of Water-Level Residuals
4-18a-d Sensitivity Test of the Central Low-K_H Zone

List of Sheets

2-1 Sections Parallel 1 through Parallel 4
2-2 Sections Parallel 5 through Parallel 8
2-3 Sections Parallel 9 through Parallel 12
2-4 Sections Cross 1 through Cross 4
2-5 Sections Cross 5 through Cross 8
2-6 Sections Cross 9 through Cross 12

List of Acronyms

AFY	acre-feet per year
Bay	San Francisco Bay
CHD	constant head boundary
CIMIS	California Irrigation Management Information System
District	Santa Clara Valley Water District
DWR	California Department of Water Resources
ET	evapotranspiration
ETo	reference evapotranspiration
ft	feet
ft/d	feet per day
GHB	general head boundary
GIS	Geographic Information System
IMOD	MODFLOW model developed for IPR Groundwater Study
in/d	inches per day
in/yr	inches per year
IPR	indirect potable reuse
K_H	horizontal hydraulic conductivity
K_V	vertical hydraulic conductivity
MAR	managed aquifer recharge
mg/L	milligrams per liter
NAD	North American Datum
NAVD88	North American Vertical Datum of 1988
NGVD29	National Geodetic Vertical Datum of 1929
SCVWD	Santa Clara Valley Water District
S_0	specific storativity
S_Y	specific yield
Subbasin	Santa Clara Groundwater Subbasin
USEPA	U.S. Environmental Protection Agency
USGS	U.S. Geological Survey

Executive Summary

A numerical groundwater flow model (IMOD) of the Santa Clara Groundwater Subbasin (excluding the Coyote Valley Region) (Subbasin) was developed for Santa Clara Valley Water District (SCVWD or District) to support groundwater management activities, including evaluation of proposed spreading and injection of advanced treated recycled water (purified water) into the Subbasin. This regional model is suitable for simulating a wide range of groundwater conditions and management scenarios. Subsequent local refinements were implemented to simulate the purified water recharge projects.

The model draws on two predecessors: the GMOD model originally developed in 1992 and the XMOD model developed in 2004. Some model features such as its areal extent and basic layering are very similar to the prior models, while other features and inputs are new and substantially different.

The model simulates groundwater flow in unconsolidated alluvial sediments beneath the Santa Clara Plain at the southern end of San Francisco Bay. It extends north to Milpitas on the east side of the Bay and north to Atherton on the west side. The finite-difference model grid consists of 172 columns and 106 rows of cells with 1,000 x 1,000 foot spacing, and six layers. In some places, the layers correspond to specific hydrogeologic features, such as the regional confining layer or bedrock surface, but in many places the layers are arbitrary subdivisions of the complexly-layered alluvial sediments down to an elevation of 1,000 feet below sea level. The modeling software consists of MODFLOW-2005 operated through Groundwater Vistas, with model inputs and outputs processed using ArcGIS, Excel, and custom Fortran utility programs.

Recent geologic studies and data were reviewed to revise the conceptual hydrogeologic model and determine whether a different layering scheme would more accurately reflect the distribution of aquifers and aquitards within the Subbasin. In the end, the layering used in GMOD and XMOD was retained, except that the two uppermost model layers were extended to cover the entire basin, not just the confined area in the central part of the Subbasin.

Dispersed recharge through the top surface of the groundwater basin was simulated using a recharge model operated as a pre-processor to the groundwater flow model. Recharge from rainfall, irrigation return flow and pipe leaks was simulated separately for 174 zones delineated based on their percent impervious and irrigated land cover. Recharge was simulated daily and subtotaled to monthly values for input to the groundwater model.

Recharge from stream percolation and groundwater discharge into streams was simulated using the MODFLOW stream package. Monthly flows in 48 streams that enter the Subbasin were obtained directly from an extensive network of existing stream gages or by correlation from gaged to ungaged watersheds. The stream package routes flow down the network of stream channels from the mountains to the Bay, calculating gains and losses based on adjacent groundwater levels and stream hydraulic characteristics.

Groundwater inflow from the upgradient Coyote Valley Region of the Santa Clara Subbasin, mountain front recharge along the Diablo Range and groundwater outflow to San Francisco Bay were all represented in the model using general-head boundary conditions.

The District's managed aquifer recharge program introduces large amounts of water into the Subbasin through percolation ponds and percolation along stream channels. Pond percolation was represented as injection wells in model layer 1, and stream channel recharge was included by adding managed aquifer recharge discharges to natural flows in the stream package.

The model simulated transient groundwater flow and levels during calendar years 1985-2014 using monthly stress periods. This calibration period reflects current land and water use conditions and includes significant wet and dry periods. The recharge model and groundwater flow models were calibrated jointly, mostly based on visual comparison of simulated and measured groundwater hydrographs at 73 wells and stream flow hydrographs at 16 gages. Aquifer characteristics in each model layer were defined as broad zones of uniform values. Simulation results proved to be most sensitive to horizontal hydraulic conductivity, and to a lesser extent to vertical hydraulic conductivity and storativity. Consistent with the principle of parsimony, calibration commenced with a small number of parameter zones. Zone boundaries were adjusted and zones were subdivided only if multiple wells in an area exhibited similar discrepancies between measured and simulated water levels. Because land use is relatively uniform (urban), recharge model parameters were adjusted when the groundwater balance appeared to have too little or too much water overall. The primary recharge calibration variables were pipe leak rates, root depths of non-irrigated vegetation, and the threshold and slope of the rainfall-infiltration function.

Simulated groundwater levels generally matched measured water levels reasonably well throughout the Subbasin and calibration period. In some locations, discrepancies remained after extensive calibration efforts. Often, a parameter adjustment that improved results for several wells in an area worsened the results for other wells in that area. At some multiple-depth monitoring well clusters, discrepancies could not be eliminated because measured water levels were very different for two wells screened at different depths but within the same model layer. For the 12,925-measured water-level data points used in the calibration, simulated water levels were slightly high overall. Much of this statistical finding is derived from errors at some of the multi-depth monitoring well clusters, where measured water levels appeared to be influenced by nearby pumping that was either not included in the model, incorrectly specified in terms of depth and location, or within a localized area of low hydraulic conductivity.

Simulated stream base flow also matched the general magnitude of measured base flow at twelve of the stream gage locations. Measured flows at two gages close to San Francisco Bay were much higher than simulated flows, possibly due to active discharges from shallow groundwater dewatering systems into the streams, which is not included in the model.

Average annual inflows to the groundwater Subbasin during 1985-2014 totaled 160,000 acre-feet per year (AFY), and consisted of percolation of natural and managed aquifer recharge flows in streams (42 percent), dispersed recharge (28 percent), percolation at recharge ponds (25 percent), and subsurface inflow (5 percent). Outflows averaged 149,000 acre-feet per year, with well production accounting for the majority (72 percent), followed by discharges to streams (23 percent) and subsurface outflow to the Bay (5 percent). The average annual storage change was an increase of 11,000 acre-feet per year (AFY).

1 Introduction

1.1 Purpose and Goals of Model

The District is planning to augment local and imported water supplies by percolating and/or injecting purified water into the Santa Clara Groundwater Subbasin, a process known as indirect potable reuse (IPR). A groundwater model is needed to manage groundwater levels and storage and to estimate subsurface travel time of the recycled water once it enters the Subbasin. Because recharge and subsurface flow of recycled water are likely to occur in various locations throughout the Subbasin, the model needs to simulate the regional flow system at the Subbasin scale as well as local flow patterns around injection and spreading sites. This resulted in a two-phased approach. In the first phase, a basin-scale model was developed capable of accurately simulating historical groundwater conditions throughout the Subbasin over a 30-year historical calibration period. In the second phase, the model grid was refined in the vicinity of several potential recharge sites and the fine-grid model was used to simulate future groundwater conditions with and without recharge of purified recycled water. This report describes the development and calibration of the uniform-grid, Subbasin-scale model developed in the first phase.

1.2 Description of Model Area

The groundwater model simulates groundwater flow beneath the portions of Santa Clara Valley Basin, including the Santa Clara Plain Subbasin as shown in **Figure 1-1**. The modeled area is comprised of the Santa Clara Subbasin portion of the Santa Clara Valley Groundwater Basin formally recognized by the California Department of Water Resources (DWR, 2003). The model omits the Coyote Valley Region of the Santa Clara Subbasin, from which groundwater and surface water drain into the Santa Clara Plain area through the Coyote Narrows. San Francisco Bay (Bay) is at the northern end of the Santa Clara Plain, and the modeled area extends several miles out beneath the Bay. The alluvial deposits of the groundwater Subbasin continue northeastward into the Niles Cone Subbasin on the East Bay Plain. Similarly, the deposits continue northwestward beyond San Francisquito Creek into the San Mateo Plain Subbasin on the west side of San Francisco Bay. The modeled area will be referred to as the Santa Clara Plain, Santa Clara Subbasin or Subbasin in this report.

Land use overlying the Subbasin is almost entirely urban and includes the cities of San Jose, Santa Clara, Sunnyvale, Cupertino, Los Altos, Mountain View, Palo Alto and part of Milpitas. The combined population of those communities was approximately 1.5 million as of 2010.

The relatively flat valley floor is bounded by rugged hills of the Diablo Range to the northeast and the Santa Cruz Mountains to the southwest. These rise to elevations of 4,200 and 3,200 feet above sea level, respectively. Numerous creeks drain the hills and flow into the valley, where they merge into a handful of large creeks and the Guadalupe River and empty into the Bay.

Groundwater was originally the primary source of supply for urban and agricultural uses on lands overlying the Subbasin. As early as the 1920’s however, over-pumping had lowered groundwater levels by tens of feet, resulting in compaction of clay layers in the Subbasin fill deposits and subsidence of the ground surface. By the time surface water supplies from local reservoirs came on-line in 1935, groundwater levels in parts of the Subbasin had declined by 100 feet (ft). However, demand continued to outstrip supply, and water levels declined by more than 200 ft from pre-development levels by the early 1960s, when imports of water from the State Water Project commenced. Cumulative subsidence from 1934 to 1967 in the Mountain View-San Jose area was 6-8 feet (Poland and Ireland, 1988). Cumulative subsidence from 1915 to 1970 for the Santa Clara-San Jose area was 13 feet (SCVWD, 2010).

Deliveries of water from the federal Central Valley Project commenced in the mid-1980s and accelerated the rate of water-level recovery. Groundwater levels have approached pre-development levels in some parts of the Subbasin, but the imported supplies that made the recovery possible are not expected to be as reliable in the future as they have been in the past. Accordingly, the District is proceeding with plans to recharge the basin with fully advanced treated recycled water.

1.3 Previous Groundwater Modeling Investigations

The groundwater model described in this report is a new basin-wide groundwater flow model that combines elements of two previous models. The GMOD model was developed in 1991 by CH2M HILL (1992), and the XMOD model was developed by the U.S. Geological Survey in 2002 (Hanson and others, 2004). Both models cover the same area and have the same number of layers, but GMOD is simpler than XMOD in terms of spatial resolution and the level of detail in representing hydrologic processes. The District currently uses GMOD to support its groundwater management activities. While suitable for current District management purposes, for simulating percolation, injection and movement of recycled water, some aspects of GMOD were considered too simplistic, whereas some elements of XMOD were considered unnecessarily elaborate. The pros and cons of the two previous models are discussed under each modeling topic, below. In some cases, an entirely new approach or algorithm was adopted for the IMOD model if it offered significant advantages for a reasonable level of effort.

2 Hydrogeologic Conceptual Model

2.1 Subbasin Boundaries

Conceptually, the geographic boundaries of the Subbasin follow the contact between the unconsolidated alluvial deposits that underlie the Santa Clara Plain and the consolidated bedrock materials present in the adjacent hills and mountains. In some locations, this conceptual boundary is not clear-cut in practice. This occurs where the alluvial materials continue unbroken from the Santa Clara Plain up the east and west sides of San Francisco Bay, where fingers of alluvium extend from the plain up the valleys of tributary streams, and where semi-consolidated geologic formations could be considered “bedrock” but produce significant quantities of groundwater. Each of these situations is discussed below. In the numerical model, grid cells in areas classified as bedrock are set to be inactive, which means they do not store or transmit groundwater. They form a no-flow boundary with respect to the adjoining active flow cells. The model boundary corresponds to the boundary delineation in California Department of Water Resources’ Bulletin 118 (2003). Boundaries of the Santa Clara Subbasin and the active flow regions of the groundwater model are shown in **Figure 2-1.**

Along the east side of San Francisco Bay, the Subbasin boundary is in Milpitas at Scott Creek. Although permeable deposits continue north beyond this boundary into the East Bay Plain area, groundwater flow at that location is roughly parallel to the edge of the grid, from the Diablo Range toward San Francisco Bay. Because there is negligible flow in the north-south direction, areas north of that boundary are treated in much less detail in the model.

A similar situation is present along the southwestern edge of the Bay, in the northwestern portion of the Santa Clara Plain. In the GMOD and XMOD models, the active flow domain was truncated at San Francisquito Creek, which is the boundary between San Mateo and Santa Clara counties. It is noted that there is no hydrogeologic boundary at this location. The boundary along San Francisquito Creek is a jurisdictional boundary that follows the Santa Clara/San Mateo County line. Under pre-development conditions, recharge from the creek probably formed a flow divide at that location. However, the alluvial deposits are continuous across the County line, and recharge and pumping in San Mateo County could affect groundwater levels in adjacent parts of the Santa Clara Plain. The active domain of the IMOD model was moved to the northern edge of Atherton in San Mateo County to test a hypothesis that calibration errors at a monitoring well next to San Francisquito Creek might have resulted from the omission of groundwater pumping in Menlo Park, Atherton and East Palo Alto. The new boundary alignment is also roughly parallel to the usual direction of groundwater flow, and hence also reasonable to represent as a no-flow boundary.

The second boundary condition treated as a no-flow boundary in the model is the omission of groundwater flow in the fingers of alluvium beneath creek channels where they approach the Santa Clara Plain from the surrounding hills. The effect of inflow through stream channel alluvium on simulated water levels at downgradient wells would likely be indistinguishable from the effect of subsurface mountain front recharge distributed along the length of the mountain front. Near the streams, any subsurface inflow through channel alluvium not included in the model is compensated by increased stream percolation along the reach just inside the model boundary because percolation is simulated as a head-dependent process. The one exception is groundwater inflow at Coyote Narrows, where highly permeable stream channel deposits and a substantial reservoir of upstream groundwater (in the Coyote Valley Region) support a relatively large amount of inflow.

The GMOD and XMOD models used almost identical inland boundaries of their active flow domains. Those boundaries followed the edge of geologic materials mapped as Holocene basin and alluvial fan deposits. One difference was that XMOD included the Evergreen area, which is a triangular region of relatively thin Pleistocene alluvial fan deposits extending from the main Subbasin area into the Diablo Range hills near the southeastern corner of Santa Clara Plain (see **Figure 2-1**).

The IMOD model differs from the GMOD and XMOD models by including portions of the Santa Clara Formation in the active flow domain. Both of those models excluded the outcrop of the Santa Clara Formation along the southwestern edge of the basin. A geologic map showing the outcrop area of the Santa Clara Formation and the GMOD/XMOD basin boundary delineation is presented in **Figure 2-2**. This formation, deposited from late Tertiary through Pleistocene time, contains unconsolidated to lightly consolidated sedimentary deposits and has been considered non-water-bearing where it crops out in the foothills (despite the presence of numerous domestic wells) and water-bearing where it occurs at depth within the basin (Iwamura, 1995). Several lines of evidence suggest that the formation should be included in the active flow domain of the groundwater Subbasin. First, the formation is present beneath the Old and Young Alluvium throughout the Santa Clara Plain, where it is tapped by water supply wells. Second, the outcrop area of the formation is included within the basin in Bulletin 118, which functions as the official delineation of groundwater basins and subbasins for management purposes in California. The Bulletin 118 boundary follows the contact between the Santa Clara Formation and much more impermeable Franciscan bedrock units. Third, as shown in **Figure 2-2**, numerous wells produce groundwater from the Santa Clara Formation outcrop area. Most if not all those wells are for domestic use. Although the quantity produced at each well is relatively small, the use of the water is economically significant, and wells in that area intercept water that would otherwise flow into the main Subbasin area. Finally, simulated groundwater levels near the initial (GMOD and XMOD) model boundary near the area with numerous external wells were too high at first, suggesting that the external wells were in fact affecting downgradient water levels. The active area of the IMOD model was expanded to include the Santa Clara Formation and coincide with the Bulletin 118 boundary along the southwestern edge of the model. The external wells were included in the simulation, and the calibration water levels that had been too high were lowered by several feet (but not enough to completely match measured water levels).

2.2 Basin Fill Materials and Layering

The alluvial deposits that fill the basin consist of discontinuous layers of clay, silt, sand and gravel. An extensive, thick compacted clay layer forms a regional aquitard at a depth of approximately 100 feet below ground surface near the forebay and 150-250 feet below ground surface in the interior portion of the basin and substantially impedes the vertical flow of groundwater. The part of the Subbasin where the aquitard is present is known as the confined area (see **Figure 2-1**). At greater depth, however, previous hydrogeologic investigations have reached different conclusions about the continuity of aquifer and aquitard layers and their effects on vertical groundwater flow. The GMOD model assumed broad zones of uniform horizontal hydraulic conductivity and a horizontal-to-vertical conductivity ratio of 10:1. This represents a relatively low degree of vertical anisotropy such as might be expected within a single layer of relatively uniform material. Horizontal hydraulic conductivity in the XMOD model was based on interpolation of sediment texture reported in drillers' logs and as a result is highly variable in the horizontal direction. Vertical hydraulic conductivity is a much smaller fraction of horizontal hydraulic conductivity in the XMOD model as compared with the GMOD model, in part because XMOD explicitly simulates passive vertical flow through boreholes separately from vertical flow through the aquifer materials.

A more recent study of borehole geophysical and geologic data asserted that repeating cycles of coarse-to-fine sediment deposition could be identified and correlated among boreholes across the entire Subbasin (Wentworth and others, 2015). A total of eight depositional cycles were identified, and the cyclic pattern was attributed to transgression and regression of San Francisco Bay as sea level rose and fell multiple times during the Pleistocene Epoch.

2.2.1 Hydrogeologic Conceptual Model Geometry Refinement

As part of the first phase of model development, the hydrogeologic conceptualization model geometry in the area of the potential IPR projects was assessed. The goals of this assessment were to identify any local hydrogeologic structures that should be reflected in the model to allow for better simulation of groundwater flow, pond recharge, injection, and pumping distribution.

This hydrogeologic conceptual model geometry refinement focused on conditions relevant to layering in and around the four originally identified IPR areas and the revised injection well area. The assessment was designed to use and combine existing information in a data format that supports application of geographic evaluation tools within a Geographic Information System (GIS) platform. The information assessed in this evaluation included:

- Lithology and geophysical logs,
- Well construction logs,
- Groundwater elevations,
- Recently completed stratigraphic studies (Wentworth and others, 2015), and
- Existing GMOD and XMOD layering.

This information was collected and translated into a unified GIS compatible database structure for cross section construction and geographic evaluation. This approach allows any hydrostratigraphic structures relevant to groundwater flow in the IPR areas to be easily translated from GIS to the revised model.

2.2.1.1 Available Data and Information

Existing datasets and information were collected from all available sources.

The District provided locations for nearly 42,000 wells within Santa Clara County, as shown on **Figure 2-3**. The District's database and well completion reports provided lithologic records for over 3,200 of these wells (**Figure 2-4**) and construction records for over 1,600 wells[1] (**Figure 2-5**). These lithologic and well construction records were combined into a unified dataset extending well beyond the extents of the IPR areas. The effort required to compile these data and convert them to a format compatible with use in GIS is similar for small and large datasets. Therefore, extending the compilation of the dataset to include all provided data did not represent significant increased effort, and may provide the District with a resource for use in future hydrogeologic and hydrostratigraphic evaluations. The wells with either lithologic records, construction records, or both are shown on **Figure 2-6**. Construction of the unified database required combination of well location, lithologic, and well construction data from multiple data sources. These data sources often contained different information types. At each stage of the database construction process care was taken to include all the data from each data source. In addition, many records were included in multiple data sources, and often the records from two or more data sources had differences in locations or information for wells. Duplicate well locations or records were combined into single records preserving all the information from each individual data source.

The District also provided historical groundwater elevation data for wells throughout Santa Clara County. These data were primarily used to assess historical groundwater elevation patterns and in model calibration, as discussed in **Sections 2.4** and **4**. The average minimum and maximum groundwater elevations discussed in **Section 2.4** were translated into the GIS database for evaluation alongside conceptual and numerical model geometries.

Previously developed numerical model layers were exported from the GMOD model and imported to GIS for use in the geometry evaluation. The model layers for the GMOD model were the same as those used by the USGS in the XMOD model.

As noted above, Wentworth and others (2015) recently published the results of a large-scale evaluation of depositional environments in the Subbasin. The depositional cycle elevation surfaces developed by Wentworth are available from the USGS, and these data were imported to the GIS database for further evaluation in the context of conceptual and numerical model geometries.

Previously completed studies relating to environmental site investigations that included the development of conceptual and numerical groundwater models were also collected and reviewed.

2.2.1.2 Cross Section Construction and Hydrostratigraphic Evaluation

The study area for conceptual model geometry refinement was the four original IPR areas and revised injection well area shown in **Figure 2-7**. A total of 21 individual cross sections (which will hereafter be referred to as sections) were developed covering this study area, as shown on **Figure 2-8**. These sections are designated as parallel and cross oriented sections. The parallel sections are oriented parallel to the long axis of the model domain, and the cross oriented sections are perpendicular to the long axis. These 21 sections cover all the IPR areas, and extend between them to provide buffering around the areas. The sections are each separated by approximately 4,000 feet, providing good coverage of the study area.

---

[1] Construction records provided for Santa Clara Plain only.

The datasets incorporated into the GIS database discussed above were used to populate the sections with information from the subsurface and previous investigations. These data were applied to the sections using the ArcHydro Groundwater extension to ESRI's ArcGIS Desktop software. ArcHydro Groundwater includes tools for plotting lithologic and construction records from wells in a two-dimensional map to a two-dimensional section. The wells with lithologic and construction information in the vicinity of the sections are shown on **Figure 2-9**. ArcHydro Groundwater also includes the ability to plot surfaces, like ground surface, groundwater elevation surfaces, and model layers as lines on sections. These tools were used to populate each section with the following datasets:

- Ground surface elevations;
- Well and borehole lithology and well construction;
- High and low groundwater elevations from 2012 and 1989, respectively;
- GMOD / XMOD /IMOD model layers
- USGS (Wentworth) hydrostratigraphic cycle and bedrock boundaries.

These data were interpreted to the sections in a stepwise manner, with thorough review of the results following each interpretive step. Ground surface elevations and well locations with lithology and construction details were added to the sections first. Two example sections (Parallel 3 and Cross 3) showing ground surface elevations, minimum and maximum groundwater elevations, and lithology and well perforated intervals are included on **Figure 2-10**. The wells within 2,000 feet of either side of each section were used populate the sections, thus covering all the space between sections. The thickness of the lines representing lithology and perforated intervals in the wells shown on these example sections are inversely proportional to the distance of the well from the section line; the closer the well to the section, the thicker the line representing lithology or perforations. The GMOD and XMOD model layers were then added to each section and assessed in comparison to lithology and well construction, as shown in the example sections on **Figure 2-11**. Following this evaluation, the Wentworth cycle boundaries were plotted on each section and evaluated in combination with the lithology, well construction, and GMOD/XMOD model layers, as shown on **Figure 2-12**. Example sections showing all the information together are shown on **Figure 2-13**.

Each of the datasets used to populate the sections was evaluated alone and in combination with the other data on each section to check for the presence of local or study area wide hydrogeologic structures that should be represented in the model. This series of evaluations showed the subsurface in the study area to be composed of discontinuous sedimentary materials with limited distinct patterns at either a local or study area wide scale. There is some consistency in well construction at a local scale that roughly corresponds to the top of GMOD model layer three. Comparison to the depositional cycle boundaries described by Wentworth and others (2015) showed no correlation to lithology in logged wells and boreholes.

Evaluation of GMOD/XMOD model layering in the study area did indicate that layers one and two were essentially inactive in much of the model, but could be used to simulate shallow saturated aquifer materials in the unconfined IPR areas for better simulation of shallow groundwater conditions. The minimum groundwater elevations from 1989 were used to identify the maximum elevations these model layers could be set to while maintaining saturated model conditions.

The sections are all shown individually with lithology, groundwater surfaces, and IMOD model layers on **Sheets 2-1** through **2-6**.

2.2.1.3 Geophysical Log Review

A total of 34 geophysical logs were available for wells near the IPR areas, as shown on **Figure 2-14**. These geophysical logs were assessed in relation to one another and to surrounding lithology. This evaluation showed some correlation between geophysical logs from wells close to one another, but no locally or study area-wide patterns that could affect groundwater flow were indicated.

2.2.1.4 Depth Discrete Groundwater Elevation Monitoring

GMOD and XMOD pre-dated the installation of eight depth-discrete monitoring well clusters by the District. Those wells, shown on **Figure 2-15,** have now been monitored for over a decade, and their water-level patterns shed new light on the extent to which aquifer layering results in vertical gradients in groundwater levels. Well screens separated by as little as 100 feet vertically often have substantially different water levels and ranges of seasonal water-level fluctuation (see data presented below in **Section 2.4** "Groundwater Levels and Flow"). Also, the vertical distribution of water levels varies considerably among the cluster sites, which supports a conclusion that geographic variability in aquifer characteristics is also high.

The conceptual model geometry evaluation discussed above did not identify any hydrostratigraphic basis for modifying the numerical model layers from the GMOD or XMOD layering. The well logs and cross sections did not indicate any lithologic or geophysical structures that are consistent throughout or within the IPR areas. Well construction logs do indicate some consistency in the top of screens for municipal wells near individual IPR areas; however, vertical hydraulic gradients show variable patterns that are not depth specific.

Layering in the IMOD model is similar to layering in the GMOD and XMOD models. All three models have six layers. In GMOD and XMOD, the two uppermost layers (1 and 2) were intended to represent the upper groundwater system and regional aquitard layer; those layers were only active in the northern and central parts of the basin where the aquitard is present. The thicknesses of layers 1 and 2 were based on drillers' logs, with layer 1 representing permeable materials above the aquitard layer and layer 2 representing the aquitard itself. Model layer 3 covered the full extent of the basin. Oak Hill and other "islands" of bedrock that protrude upward through the alluvial deposits are incorporated as patches of no-flow cells within layer 3. Layers 4 through 6 are vertical subdivisions of alluvial deposits down to an elevation of 1,000 feet below sea level. Sediments deeper than that are not included in the model because they are generally fine-grained and because no wells extract water from those depths (Iwamura, 1995; Wentworth and others, 2015). In the IMOD model, layers 1 and 2 were given significant thickness throughout the basin, the bottom of layer 3 was modified locally to be more consistent with bedrock elevations, and the bottom elevations of layers 4-6 were essentially the same as in the previous models. Details regarding IMOD layering are presented in Section 3.3 "Model Layers".

2.3 Aquifer Hydraulic Characteristics

The hydraulic characteristics of an aquifer system are its ability to transmit and store groundwater. In the mathematical governing equations used to simulate groundwater flow, hydraulic conductivity represents the ability to transmit water at any point in the system, and specific storativity and specific yield represent the storage or release of water within the system when water levels rise or fall.

2.3.1 Hydraulic Conductivity

In layered aquifer systems, hydraulic conductivity is greater along layers than across layers, which typically are the horizontal and vertical directions, respectively. Various units are used to express this variable, but in this report units of feet per day (ft/d) are used. Hydraulic conductivity is highly dependent on sediment texture, and values for sands and gravels can be several orders of magnitude larger than for silts and clays. Due to layering in the sediments and in the model, vertical hydraulic conductivity is specified separately from horizontal hydraulic conductivity and is usually much lower. The transmissivity of an aquifer or model layer is obtained by multiplying its horizontal hydraulic conductivity by its thickness. Values of horizontal hydraulic conductivity (K_H) can be obtained from aquifer tests or from model calibration. For this study, aquifer test data were used to inform model calibration, which is described in **Section 4.1.6** "Discussion of Calibrated Parameters".

Aquifer tests consist of pumping water from a well at a controlled, constant rate and observing the change in water levels in the pumping well and/or nearby wells. Multiple-well aquifer tests have been done at several groundwater remediation sites in the Subbasin, resulting in a large number of K_H estimates. However, those estimates are for wells that are typically shallow and concentrated in relatively small geographic areas. Measurements of specific capacity are commonly done at large production wells and can be used as informal aquifer tests. Specific capacity is the flow rate in a well divided by the amount of drawdown (decline from static conditions) of the water level in the well when it reaches a stable level after turning the pump on. With simplifying assumptions, specific capacity can be converted to an estimate of transmissivity, which can then be divided by thickness to obtain K_H.

Compilations of K_H estimates from previous studies and new estimates from specific capacity data are presented in **Figure 2-16**. The figure shows the cumulative probability distribution of K_H values from each data source, plotted as the percent of sampled wells that were less than or equal to the corresponding K_H value. Several patterns stand out. One is the large variation in K_H values, both within and among sample data sets. In particular, most of the curves are concave to the right, indicating the presence of high outlier values, or a positively skewed distribution. The high values in the data set for the IBM remediation site (170-7,700 ft/d; log-mean value of 1,300 ft/d) reflect geographic variations in K_H (Harding Lawson Associates, 1987b). That site is in the Santa Teresa area, where coarse gravel deposits are relatively abundant in the subsurface. An aquifer test at Edenvale Gap at the downstream end of that area (**Figure 2-1**) produced a similar K_H estimate of 2,000 ft/d (Harding Lawson Associates, 1987a). The specific capacity data consist of measurements from 185 production wells, most of them relatively deep municipal wells. When K_H was calculated by dividing transmissivity by well screen length, the resulting cumulative distribution curve ranged from 0.1-212 ft/d (median = 7.8 ft/d). For reasons that are not clear, specific capacity tests from 23 water supply wells in the 1960s indicated consistently higher values (0.3-410 ft/d; median =78 ft/d) (Graveto and Majumdar, 1971).

Vertical hydraulic conductivity (K_V) is not measured by specific capacity tests or most multiple-well aquifer tests. Laboratory tests of cores of aquitard material often produce values that are smaller than regional average values because vertical flow at the regional scale is dominated by flow through local discontinuities in the clay aquitard. It is unlikely that a borehole at any given location will encounter these "leaky" spots. A well can significantly increase vertical flow across an aquitard if it is screened above and below it and/or the gravel pack is continuous across it. The cumulative effect of the thousands of wells in the Santa Clara Plain—most of which are screened across several hundred feet of basin thickness—is undoubtedly substantial. For practical purposes, model calibration is the best method for estimating the net effect of numerous aquitards, their spatial discontinuities, and passive vertical flow via boreholes.

2.3.2 Storativity and Specific Yield

The storage response of an aquifer system consists of two components: the very small elastic compressibilities of water and mineral grains (specific storativity, or S_0), and the much larger amounts of water stored and drained in aquifer pores as the water table rises and falls (specific yield, or Sy). Specific storativity occurs throughout the thickness of the aquifer system, whereas specific yield occurs only at the water table, which is the top surface of the flow system. This spatial separation combined with the relatively low bulk vertical hydraulic conductivity of layered aquifer systems produces a storage response that increases as the duration of pumping increases. If a new pumping stress is suddenly introduced far below the water table, the initial storage response will be from elastic storativity. Over time, the decrease in pressure (water level) in the pumped interval will propagate up to the water table and engage the larger storage response provided by specific yield. Empirically, storage responses obtained from aquifer tests lasting hours to days are smaller than storage responses obtained by calibrating groundwater models to observed water-level declines during multi-year droughts. The purpose of the present study is to support groundwater management over periods of years to decades, and consequently, the appropriate storativity and specific yield values are the ones obtained from model calibration. These are described in **Section 3.4** "Aquifer Characteristics".

A third component of storage response that has historically been present in the Santa Clara Plain is the release of water from aquitards as they compress during the process of inelastic subsidence. Historical subsidence is described in **Section 2.6** "Subsidence". In terms of storage, subsidence contributed an estimated 11,275 AFY of stored water to the active groundwater flow system during 1970-1999 (Hanson and others, 2004).

2.4 Groundwater Levels and Flow

Under pre-development conditions, groundwater flowed from the interior of the Subbasin toward San Francisco Bay, discharging upward through the regional confining layer into the Bay or into the channels of creeks as they approached the Bay. This discharge was associated with downward vertical water-level gradients around the inland periphery of the Subbasin and upward vertical gradients near the Bay. These patterns were confirmed by water levels and the locations of flowing wells prior to 1920 as reported by Clark (1924).

During 1915-1965 annual groundwater pumping in the Subbasin increased from approximately 49,000 to 185,000 AFY (Poland and Ireland, 1988). Groundwater levels in the central part of the Subbasin declined up to 240 feet during that period, to elevations more than 150 feet below sea level[2]. A hydrograph illustrating this history is shown in **Figure 2-17**. Groundwater levels did not begin their long-term recovery until 1965, when deliveries of imported surface water through the State Water Project commenced. The new supply of water enabled a decrease in groundwater pumping and increased MAR and a recovery of water levels. Groundwater levels at the hydrograph well rose 200 feet by the mid-1990s, and hydrographs for other wells confirm that the recovery was widespread and continued into the 2000s.

Spatial patterns of groundwater flow also changed in response to pumping. In past decades, heavy pumping near the center of the basin created a “pumping trough” in the water-level surface. **Figure 2-18** shows contours of water levels measured in June 1989, which at most wells were the lowest water levels during the calibration period (though not nearly as low as during the 1960s). Water levels were below sea level throughout a region extending from Santa Clara and downtown San Jose out to San Francisco Bay. Water levels were as low as 40 feet below sea level in a few wells. By 2012, water levels had recovered to their highest elevations during the calibration period. Contours of groundwater levels in spring 2012 are shown in **Figure 2-19**. Water levels were above sea level almost everywhere at that time, but were lowest in the center of the basin. Water levels were only 20-40 feet above sea level at the center of the pumping trough but 50-70 feet above sea level between the trough and San Francisco Bay.

The high water levels near the Bay could not have resulted from groundwater flow from the Bay or from the pumping trough, because the water would have had to flow uphill. Inflow from the Niles Cone area also could not have created the high water levels, because water levels in the Niles Cone aquifers range from a few feet above sea level to about 16 feet below sea level (Alameda County Water District, 2015). High water levels in the Bay Plain part of the Santa Clara Plain result from recharge in the unconfined “forebay” areas along the inland margins of the Subbasin that generates pressure head in the aquifers of the confined area, and that pressure head is not everywhere captured by the pumping trough near the center of the Subbasin.

---

[2] At the southern end of San Francisco Bay mean sea level is 1.30 feet above the National Geodetic Vertical Datum of 1929, which is the vertical datum used for all water level data collected by the District and also for all elevations in the groundwater model.

There are large vertical water-level gradients in the confined part of the Subbasin, which means that wells with short screens at different depths have substantially different water levels. The magnitude and variability of these gradients have only become evident since five multiple-completion monitoring wells were installed in the early 2000s. Although the largest water-level difference is often across the regional aquitard, the cluster wells confirm that the aquifer system below that aquitard is also highly stratified, with multiple confining layers at various depths. This pattern is consistent with the recent study of geologic and geophysical data by Wentworth and others (2015), who identified eight repeated sequences of coarse-to-fine upward-grading depositional cycles that appeared to be laterally extensive in the confined area.

Each of the five multiple-depth monitoring well clusters presents a different pattern of vertical water-level gradients, underscoring the ubiquitous presence of aquifer-aquitard layers and also the high degree of spatial variability across the Subbasin. **Figure 2-20** shows hydrographs of measured water levels at the monitoring well clusters. At the Guadalupe cluster, there is very little variation in water level with depth, indicating an absence of nearby pumping and little pressure head derived from upgradient recharge outside the confined area. At the Willow cluster, the highest water levels are in the shallowest and next-to-deepest well screens. This presumably results from the depth distribution of pumping in nearby production wells, combined with aquifer-aquitard layering that restricts the vertical propagation of drawdown. The other depth intervals have lower water levels and larger seasonal water-level fluctuations, both of which are signs of nearby pumping. At the Coyote Creek Outdoor Classroom (CCOC) cluster well, most of the vertical gradient is between model layers 1 and 4, with only a small additional increment between layer 4 and 5. The gradient is consistently downward. At the Saratoga cluster well, there is a very large water-level difference between two screened intervals that are both within the depth range corresponding to model layer 4. Water levels in the layer 5 screen are intermediate between those, and water levels in the layer 3 screen are only slightly higher. This pattern suggests the presence of a heavy nearby pumping stress that is hydraulically coupled to the deeper of the two layer 4 well screens. At the McGlincy cluster well, there is almost no water-level difference between screens corresponding to model layers 1 and 3. Two screens in layer 4 are somewhat lower and have generally similar elevations, but seasonal fluctuations are more pronounced in the deeper of those two screens. Water levels are higher in the layer 5 screen than the layer 4 screens. This pattern suggests the presence of a nearby pumping stress hydraulically coupled to the lower of the two layer 4 screens.

2.5 Sources of Inflow and Outflow

There are numerous sources of groundwater inflow (recharge) because Subbasin land use and hydrology include natural recharge from rainfall and stream percolation, urban effects related to pervious surfaces, irrigation and pipe leaks, and active percolation of local reservoir releases and imported water in ponds and creek channels. In addition, groundwater flows into the Subbasin through the alluvium beneath Coyote Creek at the southeastern corner of the Subbasin (Coyote Narrows) and also in small quantities from adjacent bedrock hills along the northeastern Subbasin margin. Methods for estimating these flows range from simple empirical rules of thumb to complex simulations of physical processes involved in soil zone and stream hydrology. For some inflows (for example, stream percolation and groundwater inflows) the groundwater model provides the best estimate, and for all other inflows, model calibration might reveal a need to revise prior estimates.

Groundwater pumping is by far the largest outflow from the Subbasin. Other outflows include evapotranspiration (ET) by phreatophytic riparian vegetation (riparian ET), discharge into stream channels where the water table is higher than the stream surface, and discharge through the regional confining layer and Bay Mud into San Francisco Bay. The last three of these are functions of groundwater levels and are best estimated by the groundwater model.

Details of the estimated Subbasin inflows and outflows are presented in the discussion of the groundwater model because many of them were estimated by the model or adjusted during joint calibration of the groundwater model and recharge model.

2.6 Subsidence

Subsidence occurs when pumping from wells lowers the water pressure in aquifer units below the pore pressure in the intervening fine-grained aquitard units. Certain types of clay minerals will compact under these circumstances, and those types of clays are common in this Subbasin. Groundwater levels in the central part of the Subbasin declined by as much as 240 feet between 1912 and 1965 (**Figure 2-17**), and this resulted in up to 13 feet of compaction in the area between Mountain View and downtown San Jose, as measured by lowering of the ground surface between 1915 and 1970 (Ingebritsen and Jones, 1999). The XMOD model explicitly simulated the subsidence process and concluded that water released from clay compaction contributed six percent of total inflow to the groundwater system during the 1970-1999 calibration period. Subsidence is not included in the present model because water levels during the 1985-2014 calibration period have been far above the minimum historical levels. Inelastic compaction is a one-time process that occurs when pore pressure in aquifers is first decreased. Although compaction is not instantaneous, any compaction potential associated with 1985-2014 water levels would almost certainly have come to completion during the preceding 50 years when water levels were much lower. The omission of subsidence from the model also implicitly assumes that future groundwater management will prevent groundwater levels from declining to near or below the historical minimums, which would trigger renewed subsidence.

3 Numerical Model Development

The numerical model was developed in two phases. In the first phase, an all-purpose, Subbasin-wide model with a uniform-grid was created and calibrated. In the second phase, the model grid was reduced in regions surrounding proposed IPR sites to add precision to simulated subsurface travel times. This report describes the model developed during the first phase, which is referred to as the IMOD model. The refined model used for IPR scenario simulation is called the fine-grid model. IMOD model incorporates elements of the two previous models of the Subbasin—GMOD and XMOD—but also includes numerous new components and details intended to improve model accuracy and enable the subsequent simulation of IPR projects and other types of groundwater management.

3.1 Software Used for Modeling

To simulate groundwater flow, the model uses MODFLOW-2005, the current version of the MODFLOW finite-difference computer program developed by the U.S. Geological Survey (Harbaugh, 2005). To expedite preparing and checking model input and processing model output, the MODFLOW program was operated from within Groundwater Vistas v.6.1, which is a widely-used graphical user interface program developed by and available from Environmental Simulations, Inc.

Additional steps in data preparation and model post-processing were completed using Microsoft Excel spreadsheets and custom Fortran utility programs developed by Todd Groundwater. Processing of variables with geographic distributions was completed using ArcGIS 10 geographic information system (GIS) software available from the ESRI company.

3.2 Model Grid and Active Flow Area

The footprint of the rectangular model grid and the number of layers was the same as for the XMOD model. The model grid is 172,000 feet in width and 106,000 feet in height, and these dimensions are divided into 172 columns and 106 rows of uniform 1,000 foot spacing, respectively. The lower-left corner of the grid has California State Plane Zone III (North American Datum [NAD] 1983) coordinates of 6,032,826 feet in the X direction and 1,959,735 feet in the Y direction. The grid is rotated -29.3 degrees about the lower left corner (that is, clockwise from east-west). The GMOD grid is 1,000 feet shorter in width and height than XMOD and the IMOD model, and based on report figures, the differences appear to be at the bottom and right edges.

The grid extends beyond the Subbasin in various places (**Figure 2-1**), and model cells outside the Subbasin are specified as no-flow cells. The active areas of model layers 1, 2 and 3 are identical, and they all cover the entire basin. The bedrock surface that defines the bottom of the basin is much deeper below the ground surface at the center of the basin than along the edges. Accordingly, the active flow regions of layers 4, 5 and 6 become progressively smaller, shrinking from the northeastern and southwestern Subbasin margins toward the center of the Subbasin.

3.3 Model Layers

The purpose of including multiple layers in the model was to enable the simulation of vertical groundwater movement within the Subbasin. Water-level data from the multiple-completion monitoring well clusters confirms that vertical gradients are large and water levels are very different between wells screened at different depths. In some locations, some of the boundaries between layers correspond to specific geologic horizons, and in others they simply subdivide the complexly layered sequence of aquifers and aquitards into depth intervals.

The IMOD model grid has six layers, and the layering scheme is similar to the layers in GMOD and XMOD. There are a few differences in model layers 1-3, however. Unlike the previous models, layers 1 and 2 are active over the entire basin, not just in the confined area. This change was implemented to simulate vertical flow near percolation ponds more precisely. The top of layer 1 and the bottoms of layers 1-3 were defined as sets of points from which smooth surfaces were generated using contouring software (Surfer), followed by grid subtraction procedures that ensured all cells in all layers had at least 20 feet of thickness. This minimum thickness was considered thick enough to decrease the risk of having model cells go dry during the numerical iterations used to solve for groundwater levels at each time step yet not so thick that bedrock elevation and total groundwater storage is misrepresented along the perimeter of the active flow domain. The data and procedures for those elevation surfaces are described in the following sections.

3.3.1 Top of Layer 1

The top of layer 1 equals the ground surface elevation. This was obtained from a 3-meter digital elevation model raster data set (National Elevation Dataset), converted from meters to feet and from the North American Vertical Datum of 1988 (NAVD88) datum to the National Geodetic Vertical Datum of 1929 (NGVD29) datum (by subtracting 2.68 feet).

3.3.2 Bottom of Layer 1

The bottom elevation for layer 1 was set slightly below the minimum measured water levels during the calibration period, which in most cases occurred around 1989. The purpose of this criterion was to prevent layer 1 cells from going dry during the simulation and thereby avoid the need to use the cell rewetting algorithm in MODFLOW (which tends to destabilize numerical convergence). Beneath San Francisco Bay, an elevation of -22 feet was used. Because contouring of measured water levels was unreliable around the Subbasin margins, an additional criterion was implemented that required the bottom of layer 1 to be at least 20 feet below the top of layer 1. Because groundwater levels recovered substantially after 1989, the saturated thickness of model layer 1 was moderately large toward the end of the calibration period. In spring 2012, for example, the saturated thickness was 100-120 feet throughout most of the central part of the Subbasin and the Santa Teresa area. Thickness decreased steadily to about 40 feet near San Francisco Bay. Along the southwest margin of the Subbasin saturated thickness was as much as 200 feet.

3.3.3 Bottom of Layer 2

In the confined area, the bottom of layer 2 represents the bottom of the older Bay Mud regional confining layer, and the GMOD elevations were retained. Outside the confined area, the bottom elevation was set roughly equal to the typical top-of-screen elevations in municipal wells. The purpose of this distinction was to focus pumping into layers 3-6 and let flow in layer 2 be primarily downward. A review of well construction data revealed some general patterns in the depths to the tops of municipal well screens: around 200 feet in the Santa Clara area, increasing southward to 300 feet near Highway 85 and decreasing to about 100 feet in the Santa Teresa area. After broadly contouring between these locations and merging with the GMOD layer 2 bottom elevations in the confined area, the minimum 20-foot layer thickness criterions was applied to obtain bottom elevations for layer 2 throughout the basin.

3.3.4 Bottom of Layer 3

The IMOD model uses the GMOD elevation for the bottom of layer 3 except along the southwest margin of the Subbasin and the Santa Teresa area. In those areas, the bottom of layer 3 is the bedrock surface, which was re-contoured for the IMOD model to project bedrock slopes from hillsides adjacent to the basin and to eliminate major deviations from bedrock elevation that GMOD included in the Santa Teresa area. Point elevations for the bedrock surface were obtained from a database of well completion reports, and these were combined with ground elevation points where bedrock crops out on hillsides adjacent to the basin. These points were contoured to obtain a continuous bedrock elevation surface. This was merged with the GMOD layer 3 bottom elevation at the locations where contoured bedrock dropped below the GMOD layer 3 bottom elevation. A minimum 20-foot layer thickness was imposed.

3.3.5 Bottom of Layers 4 through 6

The bottom elevations of model layers 4 through 6 are identical to their respective GMOD elevations, except that a minimum 20-foot layer thickness was required (in practice, few cells were affected by that criterion). The bottom of layer 6 is basically flat at an elevation of -1,000 feet. GMOD assumed that deeper parts of the basin are not actively involved in groundwater flow, and that assumption has been carried forward to XMOD and the IMOD model.

3.4 Aquifer Characteristics

Hydraulic conductivity and storativity were specified in the model as zones of cells with uniform values. The pattern of zonation and the values of horizontal and vertical hydraulic conductivity (K_H and K_V) and specific storativity and specific yield (S_0 and S_Y) assigned to the zones were a major focus of the model calibration process. It was found that simulated water levels were generally more sensitive to changes in K_H and K_V than in either storativity parameter. Accordingly, one zonation pattern was used for all four variables in each model layer. The zonation patterns and values for all six model layers are shown in **Figures 3-1** through **3-4**. The patterns and values for layers 3-5 were identical. The regional confining layer occupies the confined area of model layers 1 and 2, and its low permeability is represented by a vertical hydraulic conductivity of 0.0001 ft/d in layer 2. With two exceptions, K_H has moderate values in most parts of the basin: 10-15 ft/d along the mountain fronts and 70-90 ft/d in the central and southeastern parts of the basin. The exceptions are a zone of high conductivity (300 ft/d) in the Santa Teresa area and a zone of low conductivity (6 ft/d) in the center of the basin.

The calibrated values of specific yield apply mainly to model layer 1, which contained the water table at all locations throughout the calibration period. In that layer, the specific yield was 0.003 in the confined zone, 0.03 in most other areas including the Santa Teresa subarea, and 0.12 along the southwestern mountain front and in the Evergreen area. Specific storativity represents the storage response in layers 2-6. It ranged from 0.000003 ft^{-1} in the confined area in layers 3-6, 0.00003 in most other areas and 0.0001 ft^{-1} in the Evergreen and southwestern mountain front areas.

The patterns and values of hydraulic conductivity and storativity are discussed in greater detail in **Section 4.1.6** "Discussion of Calibrated Parameters".

3.5 Simulation Period and Time Increments

The model simulates calendar years 1985-2014 using monthly stress periods, which are the increments of time for which input data are specified. A steady-state simulation was not completed because groundwater conditions were changing fairly rapidly during 1985-1999 as the basin recovered from previous decades of overdraft and responded to wet years in the mid-1990s. Although steady-state simulations allow K to be calibrated independently of S, their separate effects can usually be differentiated in transient simulations. In this case, it was considered more efficient to proceed directly with transient calibration. The simulation period was selected based on several criteria:

- Land and water use conditions were similar to current conditions. Calibrating the model to conditions during 1985-2014 provides a more reliable basis for simulating future scenarios than calibrating to an older historical period.
- Thirty years is sufficiently long to simulate long-term responses to changes in recharge and pumping. It is relatively easy to switch the 30-year simulation from retrospective (1985-2014) to prospective (2015-2044), whereas changing the duration of the simulation requires more comprehensive modification of model pre-processing and post-processing files.
- Climatic conditions during 1985-2014 reflected the average for the historical period of record and also included multi-year wet and dry periods (see **Section 3.7.1.1** "Rainfall and Interception").

Monthly stress periods offer a reasonable compromise between accurately simulating short-term non-linear hydrologic processes (such as recharge from large stream flow events) and simulating long-term changes in groundwater conditions with manageable data file sizes and model run times. The GMOD and XMOD models also use monthly stress periods.

3.6 Initial Water Levels

Initial water levels representing groundwater conditions on December 31, 1984 were based on a combination of measured water levels, simulated water levels and hydrograph errors during the first 3 years of the calibration period. An initial water level is required for every active cell in every model layer. Measured water levels alone do not provide this information because they indicate water levels at a relatively small number of point locations, and the measured water levels are vertically averaged over the length of the well screen (which commonly spans multiple model layers). Mathematical methods such as kriging can be used to interpolate and extrapolate water levels from well locations to the rest of the Subbasin, but those mathematical procedures are entirely unrelated to the physical processes of groundwater flow. As a result, the interpolated/extrapolated values will be inconsistent with simulated groundwater levels, which leads to large water-level “adjustments” during the first few years of the simulation. Also, most measured water levels represent an average water level over a large depth interval because well screens are long, and those water levels must be expanded into a set of six water levels representing each model layer at that location. The challenge is to obtain a set of initial water levels that honors the measured data while simultaneously representing horizontal and vertical water-level gradients that are consistent with the flows and aquifer characteristics of the groundwater system. By calibrating vertical hydraulic conductivity to replicate vertical water-level gradients at cluster well sites and assuming those conductivity values apply to surrounding areas in the basin, the model can be used to estimate water levels in all layers at all locations, including at the start of the simulation.

Errors in initial water levels often take several years to dissipate as groundwater moves between layers to achieve water levels that are hydraulically consistent with inflows, outflows and horizontal hydraulic conductivities throughout the flow domain. Accordingly, initial water levels were obtained through an iterative process in which simulated water levels in April 1988—which appeared to be after initial head errors had dissipated—were adjusted back to December 1984 to create a new set of estimated initial water levels. Iteration was necessary because there were real trends in groundwater levels during the first few years of the simulation, not just adjustments to initial-head errors. The adjustments were specified at hydrograph locations. For each layer, those adjustments were converted to a smooth surface over the entire Subbasin using contouring software. This process was repeated until simulated hydrographs matched measured hydrographs during the first few years of the calibration period with no large initial water-level rises or declines resulting from inconsistency between the estimated initial water level and the groundwater conditions prevailing at that time. **Figures 3-5** through **3-7** shows contours of estimated December 1984 water levels in model layers 1, 3 and 5, respectively, to illustrate the results of this process.

Steady-state simulation is an alternative method for obtaining estimates of initial water levels, but it is only appropriate if groundwater conditions were in fact stable at that time. In 1984, the Santa Clara Plain was still recovering from decades of historical water-level declines and had just experienced an exceptionally wet year in 1983 (see long-term hydrograph in **Section 2.6** “Subsidence”). Therefore, the steady-state assumption would not be valid.

3.7 Inflows

3.7.1 Dispersed Recharge

A substantial amount of recharge to the groundwater Subbasin consists of percolation of infiltrated rainwater, irrigation return flow and pipe leaks distributed widely across the

Subbasin. These hydrologic processes involve nonlinear relationships among variables, which means that the resulting recharge cannot be accurately estimated on an annual or even monthly basis. Instead, the processes were simulated concurrently using a recharge model with daily time steps, and the estimated daily recharge amounts were subtotaled monthly for input to the groundwater model. The recharge model includes precipitation, interception, direct runoff (from pervious and impervious surfaces), infiltration, soil moisture storage in the root zone, evapotranspiration, irrigation, leaks from water and sewer pipes, and the attenuating effects of shallow groundwater storage on recharge to deeper aquifers.

The surface of the Santa Clara Plain is almost completely urbanized, but there are a few undeveloped areas as well as variations in the percentages of impervious and irrigated land cover. For simulating recharge, land use in the Subbasin was divided into 174 recharge zones delineated from 2012 high-resolution aerial photography based on visual differences in percentage of impervious and irrigated area. The modeling extended beyond the groundwater Subbasin to include watersheds in the Diablo Range and Santa Cruz Mountains that drain to the Subbasin. Simulating recharge in tributary watershed areas provided a constraint on estimated amounts of subsurface inflow and also provided a means of simulating the potential effects of changes in climate or land use on surface and subsurface inflows along the groundwater model boundary. One exception was the large Coyote Creek watershed, which was clipped at the groundwater model boundary. Surface and subsurface inflow from that watershed were estimated by stream gage records and groundwater flow calculations using the Darcy Equation. **Figure 3-8** shows a map of the recharge zones.

Each recharge zone consists of impervious, pervious (nonirrigated) and irrigated subareas that are not mapped explicitly but simulated as percentages of the zone area. A one-dimensional soil moisture and shallow groundwater water balance is calculated separately for the three component subareas, multiplied by their respective areas, then totaled to obtain volumetric daily recharge for the entire zone. Parameters used to characterize physical conditions in each zone are listed in **Table 3-1** and are described in the following sections.

3.7.1.1 Rainfall and Interception

The climate in the San Jose area is Mediterranean, with wet winters and dry summers. Precipitation in downtown San Jose averages 14.05 inches per year (in/yr), of which 81 percent typically falls between November and March. **Figure 3-9** shows annual rainfall and the cumulative departure of annual rainfall during the 1933-2014 period of record. Rainfall averaged 14.22 in/yr during the 1985-2014 calibration period, which was 1.2 percent more than the long-term average. On an annual basis, rainfall is greater in the mountains than on Santa Clara Plain and San Francisco Bay. The distribution of average annual rainfall is shown in **Figure 3-10** and ranges from 12 in/yr near the southern tip of San Francisco Bay to 30-50 in/yr near the crests of the Diablo Range and Santa Cruz Mountains. Average annual rainfall at each recharge zone was estimated from this isohyetal map, and daily rainfall at each zone was calculated by multiplying daily rainfall at the San Jose gage by the ratio of average annual zone rainfall to average annual San Jose rainfall.

Interception refers to rainwater that adheres to the leaves of plants and does not reach the ground. The amount is small at any time, but interception occurs repeatedly throughout the rainy season and can substantially decrease the amount of soil infiltration on days with small amounts of rain. In the recharge model, interception was estimated to be 0.08 inch for evergreen trees and shrubs, 0.04 inch for crops and urban residential (where vegetation is a mix of turf, shrubs and trees), 0.02 inch for turf, and 0 inch for impervious surfaces. These values are consistent with field studies of interception in other areas (Viessman and others, 1977). Interception was subtracted from rainfall on a daily basis.

3.7.1.2 Runoff and Infiltration

Most rainfall reaching the ground surface (net rainfall) infiltrates into the soil, but direct runoff occurs when net rainfall exceeds a certain threshold. The threshold at which runoff commences and the percent of additional rainfall that runs off are significantly influenced by a number of variables, including soil texture, soil compaction, leaf litter, ground slope, and antecedent moisture. These factors can be highly variable within a recharge zone, and data are not normally available for them. Also, the intercept and slope of the rainfall-runoff relationship depends on the time increment of analysis. Most analytical equations for infiltration and runoff apply to spatial scales of a few square meters over periods of minutes to hours (Viessman and others, 1977). They are suitable for detailed analysis of individual storm events. The curve number approach to estimating runoff also applies to single, large storm events. It is not suitable for continuous simulation of runoff over the complete range of rainfall intensities (Van Mullen and others, 2002). The approach used in the recharge model is similar but less complex than the approach used in popular watershed models such as HSPF (Bicknell and others, 1997).

In the recharge model, daily infiltration is simulated as a three-segment linear function of net rainfall, and net rainfall in excess of infiltration is assumed to become runoff. The general shape of the relationship of daily infiltration to daily net rainfall is shown in **Figure 3-11** (upper graph). Below a specified runoff threshold, all daily net rainfall is assumed to infiltrate. Above that amount, a fixed percentage of rainfall is assumed to infiltrate, which is the slope of the second segment of the infiltration function. Finally, an upper limit is imposed that represents the maximum infiltration capacity of the soil. The runoff threshold, the percentage of excess net rainfall that infiltrates, and the maximum daily infiltration capacity were assumed to vary by land use and were among the variables adjusted for model calibration. The runoff threshold ranged from 0.2 inches per day (in/d) for unpaved areas in industrial and commercial zones to 0.8 in/d for turf and natural vegetation areas. The infiltration percentage for excess rainfall ranged from 55 percent in commercial and industrial areas to 87 percent in large turf areas and upland natural vegetation. In urban residential areas—which comprise most of the land cover over the Subbasin—the runoff threshold was 0.35 in/d and the infiltration percentage was 80 percent. The maximum daily infiltration was set to 3 in/d for all land uses and soil types.

The above parameter values are for soils that are relatively dry. Infiltration rates decrease as soils become more saturated. This phenomenon led to the development of the Antecedent Runoff Condition adjustment factor for rainfall-runoff equations (Rawls and others, 1993). However, application of the concept has been focused on individual storm events. For the purpose of the recharge model, the adjustment provides a means of simulating empirical observations that a given amount of rainfall produces less runoff at the beginning of the rainy season when soils are relatively dry than at the end of the rainy season when soils are relatively wet. This effect is included in the recharge model as a multiplier that decreases the estimated infiltration as soil saturation increases. This multiplier is applied to the runoff threshold, the infiltration slope and the maximum infiltration rate. The multiplier decreases from 1.0 when the soil is dry to a user-selected value between 1.0 and 0.60 when the soil is fully saturated (lower graph in **Figure 3-11**). A low value has the effect of decreasing infiltration (and potential groundwater recharge) toward the end of the rainy season or in very wet years, and also to increase simulated peak runoff during large storm events. The multiplier under saturated conditions was assumed to be 0.75 for the Santa Clara Plain recharge model.

Runoff from impervious surfaces was assumed to equal 100 percent of rainfall. Runoff that flows into a storm drain system (known as “connected impervious runoff”) contributes to stream flow but not groundwater recharge. However, runoff from some impervious surfaces flows onto adjacent areas of pervious soils (“disconnected impervious runoff”). The surface hydrology model treats this type of runoff as if it were a large increment of additional rainfall where it flows over or ponds on the pervious soils. The excess water can quickly saturate the soil and initiate deep percolation. The model incorporates this process by means of a variable representing the fraction of impervious runoff that becomes deep percolation. Data and literature values are not available for this variable, so it was included among the recharge variables adjusted during calibration. The final estimates were that 7 percent of impervious runoff becomes deep percolation in urban residential areas, 3 percent in commercial and industrial areas and 100 percent in rural residential areas.

The amount of connected impervious runoff in the Santa Clara Plain was estimated from observed increases in stream flow during small rainfall events, during which all the runoff was probably from impervious surfaces.

3.7.1.3 Root Zone Depth and Moisture Content

The storage capacity of the root zone equals the product of the vegetation root depth and the available water capacity of the soil. The available water capacity for each recharge zone was a depth-weighted average for the dominant soil type, as reported in the soil survey (Natural Resources Conservation Service, 2015). Root depth is a complex variable. Except for cropland, vegetation cover typically consists of a mix of species with different root depths. At a very local scale, roots are deepest directly beneath a plant and shallower between plants. Root density and water extraction also typically decrease with depth within the root zone. To complicate matters, root depth is somewhat facultative for many plants, which means that roots will tend to grow deeper in soils with low available water capacity, such as sands. Finally, root depth in many upland watershed areas is restricted by shallow bedrock. The root depth selected for each recharge zone represents an average of all these factors such that simulated deep percolation and stream flow are the same as the actual values averaged over the area of the zone. Separate root depths were specified for irrigated and non-irrigated vegetation in each recharge zone. Root depths for any given vegetation type (such as lawn or truck crops) was required to be the same in all zones.

In the Santa Clara Plain, the most common irrigated vegetation is lawns, for which a root depth of 18 inches was assumed. An average root depth for non-irrigated vegetation (primarily shrubs and trees) of 72 inches was assumed in urban areas and 84 inches in upland watershed areas. Root depth has a large effect on simulated deep percolation and hence groundwater recharge. The above values were obtained partly by model calibration.

3.7.1.4 Evapotranspiration

Evapotranspiration is affected by meteorologic conditions, plant type and growth stage, and soil moisture availability. All of these factors are included in the recharge model. The evaporative demand created by meteorological conditions is represented by reference evapotranspiration (ETo). Numerous equations have been developed over the years relating ETo to solar radiation, air temperature, relative humidity and wind speed. For the purposes of the Santa Clara Plain model, ETo values were extrapolated from a California Irrigation Management Information System (CIMIS) microclimate station in Union City to San Jose. Based on a statewide ETo map (Jones, 1999), average annual ETo in San Jose and Union City are 49.4 and 44.8 inches, respectively. Daily ETo data for Union City are available for 2001-2014 and were extrapolated to San Jose based on ratios of long-term average ETo for each month of the year. All recharge zones in the recharge model are in the same climate zone and were assumed to have the same annual ETo. For years prior to 2001, Daily ETo in Union City was estimated to equal average ETo for that month of the year multiplied by an adjustment factor derived from the relationship between ETo and air temperature. The factor equaled 0.0055, which was the slope of a linear regression of daily ETo versus daily maximum air temperature for that month of the year, using data from the period of record for the Union City CIMIS station.

Evapotranspiration varies by vegetation type and growth stage. Reference ET is the amount of water evapotranspired from a broad expanse of turf mowed to a height of 4-6 inches with ample irrigation. ETo is multiplied by a crop coefficient to obtain the actual ET of a different crop or vegetation type at a particular point in its growth and development. Although primarily used for agricultural crops, crop coefficients can also be applied to urban landscape plants and natural vegetation. Compilations of crop coefficients for many plant types based on field studies are available from numerous sources, in some cases specified by calendar month and in others by growth stage of the plant. Monthly crop coefficients for the ten land use categories in the recharge model are shown in **Table 3-2** and were developed from a comparison of published values from various published sources.

3.7.1.5 Irrigation

Evapotranspiration gradually depletes soil moisture, and for irrigated areas the recharge model triggers an irrigation event whenever soil moisture falls below a specified threshold. The amount of applied irrigation water is equal to the volume required to refill soil moisture storage to field capacity, divided by the assumed irrigation efficiency. An irrigation threshold equal to 80 percent of maximum soil moisture storage was used for urban landscaping and all crops. This variable primarily affects the frequency of irrigation; a higher threshold results in more frequent irrigation but approximately the same total amount of water applied annually. Irrigation efficiency was assumed to be 80 percent for urban residential irrigated areas and 90 percent for parks, playing fields and commercial and industrial irrigated areas. These efficiencies are with respect to deep percolation only. That is, an efficiency of 90 percent means that 10 percent of the applied water is assumed to percolate beneath the root zone, largely due to low uniformity of application. In urban areas, there are additional large sources of inefficiency, such as direct evaporation from spray droplets and sprinkler overspray onto driveways, sidewalks and other impervious surfaces (Baum and others, 2005; Xiao and others, 2007; Kumar and others, 2009). Those losses can affect water use and runoff, but are not part of the calculation of dispersed groundwater recharge.

Because irrigation is assumed to completely refill the soil moisture storage and is less than 100 percent efficient, soil moisture exceeds capacity immediately following an irrigation event. The excess is assumed to become deep percolation beneath the root zone.

The percent irrigated area for each urban land use category was estimated by curve separation of seasonal variations in monthly water use. For each water purveyor, water use during the minimum-use month (typically December, January or February) was assumed to represent only indoor water use because irrigation is generally unnecessary in mid-winter. Indoor water use was assumed to be constant year-round, and excess water use in all other months was attributed to irrigation. Data for 2000-2003 was selected because climatic conditions were fairly normal during that period and complete water use data were available. The calculations indicated that about 97,300 AFY were used for irrigation during that period, or 36 percent of total municipal water use. The calculations were also broken down by user category. For the largest purveyor (San Jose Water Company) outdoor water use for residential, commercial, industrial and institutional users was 37 percent, 29 percent, 21 percent and 67 percent of total water use, respectively.

Irrigation efficiency is commonly low for urban landscape vegetation because of irregular vegetation patch shapes, mixed types of vegetation, and homeowner management of irrigation. Application efficiencies of 50 percent are common for the San Francisco Bay Area (Sandoval-Solis and others, 2013). Much of the inefficiency is loss of water to direct evaporation of sprinkler spray and overspray onto impervious surfaces such as driveways and streets. Additional inefficiency results from non-uniform application of water, which results in deep percolation out of the root zone at various locations within the irrigated area. For this analysis, the 80-90 percent efficiency described above refers to the deep percolation component of inefficiency that becomes groundwater recharge.

The amount of irrigated area in the Subbasin was estimated by dividing the estimated total volume of water used for irrigation by an estimated irrigation rate. Assuming 75 percent irrigation efficiency, the average annual applied water requirement for turf in San Jose is 47 inches, based on a daily simulation of soil moisture for a hypothetical turf root zone during 1985-2014 using local rainfall and ET data. This indicates a total of 25,000 irrigated acres for the eight purveyors used in the analysis, which corresponds to 14 percent of their total combined service areas. This was broken down by user category so that the percent irrigated area in each category was consistent with the percent outdoor water use. The resulting estimates of percent irrigated area were 16 percent for residential, and 12 percent, 9 percent and 29 percent for commercial, industrial and institutional land uses, respectively.

For the recharge model, the foregoing parameters were used to estimate applied irrigation water in each recharge zone, and 10 percent of the applied irrigation water was assumed to percolate past the root zone to become groundwater recharge.

3.7.1.6 Deep Percolation from Root Zone to Shallow Groundwater

The recharge model updates soil moisture storage each day to reflect inflows and outflows. Rainfall infiltration and applied irrigation water are added to the ending storage of the previous day, and ET is subtracted. If the resulting soil moisture storage exceeds the root zone storage capacity, all the excess is assumed to percolation down from the root zone to shallow groundwater. These continuous water balances are calculated separately for the pervious, impervious and irrigated subareas of each recharge zone.

3.7.1.7 Pipe Leaks

Water, sewer, and storm drain pipes in urban areas leak to some extent, creating a source of recharge to the underlying groundwater system. Conversely, sewer and storm drain pipes can gain flow from infiltration of groundwater where the water table is high. Leaks are often small and difficult to detect. Of the three types of pipelines, municipal water distribution systems are typically the most studied and best maintained. Leak rates are relatively high because the pipes are pressurized, but leak detection is relatively aggressive because the leakage can be a significant economic loss and because leak detection is a best management practice for water conservation. One leak detection program audited 47 California water utilities and found an average loss of 10 percent, with a range of 30 percent to less than 5 percent of the total annual flow.[3] Another study monitored water use at numerous individual residences in ten medium to large California water systems using data loggers, and it found an average leak rate of 18 percent of the delivered volume (Aquacraft, 2011). A U.S. Environmental Protection Agency (USEPA) study found that “unaccounted for water” (which includes incidental unmetered uses in addition to leaks) in the range of 10-20 percent of total volume delivered is normal (Lahlou, 2001).

Unaccounted for water is estimated in urban water management plans prepared by local water purveyors. Those losses are typically estimated as a residual, that is, as the difference between metered production and the sum of metered deliveries, minus known unmetered uses (fire hydrants, main flushing, etc.). The water system leak rate is commonly expressed as a percentage of flow because of the water-balance approach used to estimate it. However, it is actually independent of flow because the network of pressurized pipes would leak even if all faucets and other outlets were turned off. Unaccounted-for system losses were tabulated from the 2010 urban water management plans prepared by each of the ten large municipal water purveyors in the Subbasin. Those volumes were divided by total water production (from all sources) to estimate the leak rate. Leak rates were 5-9 percent of annual water use. Due to the inherent uncertainty in estimating leak rates, a uniform value of 7 percent was assumed for all purveyors, which also equaled the percentage reported by the largest purveyor (San Jose Water Company).

---

[3] DWR website http://www.water.ca.gov/wateruseefficiency/leak/ accessed 5/2/13

Leak detection is a higher priority for water purveyors now than it was in 1985, due to statewide mandates for water conservation. It was assumed that leak rates in 1985 were higher than in 2010 by 2 percent of total water production. Also, the extent of the water distribution system was assumed to be correlated with population, and total water use was projected backward from 2010 to 1985 in proportion to population.

Plant roots probably intercept a substantial amount of leaked water, consuming it as evapotranspiration and preventing it from becoming groundwater recharge. That interception presumably depends strongly on the sizes and locations of leaks and the proximity of nearby vegetation. Given the absence of such detailed information, interception by plants was estimated by overall joint calibration of the recharge model and groundwater model. In the final calibration, the amount of water pipe leakage that becomes groundwater recharge was assumed to decrease from 4 percent of total water use in 1985 to 2 percent in 2014.

Sewer pipes also leak, and their leak rate was assumed to be half of the water pipe leak rate (as a percentage of annual flow). Sewer flow was estimated in a two-step process. First indoor use was estimated by curve separation of monthly purveyor water production. This separation assumes than in the minimum-use month (usually February), all water is used indoors and none is used for irrigation. Furthermore, indoor use was assumed to remain constant year-round. Almost all water used indoors leaves the building as wastewater in drains; only about 2 percent is consumed (Mitchell and others, 2001). Sewer leaks receive less attention than water pipe leaks, and few studies are available in the literature. Because sewer pipes are mostly not pressurized, and leaks probably self-seal to some extent due to clogging by solids and biofilms, the sewer pipe leak rate was assumed to be half the water pipe leak rate. Interception by plants and decreases in leak rates over time due to conservation efforts were assumed to be the same as for water pipe leaks.

On a volumetric basis over the entire basin, estimated groundwater recharge from water and sewer pipe leaks decreased from 10,200 AF in 1985 to 7,000 AF in 2014 (excluding the San Mateo County area).

3.7.1.8 Movement of Shallow Groundwater to Deep Recharge and Stream Base Flow

In some basins, deep percolation from the root zone does not appear to flow directly to regional water supply aquifers but rather to a shallow groundwater zone from which it slowly dissipates as lateral flow to streams or steady downward recharge to deeper aquifers (Yates and others, 2002; Johnson and others, 2004) Lateral flow to streams is usually substantial only in upland watersheds, which were not a major focus of the present modeling effort. Groundwater discharges to stream channels as they approach San Francisco Bay in the Santa Clara Plain basin, but that process is adequately represented by the stream package within MODFLOW-2005 and did not need to be represented in the recharge model. Shallow groundwater zones do appear to attenuate pulses of deep percolation leaving the root zone, and that effect was implemented by assuming a deep recharge rate of 0.2 in/d in all the valley-floor recharge zones. Recharge to model layer 1 continues at that rate until shallow groundwater storage is exhausted, and it resumes whenever shallow storage is replenished by deep percolation.

3.7.2 Managed Aquifer Recharge

For many years, the District has supplemented natural groundwater recharge with managed aquifer recharge (MAR), which consists of percolating imported water and storage releases from local reservoirs at ponds operated for that purpose and along stream channels.

There are 70 percolation ponds in the Santa Clara Plain area, in groups at nine recharge facility locations. The District monitors monthly percolation by facility, and the facility totals were allocated to individual ponds based on pond area for input to the groundwater model. The locations of MAR ponds and percolation discharges to stream channels are shown in **Figure 3-12**. After subtracting net evaporation (monthly evaporation minus monthly rainfall) from each pond, the net recharge was added to the groundwater model as if the recharge were injected by a well into model layer 1 at the pond location.

The Coyote Ponds and Ford Ponds on Coyote Creek were simulated as stream reaches rather than injection wells. At those locations, the creek flows through the ponds and it was more logical to simulate percolation using the MODFLOW stream package with the pond represented as a wide reach of stream channel.

Annual percolation at MAR pond facilities during 1985-2014 is shown in **Figure 3-13**. Total pond percolation was 35,000-55,000 AFY in almost all years during that period, and the proportional allocations among the facilities also remained fairly uniform. One exception was the large decrease in MAR recharge in 2014, when statewide drought conditions greatly reduced the availability of imported and local surface water.

MAR percolation along stream channels was included in the groundwater model by adding the discharge from pipelines to the flow in the stream segment that receives the water. The groundwater model then calculates the percolation from the stream channel based on the flow, elevation and hydraulic geometry of the stream, as described in the next section.

3.7.3 Percolation from Streams

Numerous creeks cross the Santa Clara Plain and discharge into San Francisco Bay. Where the creek channel is far above the adjacent groundwater table, stream percolation provides a source of recharge, and the rate is independent of water table elevation. This is common along stream reaches in interior parts of the basin, near the mountains. If the water table elevation is close to the channel elevation, flow can be from the creek to the aquifer or vice versa, depending on which has the higher elevation. In most of the area underlain by the regional confining layer creeks gain flow from groundwater because discharge to the creek is the primary pathway for groundwater outflow. Except near the Bay shoreline, creek channels are generally closer to sources of recharge than the Bay is. Also, water-level gradients across the confining layer are usually upward, and consequently local recharge cannot percolate downward the way it typically does outside the confined area. A substantial amount of groundwater is pumped from the shallow aquifer above the confining layer by remediation wells at groundwater contamination sites and dewatering systems. In most cases the pumped water is discharged to local creek channels, thereby accelerating the rate at which shallow groundwater flows into the creek channels.

Because groundwater and surface water are hydraulically connected along many stream reaches, the exchange of water between them was simulated using the MODFLOW stream package. This program module calculates the direction and rate of flow between streams and model layer 1 based on current groundwater elevation, current stream flow, and the length, width, depth and water surface elevation of the wetted stream channel. Implementation of the stream package in the model was very similar to the implementation in the XMOD model. The network of stream channels was divided into 116 stream segments, which are lengths of channel between confluence and boundary points. Each segment is divided into a series of stream reaches, with one reach for every model cell traversed by the segment. There are 1,178 stream reaches in the model. A map of the stream segments is shown in **Figure 3-14**. Stream segments 1 through 48 correspond to the 48 tributary watersheds around the perimeter of the Subbasin (clockwise from Calera Creek to San Francisquito Creek). Stream segments 49-58 are used to represent pipeline discharges to various creeks and diversions from creeks for MAR purposes. The remaining segments are located below confluences, and inflow to those segments equals the model-simulated outflow from the upstream segments.

There are stream flow gages at or near the model boundary on sixteen of the tributary streams. In some cases, MAR discharges occur upstream of the gage and are included in the gaged flow. Where MAR discharges are downstream of the gage, the discharge is added to the gaged flow to obtain total inflow at the model boundary. **Table 3-3** lists the sources of flow data for each of the tributary streams where they enter the groundwater model active flow area. Flow in ungaged streams was estimated by correlation with gaged streams. For streams entering from the Diablo Range, Thompson, Berryessa and Penitencia Creeks were used as the reference streams. Daily flows for each of those streams were divided by the drainage area and average annual rainfall of the tributary watershed to obtain a unit runoff value. Unit runoff was averaged for the three reference gages and then multiplied by the drainage area and average annual rainfall of each ungaged watershed to obtain estimated daily flows for those watersheds. Daily flows were subtotaled to monthly flows for input to the groundwater model. The same procedure was applied to streams entering from the Santa Cruz Mountains, with Ross, Smith and San Tomas Aquino Creeks serving as the reference gages.

The flow of water between a stream reach and the model cell in which it is located is proportional to the length and width of the wetted area, the difference in water level between the stream surface and the water table, and the vertical hydraulic conductivity of the stream bed. The lengths of stream channel in each reach were calculated by intersecting the stream network and model grid in GIS. The water-level difference is partly a function of stream flow, because higher flow increases flow depth in the channel. Plots of stream depth versus stream flow were prepared from historical data for 30 District stream gages and several U.S. Geological Survey gages. Differences between the curves were generally small relative to the uncertainty in stream bed elevation and in simulated groundwater levels. For purposes of the groundwater model, one depth-flow function was used for small channels and a second for large channels, which included the Guadalupe River and the downstream ends of other creeks where they widen into flood control channels near the Bay. A similar classification was done for width versus flow. The resulting functions are shown in **Figure 3-15**.

The vertical hydraulic conductivity of the stream bed can vary substantially along a stream segment. The average hydraulic conductivity can be estimated by measuring the amount of flow gain or loss along the segment. Stream flow is gaged at a number of locations within the Santa Clara Subbasin (**Figure 3-14**), and it was possible to calibrate stream bed hydraulic conductivity to match observed flow gains or losses between gages near the model boundary and gages farther downstream. Initially, all stream segments were assigned a conductivity of 1 ft/d except segments flowing through pipes, concrete-lined channels or representing pipeline discharges, which were assigned near-zero values (0.1, 0.3 and 0.2 ft/d, respectively). During model calibration, only hydraulic conductivity was varied; reach length and the width and depth functions were not changed. Stream bed hydraulic conductivity was adjusted up or down to match nearby layer 1 groundwater hydrographs and stream base flow hydrographs to the extent possible. The resulting calibrated estimates of stream bed hydraulic conductivity ranged from 0.1 to 8 ft/d (**Figure 3-14**). Stream flow hydrographs and additional discussion of the calibration process are presented in **Section 4.1.4** “Stream Flow Results”.

3.7.4 Subsurface Inflow across Inland Subbasin Boundaries

In additions to the stream flow described above, water can also flow from tributary watersheds into the Santa Clara Plain via the subsurface. The tributary watersheds are underlain by consolidated bedrock and accordingly treated as inactive in the groundwater flow model. However, small amounts of water can enter the Subbasin through bedrock fractures or the thin ribbons of alluvium beneath stream channels where they cross the Subbasin boundary. Groundwater recharge in tributary watersheds is likely to flow directly to the groundwater Subbasin only if it occurs close to the model boundary. Farther from the Subbasin, recharge is more likely to flow toward the tributary stream channel than directly to the Subbasin. The initial assumption—which was conservative from a water-supply standpoint—was that subsurface inflow from bedrock and through narrow ribbons of stream channel alluvium was zero.

One exception to this assumption was made for Coyote Narrows, where permeable alluvial deposits connect the upgradient Coyote Valley Region with the Santa Clara Plain within the Santa Clara Subbasin. This flow was included in the model as a general-head boundary, which means inflow is calculated by the Darcy Equation based on the current simulated groundwater level near that boundary. The assumed values of the other variables in the equation were a flow width of 2,000 feet (two model cells), a flow thickness of 150 feet, a horizontal hydraulic conductivity of 100 ft/d, and an external head 1,000 feet upgradient in the Coyote Valley of 230 feet above sea level. This boundary accounted for an average of 5,500 AFY of inflow to the Santa Clara Plain during 1985-2014.

A second exception was made along the Diablo Range mountain front. Simulated water levels along that margin of the Subbasin were generally too low when only in-basin recharge was present, and this held true over a range of horizontal hydraulic conductivity values. Results improved if a small amount of subsurface inflow was added to layer 3 cells along that boundary.

Those cells were converted to general-head boundary cells with widths of 1,000 feet, horizontal hydraulic conductivity of 2 ft/d, an external head at a distance of 1 mile from the model boundary increasing from 200 feet above sea level near Calera Creek to 300 feet above sea level near Evergreen Creek. The resulting subsurface boundary inflow averaged 2,500 AFY during 1985-2014.

3.7.5 Inflow from San Francisco Bay

Saltwater from San Francisco Bay historically intruded into the upper aquifer zone above the regional confining layer due to a landward gradient in water levels. From Palo Alto to Milpitas chloride concentrations exceeding 100 milligrams per liter (mg/L) were present in most areas within 1 mile of the shoreline. The greatest inland extent was along the Guadalupe River channel, where the 100 mg/L isochlor extended 3 miles inland in 1980. Small pockets of elevated chloride in the lower aquifer were attributed to leakage through wells across the confining layer. At that time groundwater elevations were rapidly recovering from the historical lows of the 1960s, and the extent of saltwater intrusion was thought to be static (Iwamura, 1980).

The floor of San Francisco Bay (model layer 1 cells throughout the offshore area) and the edge cells of model layers 2-6 are designated as general-head boundary cells in the model. The external head at all the cells was set to 1.3 ft NGVD29, which is equal to mean sea level at the south end of San Francisco Bay. For model layer 1, the external head was assumed to be at a distance of 20 ft and the vertical hydraulic conductivity was assumed to be 0.001 ft/d. For the edge cells of layers 2-5, a distance of 1,000 ft and a horizontal hydraulic conductivity of 0.0001 ft/d were assumed. The low K_H was selected during calibration to help elevate water levels and increase upward gradients near the southern margin of San Francisco Bay. The same external head was assigned to all model layers because the offshore boundary is located far from pumping and sources of recharge.

Because groundwater levels beneath the Bay were above sea level throughout the calibration period, there was no simulated inflow from the Bay into the aquifer system. All flow was outflow to the Bay. Density effects stemming from the salinity of sea water or brines beneath salt evaporation ponds were not included in the model.

3.8 Outflows

Groundwater pumping is by far the largest outflow from the Santa Clara Subbasin. However, smaller outflows include seepage into streams, evapotranspiration by riparian vegetation, and outflow to San Francisco Bay. Each of these outflows is described below.

3.8.1 Groundwater Pumping

All groundwater users in the Santa Clara Subbasin report their production amounts to the District, and those records cover the entire 1985-2014 calibration period. The reporting interval ranges from 1 month to 1 year depending on well type, with large wells reporting more frequently. The database for 1985-2014 contained 148,002 records of production at 4,196 water supply wells and 272 “totalizer” wells. Totalizers are meters at groundwater remediation sites that measure the combined production of multiple wells at the site. The District provided well numbers for each of the wells contributing to each totalizer. A Fortran utility program was used to distribute totalizer volumes among the contributing wells and to parse well and totalizer data from long sampling intervals into monthly values. The parsing procedure used the average monthly distribution of production at wells with monthly data to pro-rate the data from long-interval wells. Separate monthly patterns were developed for each of the four well categories used by the District: agricultural, municipal/industrial, domestic and other.

A few wells were added that were not included in the database. When the active area of the groundwater model was expanded to include East Palo Alto, Menlo Park and Atherton, recent annual production at five wells in Menlo Park were obtained from an East Palo Alto study (Todd Engineers and others, 2012) and applied to all years during the calibration period. Estimated total production by numerous private wells in Atherton (Metzger and Fio, 1997) was divided among seven hypothetical pumping locations and also assumed to have remained constant throughout the calibration period.

The vertical distribution of pumping among model layers at each well was based on the percent of well screen overlapping each model layer and the transmissivities of the model layers at the well locations. Construction information was available for about half the wells in the production database. For the remaining wells, hypothetical screened intervals were based on the average screen length, top elevation and bottom elevation for wells in that well category at that location in the Subbasin. The average values were obtained by gridding and contouring the three variables for wells in each category, using data from wells for which construction information was available. The vertical distribution of pumping was periodically updated during the calibration as horizontal hydraulic conductivity values in the model were adjusted.

Annual groundwater production by user category during 1985-2014 is shown in **Figure 3-16**. Total groundwater production averaged about 170,000 AFY during 1985-1989, then dropped abruptly to around 110,000 AFY when a large new increment of imported water came on-line. Total production partly reflects the availability of local and imported surface water supplies. Those supplies decrease during droughts, and the shortfall is made up with increased groundwater pumping. For example, the relatively high amounts of pumping in 2007-2009 and 2013-2014 can be attributed to statewide drought conditions.

Municipal well pumping accounted for 98 percent of total production since 1985. Agricultural production decreased from about 4 percent to less than 1 percent of total production during that period, and domestic pumping has been consistently less than 0.4 percent.

Groundwater production is distributed throughout the Subbasin but is relatively concentrated along a swath extending from Los Altos to downtown San Jose and in the Santa Teresa area. **Figure 3-17** shows average annual pumping at individual wells during 1989-2014, which is more representative of current conditions than the 1985-1988 period. The areas of the circular symbols are proportional to the amount of pumping.

3.8.2 Seepage into Streams

Groundwater seeps into streams when the layer 1 water level at a stream cell is higher than the water level in the stream. This occurs predominantly along stream reaches in the confined area as the streams approach San Francisco Bay. Seepage into streams is calculated by the groundwater model during each simulation because it is a function of groundwater level and stream flow, both of which change over time. The equations used to calculate the flux are the same as for percolation from streams, as described above in **Section 3.7.3** “Percolation from Streams”. Contours of simulated layer 1 groundwater levels showing convergent flow toward stream channels are discussed in **Section 4.1.3.2** “Contours”.

3.8.3 Evapotranspiration by Riparian Vegetation

Evapotranspiration (ET) of groundwater by phreatophytic riparian vegetation is simulated differently in the IMOD model than in either GMOD or XMOD. GMOD applied a constant loss of 50 in/yr of water over a 100-foot-wide vegetation corridor along selected stream reaches outside the confined area. The annual amount was combined into the distributed recharge term and was not stated in the report. XMOD used the same base rate of 50 in/yr and vegetation corridor width, but extended it to include stream reaches in the confined area. Also, ET was dynamically simulated within the model as a function of water table depth. The base rate was assumed to decrease linearly to zero at a water table depth of 5 ft. This resulted in a highly variable ET rate along the stream channels.

The IMOD model refines the calculations of the base ET rate but does not relate ET to water table depth within the model. ET varies seasonally due to variations in reference ET and in leaf area. Annual reference ET in San Jose (CIMIS Zone 8) is 50 in/yr, consistent with the rate assumed in the previous models. However, it varies from 0.93 inch in December to 7.44 inches in July (Jones, 1999). Also, some common phreatophytes such as sycamores and cottonwoods are partially or completely deciduous in winter, which changes their “crop coefficient”. Monthly crop coefficients were estimated to range from 0.40 in winter to 1.20 in summer, with the high summer values reflecting the large height of the vegetation and the distribution of riparian vegetation as narrow strips surrounded by a relatively hot and dry urban environment (Allen and others, 2006). Phreatophytes also preferentially use soil moisture derived from infiltrated rainfall when it is available because of its higher head. These factors result in a variable time series of riparian ET. The one-dimensional ET rate was estimated using the recharge model by simulating riparian vegetation as irrigated and allowing the model to estimate the amounts and timing of simulated irrigation depending on current soil moisture status. The simulated amount of irrigation was assumed to equal the amount of water the trees would draw from groundwater. The average annual simulated groundwater ET rate was 42 in/yr and ranged from 38 to 47 in/yr.

Riparian vegetation along stream channels ranges from sparse and narrow to dense and wide. Based on high-resolution aerial photography taken in 2012, stream channel segments with relatively dense riparian vegetation 80 or more feet in width were tabulated. The presence of dense vegetation indicates that it has perennial access to water, either directly from the water table or by intercepting stream percolation that would otherwise reach the water table. A total of 1,560 acres of riparian phreatophytic vegetation distributed over 421 stream cells was inventoried. These areas were assumed to remain constant throughout the 30-year calibration period, and volumetric rate of groundwater consumption was included in the model as a “well” in layer 1 at each stream reach cell with riparian vegetation. The annual volume of groundwater consumed by riparian ET averaged 5,480 AFY over the calibration period, with a range of 4,890-

6,100 AFY. The monthly riparian ET volumes were entered as fixed inputs to the model and did not vary as a function of water-table depth during the simulation. This was considered reasonable because shallow-zone water levels remain much more stable than water levels in deep aquifers tapped for water supply. Also, shallow groundwater adjacent to many streams is sustained by percolation from the creek and is thus somewhat buffered from the effects of pumping and groundwater fluctuations farther from the creek. Finally, annual variations in riparian ET would amount to a very small percentage of the overall Subbasin-wide water balance. Thus, the small potential increase in model accuracy would not justify adding another nonlinear component to the model, which would retard and potentially destabilize numerical convergence.

Net evaporation from MAR percolation ponds was included in the model in the same way as riparian ET. The surface area of each MAR pond was tabulated and assigned to one or model cells at the pond location. MAR percolation at each facility was divided uniformly among the model cells corresponding to the locations of the ponds at that facility. Percolation volumes reported by the District were adjusted by net evaporation, which is the monthly difference between evaporation and rainfall multiplied by the pond area. The open-water evaporation rate was assumed to equal the reference ET rate, because the pan-to-lake coefficient that converts point evaporation to large area evaporation approximately cancels out the difference between open-water evaporation and reference ET at a point. There are 171 acres of MAR ponds in the Subbasin (excluding Coyote and Ford Ponds, which were simulated as stream reaches). On an average annual basis, net evaporation was 36 inches, or 513 AFY for all MAR ponds collectively. After adjusting for net evaporation, MAR percolation was entered into the groundwater model as a set of layer 1 injection wells, with one well for each model cell at a pond location.

3.8.4 Outflow to San Francisco Bay

Outflow through the general-head boundary cells representing San Francisco Bay depends on groundwater levels and accordingly is calculated by the IMOD model during each simulation. The general-head boundary cell parameters were described in **Section 3.7.5** “Inflow from San Francisco Bay”. Simulated outflow averaged 2,250 AFY and ranged from 1,160 AFY in 1990 to 3,220 AFY in 2006.

The active flow domain of the groundwater flow model includes part of the Niles Cone area near Newark, on the East Bay Plain. However, recharge and pumping in that region are not included in the model, consistent with the GMOD and XMOD models. Water levels in the Centerville-Fremont and deep aquifers were as much as 16-20 feet below sea level in the pumping trough centered beneath Newark (Alameda County Water District, 2015). It is possible that some of the simulated outflow to San Francisco Bay in the groundwater model actually flows to the Newark pumping trough instead. The Niles Cone area is sufficiently far from prospective IPR sites that improving that region of the IMOD model was considered to be beyond the scope of the current effort. It would be a worthwhile future improvement.

3.9 Water Balance Summary and Change in Storage

The inflows and outflows described in the preceding sections collectively comprise the water balance of the Santa Clara Subbasin. Any imbalance between inflows and outflows in a given year results in a change in groundwater storage. The annual water balances and storage changes for 1985-2014 are listed in **Table 3.4** and displayed as a stacked-bar chart in **Figure 3-18**. Inflows are shown as positive values above the X axis, and outflows are negative values below the axis. Net annual storage changes are indicated by the line. Stream percolation and dispersed recharge provide the largest amounts of Subbasin inflow, and they are both noticeably larger in wet years than in normal and dry years. Percolation from MAR ponds is the third-largest source of inflow and is relatively steady from year to year. Groundwater pumping is by far the largest outflow, although groundwater seepage into streams gradually increased during the calibration period as groundwater levels in the Subbasin recovered. In recent years, seepage into streams has been 25-30 percent of total outflow.

The annual net change in storage ranged from a decrease of 86,000 AF in 2014 to an increase of 104,000 AF in 1995. Over the entire 1985-2014 period there was an average annual storage increase of 11,000 AFY.

The average annual water balance for the IMOD model is compared with the average annual water balances for the GMOD and XMOD models in **Figure 3-19**. Differences among the balances reflect differences in the geographic area covered by each model, how inflows and outflows were grouped, different methods for estimating the flows, and differences in hydrologic conditions during the periods simulated by the models. To facilitate a comparison among models, the southern San Mateo County part of the IMOD model was excluded from the budget tabulations, but the flow domain still differs from GMOD by including the Santa Clara Formation and the Evergreen area. The District has continued to update the GMOD model since it was first developed in 1992, and the water balance in the figure is the average for the current 1970-2014 simulation period. Many inflows that are simulated separately in the IMOD model are grouped into an overall recharge term in GMOD. The magnitude of subsurface inflow at Coyote Narrows (the CHD inflow in GMOD) is considerably larger than the estimate in the IMOD model (the GHB inflow includes 7,100 AFY at Coyote Narrows and 2,500 along the Diablo Range mountain front). The other inflows are difficult to compare due to lumping in GMOD. The XMOD model does not include subsurface inflow but does include water yielded by compaction of clays during subsidence. The values for stream recharge and MAR recharge cannot be compared individually because the IMOD model classifies MAR percolation in stream channels as stream recharge. However, the total of the two inflows differs by only 13 percent between the models. Similarly, dispersed recharge differs by only 8 percent despite the very different methods and assumptions used to obtain the estimates.

Average annual groundwater pumping is much larger in GMOD and XMOD than in the IMOD model, mostly because those models included more years of high pumping rates before 1989. GMOD has only a single other outflow (discharge to San Francisco Bay), whereas XMOD and the IMOD model also simulate groundwater seepage into streams. Outflow to the Bay in GMOD is smaller than the combined stream and Bay outflows in the IMOD model, and much of that difference might be attributable to the different simulation periods. Groundwater levels were on average much higher during the 1985-2014 period simulated by the IMOD model, and the higher levels resulted in increased groundwater seepage into streams. The combined stream and Bay outflows in XMOD are smaller than in GMOD, partly due to the older simulation period when outflows were in fact smaller. The relative proportions of Bay and stream outflows in XMOD are different than in the IMOD model, probably due to different parameters used to simulate those outflows. Outflow to the Bay was reduced during calibration of the IMOD model to elevate on-shore groundwater levels near San Francisco Bay and thereby replicate the large observed upward water-level gradients. Most of the data used to characterize vertical gradients was collected after XMOD was developed.

4 Numerical Model Calibration

Model calibration is the process of adjusting model input data and parameters so that model output matches observed groundwater elevations and stream flow for a specified historical simulation period. Modifying the initial estimates of model inputs is justifiable because many inputs are imprecisely known or are valid only for selected locations and times. Although historical data for pumping, stream flow and water levels are much more abundant for the Santa Clara Plain than for most groundwater basins in California, some variables remain that can only be estimated indirectly.

The historical calibration period selected for the model is January 1985-December 2014. The model uses monthly time increments (stress periods), which results in a total of 360 stress periods in the calibration simulations.

4.1.1 Objectives

The calibration objective for the general model was to reasonably match measured historical water levels and stream base flow at gages within the Subbasin. This subjective criterion was deemed to be met when residuals exhibited no further spatial or temporal trends among groups of wells that could be attributed to a hydrologic process and corrected by changing the parameters or data associated with that process. That is, the remaining residuals were random, or were not diminished by adjustments to inputs, or those adjustments increased some residuals while diminishing others.

For individual well hydrographs, the calibration objective was to obtain a simulated hydrograph that matched the dominant trend of the measured water levels, which is the pattern represented by most of the data points. This includes the timing and magnitude of long-term (multi-year) water-level trends and the magnitude of seasonal water-level fluctuations. This objective emphasizes the central tendency of the data rather than minimization of outlier residuals.

Model calibrations generally are not unique. Often, two or more variables can trade off against each other to produce nearly identical simulated water levels. For example, increasing the estimate of a flow—such as pumping at a well or inflow from recharge—can often be balanced by an increase in hydraulic conductivity to obtain similar results. The calibration objective was to obtain one good calibration using realistic values of all data and parameters, but not to explore possible alternative calibrations. In practice, some exploration inevitably occurred during model calibration. For example, in an attempt to correct an excessive long-term rising trend in some simulated hydrographs, selected parameters in the recharge model were adjusted within their ranges of uncertainty to decrease average annual recharge by 15,000 AFY (about 25 percent). This noticeably lowered simulated water levels throughout the Subbasin, but subsequent adjustments to hydraulic conductivity and other model parameters were able to re-tune the simulated hydrographs to match measured hydrographs as well as or better than they had before.

4.1.2 Method

The model was calibrated manually by trial-and-error primarily based on visual comparison of simulated and measured water-level hydrographs. Simulated hydrographs are produced by transient model simulations. Steady-state simulations can be used to isolate the effects of hydraulic conductivity from the effects of storativity and are sometimes used as an initial step in model calibration. Steady-state calibration was not done in this case because groundwater levels exhibited strong trends throughout most of the calibration period in response to long-term changes in pumping as well as wet and dry climatic periods. Also, inspection of hydrographs from transient simulations reveals spatial and temporal patterns in residuals, and those patterns often indicate which hydrologic process or model variable caused the residual. That is, the different effects of storativity and hydraulic conductivity can be identified from transient simulations without a need for steady-state simulations. Adjustments could then be made in variables logically linked to the residuals. Also, it is easy to discern the central tendency of simulated and measured water levels at each well, and disregard outlying points that are not representative of ambient groundwater conditions. Hydrographs of simulated stream base flow were also compared with measured data at gage locations within the Subbasin. Automated methods that seek to minimize an objective function such as the sum of squared residuals were not used.

The principle of parsimony was applied, which is a general concept in modeling that between two models that perform equally well, the one with the smaller number of parameters is preferable (Forster, 2001). More complex models can generally fit measured data more precisely, but beyond a point the model might simply be replicating “noise” in the data. In other words, by specifying unique parameter values at individual wells, the model might be able to match historical water levels almost perfectly. However, by acknowledging such local variability, parameter values between well locations are more uncertain and model performance in those areas is also more uncertain. In the present context, parsimony was implemented by assuming that hydraulic conductivity and storativity were homogeneous within broad zones, and those zones were only subdivided or re-shaped if the changed corrected a residuals pattern shared by multiple wells in that region. The model is intended to provide the best estimate of aquifer characteristics for any location within the Subbasin.

The variables most frequently adjusted during model calibration were horizontal and vertical hydraulic conductivity and the zonal patterns representing those variables. Other internal variables adjusted during calibration included streambed hydraulic conductivity, streambed elevation, and the locations and conductances of general-head boundaries where groundwater flows into or out of the Subbasin. Simulation results were not very sensitive to storativity, so few adjustments were made and final values were relatively homogeneous.

The recharge model was jointly calibrated with the groundwater flow model. Variables adjusted during calibration included water and sewer pipe leak rates, irrigated percentage of recharge zone area, average root depth of non-irrigated vegetation in urban zones, the threshold and slope of the rainfall-runoff relationship for pervious soils, and the fraction of impervious runoff that percolates past the root zone. These adjustments were made uniformly to all zones of the same land use type.

All other input data remained at their initial estimates. Notably, this includes groundwater pumping, stream flow entering the Subbasin, percolation from MAR ponds, and evapotranspiration by riparian vegetation.

4.1.3 Water Level Results

4.1.3.1 Hydrographs

Hydrographs of simulated and measured water levels for all 73 calibration wells are presented in **Figures 4-1** to **4-8**. In each hydrograph, measured water levels are shown as connected black dots, and simulated water levels in all active model layers are displayed as colored curves. The colors are consistently matched to model layers in all hydrographs, and the Y axis span is also a constant 200 feet in all hydrographs. The plot title indicates the model layer that contains the largest percentage of well screen length. The simulated water levels for the corresponding model layer are shown with a heavier line weight than for the other model layers, to facilitate a comparison between simulated and measured water levels. Finally, the hydrographs are grouped by region for the purposes of discussion. A location map is included on each hydrograph plot to assist the reader in following the discussion of regional patterns. The following paragraphs discuss water-level patterns by region within the Subbasin. Lessons learned during calibration are described, as well as stubborn residuals patterns that calibration adjustments were unable to eliminate.

4.1.3.1.1 Northeast Subbasin Margin

Four calibration wells are located along the northeast Subbasin margin, near the Diablo Range foothills. **Figure 4-1** shows hydrographs for the two calibration wells near the northern half of that boundary. Their water levels reflect a regional gradient from the edge toward the center of the Subbasin. The east side wells responded differently to decreases in horizontal hydraulic conductivity, so that a single uniform K_H value along the mountain front did not obtain a good calibration for all the wells. After some experimentation, simulation results were slightly improved when a moderately low K_H value (10 ft/d) was combined with a small amount of mountain-front recharge. That recharge was implemented by a row of general-head-boundary cells in model layer 3 along the northeast edge of the active flow area.

4.1.3.1.2 Southeast Subbasin Margin

Observed and simulated groundwater level hydrographs for two wells along the southern part of the eastern Subbasin boundary are shown in **Figure 4-2**. Well 07S01E02J006 is the only east side well that shows significant influence of local pumping. Well 07S02E19B009 is located at the mouth of the Evergreen area, which is a triangular region of relatively thin alluvium extending from the southeast corner of the Subbasin into the foothills. Its water levels are typically 120 feet higher than at a well located 10,000 feet closer to the center of the Subbasin (well 07S01E26B011 in the southeast-central part of the Subbasin). The XMOD model achieved some of this water-level difference by including the Silver Creek Fault as a partial barrier to groundwater flow. Calibration of the IMOD model demonstrated that the water-level difference can also be achieved by means of a low but reasonable K_H value (6 ft/d) throughout the Evergreen area and extending a short distance out into the main Subbasin area.

4.1.3.1.3 Northwest Subbasin Margin

A variety of residuals patterns were present along the northwest margin of the Subbasin, adjacent to the Santa Cruz Mountains (**Figures 4-3a** and **4-3b)**. These are described from north to south. Wells 06S03W12R010 and 06S03W13A010 near Adobe, Barron and Matadero Creeks had similar measured hydrographs and similar residuals patterns. The model matched the first half of the hydrograph well, but simulated water levels were consistently about 15 feet too high during the second half. This pattern led to the inclusion of the Santa Clara Formation in the active flow domain of the model. Numerous domestic wells pump from that formation in this area, and it was hypothesized that the absence of that pumping might explain the excessively high simulated water levels. Including the Santa Clara Formation and associated pumping in the model did in fact lower simulated water levels at these wells by a few feet but did not completely eliminate the entire residual pattern.

Wells 06S02W28N001 and 06S02W33A002 near Stevens, Permanente and Hale Creeks exhibited an opposite residuals pattern: simulated water levels were consistently lower than measured water levels by 5-10 feet. Initially, the residuals were larger, but increasing the hydraulic conductivity of the creek beds near the Subbasin boundary increased the simulated amount of stream recharge and raised the simulated hydrographs by several feet. The simulated hydrographs now show upward spikes associated with slugs of recharge that occur during storm-generated periods of high stream flow.

4.1.3.1.4 Southwest Subbasin Margin

Hydrographs for wells located along the southwest Subbasin margin are shown in **Figures 4-4a** through **4-4i**. The model generally matched measured hydrographs reasonably well between Stevens Creek and San Tomas Aquino Creek (calibration wells 07S02W13C001 to07S01W33M002). Results at the Saratoga multi-completion well (07S01W29C003 through 07S01W29C006) revealed some calibration limitations, however. The model matched layer 1 water levels well but could match only one of the two measured hydrographs corresponding to model layer 4, which differed by 60-70 feet in elevation.

Simulated water levels were consistently too high at monitoring wells 07S01W34F002 and 07S01W35L013 through 07S01W35L018 (McGlincy multi-completion well), near San Tomas Aquino and Los Gatos Creeks. Percolation at the nearby recharge ponds did not appear to be the cause of the discrepancy. When percolation at the McGlincy pond was eliminated from the model, simulated water levels at the McGlincy multi-completion well were lower by only 5 feet in layer 1, decreasing to 1 foot in layer 4. Experiments with the “New Cascade Fault” that was included in the XMOD model immediately upgradient of these wells also did not significantly lower simulated water levels. The cause of the water-level discrepancy is not known, although a comparison of the hydrographs for individual well screens at the McGlincy site suggests that there may be a nearby unregistered pumping well not included in the pumping database that might be lowering the measured water levels. At that location, the lowest water levels are at one of the intermediate-depth screens (in layer 4), and the hydrograph for that screen also exhibits the largest seasonal fluctuations.

Farther up Los Gatos Creek, wells 08S01W03K013 and 08S01W10F002 exhibited opposite residuals, and no calibration adjustment enabled the model to match both hydrographs simultaneously. Simulated water levels were always too low at 3K13 and too high at 10F2. Well 3K13 is next to the Oka MAR ponds, and its hydrograph is relatively stable. This suggests that pond percolation might be elevating the water levels at that well, but its screen is fairly deep (model layer 4). In any event, the final calibration splits the difference and produces water levels that match the two wells equally poorly.

Farther south along the southwest Subbasin margin, pumping stresses are smaller and the measured hydrographs were generally easier to fit. The model matches wells 08S01E05N002 and 08S01E08R001 near Ross and Guadalupe Creeks relatively well. Farther up Alamitos Creek at well 08S01E27C002 simulated water levels turned out to be controlled primarily by the estimated creek bed elevation, and an excellent match was achieved.

4.1.3.1.5 Santa Teresa Area

There are only four calibration wells in the Santa Teresa area, and their hydrograph trends and residuals patterns were similar (**Figures 4-5a** and **4-5b**). Simulated water levels declined too steeply during the first three years of the simulation, then recovered slightly faster than measured water levels during 1989-1998. The measured and simulated hydrographs converged at that point and simulated water levels remained close to (slightly higher) than measured water levels thereafter. This pattern was most pronounced in the hydrographs for well08S01E10J002, but also evident at wells 08S02E06R008, 08S02E07A003 and 08S02E18L001. The recovery rate during 1989-1998 at the latter three wells proved to be affected by the streambed hydraulic conductivity in Coyote Creek and the conductance of the general-head boundary at Coyote Narrows, with higher values accelerating the rate of recovery. This improved the hydrograph match during the first half of the simulation period, but tended to overestimate water levels during the second half. Also, high stream bed K values resulted in excessive percolation losses from Coyote Creek. The final calibration splits the difference and includes moderate K and conductance values with moderate-to-large residuals during the first half of the simulation. Regional adjustments to aquifer K in that area had opposite effects on wells 6R8 and 7A3 compared to 18L1. There is little pumping at the former wells, and lower K values steepened the regional gradient within the Santa Teresa area and raised simulated water levels at those wells. In contrast, there was significant pumping at or near 18L1, and lower K values consequently resulted in lower simulated water levels. A final possible cause of the sagging simulated water levels during the first half of the calibration period is incorrect specification of initial water levels. A few small adjustments of initial water levels were tested, but they did not dramatically improve results.

4.1.3.1.6 Southeast-Central Area

The southeast-central area refers to the region between Edenvale Gap and Oak Hill at the downgradient edge of the Santa Teresa area and the low- K_H zone in the central part of the Subbasin. Hydrographs for this area are presented in **Figures 4-6a** through **4-6j**). Water levels consistently slope toward the center of the Subbasin, but residuals are highly variable among the wells in this area. Tests of alternative aquifer K_H values commonly had surprisingly little impact on simulated water levels or affected half the hydrographs favorably and half unfavorably. This result probably reflects the different response in water levels at non-pumping wells versus pumping wells. At non-pumping wells, water levels are controlled by the regional gradient, and lower K_H values tend to raise water levels, especially toward the upgradient end of this area. At pumping wells (and nearby non-pumping wells), lower K_H values tend to increase simulated drawdown and generally lower the simulated hydrograph.

At the upgradient end of this area, simulated water levels at well 07S01E33M003 on the west side of Oak Hill are generally too low during the first part of the calibration period, with a residuals pattern similar to the Santa Teresa area wells. In contrast, simulated water levels were always too high at well 07S01E24P010 in Edenvale Gap on the east side of Oak Hill. Simulated water levels were also too high at nearby well07S01E26B001. Many tests of alternative aquifer K values failed to lower simulated water levels at these wells to the observed levels.

Farther to the northwest, the model simulated water levels at wells 07S01E19B002 and 07S01E24H004 matched observed water levels very well. However, results were variable at the Willow multi-completion well (07S01E19B002 through 19B007). For example, the model closely matched measured water levels at one layer 5 screen (19B6) but were 20-60 feet higher than measured water levels at the two other layer 5 screens (19B3 and 19B4). The match was also reasonably good for layer 1, but simulated water levels were too high for layer 3. At the CCOC multi-completion well (07S01E09L004 through 09L007) simulated water levels were substantially too high at three of the four well screens; only layer 1 matched reasonably well. Simulated water levels at nearby well 07S01E16C006 were also too high.

The pattern of generally high simulated water levels at the above wells does not appear to reflect a regional bias, however. At well 07S01E07R013 simulated water levels are chronically too low, and at well 07S01E06L001 they are nearly perfect. Based on the experience calibrating K_H in the low- K_H zone, the most likely causes of high simulated water levels are under-reported pumping or locally-low K_H.

4.1.3.1.7 Central Low- K_H Zone

The central low- K_H zone was delineated based on distinct patterns in measured water levels. Hydrographs for wells in this area are presented in **Figures 4-7a** through **4-7i**). At all wells in this zone the amplitude of seasonal water-level fluctuations is much larger than elsewhere in the Subbasin. Calibration tests showed that this pattern was clearly linked to low horizontal K. Vertical K values contributed somewhat to the spread in water levels between model layers, but results were relatively insensitive to storativity values. There are 18 calibration wells in this zone, and the model performs consistently well at all those locations. Pumping stresses are moderate in the northeastern part of this zone near wells 06S01W26D002 and the Guadalupe multi-completion well (06S01W26R001 through 26R004). The model reproduces the measured water levels and the small vertical gradient quite well.

Pumping stresses are larger to the southwest, in the City of Santa Clara, and seasonal water level fluctuations of 60 feet are common. The model does a reasonably good job of matching observed water levels at all the wells using only a single K_H value (6 ft/d) throughout the zone.

The boundary between the low- K_H zone and adjoining areas of higher K_H is abrupt in some places and associated with distinctly different hydrograph patterns. At the west edge, for example, well 07S01W06P001 is within the low- K_H zone but well 07S02W01B001 located 5,000 feet away is clearly outside the zone (and included in the southwest Subbasin margin group). At the east edge, well 07S01W22E002 is inside the low- K_H zone, while well 07S01W24H004 located 14,000 feet to the east is not. Well 07S01W20C001 appeared to be transitional between the low- K_H zone and the southwest Subbasin margin area.

4.1.3.1.8 San Francisco Bay Margin

Hydrographs of wells near the San Francisco Bay margin are shown in **Figures 4-8a** through **4-8c**). The model successfully produced simulated groundwater levels in layers 3-6 that were tens of feet above the San Francisco Bay general-head boundary and water levels in the pumping trough centered on the low- K_H zone. Results were variable on a well-by-well basis. They are described here from west to east along the Bay margin.

Well 05S03W35G010 is located next to San Francisquito Creek. Simulated water levels at this well remained stubbornly high despite numerous calibration adjustments. Measured water levels at this location are below the ground surface and only slightly above sea level, whereas water levels are typically tens of feet above both benchmarks at the other Bay margin wells. Expanding the model to include pumping from wells in East Palo Alto, Menlo Park and Atherton lowered the simulated water levels by a few feet but a large residual remains. Adjustments to creek parameters had little effect, which is not surprising given that the well is screened in layer 5.

At wells 06S02W21A001 and 24C008 simulated water levels are lower than measured, but still 50-60 feet above sea level. The discontinuity in the observed hydrograph for 24C8 appears unrealistic and might indicate a data error. Farther east, wells 06S01W17F002 and 06S01W17F002 have short periods of record. Once again, simulated water levels are somewhat below measured water levels, but still 35-45 feet above sea level.

4.1.3.2 Contours

Contours of simulated groundwater elevations in model layers 1-6 in March 2012 are shown in **Figures 4-9** through **4-14**). Contours are simply another way of presenting residual differences between simulated and measured water levels. Measured water levels are shown as points, and each map includes only data for wells screened primarily in that layer. At the regional scale, the contours of simulated water levels are generally consistent with measured water levels. In some cases, there are substantial differences, but differences within clusters of measured water levels are also often large. This reflects a degree of local spatial variability not captured in the model.

Differences between simulated and measured contours are not necessarily model errors, because there may be errors associated with the measured data. For example, measured water levels can be affected by residual drawdown in a well that was pumped a short time before the measurement was made. In contrast, model calibration strove to achieve water levels that represented the region surrounding a well—including nearby wells—not just each individual well location. Also, measured water levels in wells with long screens represent an average water level for that depth interval. Although each well is displayed only on the map for the layer in which it has the most screen length, the screen might overlap other model layers. Finally, the simulated contours are different for model layers 3-6, whereas the measured water levels represent an average of those layers. The fact that simulated contours for model layers 3-

6 are noticeably different from each other underscores the presence of spatial variability in the vertical dimension, which can also contribute to differences between measured and simulated contours.

4.1.3.3 Flooded Cells

Toward the end of the calibration period, simulated groundwater levels in model layer 1 were above the ground surface in the confined area near San Francisco Bay. The extent of the area with "flooded" cells in March 2012—which for many simulated and measured hydrographs had the highest groundwater levels of the entire calibration period—is shown on the upper plot in **Figure 4-15**. For comparison, the lower plot shows a map of the extent of shallow groundwater conditions in 2003 (URS Corporation, 2009). The criterion for the shallowest depth category in the 2003 map is a water table depth of less than 10 feet, which is lower in elevation than the criterion for flooded cells (a depth of 0 feet or less). The larger extent of the shallow groundwater zone in the 2003 map is partly attributable to the difference in mapping criteria. Nevertheless, both maps show shallow groundwater occurring along the entire Bay margin and inland as far as downtown San Jose. The 2003 study also documented 28 dewatering sites within the confined part of the Subbasin and 20 sites where water tables near the land surface created nuisance conditions. This confirms that the water table is close to the land surface in that region.

There are mechanisms not included in the model by which shallow groundwater may flow to nearby streams. These include basement and french drain sump pumps at individual buildings that discharge to street gutters or storm drains, groundwater extraction at dewatering sites and groundwater remediation sites not included in the District's groundwater production database, and possibly secondary porosity in near-surface soils associated with root tubes, bioturbation and desiccation cracks.

Overall, the simulation of flooded cells in the model appears reasonably consistent with available data and hydrologic processes.

4.1.4 Stream Flow Results

Hydrographs of simulated monthly stream flow superimposed on measured monthly stream flow at 16 gage locations in the interior of the Subbasin are shown in **Figure 4-16**, arranged in clockwise order around the Subbasin. High stream flows tend to pass through from the mountains to the Bay, and the effects of seepage to or from groundwater is typically too small to be noticeable. Calibration focused on achieving a pattern of low, sustained base flows at each gage similar to the measured pattern. At some gage locations, measured flows consisted of storm peaks with little or no sustained base flow. These included the gages on Thompson, Ross, San Tomas Aquino, Saratoga and Stevens Creeks. Simulated flows also showed no evidence of base flow sustained by groundwater seepage.

At other gages, not close to San Francisco Bay, the model replicated the magnitude of base flow reasonably well. These included the gages on Thompson Creek, Alamitos Creek, Canoas Creek, and the two upper gages on Coyote Creek (gages SF89 and SF58) and Guadalupe River (gages SF23.2 and 11169000). One exception was at Los Gatos Creek gage, where simulated base flow was consistently too low after 1997. Several attempts to correct this error during calibration failed.

Simulated base flows were too small at the two gages located far downstream in the confined area: Coyote Creek above Highway 237 and Guadalupe River above Highway 101. The high observed flows could result from accelerated discharge of shallow groundwater into local streams by mechanisms not included in the model, such as discharges from sump pumps, dewatering facilities, groundwater remediation sites and relatively permeable flow paths through soil zones. The errors are thus consistent with the occurrence of simulated layer 1 water levels above the ground surface in the coastal part of the Subbasin.

4.1.5 Residuals Statistics

The differences between each measured water level and the corresponding simulated water level is the residual. Residuals can be summarized statistically to obtain an objective measure of model performance. The model calibration guidelines presented in ASTM D-5490-93 recommends that these statistical summaries be calculated. Residuals statistics are not a completely objective measure of model performance because the process of selecting and evaluating measured data is subjective, as follows:

- Often, some wells are excluded from the calibration data set because they are geographically clustered, have too few data points to be useful, or have erratic or apparently abnormal water levels. In this case, 73 wells were selected from a County-wide data base of 900 wells. The subjective selection process attempted to achieve a relatively even geographic distribution and retain wells with long periods of record and regular patterns of seasonal and long-term water levels.
- Some water-level measurements at a given well are omitted or assigned a low weight based on a subjective conclusion that they are not representative of ambient groundwater conditions (such as a measurement made while the well pump was operating). A few highly unusual measurements were omitted from the calibration set in this case, but most were retained even if they seemed “noisy”. High-frequency measurements from data loggers were also thinned to approximately one measurement every 3 weeks to be more consistent with manually measured wells.
- Deciding whether model performance is “good enough” based on residuals statistics is subjective. A common rule of thumb is that model performance can be considered acceptable if the root-mean-squared residual is less than 10 percent of the total range of measured water levels (Environmental Simulations, Inc., 2011). In the present case, no statistical performance criterion was applied to determine when to stop the calibration process.

Groundwater Vistas interpolates simulated water levels in space and time—that is, between cell centers and between stress periods—to more precisely match simulated water levels with measured water levels. A scatterplot of the 12,114 pairs of measured and simulated water levels is shown in **Figure 4-17**, and the summary statistics are displayed on the graph.

The mean residual is --17.14 ft, which indicates that on average simulated water levels are higher than measured water levels. Looking at the scatterplot, this error is most pronounced for low water levels (where the cloud of points is centered slightly above the 1:1 line). Those measured water levels are mostly summer water levels in the confined area. This residual pattern is not surprising because most of the measured wells are also production wells. The model simulates the average water level over the cell area, whereas the water level at the well location is likely to be the lowest level within the cell area.

The standard deviation of the residuals provides a quantitative measure of goodness-of-fit between simulated and measured water levels per industry standard ASTM D-5490-93 (American Society for Testing and Materials, 2014). For the IMOD model all measured values were assigned the same weight, so no adjustments related to weighting were necessary. The standard deviation of the residuals was 25.49 ft. To compare model accuracy with models in general, the standard deviation is commonly divided by the overall range in measured water levels to obtain a dimensionless metric known as the normalized standard deviation. In this case, the range of water levels was 384.4 ft, and the normalized standard deviation was 6.6 percent.

The residuals scatterplot exhibits several "tails" where groups of points extend horizontally out from the 1:1 line. These groups of points are usually associated with one or two wells that have high residuals. **Table 4-1** lists the wells responsible for almost all of the 100 largest residuals in each model layer. Inspection of the hydrographs for these wells (**Figures 4-1** through **4-8**) provides a clearer picture of how their simulated water levels deviate systematically from measured water levels.

4.1.6 Discussion of Calibrated Parameters

The calibrated values of parameters in the recharge model and groundwater flow model are all within typical ranges for those variables. A few of them warrant additional corroboration and explanation, however. For example, the K_H value of 6 ft/d in the central low- K_H zone is only one-fifth as large as the value for that region in the GMOD model and might seem inconsistent with pumping rates in excess of 1,000 gallons per minute achieved by some municipal wells in that area. However, three lines of follow-up investigation all corroborated that the 6 ft/d value was reasonable. Those tests are described below.

The estimates of K_H obtained from measured specific capacity of water supply wells presented in **Section 2.3.1** "Hydraulic Conductivity" were obtained by dividing estimated transmissivity by the length of the well screen. This implicitly assumes that all horizontal flow occurs only through the screened depth interval. In the groundwater model, horizontal flow occurs over the full thickness of each model layer. Dividing transmissivity by layer thickness rather than screen length would result in a lower estimate of K_H. The magnitude of the adjustment depends on the ratio of layer thickness to screen length in each model layer. These ratios were calculated for 189 wells that had specific capacity data and well screen information. The length of well screen in each model layer was calculated, using layer elevations at the well locations. Layers containing less than 25 percent of the well screen length were discarded because they would result in unreasonably large adjustment ratios while contributing relatively little to the measured specific yield. This resulted in a data set of 279 screen-layer ratios. The mean value of K_H based on well screen length was 24 ft/d and the median value was 8 ft/d. After adjusting to reflect model layer thickness, the mean value was 6 ft/d and the median value was 3 ft/d. The adjusted values are similar to the calibrated K_H value of 6 ft/d. The large difference between average and median values results from the positive skew in the data set. This means that there are high outliers, which would likely include the wells capable of pumping at high rates. In other words, high-yield wells are present but they do not represent typical conditions in the low- K_H zone.

K_H is much more variable in XMOD than in GMOD or the IMOD model. GMOD and the IMOD model have K_H values that range over about 1.5 orders of magnitude, whereas in XMOD the range is 3-4 orders of magnitude. Notably, the additional range in XMOD is at the low end, suggesting that flow through high- K_H areas is balanced by lack of flow through low- K_H areas. Visual averaging of the continuous distributions of K_H shown in Figure 6 of the XMOD documentation report (Hanson and others, 2004) is difficult. Rough averages for the central low- K_H zone are 38 ft/d for layer 3, and 1.0-1.3 ft/d for layers 4 and 5. Thus, an average of 6 ft/d for all three layers appears reasonable.

Finally, a sensitivity test of the IMOD model was completed in which K_H in the central low- K_H zone was increased to the GMOD value of 30 ft/d. No other changes were made to the model. The results are shown in **Figure 4-18a through 4-18d** for a sample of eight wells. In all cases, simulated water levels were higher with the higher K_H value, often by a large amount (40-80 feet) and the amplitude of seasonal water-level fluctuations was smaller by a factor of about four. The results using a K_H of 30 ft/d are clearly inferior to the results using 6 ft/d.

These additional investigations confirm that the K_H value of 6 ft/d in the central low- K_H zone is reasonable.

Vertical hydraulic conductivity values are quite different among the three models. When GMOD was developed, little information regarding vertical water-level gradients was available, and K_V was in most places assumed to equal one-tenth the K_H value. Typical values were 3-10 ft/d in layer 3 and 1-6 ft/d in layers 4 and 5. K_V values in the XMOD model were spatially quite variable—similar to the K_H values—but generally much lower than the XMOD values. In the vicinity of the central low- K_H zone, for example, K_V was 0.01-0.03 ft/d. The XMOD K_V values might not be directly comparable to the other models because XMOD simulated passive vertical flow through wells separately from vertical flow within the aquifer system. K_V values in the IMOD model differ somewhat from XMOD. In the central low- K_H zone, for example, K_V of the regional confining layer is larger in the IMOD model (0.0001 versus 0.00001 ft/d), but lower in layers 3-5 (0.005 versus 0.01-0.03 ft/d). In general, K_V had less impact than K_H on simulated water levels and vertical gradients in the IMOD model.

The calibrated values of specific storativity and specific yield are typical for layered aquifer systems comprised of unconsolidated gravels, sands, silts and clays. The specific yield values in model layer 1 were 0.01 in the confined zone where clay-silt sediments likely predominate and 0.10 throughout the rest of the Subbasin, which is typical of silty-sand textures (Fetter, 1994). The values of specific storativity in layers 2-6 (0.00001 ft^{-1} in the confined area and 0.0001 ft^{-1} elsewhere) are also within the range commonly found in alluvial groundwater basins.

The calibrated values of stream bed K_V are plausible for the types of geologic materials likely present along the channels. Although the calibrated values of 0.1-8.0 ft/d might seem low for gravelly channel deposits, the values actually represent the harmonic mean K_V for vertical flow from the creek down to the midpoint depth of layer 1. Also, K_V was the only variable adjusted during calibration, so the resulting values implicitly incorporate the effects of errors in parameters related to stream depth and width.

4.1.7 Model Advantages and Limitations

The IMOD model is similar to the GMOD and XMOD models in many respects, but its unique characteristics offer the following advantages for some model uses:

- The procedures used to calculate dispersed recharge are more detailed in terms of physical processes and spatial pattern. This enabled an improvement in overall joint calibration of the recharge and groundwater model, because recharge estimates were derived from additional independent data sets such as the amount of disconnected impervious area, the amount of water applied for irrigation, and the amount of water leaking from water and sewer pipes.
- The additional details in the calculations for dispersed recharge also make it possible to simulate a wider range of water management options. For example, changes in stormwater management (such as downspout disconnection, drainage swales or dry wells), changes in irrigation (such as turf conversion rebates or weather-based irrigation controllers), and changes in pipe leak rates (through leak detection programs) could be easily simulated explicitly and quantitatively with the IMOD model.
- The calibration focuses on relatively current groundwater conditions (1985-2014 versus 1970-1989 for GMOD and 1970-1999 for XMOD).
- The IMOD model more accurately simulates vertical water-level gradients within the Subbasin because it was calibrated using the large amount of depth-specific water-level data collected since 2004.
- Simulation time is faster and numerical convergence more reliable than for the XMOD model, largely because several of the nonlinear MODFLOW packages in XMOD were not carried forward into the IMOD model (evapotranspiration, multi-node well, and subsidence).
- A larger number of well and stream hydrographs were used for model calibration than were used for XMOD calibration.
- Calibration by hydrograph inspection allowed model errors to be traced to specific parts of the hydrologic cycle based on the location and timing of residuals, which is more informative than simply evaluating residuals statistics.
- The bedrock surface in the Santa Teresa area is more accurately represented than in GMOD.
- The IMOD model includes the Santa Clara Formation and part of San Mateo County north of San Francisquito Creek in the active flow area. Simulation results are more reliable than when those areas are represented with simplified boundary conditions, as

they were in GMOD and XMOD. Also, the IMOD model is capable of simulating changes in groundwater conditions or management in those areas.

- In the IMOD model, layers 1 and 2 extend across the entire Subbasin, whereas they were restricted to the confined area in GMOD and XMOD. This increases the ability of the IMOD model to simulate vertical groundwater flow and gradients outside the confined area.
- The evaluation of faults based on groundwater levels rather than geology more accurately represents their effects on groundwater.

Despite the above improvements, the model is still a simplified representation of the physical groundwater system. Its ability to simulate all details of groundwater flow and levels is limited, and those limitations should be considered when applying the model to address groundwater management questions. Limitations of the IMOD model include the following:

- Model results are more accurate at the regional scale than at local scales. This is partly due to the high degree of horizontal and vertical spatial variability in groundwater conditions evident in measured water level data. The model provides a good estimate of the “average” groundwater conditions at any location in the Subbasin, but the actual conditions encountered if a well were drilled at that location could differ from the average.
- Accurate simulation of local groundwater conditions is also limited by the grid cell spacing. The simulated water level in each model cell represents the average water level over the 1,000 x 1,000-foot cell. The actual water level at a pumping well within the cell would be lower than the average. Thus, the model is not an appropriate tool for evaluating available drawdown or well screen dewatering in wells or the drawdown caused by a pumping well at another well located less than 1,000 feet away.
- The limitations on spatial accuracy of model results apply to vertical as well as horizontal accuracy. The complex layering of individual lenses of alluvial materials with different textures is represented crudely in the model. Vertical water-level gradients should be viewed as averages over areas encompassing several square miles. Actual gradients at specific locations are highly influenced by the screen depths at nearby production wells.
- The model is not capable of accurately simulating hydrologic processes over time intervals less than one month, which is the stress period duration used for transient simulations. This includes drawdown during pumping cycles shorter than 1 month and the effects of brief stream flow peaks on groundwater recharge.
- The IMOD model does not simulate subsidence. Consequently, results might not be accurate for scenarios in which groundwater levels approach or drop below the minimum water levels reached in the 1960s.
- The IMOD model does not simulate the difference in density between San Francisco Bay water and groundwater. Thus, for scenarios in which simulated groundwater levels near San Francisco Bay—particularly in model layer 1—approach or drop below sea level, the results might underestimate the rate and extent of saltwater intrusion.

5 References

Alameda County Water District. January 31, 2015. Groundwater Monitoring Report 2014. Fremont, CA.

Allen, R.G., L.S. Pereira, D. Raes, and M. Smith. 2006. Crop Evapotranspiration. United Nations Food and Agriculture Organization. Rome, Italy.

American Society for Testing and Materials. 2014 (periodically updated). ASTM D5490-93(2014)e1 Standard Guide for Comparing Groundwater Flow Model Simulations to Site-Specific Information. Downloaded from http://www.astm.org/search/fullsite-search.html?query=D5490-93&resStart=0&resLength=10&toplevel=products-and-services&sublevel=standards-and-publications& on December 10, 2015.

Aquacraft, Inc. July 20, 2011, California Single-Family Water Use Efficiency Study, Boulder, CO, Prepared for Irvine Ranch Water District and California Department of Water Resources.

Baum, M.C., M.D. Dukes, and G.L. Miller. July/August 2005. Analysis of Residential Irrigation Distribution Uniformity. Journal of Irrigation and Drainage Engineering. American Society of Civil Engineers Ppp 336-341.

Bicknell, B.R., Imhoff, J.C., Kittle, J.L., Jr., Donigian, A.S., Jr., and Johanson, R.C., 1997, Hydrological Simulation Program--Fortran, User's manual for version 11: U.S. Environmental Protection Agency, National Exposure Research Laboratory, Athens, Ga., EPA/600/R-97/080, 755 p.

Blaney, H.F., P.R. Nixon, G.P. Lawless and E.J. Wiedmann. October 1963. Utilization of the waters of the Santa Ynez River basin for agriculture in southern Santa Barbara County, California. U.S. Department of Agriculture, Agricultural Research Service. Riverside, CA.

Brabb, E.E., R.W. Graymer and D.L. Jones. 2000. Geologic Map and Map Database of the Palo Alto 30’ X 60’ Quadrangle, California. Miscellaneous Field Studies Map MF-2332. U.S. Geological Survey. Menlo Park, CA.

California Department of Water Resources (DWR). 2003. California’s Groundwater. Bulletin 118. Sacramento, CA

California Water Service Company. June 2011. 2010 Urban Water Management Plan, Los Altos Suburban District. Los Altos, CA.

CH2M HILL, Inc. December 1992. Santa Clara Valley Groundwater Model Project, Basinwide Groundwater Flow Model. Draft technical memorandum. Prepared for City of San Jose and Santa Clara Valley Water District, San Jose, CA.

Clark, W.O. 1924. Ground water in Santa Clara Valley, California. Water-Supply Paper 519. U.S. Geological Survey, Washington D.C.

Environmental Simulations, Inc. 2011. Guide to Using Groundwater Vistas, Version 6. Reinholds, PA.

Fetter, C.W. 1994. Applied Hydrogeology, 3rd edition. Prentice-Hall. Upper Saddle River, NJ.

Forster, M.R. 2001. The New Science of Simplicity. Chapter 5 *in* A. Zellner, H.A. Kreuzenkamp and M. McAleer, eds., Simplicity, Inference and Modeling. Cambridge University Press, Cambridge, England.

Graveto and H. Majumdar. 1971. Investigation on Permeability and Storage Coefficients. Santa Clara Valley Water District, San Jose, CA.

Hanson, R.T., Z. Li, and C.C. Faunt. 2004. Documentation of the Santa Clara Valley Regional Ground-Water/Surface-Water Flow Model, Santa Clara County, California. Scientific Investigations Report 2004-5231. U.S. Geological Survey, Reston, VA.

Harbaugh, A.W. 2005. MODFLOW-2005: the U.S. Geological Survey Modular Ground-Water Model—the Ground-Water Flow Process. Chapter 16 of Book 6 *in* Techniques and Methods. U.S. Geological Survey, Reston, VA.

Harding Lawson Associates. June 24, 1987a. Edenvale Gap Subsurface Characterization, San Jose, California. Prepared for IBM General Products Division, San Jose, CA.

Harding Lawson Associates. June 1987b. Comprehensive plan, IBM Groundwater Restoration Program, Draft Appendix B: Summary of Hydrogeologic Studies. Prepared for IBM General Products Division, San Jose, CA.

Ingebritsen, S.E. and D.L. Jones. 1999. Santa Clara Valley, California: a Case of Arrested Subsidence. *in* D. Galloway, D.R. Jones and S.E. Ingebritsen, Eds. Land Subsidence in the United States. Circular 1182. U.S. Geological Survey, Reston, VA.

Iwamura, T.I. September 1980. Saltwater Intrusion Investigation. Santa Clara Valley Water District. San Jose, CA.

Iwamura, T.I. 1995. Hydrogeology of the Santa Clara and Coyote Valleys Groundwater Basins, California. Santa Clara Valley Water District, San Jose, CA.

Johnson, N.M., D. Williams, E.B. Yates, G. Thrupp. 2004. Groundwater Use Assessment of Alternative Conjunctive Use Scenarios—Technical Memorandum 2: Hydrogeologic Conceptual Model. Prepared for Soquel Creek Water District, Soquel, CA.

Jones, D.W. 1999. California Irrigation Management Information System Reference Evapotranspiration (ETo) zones. University of California, Davis, and California Department of Water Resources. Sacramento, CA. Accessed on-line at http://wwwcimis.water.ca.gov/App_Themes/images/etozonemap.jpg on May 12, 2015.

Kumar, R., M. Seaman, W. Raff, and A. Scott. 2009. Effect of Rotary Nozzles and Cycle and Soak Scheduling on Landscape Irrigation Efficiency. California Polytechnic State University, Pomona, CA.

Lahlou, Z. May 2001. Leak Detection and Water Loss Control, Tech Brief Fact Sheet. National Drinking Water Clearinghouse, Morgantown, WV.

Metzger, L.F. and J.L. Fio. 1997. Ground-Water Development and the Effects on Ground-Water Levels and Quality in the Town of Atherton, San Mateo County, California. Water-Resources Investigations Report 97-4033. U.S. Geological Survey, Sacramento, CA.

Mitchell, V.G., R.G. Mein and T.A. McMahon. 2001. Modelling the Urban Water Cycle. Environmental Modeling and Software 16(2001):615-629.

Natural Resources Conservation Service. 2015. SSURGO Soil Survey On-line Map Database available at http://websoilsurvey.nrcs.usda.gov/app/WebSoilSurvey.aspx . Downloaded 27 March 2015.

Poland, J.F. and R.L. Ireland. 1988. Land Subsidence in the Santa Clara Valley, California, as of 1982. Professional Paper 497-F. U.S. Geological Survey, Washington, D.C.

Rawls, W.J., L.R. Ahuja, D.L. Brakensiek and A. Shirmohammadi. 1993. Infiltration and Soil Water Movement. Chapter 5 *in* D.R. Maidment, ed. Handbook of Hydrology. McGraw-Hill, Inc. New York, NY.

Sandoval-Solis, S., M. Orang, R.L. Snyder, S. Orloff, K.E. Williams and J.M. Rodriguez. June 2013. Spatial analysis of application efficiencies in irrigation for the State of California. Water Management Research Laboratory, University of California, Davis, CA.

Santa Clara Valley Water District (District). 2010. 2010 urban water management plan. San Jose, CA.

Snyder, R.L., M. Orang, K. Bali and S. Eching. Revised 2007. Basic Irrigation Scheduling (BIS). Computer Software Manual. Department of Land, Air and Water Resources, University of California. Davis, CA.

Todd Engineers, Kennedy/Jenks, and ESA. November 2012. Gloria Way Production Well Alternatives Analysis and Water Security Feasibility Study. Prepared for City of East Palo Alto, CA.

URS Corporation. December 17, 2009. Feasibility Study for the Recovery and Beneficial Use of Shallow Groundwater. Prepared for Santa Clara Valley Water District. San Jose, CA.

Van Mullen, J.A., D.E. Woodward, R.H. Hawkins, and A.T. Hjelmfelt, Jr. No date (but after 2001). Runoff Curve Number Method: Beyond the Handbook. Curve-Number Working Group, Natural Resources Conservation Service, Washington, D.C.

Viessman, W., Jr., J.W. Knapp, G.L. Lewis, and T.E. Harbaugh. 1977. Introduction to Hydrology. 2nd edition. Harper & Row, Publishers. New York, NY.

Wentworth, C.M., M.C. Blake, R.J. McLaughlin and R.W. Graymer. 1999. Preliminary Geologic Map of the San Jose 30 X 60 Minute Quadrangle, California. Digital Database. Open-File Report 98-795. U.S. Geological Survey, Menlo Park, CA.

Wentworth, C.M., R.C. Jachens, R.A. Williams, J.C. Tinsley and R.T. Hanson. 2015. Physical Subdivision and Description of The Water-Bearing Sediments of the Santa Clara Valley, California. Scientific Investigations Report 2015-5017. U.S. Geological Survey, Reston, VA.

Yates, G., M. Feeney and L.I. Rosenberg. November 2002. Laguna Seca Subarea Phase III Hydrogeologic Update. Prepared for Monterey Peninsula Water Management District, Monterey, CA.

Xiao, Q., E.G. McPherson, J.R. Simpson and S.L. Ustin. October, 2007. Hydrologic Processes at the Urban Residential Scale. Hydrologic Processes 21:2174-2188.

Tables

Table 3-1 Recharge Zone Parameters

Zone number	Land use	Zone area (ac)	Impervious fraction of total area	Irrigated fraction of total area	Average annual rainfall (in)	Average annual reference ET (in)	NRCS soil hydrologic group	Daily Interception (in)	Runoff threshold	Infiltration slope (fraction of rainfall)	Maximum daily infiltration (in)	Infiltration parameter factor at soil saturation	Root depth in irrigated areas (in)	Root depth in nonirrigated areas (in)	Available water capacity (in/in)	Initial soil moisture in irrigated areas (fraction of maximum storage)	Initial soil moisture in nonirrigated areas (fraction of maximum storage)	Irrigation efficiency (fraction)	Soil moisture trigger for irrigation (fraction)	Soil moiture threshold for ET depression	Crop coefficient set for irrigated veg	Crop coefficient set for nonirrigated veg	Fraction of impervious area that runs off to pervious soils	Municipal water service area	Ratio of muni use/acre to average muni use/acre	Shallow groundwater deep percolation rate (ft/d)	Shallow groundwater recession exponent [$S_t=(S_{t-1}+1)^a$ - 1]
1	Natural grassland	2,280	0.00	0.00	17.70	49.4	C	0.04	0.80	0.85	3.0	0.75	36	48	0.14	0.81	0.20	0.85	0.80	0.60	3	3	1.00	11	0.01	0.05	0.05
2	Natural grassland	689	0.00	0.00	16.02	49.4	C	0.04	0.80	0.85	3.0	0.75	36	48	0.14	0.81	0.20	0.85	0.80	0.60	3	3	1.00	11	0.01	0.05	0.05
3	Natural grassland	3,197	0.00	0.00	18.42	49.4	C	0.04	0.80	0.85	3.0	0.75	36	48	0.15	0.81	0.20	0.85	0.80	0.60	3	3	1.00	11	0.01	0.05	0.05
4	Natural grassland	385	0.00	0.00	16.97	49.4	C	0.04	0.80	0.85	3.0	0.75	36	48	0.15	0.81	0.20	0.85	0.80	0.60	3	3	1.00	11	0.01	0.05	0.05
5	Natural grassland	1,339	0.00	0.00	17.07	49.4	C	0.04	0.80	0.85	3.0	0.75	36	48	0.15	0.81	0.20	0.85	0.80	0.60	3	3	1.00	11	0.01	0.05	0.05
6	Natural grassland	814	0.00	0.00	17.00	49.4	C	0.04	0.80	0.85	3.0	0.75	36	48	0.15	0.81	0.20	0.85	0.80	0.60	3	3	1.00	11	0.01	0.05	0.05
7	Natural grassland	821	0.00	0.00	14.98	49.4	C	0.04	0.80	0.85	3.0	0.75	36	48	0.10	0.81	0.20	0.85	0.80	0.60	3	3	1.00	11	0.01	0.05	0.05
8	Natural trees & shrubs	4,952	0.00	0.00	27.57	49.4	C	0.08	0.80	0.85	3.0	0.75	36	84	0.14	0.81	0.20	0.85	0.80	0.60	8	8	1.00	8	0.01	0.05	0.05
9	Natural grassland	14,433	0.00	0.00	21.83	49.4	D	0.04	0.80	0.85	3.0	0.75	36	48	0.14	0.81	0.20	0.85	0.80	0.60	3	3	1.00	11	0.01	0.05	0.05
10	Natural grassland	3,642	0.00	0.00	17.47	49.4	C	0.04	0.80	0.85	3.0	0.75	36	48	0.15	0.81	0.20	0.85	0.80	0.60	3	3	1.00	11	0.01	0.05	0.05
11	Natural grassland	774	0.00	0.00	16.09	49.4	C	0.04	0.80	0.85	3.0	0.75	36	48	0.15	0.81	0.20	0.85	0.80	0.60	3	3	1.00	11	0.01	0.05	0.05
12	Natural grassland	379	0.00	0.00	15.50	49.4	C	0.04	0.80	0.85	3.0	0.75	36	48	0.14	0.81	0.20	0.85	0.80	0.60	3	3	1.00	11	0.01	0.05	0.05
13	Natural trees & shrubs	5,583	0.00	0.00	25.24	49.4	C	0.08	0.80	0.85	3.0	0.75	36	84	0.14	0.81	0.20	0.85	0.80	0.60	8	8	1.00	11	0.01	0.05	0.05
14	Natural trees & shrubs	1,652	0.00	0.00	22.69	49.4	C	0.08	0.80	0.85	3.0	0.75	36	84	0.15	0.81	0.20	0.85	0.80	0.60	8	8	1.00	11	0.01	0.05	0.05
15	Natural grassland	480	0.00	0.00	15.50	49.4	D	0.04	0.80	0.85	3.0	0.75	36	48	0.13	0.81	0.20	0.85	0.80	0.60	3	3	1.00	7	0.01	0.05	0.05
16	Natural grassland	1,881	0.00	0.00	17.79	49.4	C	0.04	0.80	0.85	3.0	0.75	36	48	0.15	0.81	0.20	0.85	0.80	0.60	3	3	1.00	11	0.01	0.05	0.05
17	Natural grassland	1,331	0.00	0.00	18.55	49.4	C	0.04	0.80	0.85	3.0	0.75	36	48	0.15	0.81	0.20	0.85	0.80	0.60	3	3	1.00	11	0.01	0.05	0.05
18	Natural trees & shrubs	8,243	0.00	0.00	40.83	49.4	B	0.08	0.80	0.85	3.0	0.75	36	84	0.14	0.81	0.20	0.85	0.80	0.60	8	8	1.00	11	0.01	0.05	0.05
19	Natural trees & shrubs	3,541	0.00	0.00	29.19	49.4	C	0.08	0.80	0.85	3.0	0.75	36	84	0.14	0.81	0.20	0.85	0.80	0.60	8	8	1.00	11	0.01	0.05	0.05
20	Natural grassland	391	0.00	0.00	23.46	49.4	C	0.04	0.80	0.85	3.0	0.75	36	48	0.17	0.81	0.20	0.85	0.80	0.60	3	3	1.00	11	0.01	0.05	0.05
21	Natural grassland	2,676	0.00	0.00	27.57	49.4	C	0.04	0.80	0.85	3.0	0.75	36	48	0.17	0.81	0.20	0.85	0.80	0.60	3	3	1.00	11	0.01	0.05	0.05
22	Natural grassland	3,370	0.00	0.00	16.24	49.4	C	0.04	0.80	0.85	3.0	0.75	36	48	0.11	0.81	0.20	0.85	0.80	0.60	3	3	1.00	9	0.01	0.05	0.05
23	Natural grassland	3,473	0.00	0.00	17.15	49.4	C	0.04	0.80	0.85	3.0	0.75	36	48	0.13	0.81	0.20	0.85	0.80	0.60	3	3	1.00	11	0.01	0.05	0.05
24	Natural grassland	3,308	0.00	0.00	16.43	49.4	C	0.04	0.80	0.85	3.0	0.75	36	48	0.13	0.81	0.20	0.85	0.80	0.60	3	3	1.00	11	0.01	0.05	0.05
25	Natural grassland	1,788	0.00	0.00	18.47	49.4	C	0.04	0.80	0.85	3.0	0.75	36	48	0.14	0.81	0.20	0.85	0.80	0.60	3	3	1.00	11	0.01	0.05	0.05
26	Natural trees & shrubs	5,859	0.00	0.00	42.91	49.4	B	0.08	0.80	0.85	3.0	0.75	36	84	0.12	0.81	0.20	0.85	0.80	0.60	8	8	1.00	11	0.01	0.05	0.05
27	Natural trees & shrubs	702	0.00	0.00	37.36	49.4	C	0.08	0.80	0.85	3.0	0.75	36	84	0.13	0.81	0.20	0.85	0.80	0.60	8	8	1.00	11	0.01	0.05	0.05
28	Natural trees & shrubs	3,306	0.00	0.00	32.20	49.4	C	0.08	0.80	0.85	3.0	0.75	36	84	0.14	0.81	0.20	0.85	0.80	0.60	8	8	1.00	11	0.01	0.05	0.05
29	Natural trees & shrubs	5,924	0.00	0.00	25.09	49.4	C	0.08	0.80	0.85	3.0	0.75	36	84	0.14	0.81	0.20	0.85	0.80	0.60	8	8	1.00	11	0.01	0.05	0.05
30	Natural trees & shrubs	1,086	0.00	0.00	27.08	49.4	C	0.08	0.80	0.85	3.0	0.75	36	84	0.14	0.81	0.20	0.85	0.80	0.60	8	8	1.00	11	0.01	0.05	0.05
31	Natural trees & shrubs	690	0.00	0.00	24.23	49.4	C	0.08	0.80	0.85	3.0	0.75	36	84	0.14	0.81	0.20	0.85	0.80	0.60	8	8	1.00	11	0.01	0.05	0.05
32	Natural trees & shrubs	798	0.00	0.00	25.51	49.4	C	0.08	0.80	0.85	3.0	0.75	36	84	0.14	0.81	0.20	0.85	0.80	0.60	8	8	1.00	11	0.01	0.05	0.05
33	Natural grassland	4,389	0.00	0.00	18.09	49.4	C	0.04	0.80	0.85	3.0	0.75	36	48	0.13	0.81	0.20	0.85	0.80	0.60	3	3	1.00	11	0.01	0.05	0.05
34	Natural trees & shrubs	1,449	0.00	0.00	31.78	49.4	C	0.08	0.80	0.85	3.0	0.75	36	84	0.13	0.81	0.20	0.85	0.80	0.60	8	8	1.00	11	0.01	0.05	0.05
35	Natural grassland	8,614	0.00	0.00	19.06	49.4	D	0.04	0.80	0.85	3.0	0.75	36	48	0.14	0.81	0.20	0.85	0.80	0.60	3	3	1.00	11	0.01	0.05	0.05
36	Natural grassland	4,871	0.00	0.00	19.99	49.4	D	0.04	0.80	0.85	3.0	0.75	36	48	0.14	0.81	0.20	0.85	0.80	0.60	3	3	1.00	11	0.01	0.05	0.05
37	Natural trees & shrubs	7,622	0.00	0.00	32.42	49.4	C	0.08	0.80	0.85	3.0	0.75	36	84	0.15	0.81	0.20	0.85	0.80	0.60	8	8	1.00	11	0.01	0.05	0.05
38	Natural trees & shrubs	13,699	0.00	0.00	38.44	49.4	C	0.08	0.80	0.85	3.0	0.75	36	84	0.13	0.81	0.20	0.85	0.80	0.60	8	8	1.00	11	0.01	0.05	0.05
39	Natural trees & shrubs	1,782	0.00	0.00	24.27	49.4	C	0.08	0.80	0.85	3.0	0.75	36	84	0.16	0.81	0.20	0.85	0.80	0.60	8	8	1.00	11	0.01	0.05	0.05
40	Urban residential	102,412	0.25	0.18	16.51	49.4	C	0.04	0.35	0.80	3.0	0.75	18	72	0.15	0.81	0.20	0.80	0.80	0.60	4	2	0.07	10	1.00	0.2	0.05
41	Open water	12,240	0.00	0.00	12.42	49.4	C	0.00	9.99	1.00	3.0	1.00	24	24	0.14	1.00	1.00	1.00	0.10	0.05	16	16	1.00	11	0.01	0.01	0.05
42	Open water	1,060	0.00	0.00	13.74	49.4	C	0.00	9.99	1.00	3.0	1.00	24	24	0.14	1.00	1.00	1.00	0.10	0.05	16	16	1.00	11	0.01	0.01	0.05
43	Open water	178	0.00	0.00	12.92	49.4	C	0.00	9.99	1.00	3.0	1.00	24	24	0.14	1.00	1.00	1.00	0.10	0.05	16	16	1.00	12	0.01	0.01	0.05
44	Open water	1,909	0.00	0.00	13.66	49.4	C	0.00	9.99	1.00	3.0	1.00	24	24	0.15	1.00	1.00	1.00	0.10	0.05	16	16	1.00	11	0.01	0.01	0.05
45	Open water	242	0.00	0.00	13.27	49.4	C	0.00	9.99	1.00	3.0	1.00	24	24	0.14	1.00	1.00	1.00	0.10	0.05	16	16	1.00	9	0.01	0.01	0.05
46	Industrial	306	0.30	0.09	15.79	49.4	C	0.00	0.20	0.65	3.0	0.75	18	72	0.16	0.81	0.20	0.90	0.80	0.60	4	3	0.03	9	0.50	0.2	0.05
47	Natural grassland	68	0.00	0.00	15.53	49.4	C	0.04	0.80	0.85	3.0	0.75	36	48	0.21	0.81	0.20	0.85	0.80	0.60	3	3	1.00	7	0.01	0.05	0.05
48	Natural grassland	39	0.00	0.00	15.61	49.4	C	0.04	0.80	0.85	3.0	0.75	36	48	0.21	0.81	0.20	0.85	0.80	0.60	3	3	1.00	9	0.01	0.05	0.05
49	Riparian vegetation	70	0.00	0.00	16.38	49.4	B	0.08	0.80	0.96	3.0	0.75	30	180	0.15	0.81	0.20	0.85	0.80	0.60	1	1	1.00	9	0.01	0.01	0.05
50	Natural grassland	30	0.00	0.00	17.00	49.4	A	0.04	0.80	0.85	3.0	0.75	36	48	0.15	0.81	0.20	0.85	0.80	0.60	3	3	1.00	9	0.01	0.05	0.05
51	Commercial	67	0.30	0.12	17.00	49.4	C	0.01	0.20	0.65	3.0	0.75	18	72	0.21	0.81	0.20	0.90	0.80	0.60	4	3	0.03	7	0.50	0.2	0.05
52	Urban residential	71	0.25	0.18	17.00	49.4	C	0.04	0.35	0.80	3.0	0.75	18	72	0.14	0.81	0.20	0.80	0.80	0.60	4	2	0.07	7	0.50	0.2	0.05
53	Natural grassland	355	0.00	0.00	16.94	49.4	C	0.04	0.80	0.85	3.0	0.75	36	48	0.16	0.81	0.20	0.85	0.80	0.60	3	3	1.00	7	0.01	0.05	0.05
54	Natural grassland	74	0.00	0.00	17.00	49.4	C	0.04	0.80	0.85	3.0	0.75	36	48	0.14	0.81	0.20	0.85	0.80	0.60	3	3	1.00	7	0.01	0.05	0.05
55	Open water	140	0.00	0.00	17.00	49.4	C	0.00	9.99	1.00	3.0	1.00	24	24	0.14	1.00	1.00	1.00	0.10	0.05	16	16	1.00	11	0.01	0.01	0.05
56	Industrial	368	0.30	0.09	17.00	49.4	C	0.00	0.20	0.65	3.0	0.75	18	72	0.19	0.81	0.20	0.90	0.80	0.60	4	3	0.03	7	1.00	0.2	0.05
57	Urban vacant	166	0.40	0.02	17.00	49.4	C	0.00	0.20	0.55	3.0	0.75	30	72	0.16	0.81	0.20	0.90	0.80	0.60	4	3	0.03	12	1.00	0.2	0.05
58	Natural grassland	40	0.00	0.00	17.00	49.4	C	0.04	0.80	0.85	3.0	0.75	36	48	0.17	0.81	0.20	0.85	0.80	0.60	3	3	1.00	7	0.01	0.05	0.05
59	Urban residential	247	0.25	0.18	16.75	49.4	C	0.04	0.35	0.80	3.0	0.75	18	72	0.20	0.81	0.20	0.80	0.80	0.60	4	2	0.07	7	0.50	0.2	0.05
60	Urban residential	149	0.25	0.18	15.50	49.4	C	0.04	0.35	0.80	3.0	0.75	18	72	0.22	0.81	0.20	0.80	0.80	0.60	4	2	0.07	7	0.50	0.2	0.05
61	Urban vacant	106	0.40	0.02	15.96	49.4	C	0.00	0.20	0.55	3.0	0.75	30	72	0.21	0.81	0.20	0.90	0.80	0.60	4	3	0.03	7	0.50	0.2	0.05
62	Industrial	307	0.30	0.09	16.64	49.4	C	0.00	0.20	0.65	3.0	0.75	18	72	0.20	0.81	0.20	0.90	0.80	0.60	4	3	0.03	12	0.50	0.2	0.05
63	Natural grassland	244	0.00	0.00	16.75	49.4	C	0.04	0.80	0.85	3.0	0.75	36	48	0.18	0.81	0.20	0.85	0.80	0.60	3	3	1.00	11	0.01	0.05	0.05
64	Commercial	282	0.30	0.12	19.08	49.4	C	0.01	0.20	0.65	3.0	0.75	18	72	0.10	0.81	0.20	0.90	0.80	0.60	4	3	0.03	10	1.00	0.2	0.05
65	Open water	11	0.00	0.00	18.63	49.4	C	0.00	9.99	1.00	3.0	1.00	24	24	0.14	1.00	1.00	1.00	0.10	0.05	16	16	1.00	10	0.01	0.01	0.05
66	Open water	2	0.00	0.00	19.00	49.4	C	0.00	9.99	1.00	3.0	1.00	24	24	0.13	1.00	1.00	1.00	0.10	0.05	16	16	1.00	10	0.01	0.01	0.05
67	Open water	36	0.00	0.00	19.00	49.4	C	0.00	9.99	1.00	3.0	1.00	24	24	0.14	1.00	1.00	1.00	0.10	0.05	16	16	1.00	10	0.01	0.01	0.05
68	Riparian vegetation	35	0.00	0.00	18.97	49.4	A	0.08	0.80	0.96	3.0	0.75	30	180	0.14	0.81	0.20	0.85	0.80	0.60	1	1	1.00	10	0.01	0.01	0.05
69	Urban large landscaping	7	0.00	0.29	17.42	49.4	A	0.02	0.80	0.87	3.0	0.75	18	72	0.14	0.85	0.20	0.90	0.80	0.60	4	3	0.70	10	1.00	0.2	0.05

Table 3-1 Recharge Zone Parameters

Zone number	Land use	Zone area (ac)	Impervious fraction of total area	Irrigated fraction of total area	Average annual rainfall (in)	Average annual reference ET (in)	NRCS soil hydrologic group	Daily Interception (in)	Runoff threshold	Infiltration slope (fraction of rainfall)	Maximum daily infiltration (in)	Infiltration parameter factor at soil saturation	Root depth in irrigated areas (in)	Root depth in nonirrigated areas (in)	Available water capacity (in/in)	Initial soil moisture in irrigated areas (fraction of maximum storage)	Initial soil moisture in nonirrigated areas (fraction of maximum storage)	Irrigation efficiency (fraction)	Soil moisture trigger for irrigation (fraction)	Soil moiture threshold for ET depression	Crop coefficient set for irrigated veg	Crop coefficient set for nonirrigated veg	Fraction of impervious area that runs off to pervious soils	Municipal water service area	Ratio of muni use/acre to average muni use/acre	Shallow groundwater deep percolation rate (ft/d)	Shallow groundwater recession exponent [$S_t=(S_{t-1}+1)^a - 1$]
70	Open water	17	0.00	0.00	19.06	49.4	C	0.00	9.99	1.00	3.0	1.00	24	24	0.14	1.00	1.00	1.00	0.10	0.05	16	16	1.00	10	0.01	0.01	0.05
71	Urban residential	33	0.25	0.18	20.73	49.4	A	0.04	0.35	0.80	3.0	0.75	18	72	0.15	0.81	0.20	0.80	0.80	0.60	4	2	0.07	10	1.00	0.2	0.05
72	Urban residential	151	0.25	0.18	22.40	49.4	B	0.04	0.35	0.80	3.0	0.75	18	72	0.13	0.81	0.20	0.80	0.80	0.60	4	2	0.07	10	1.00	0.2	0.05
73	Urban vacant	224	0.40	0.02	18.91	49.4	C	0.00	0.20	0.55	3.0	0.75	30	72	0.13	0.81	0.20	0.90	0.80	0.60	4	3	0.03	10	1.00	0.2	0.05
74	Commercial	152	0.30	0.12	16.02	49.4	B	0.01	0.20	0.65	3.0	0.75	18	72	0.16	0.81	0.20	0.90	0.80	0.60	4	3	0.03	10	1.00	0.2	0.05
75	Riparian vegetation	42	0.00	0.00	15.82	49.4	A	0.08	0.80	0.96	3.0	0.75	30	180	0.14	0.81	0.20	0.85	0.80	0.60	1	1	1.00	10	0.01	0.01	0.05
76	Commercial	187	0.30	0.12	16.21	49.4	B	0.01	0.20	0.65	3.0	0.75	18	72	0.13	0.81	0.20	0.90	0.80	0.60	4	3	0.03	10	1.00	0.2	0.05
77	Urban vacant	30	0.40	0.02	16.51	49.4	C	0.00	0.20	0.55	3.0	0.75	30	72	0.16	0.81	0.20	0.90	0.80	0.60	4	3	0.03	10	1.00	0.2	0.05
78	Urban large landscaping	26	0.00	0.29	17.00	49.4	C	0.02	0.80	0.87	3.0	0.75	18	72	0.10	0.85	0.20	0.90	0.80	0.60	4	3	0.70	10	1.00	0.2	0.05
79	Open water	8	0.00	0.00	17.00	49.4	C	0.00	9.99	1.00	3.0	1.00	24	24	0.14	1.00	1.00	1.00	0.10	0.05	16	16	1.00	10	0.01	0.01	0.05
80	Urban vacant	179	0.40	0.02	20.22	49.4	C	0.00	0.20	0.55	3.0	0.75	30	72	0.12	0.81	0.20	0.90	0.80	0.60	4	3	0.03	10	1.00	0.2	0.05
81	Riparian vegetation	14	0.00	0.00	19.16	49.4	C	0.08	0.80	0.96	3.0	0.75	30	180	0.14	0.81	0.20	0.85	0.80	0.60	1	1	1.00	10	0.01	0.01	0.05
82	Commercial	31	0.30	0.12	19.00	49.4	C	0.01	0.20	0.65	3.0	0.75	18	72	0.10	0.81	0.20	0.90	0.80	0.60	4	3	0.03	10	1.00	0.2	0.05
83	Urban large landscaping	14	0.00	0.29	19.00	49.4	C	0.02	0.80	0.87	3.0	0.75	18	72	0.11	0.85	0.20	0.90	0.80	0.60	4	3	0.70	10	1.00	0.2	0.05
84	Urban large landscaping	12	0.00	0.29	21.00	49.4	C	0.02	0.80	0.87	3.0	0.75	18	72	0.10	0.85	0.20	0.90	0.80	0.60	4	3	0.70	10	1.00	0.2	0.05
85	Commercial	57	0.30	0.12	19.00	49.4	B	0.01	0.20	0.65	3.0	0.75	18	72	0.16	0.81	0.20	0.90	0.80	0.60	4	3	0.03	10	1.00	0.2	0.05
86	Commercial	314	0.30	0.12	17.01	49.4	C	0.01	0.20	0.65	3.0	0.75	18	72	0.18	0.81	0.20	0.90	0.80	0.60	4	3	0.03	10	1.00	0.2	0.05
87	Riparian vegetation	40	0.00	0.00	17.90	49.4	B	0.08	0.80	0.96	3.0	0.75	30	180	0.17	0.81	0.20	0.85	0.80	0.60	1	1	1.00	10	0.01	0.01	0.05
88	Urban residential	37	0.25	0.18	17.00	49.4	C	0.04	0.35	0.80	3.0	0.75	18	72	0.17	0.81	0.20	0.80	0.80	0.60	4	2	0.07	10	1.00	0.2	0.05
89	Urban large landscaping	23	0.00	0.29	17.00	49.4	C	0.02	0.80	0.87	3.0	0.75	18	72	0.15	0.85	0.20	0.90	0.80	0.60	4	3	0.70	10	1.00	0.2	0.05
90	Commercial	92	0.30	0.12	18.67	49.4	C	0.01	0.20	0.65	3.0	0.75	18	72	0.16	0.81	0.20	0.90	0.80	0.60	4	3	0.03	10	1.00	0.2	0.05
91	Commercial	46	0.30	0.12	19.61	49.4	C	0.01	0.20	0.65	3.0	0.75	18	72	0.15	0.81	0.20	0.90	0.80	0.60	4	3	0.03	10	1.00	0.2	0.05
92	Natural grassland	729	0.00	0.00	13.07	49.4	C	0.04	0.80	0.85	3.0	0.75	36	48	0.16	0.81	0.20	0.85	0.80	0.60	3	3	1.00	6	0.01	0.05	0.05
93	Urban large landscaping	165	0.00	0.29	13.50	49.4	C	0.02	0.80	0.87	3.0	0.75	18	72	0.16	0.85	0.20	0.90	0.80	0.60	4	3	0.70	5	1.00	0.2	0.05
94	Industrial	1,686	0.30	0.09	13.83	49.4	C	0.00	0.20	0.65	3.0	0.75	18	72	0.14	0.81	0.20	0.90	0.80	0.60	4	3	0.03	5	1.00	0.2	0.05
95	Commercial	3,552	0.30	0.12	13.67	49.4	C	0.01	0.20	0.65	3.0	0.75	18	72	0.14	0.81	0.20	0.90	0.80	0.60	4	3	0.03	5	1.00	0.2	0.05
96	Urban vacant	933	0.40	0.02	14.10	49.4	C	0.00	0.20	0.55	3.0	0.75	30	72	0.14	0.81	0.20	0.90	0.80	0.60	4	3	0.03	10	1.00	0.2	0.05
97	Industrial	190	0.30	0.09	14.50	49.4	C	0.00	0.20	0.65	3.0	0.75	18	72	0.14	0.81	0.20	0.90	0.80	0.60	4	3	0.03	10	1.00	0.2	0.05
98	Natural grassland	131	0.00	0.00	14.50	49.4	C	0.04	0.80	0.85	3.0	0.75	36	48	0.15	0.81	0.20	0.85	0.80	0.60	3	3	1.00	10	0.01	0.05	0.05
99	Urban large landscaping	50	0.00	0.29	14.50	49.4	C	0.02	0.80	0.87	3.0	0.75	18	72	0.17	0.85	0.20	0.90	0.80	0.60	4	3	0.70	10	1.00	0.2	0.05
100	Commercial	1,312	0.30	0.12	14.50	49.4	C	0.01	0.20	0.65	3.0	0.75	18	72	0.18	0.81	0.20	0.90	0.80	0.60	4	3	0.03	10	1.00	0.2	0.05
101	Riparian vegetation	186	0.00	0.00	14.12	49.4	A	0.08	0.80	0.96	3.0	0.75	30	180	0.15	0.81	0.20	0.85	0.80	0.60	1	1	1.00	10	0.01	0.01	0.05
102	Urban residential	994	0.25	0.18	13.50	49.4	C	0.04	0.35	0.80	3.0	0.75	18	72	0.16	0.81	0.20	0.80	0.80	0.60	4	2	0.07	5	1.00	0.2	0.05
103	Commercial	51	0.30	0.12	13.50	49.4	C	0.01	0.20	0.65	3.0	0.75	18	72	0.16	0.81	0.20	0.90	0.80	0.60	4	3	0.03	5	1.00	0.2	0.05
104	Urban residential	168	0.25	0.18	13.50	49.4	C	0.04	0.35	0.80	3.0	0.75	18	72	0.16	0.81	0.20	0.80	0.80	0.60	4	2	0.07	9	1.00	0.2	0.05
105	Urban residential	124	0.25	0.18	14.50	49.4	C	0.04	0.35	0.80	3.0	0.75	18	72	0.17	0.81	0.20	0.80	0.80	0.60	4	2	0.07	10	1.00	0.2	0.05
106	Commercial	161	0.30	0.12	14.50	49.4	C	0.01	0.20	0.65	3.0	0.75	18	72	0.17	0.81	0.20	0.90	0.80	0.60	4	3	0.03	10	1.00	0.2	0.05
107	Urban residential	86	0.25	0.18	13.50	49.4	C	0.04	0.35	0.80	3.0	0.75	18	72	0.17	0.81	0.20	0.80	0.80	0.60	4	2	0.07	9	1.00	0.2	0.05
108	Commercial	3,247	0.30	0.12	13.79	49.4	C	0.01	0.20	0.65	3.0	0.75	18	72	0.16	0.81	0.20	0.90	0.80	0.60	4	3	0.03	9	1.00	0.2	0.05
109	Urban residential	178	0.25	0.18	13.50	49.4	C	0.04	0.35	0.80	3.0	0.75	18	72	0.17	0.81	0.20	0.80	0.80	0.60	4	2	0.07	9	1.00	0.2	0.05
110	Urban residential	156	0.25	0.18	14.01	49.4	A	0.04	0.35	0.80	3.0	0.75	18	72	0.14	0.81	0.20	0.80	0.80	0.60	4	2	0.07	9	1.00	0.2	0.05
111	Industrial	160	0.30	0.09	14.43	49.4	C	0.00	0.20	0.65	3.0	0.75	18	72	0.17	0.81	0.20	0.90	0.80	0.60	4	3	0.03	9	1.00	0.2	0.05
112	Natural grassland	1,378	0.00	0.00	13.85	49.4	C	0.04	0.80	0.85	3.0	0.75	36	48	0.16	0.81	0.20	0.85	0.80	0.60	3	3	1.00	11	0.01	0.05	0.05
113	Riparian vegetation	131	0.00	0.00	14.50	49.4	B	0.08	0.80	0.96	3.0	0.75	30	180	0.15	0.81	0.20	0.85	0.80	0.60	1	1	1.00	9	0.01	0.01	0.05
114	Natural grassland	455	0.00	0.00	13.92	49.4	C	0.04	0.80	0.85	3.0	0.75	36	48	0.16	0.81	0.20	0.85	0.80	0.60	3	3	1.00	9	0.01	0.05	0.05
115	Natural grassland	142	0.00	0.00	14.28	49.4	C	0.04	0.80	0.85	3.0	0.75	36	48	0.15	0.81	0.20	0.85	0.80	0.60	3	3	1.00	2	0.01	0.05	0.05
116	Commercial	3,200	0.30	0.12	14.35	49.4	B	0.01	0.20	0.65	3.0	0.75	18	72	0.16	0.81	0.20	0.90	0.80	0.60	4	3	0.03	10	1.00	0.2	0.05
117	Industrial	1,511	0.30	0.09	13.58	49.4	C	0.00	0.20	0.65	3.0	0.75	18	72	0.14	0.81	0.20	0.90	0.80	0.60	4	3	0.03	3	1.00	0.2	0.05
118	Urban vacant	722	0.40	0.02	13.48	49.4	C	0.00	0.20	0.55	3.0	0.75	30	72	0.13	0.81	0.20	0.90	0.80	0.60	4	3	0.03	12	1.00	0.2	0.05
119	Natural grassland	562	0.00	0.00	13.48	49.4	C	0.04	0.80	0.85	3.0	0.75	36	48	0.15	0.81	0.20	0.85	0.80	0.60	3	3	1.00	3	0.01	0.05	0.05
120	Urban large landscaping	326	0.00	0.29	13.50	49.4	B	0.02	0.80	0.87	3.0	0.75	18	72	0.13	0.85	0.20	0.90	0.80	0.60	4	3	0.70	3	1.00	0.2	0.05
121	Urban large landscaping	180	0.00	0.29	13.39	49.4	C	0.02	0.80	0.87	3.0	0.75	18	72	0.16	0.85	0.20	0.90	0.80	0.60	4	3	0.70	12	1.00	0.2	0.05
122	Industrial	1,344	0.30	0.09	13.15	49.4	C	0.00	0.20	0.65	3.0	0.75	18	72	0.14	0.81	0.20	0.90	0.80	0.60	4	3	0.03	6	1.00	0.2	0.05
123	Urban large landscaping	163	0.00	0.29	13.72	49.4	C	0.02	0.80	0.87	3.0	0.75	18	72	0.14	0.85	0.20	0.90	0.80	0.60	4	3	0.70	6	1.00	0.2	0.05
124	Commercial	275	0.30	0.12	14.44	49.4	C	0.01	0.20	0.65	3.0	0.75	18	72	0.14	0.81	0.20	0.90	0.80	0.60	4	3	0.03	6	1.00	0.2	0.05
125	Urban residential	2,012	0.25	0.18	13.63	49.4	C	0.04	0.35	0.80	3.0	0.75	18	72	0.14	0.81	0.20	0.80	0.80	0.60	4	2	0.07	6	1.00	0.2	0.05
126	Commercial	1,192	0.30	0.12	14.23	49.4	C	0.01	0.20	0.65	3.0	0.75	18	72	0.15	0.81	0.20	0.90	0.80	0.60	4	3	0.03	6	1.00	0.2	0.05
127	Urban residential	71	0.25	0.18	14.88	49.4	C	0.04	0.35	0.80	3.0	0.75	18	72	0.18	0.81	0.20	0.80	0.80	0.60	4	2	0.07	2	1.00	0.2	0.05
128	Commercial	2,489	0.30	0.12	14.98	49.4	C	0.01	0.20	0.65	3.0	0.75	18	72	0.16	0.81	0.20	0.90	0.80	0.60	4	3	0.03	2	1.00	0.2	0.05
129	Urban residential	345	0.25	0.18	14.50	49.4	C	0.04	0.35	0.80	3.0	0.75	18	72	0.19	0.81	0.20	0.80	0.80	0.60	4	2	0.07	2	1.00	0.2	0.05
130	Urban large landscaping	150	0.00	0.29	14.50	49.4	C	0.02	0.80	0.87	3.0	0.75	18	72	0.16	0.85	0.20	0.90	0.80	0.60	4	3	0.70	10	1.00	0.2	0.05
131	Commercial	398	0.30	0.12	14.50	49.4	C	0.01	0.20	0.65	3.0	0.75	18	72	0.14	0.81	0.20	0.90	0.80	0.60	4	3	0.03	10	1.00	0.2	0.05
132	Urban large landscaping	148	0.00	0.29	14.50	49.4	C	0.02	0.80	0.87	3.0	0.75	18	72	0.18	0.85	0.20	0.90	0.80	0.60	4	3	0.70	10	1.00	0.2	0.05
133	Urban residential	146	0.25	0.18	14.50	49.4	C	0.04	0.35	0.80	3.0	0.75	18	72	0.12	0.81	0.20	0.80	0.80	0.60	4	2	0.07	10	1.00	0.2	0.05
134	Commercial	1,478	0.30	0.12	14.50	49.4	C	0.01	0.20	0.65	3.0	0.75	18	72	0.18	0.81	0.20	0.90	0.80	0.60	4	3	0.03	10	1.00	0.2	0.05
135	Urban vacant	113	0.40	0.02	14.50	49.4	C	0.00	0.20	0.55	3.0	0.75	30	72	0.18	0.81	0.20	0.90	0.80	0.60	4	3	0.03	11	1.00	0.2	0.05
136	Commercial	226	0.30	0.12	14.75	49.4	C	0.01	0.20	0.65	3.0	0.75	18	72	0.18	0.81	0.20	0.90	0.80	0.60	4	3	0.03	10	0.50	0.2	0.05
137	Riparian vegetation	136	0.00	0.00	14.50	49.4	A	0.08	0.80	0.96	3.0	0.75	30	180	0.12	0.81	0.20	0.85	0.80	0.60	1	1	1.00	10	0.01	0.01	0.05
138	Urban large landscaping	76	0.00	0.29	14.50	49.4	B	0.02	0.80	0.87	3.0	0.75	18	72	0.16	0.85	0.20	0.90	0.80	0.60	4	3	0.70	10	1.00	0.2	0.05

Table 3-1 Recharge Zone Parameters

Zone number	Land use	Zone area (ac)	Impervious fraction of total area	Irrigated fraction of total area	Average annual rainfall (in)	Average annual reference ET (in)	NRCS soil hydrologic group	Daily Interception (in)	Runoff threshold	Infiltration slope (fraction of rainfall)	Maximum daily infiltration (in)	Infiltration parameter factor at soil saturation	Root depth in irrigated areas (in)	Root depth in nonirrigated areas (in)	Available water capacity (in/in)	Initial soil moisture in irrigated areas (fraction of maximum storage)	Initial soil moisture in nonirrigated areas (fraction of maximum storage)	Irrigation efficiency (fraction)	Soil moisture trigger for irrigation (fraction)	Soil moiture threshold for ET depression	Crop coefficient set for irrigated veg	Crop coefficient set for nonirrigated veg	Fraction of impervious area that runs off to pervious soils	Municipal water service area	Ratio of muni use/acre to average muni use/acre	Shallow groundwater deep percolation rate (ft/d)	Shallow groundwater recession exponent [$S_t=(S_{t-1}+1)^a - 1$]
139	Natural grassland	88	0.00	0.00	14.81	49.4	B	0.04	0.80	0.85	3.0	0.75	36	48	0.17	0.81	0.20	0.85	0.80	0.60	3	3	1.00	10	0.01	0.05	0.05
140	Natural grassland	155	0.00	0.00	15.50	49.4	B	0.04	0.80	0.85	3.0	0.75	36	48	0.14	0.81	0.20	0.85	0.80	0.60	3	3	1.00	11	0.01	0.05	0.05
141	Open water	16	0.00	0.00	15.50	49.4	B	0.00	9.99	1.00	3.0	1.00	24	24	0.13	1.00	1.00	1.00	0.10	0.05	16	16	1.00	10	0.01	0.01	0.05
142	Riparian vegetation	118	0.00	0.00	15.36	49.4	A	0.08	0.80	0.96	3.0	0.75	30	180	0.12	0.81	0.20	0.85	0.80	0.60	1	1	1.00	10	0.01	0.01	0.05
143	Urban large landscaping	176	0.00	0.29	15.90	49.4	C	0.02	0.80	0.87	3.0	0.75	18	72	0.10	0.85	0.20	0.90	0.80	0.60	4	3	0.70	11	1.00	0.2	0.05
144	Natural grassland	640	0.00	0.00	16.41	49.4	C	0.04	0.80	0.85	3.0	0.75	36	48	0.14	0.81	0.20	0.85	0.80	0.60	3	3	1.00	9	0.01	0.05	0.05
145	Commercial	91	0.30	0.12	15.50	49.4	C	0.01	0.20	0.65	3.0	0.75	18	72	0.12	0.81	0.20	0.90	0.80	0.60	4	3	0.03	9	1.00	0.2	0.05
146	Natural grassland	37	0.00	0.00	15.50	49.4	C	0.04	0.80	0.85	3.0	0.75	36	48	0.12	0.81	0.20	0.85	0.80	0.60	3	3	1.00	11	0.01	0.05	0.05
147	Urban large landscaping	124	0.00	0.29	15.50	49.4	C	0.02	0.80	0.87	3.0	0.75	18	72	0.14	0.85	0.20	0.90	0.80	0.60	4	3	0.70	11	1.00	0.2	0.05
148	Industrial	222	0.30	0.09	15.05	49.4	C	0.00	0.20	0.65	3.0	0.75	18	72	0.15	0.81	0.20	0.90	0.80	0.60	4	3	0.03	12	1.00	0.2	0.05
149	Urban vacant	202	0.40	0.02	14.61	49.4	B	0.00	0.20	0.55	3.0	0.75	30	72	0.18	0.81	0.20	0.90	0.80	0.60	4	3	0.03	12	1.00	0.2	0.05
150	Commercial	219	0.30	0.12	14.50	49.4	C	0.01	0.20	0.65	3.0	0.75	18	72	0.18	0.81	0.20	0.90	0.80	0.60	4	3	0.03	9	1.00	0.2	0.05
151	Natural grassland	93	0.00	0.00	14.50	49.4	C	0.04	0.80	0.85	3.0	0.75	36	48	0.16	0.81	0.20	0.85	0.80	0.60	3	3	1.00	11	0.01	0.05	0.05
152	Commercial	118	0.30	0.12	14.50	49.4	C	0.01	0.20	0.65	3.0	0.75	18	72	0.15	0.81	0.20	0.90	0.80	0.60	4	3	0.03	9	1.00	0.2	0.05
153	Urban residential	22	0.25	0.18	15.52	49.4	C	0.04	0.35	0.80	3.0	0.75	18	72	0.15	0.81	0.20	0.80	0.80	0.60	4	2	0.07	10	1.00	0.2	0.05
154	Commercial	559	0.30	0.12	15.57	49.4	C	0.01	0.20	0.65	3.0	0.75	18	72	0.20	0.81	0.20	0.90	0.80	0.60	4	3	0.03	10	0.50	0.2	0.05
155	Open water	37	0.00	0.00	16.61	49.4	C	0.00	9.99	1.00	3.0	1.00	24	24	0.14	1.00	1.00	1.00	0.10	0.05	16	16	1.00	10	0.01	0.01	0.05
156	Natural grassland	303	0.00	0.00	15.50	49.4	C	0.04	0.80	0.85	3.0	0.75	36	48	0.14	0.81	0.20	0.85	0.80	0.60	3	3	1.00	11	0.01	0.05	0.05
157	Rural residential	87	0.10	0.10	23.00	49.4	C	0.04	0.90	0.92	3.0	0.75	18	72	0.13	0.81	0.20	0.75	0.80	0.60	4	3	1.00	10	0.10	0.01	0.05
158	Rural residential	306	0.10	0.10	21.30	49.4	C	0.04	0.90	0.92	3.0	0.75	18	72	0.14	0.81	0.20	0.75	0.80	0.60	4	3	1.00	11	0.10	0.01	0.05
159	Natural grassland	703	0.00	0.00	21.29	49.4	C	0.04	0.80	0.85	3.0	0.75	36	48	0.14	0.81	0.20	0.85	0.80	0.60	3	3	1.00	11	0.01	0.05	0.05
160	Commercial	127	0.30	0.12	13.86	49.4	C	0.01	0.20	0.65	3.0	0.75	18	72	0.14	0.81	0.20	0.90	0.80	0.60	4	3	0.03	3	1.00	0.2	0.05
161	Commercial	426	0.30	0.12	14.18	49.4	C	0.01	0.20	0.65	3.0	0.75	18	72	0.14	0.81	0.20	0.90	0.80	0.60	4	3	0.03	4	1.00	0.2	0.05
162	Commercial	338	0.30	0.12	20.18	49.4	C	0.01	0.20	0.65	3.0	0.75	18	72	0.16	0.81	0.20	0.90	0.80	0.60	4	3	0.03	4	1.00	0.2	0.05
163	Urban large landscaping	100	0.00	0.29	20.65	49.4	A	0.02	0.80	0.87	3.0	0.75	18	72	0.14	0.85	0.20	0.90	0.80	0.60	4	3	0.70	10	1.00	0.2	0.05
164	Commercial	831	0.30	0.12	17.28	49.4	C	0.01	0.20	0.65	3.0	0.75	18	72	0.11	0.81	0.20	0.90	0.80	0.60	4	3	0.03	1	1.00	0.2	0.05
165	Commercial	1,209	0.30	0.12	15.80	49.4	C	0.01	0.20	0.65	3.0	0.75	18	72	0.17	0.81	0.20	0.90	0.80	0.60	4	3	0.03	5	1.00	0.2	0.05
166	Natural grassland	5,313	0.00	0.00	24.70	49.4	C	0.04	0.80	0.85	3.0	0.75	36	48	0.15	0.81	0.20	0.85	0.80	0.60	3	3	1.00	8	0.01	0.05	0.05
167	Urban residential	1,237	0.25	0.18	22.56	49.4	C	0.04	0.35	0.80	3.0	0.75	18	72	0.16	0.81	0.20	0.80	0.80	0.60	4	2	0.07	8	0.01	0.2	0.05
168	Urban residential	7,720	0.25	0.18	17.50	49.4	D	0.04	0.35	0.80	3.0	0.75	18	72	0.14	0.81	0.20	0.80	0.80	0.60	4	2	0.07	13	1.00	0.2	0.05
169	Natural grassland	631	0.00	0.00	18.00	49.4	C	0.04	0.80	0.85	3.0	0.75	36	48	0.14	0.81	0.20	0.85	0.80	0.60	3	3	1.00	11	0.01	0.05	0.05
170	Natural trees & shrubs	371	0.00	0.00	21.50	49.4	C	0.08	0.80	0.85	3.0	0.75	36	84	0.14	0.81	0.20	0.85	0.80	0.60	8	8	1.00	11	0.01	0.05	0.05
171	Natural trees & shrubs	1,452	0.00	0.00	24.50	49.4	C	0.08	0.80	0.85	3.0	0.75	36	84	0.14	0.81	0.20	0.85	0.80	0.60	8	8	1.00	11	0.01	0.05	0.05
172	Rural residential	1,274	0.10	0.10	28.00	49.4	C	0.04	0.90	0.92	3.0	0.75	18	72	0.14	0.81	0.20	0.75	0.80	0.60	4	3	1.00	11	0.10	0.01	0.05
173	Natural grassland	1,198	0.00	0.00	24.50	49.4	C	0.04	0.80	0.85	3.0	0.75	36	48	0.14	0.81	0.20	0.85	0.80	0.60	3	3	1.00	11	0.01	0.05	0.05
174	Natural trees & shrubs	531	0.00	0.00	32.00	49.4	C	0.08	0.80	0.85	3.0	0.75	36	84	0.14	0.81	0.20	0.85	0.80	0.60	8	8	1.00	11	0.01	0.05	0.05

ET = evapotranpiration
ET_0 = reference evapotranspiration
NRCS = Natural Resources Consdrvation Service
AET = actual evapotranspiration
in = inches
in/d = inches per day
in/in = inches per inch
yr = year
ac = acres

Table 3-2 Monthly Crop Coefficients for Vegetation Types Simulated by the Recharge Program

Vegetation Type	JAN	FEB	MAR	APR	MAY	JUN	JUL	AUG	SEP	OCT	NOV	DEC
Natural												
Riparian phreatophytes[1]	0.75	0.75	0.75	0.75	0.85	1.00	1.10	1.10	1.10	0.95	0.85	0.75
Grass[2]	1.00	1.00	1.00	1.00	1.00	1.00	1.00	1.00	1.00	1.00	1.00	1.00
Brush and trees[3]	0.80	0.80	0.80	0.80	0.80	0.80	0.80	0.80	0.80	0.80	0.80	0.80
Water[4]	1.13	1.13	1.13	1.13	1.13	1.13	1.13	1.13	1.13	1.13	1.13	1.13
Urban[5]												
Rural residential	0.80	0.80	0.80	0.80	0.80	0.80	0.80	0.80	0.80	0.80	0.80	0.80
Commercial	0.80	0.80	0.80	0.80	0.80	0.80	0.80	0.80	0.80	0.80	0.80	0.80
Industrial	0.80	0.80	0.80	0.80	0.80	0.80	0.80	0.80	0.80	0.80	0.80	0.80
Lawn, golf course, sod farm	0.80	0.80	0.80	0.80	0.80	0.80	0.80	0.80	0.80	0.80	0.80	0.80
Residential	0.80	0.80	0.80	0.80	0.80	0.80	0.80	0.80	0.80	0.80	0.80	0.80
Vacant or paved	0.80	0.80	0.80	0.80	0.80	0.80	0.80	0.80	0.80	0.80	0.80	0.80

Data Sources and Assumptions

ET - evapotranspiration

ET_o - reference evapotranspiration

Kc - crop coefficient

[1] Assume mostly trees (cottonwood, sycamore, willow), deciduous with shrub willow understory (willow Kc in winter). Monthly Kc values reflect total canopy leaf area and unrestricted root access to water.

[2] Similar to reference ET conditions in winter. Annual grasses deplete soil moisture in summer until soil is dry, so summer Kc not important.

[3] Kc less that 1.0 because of drought-tolerant adaptation to carry some soil moisture over to following year (Blaney and others, 1963). Soil moisture depletion in summer is not as extreme as for annual grasses.

[4] Evaporation estimated as average ratio of pan evaporation to ETo (1.26) multiplied by a pan-to-lake coefficient of 0.9 (for a pond or small lake).

[5] Irrigation in all urban land use categories assumed to be for turf. Turf Kc from Basic Irrigation Scheduling software (Snyder and others, 2007).

Table 3-3 Sources of Stream Flow Data for Tributary Watersheds

Watershed Map ID	Stream Name	Data for Natural Flow	Data for Supplemental Flow (MAR)	Notes
1	CALERA CREEK	Correlation with Thompson, Berryessa & Penitencia	No supplemental flow	
2	TULARCITOS CREEK	Correlation with Thompson, Berryessa & Penitencia	No supplemental flow	
3	LOS COCHES CREEK	Correlation with Thompson, Berryessa & Penitencia	Measured facility recharge	
4	PIEDMONT CREEK	Correlation with Thompson, Berryessa & Penitencia	No supplemental flow	
5	BERRYESSA CREEK	Gage 64 minus measured facility recharge	Measured facility recharge	Missing record cfs = 1.75 * (Penitencia-correlated flow) + 2.5
6	CROSSLEY CREEK	Correlation with Thompson, Berryessa & Penitencia	No supplemental flow	
7	SIERRA CREEK	Correlation with Thompson, Berryessa & Penitencia	No supplemental flow	
8	UPPER PENITENCIA CREEK	Gage 83	Gage 1 minus gage 83	
9	MIGUELITA CREEK	Correlation with Thompson, Berryessa & Penitencia	No supplemental flow	
10	NORTH BABB CREEK	Correlation with Thompson, Berryessa & Penitencia	No supplemental flow	
11	SOUTH BABB CREEK	Correlation with Thompson, Berryessa & Penitencia	No supplemental flow	
12	FLINT CREEK	Correlation with Thompson, Berryessa & Penitencia	No supplemental flow	
13	RUBY CREEK	Correlation with Thompson, Berryessa & Penitencia	No supplemental flow	
14	NORWOOD CREEK	Correlation with Thompson, Berryessa & Penitencia	No supplemental flow	
15	QUIMBY CREEK	Correlation with Thompson, Berryessa & Penitencia	No supplemental flow	
16	FOWLER CREEK EXISTING	Correlation with Thompson, Berryessa & Penitencia	No supplemental flow	
17	EVERGREEN CREEK	Correlation with Thompson, Berryessa & Penitencia	No supplemental flow	
18	YERBA BUENA CREEK	Correlation with Thompson, Berryessa & Penitencia	No supplemental flow	
19	THOMPSON CREEK	Gage 75	No supplemental flow	
20	UPPER SILVER CREEK	Correlation with Thompson, Berryessa & Penitencia	No supplemental flow	
21	COYOTE CREEK BRANCH G	Correlation with Thompson, Berryessa & Penitencia	No supplemental flow	
22	COYOTE CREEK BRANCH F	Correlation with Thompson, Berryessa & Penitencia	No supplemental flow	
23	METCALF CREEK	Correlation with Thompson, Berryessa & Penitencia	No supplemental flow	
24	COYOTE CREEK	Gage 7 plus gage 10	Included in gaged flows	Missing record 1985-1988 set = average monthly values
25	CANOAS CREEK	Correlation with Thompson, Berryessa & Penitencia	No supplemental flow	
26	SANTA TERESA CREEK	Correlation with Thompson, Berryessa & Penitencia	No supplemental flow	
27	CALERO CREEK	Gage 13 (includes Calero Reservoir releases)	Measured facility recharge	
28	ALAMITOS CREEK	Gage 16	Measured facility recharge (Alamitos Creek)	
29	RANDOL CREEK	Correlation with Ross, Smith and San Tomas Aquino	No supplemental flow	
30	GREYSTONE CREEK	Correlation with Ross, Smith and San Tomas Aquino	No supplemental flow	
31	GOLF CREEK	Correlation with Ross, Smith and San Tomas Aquino	No supplemental flow	
32	GUADALUPE CREEK	Gage 43 (includes Guadalupe Reservoir releases)	No supplemental flow from pipeline	
33	ROSS CREEK	Gage 21	Measured facility recharge	
34	LOS GATOS CREEK	Gage 67 (includes reservoir releases)	No supplemental flow from pipeline	
35	SMITH CREEK	Correlation with Ross and San Tomas Aquino	1/3 of pipeline discharge to Smith, Wildcat and San Tomas	Gage 27 is at downstream end of Smith Creek.
36	SAN TOMAS AQUINO CREEK	Gage 29	1/3 of pipeline discharge to Smith, Wildcat and San Tomas	Supplemental flow is just above Wildcat confluence.
37	WILDCAT CREEK	Gage 30	1/3 of pipeline discharge to Smith, Wildcat and San Tomas	
38	SARATOGA CREEK	Gage 25 (= USGS 1169500)	Measured facility recharge enters 2 mi below model boundary.	
39	RODEO CREEK	Correlation with Ross, Smith and San Tomas Aquino	Measured facility recharge enters 1.2 mi below model boundary.	
40	CALABAZAS CREEK	Correlation with Ross, Smith and San Tomas Aquino	Measured facility recharge enters 0.3 mi below model boundary.	
41	REGNART CREEK	Correlation with Ross, Smith and San Tomas Aquino	Measured facility recharge enters 0.5 mi below model boundary.	
42	STEVENS CREEK	Gage 44 (includes reservoir releases)	Assume facility recharge equals reservoir release.	
43	PERMANENTE CREEK	Gage 32.1 minus measured facility recharge	Measured facility recharge	
44	HALE CREEK	Gage 33	Measured facility recharge	
45	ADOBE CREEK	Correlation with Ross, Smith and San Tomas Aquino	Measured facility recharge	
46	BARRON CREEK	Correlation with Ross, Smith and San Tomas Aquino	No supplemental flow	
47	MATADERO CREEK	USGS gage 11166000	No supplemental flow	
48	SAN FRANCISQUITO CREEK	USGS gage 11164500	No supplemental flow	

MAR - managed aquifer recharge
USGS - United States Geological Survey

Table 3-4 Annual Groundwater Balances 1985-2014

	Calendar Year														
	1985	1986	1987	1988	1989	1990	1991	1992	1993	1994	1995	1996	1997	1998	1999
Inflows (acre-feet)															
Inflow from San Francisco Bay	1,160	1,007	884	1,649	419	335	332	431	587	442	659	695	766	942	735
Inflow across inland boundaries	14,727	16,282	16,391	17,232	14,474	12,387	12,384	11,591	10,798	10,116	9,547	9,315	9,200	8,627	9,725
Percolation from streams	56,016	96,676	48,508	44,472	49,226	48,224	43,846	52,359	85,732	52,006	107,132	97,162	88,655	102,428	63,472
MAR pond percolation	36,192	67,324	40,492	32,104	51,868	44,186	37,849	35,358	44,573	55,494	54,226	45,550	45,048	37,885	48,411
Dispersed recharge	36,915	65,275	35,962	36,377	31,688	30,458	33,404	50,788	78,687	30,268	76,891	46,342	44,191	97,634	25,387
Total	145,010	246,564	142,236	131,833	147,675	135,589	127,814	150,527	220,376	148,325	248,455	199,064	187,860	247,516	147,730
Outflows (acre-feet)															
Outflow to San Francisco Bay	1,174	1,480	1,107	821	941	886	974	1,205	1,724	1,261	2,034	1,924	2,168	2,681	2,124
Outflow across inland boundaries	1,873	2,194	1,776	1,669	1,453	1,254	1,294	1,543	2,085	1,764	2,538	2,607	2,548	3,045	2,557
Groundwater pumping	173,072	169,940	163,442	162,636	86,609	104,230	90,348	103,388	101,201	117,916	107,562	107,909	116,089	97,316	105,461
Groundwater seepage to streams	13,096	21,938	12,087	9,667	9,181	12,894	16,590	25,231	43,964	28,215	55,092	42,833	45,418	71,990	42,684
Riparian evapotranspiration	5,569	5,745	5,569	5,961	5,577	5,602	5,442	5,831	5,520	5,367	5,460	5,824	6,096	5,077	5,181
Total	194,785	201,297	183,981	180,755	103,762	124,867	114,648	137,198	154,495	154,524	172,687	161,097	172,320	180,109	158,007
Net Storage Change (acre-feet)															
Inflows - outflows	-50,166	45,268	-41,745	-48,916	43,912	10,723	13,166	13,586	65,882	-6,199	75,769	37,968	15,541	67,407	-10,276

	Calendar Year														
	2000	2001	2002	2003	2004	2005	2006	2007	2008	2009	2010	2011	2012	2013	2014
Inflows (acre-feet)															
Inflow from San Francisco Bay	827	753	685	686	702	800	933	704	715	718	738	691	614	633	623
Inflow across inland boundaries	6,713	6,983	7,528	7,243	7,377	6,308	4,835	6,096	6,063	5,751	5,406	4,920	5,985	6,244	10,758
Percolation from streams	77,178	72,708	61,728	63,146	65,375	77,800	80,193	42,904	60,848	64,975	77,680	75,846	56,167	58,320	25,972
MAR pond percolation	49,711	45,217	34,767	41,151	37,995	32,559	34,935	33,466	27,207	39,068	32,101	30,741	30,411	32,585	5,162
Dispersed recharge	40,960	29,413	23,146	22,180	29,135	77,665	73,845	14,921	20,788	23,171	36,363	22,602	18,678	10,686	21,979
Total	175,390	155,074	127,854	134,406	140,583	195,131	194,742	98,091	115,621	133,683	152,287	134,800	111,855	108,468	64,494
Outflows (acre-feet)															
Outflow to San Francisco Bay	2,276	2,201	2,055	2,075	2,011	2,493	2,795	2,103	2,122	2,062	2,264	2,387	2,128	2,142	1,945
Outflow across inland boundaries	2,492	2,339	2,345	2,296	2,236	2,690	2,895	2,208	2,271	2,225	2,406	2,608	2,437	2,267	2,048
Groundwater pumping	108,476	109,898	100,027	93,042	101,749	83,134	76,070	104,357	104,036	95,427	83,488	69,260	73,379	92,546	111,269
Groundwater seepage to streams	48,648	41,726	33,996	35,667	35,874	60,478	76,170	41,028	34,887	33,885	42,597	43,751	40,484	36,978	25,375
Riparian evapotranspiration	5,583	5,573	5,655	5,465	5,431	5,156	4,886	5,128	5,519	5,069	5,058	5,327	5,366	5,805	5,687
Total	167,475	161,737	144,079	138,546	147,302	153,951	162,816	154,824	148,835	138,666	135,813	123,333	123,794	139,738	146,324
Net Storage Change (acre-feet)															
Inflows - outflows	20,694	1,354	-12,527	111	-2,212	58,270	54,414	-54,804	-34,098	-5,746	20,868	17,764	-8,424	-31,456	-85,775

MAR - managed aquifer recharge

Excludes the San Mateo County subarea of the model.

Table 4-1 Wells Responsible for Most of the 100 Largest Residuals in Each Layer

Layer and Well	Layer and Well
Model Layer 1	**Model Layer 5**
8S/1W-3K13	7S/1W-22E2
8S/1E-5N2	7S/1E-19B3 (Willow)
7S/1W-30C2	7S/1E-16C6
8S/1E-10J2	7S/1W-5P2
	7S/1W-4E2
Model Layer 3	
7S/1W-9Q1	**Model Layer 6**
7S/1W-15E1	7S/1E-9L4 (CCOC)
7S/1E-19B5 (Willow)	7S/1W-3H2
7S/1W-35L14 (McGlincey)	6S/1W-26R1 (Guadalupe)
Model Layer 4	
7S/1W-29C4 (Saratoga)	
7S/1E-19B4 (Willow)	
7S/1E-9L7 (CCOC)	
7S/1E-2J6	

Note: Few wells are completed in model layer 2.

Figures

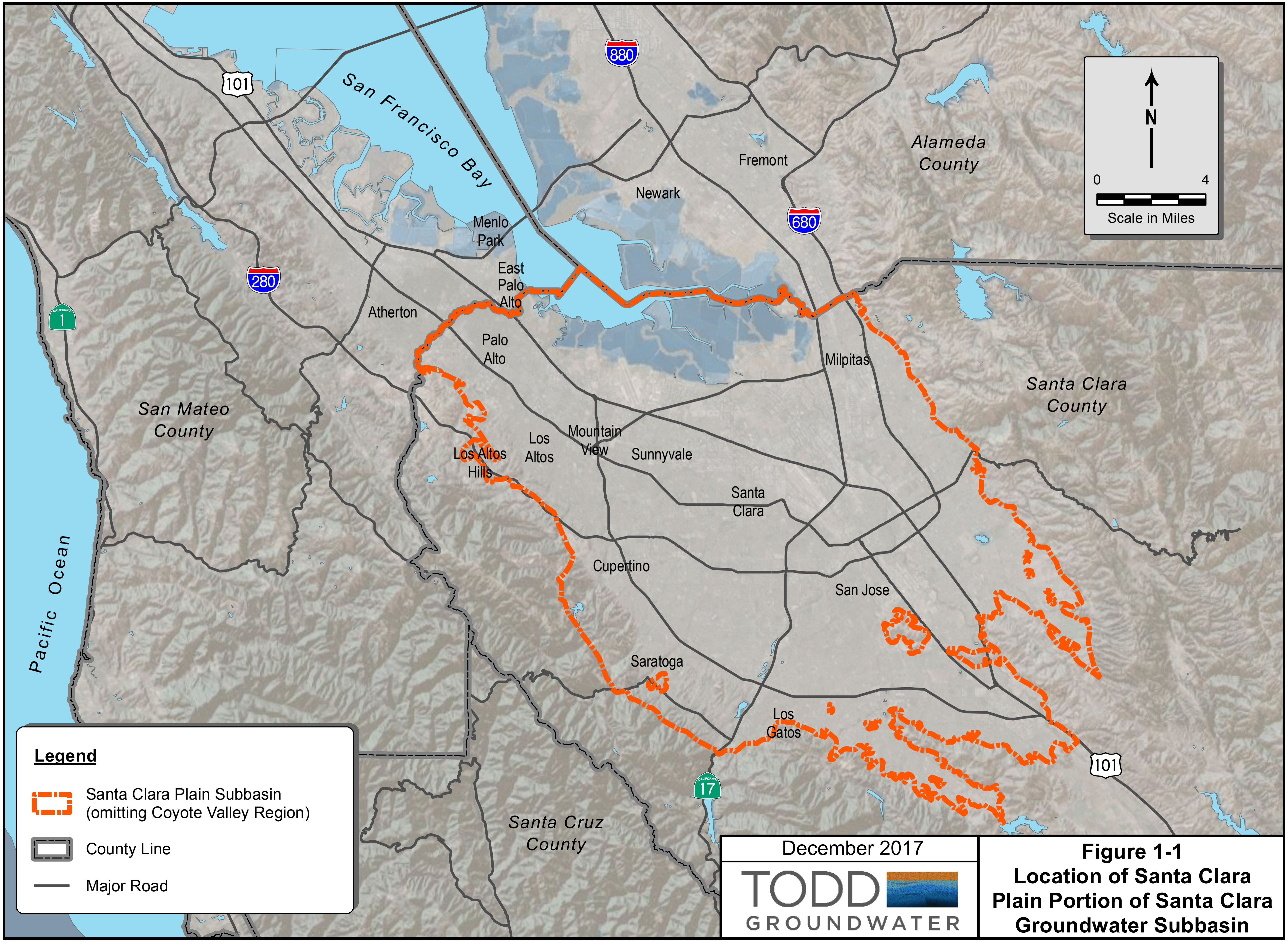

Figure 1-1
Location of Santa Clara Plain Portion of Santa Clara Groundwater Subbasin

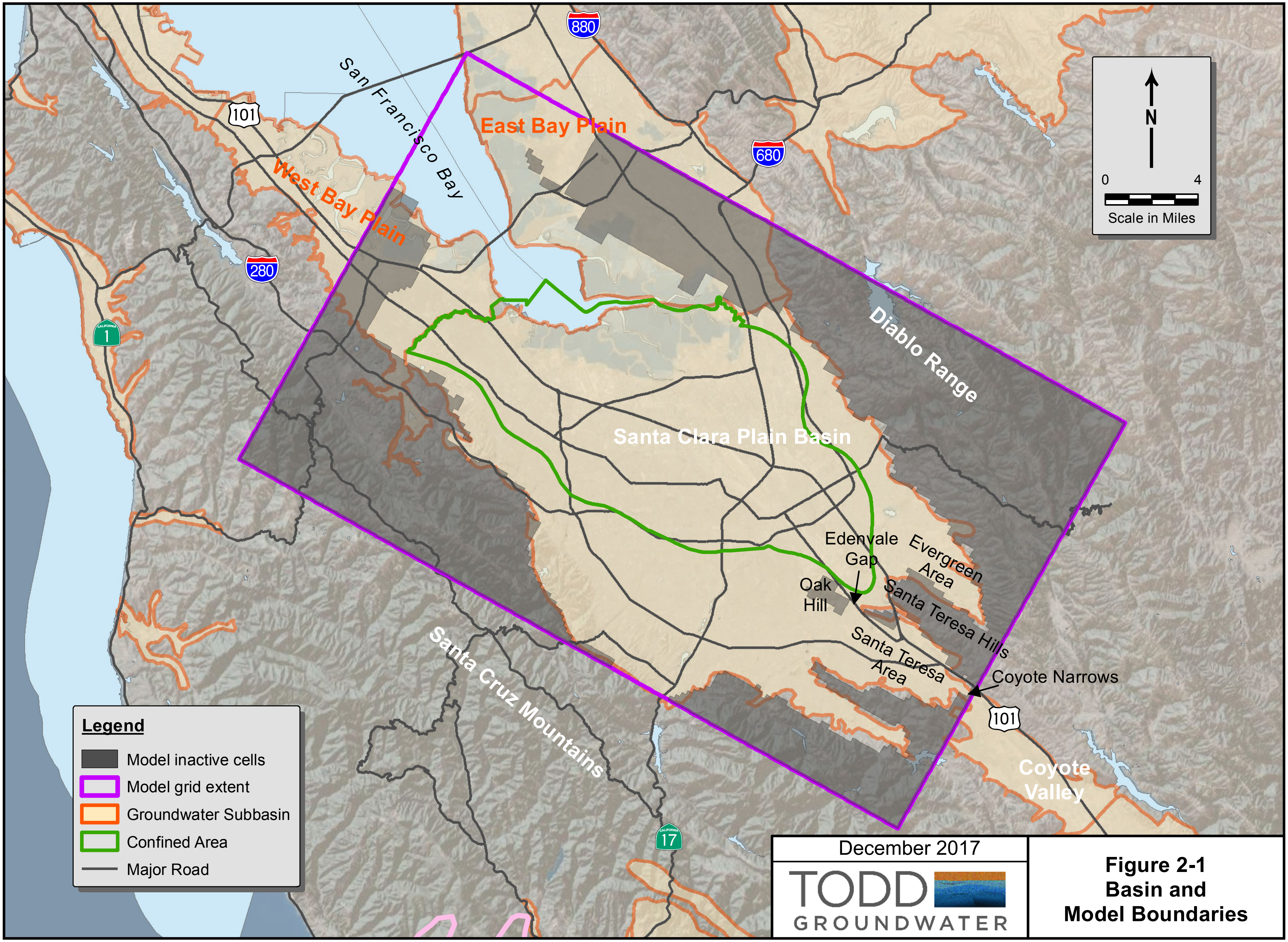

December 2017

TODD GROUNDWATER

Figure 2-1
Basin and
Model Boundaries

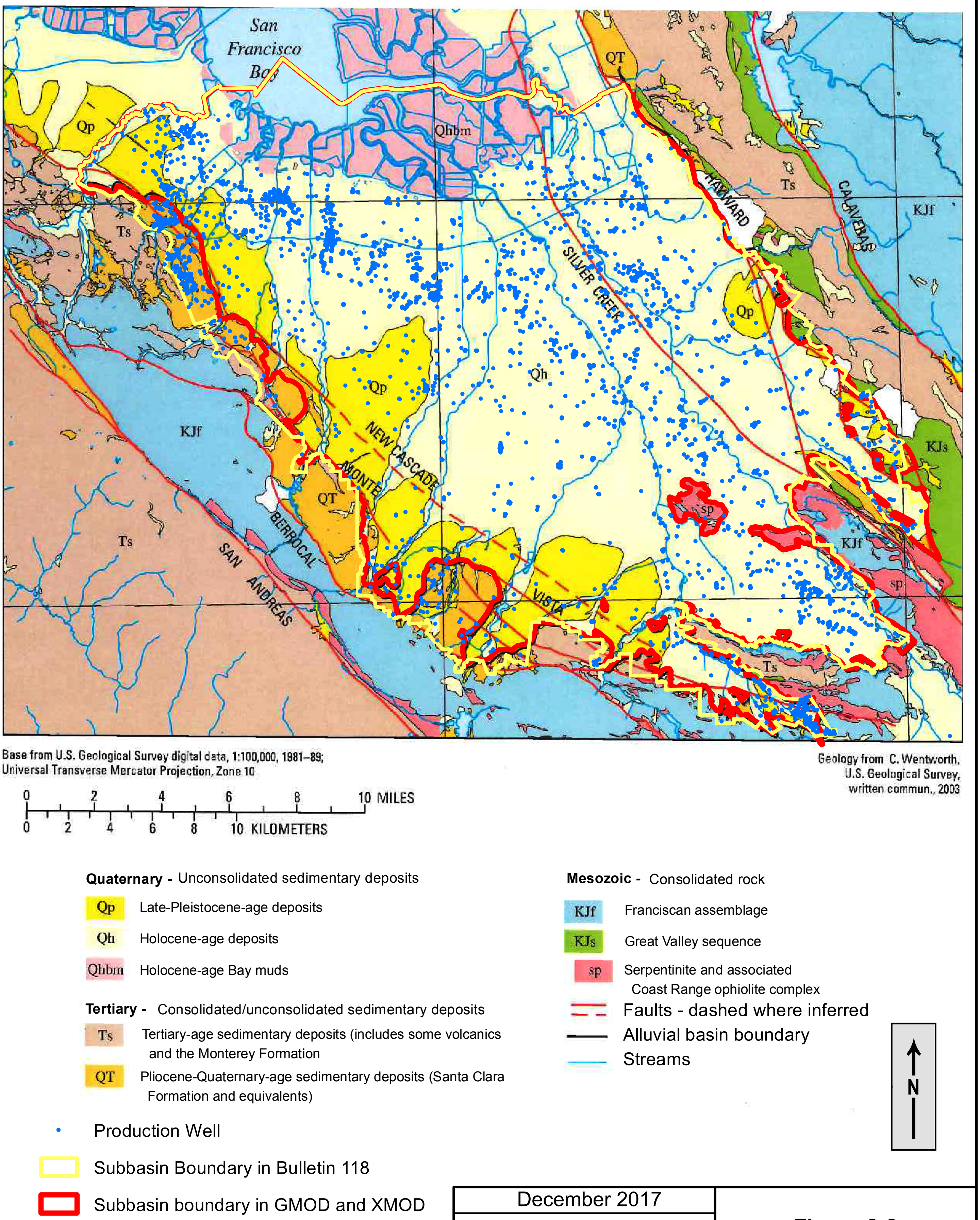
San Francisco Bay
Qp
Qhbm
QT
Ts
HAYWARD
CALAVERAS
KJf
SILVER CREEK
Qp
Qh
Qp
NEW CASCADE
MONTE
KJs
KJf
QT
BERROCAL
sp
KJf
Ts
SAN ANDREAS
VISTA
sp
Ts
0 2 4 6 8 10 MILES
0 2 4 6 8 10 KILOMETERS
Quaternary - Unconsolidated sedimentary deposits
Qp Late-Pleistocene-age deposits
Qh Holocene-age deposits
Qhbm Holocene-age Bay muds
Tertiary - Consolidated/unconsolidated sedimentary deposits
Ts Tertiary-age sedimentary deposits (includes some volcanics and the Monterey Formation
QT Pliocene-Quaternary-age sedimentary deposits (Santa Clara Formation and equivalents)
Production Well
Subbasin Boundary in Bulletin 118
Subbasin boundary in GMOD and XMOD
Mesozoic - Consolidated rock
KJf Franciscan assemblage
KJs Great Valley sequence
sp Serpentinite and associated Coast Range ophiolite complex
Faults - dashed where inferred
Alluvial basin boundary
Streams
N

Base from U.S. Geological Survey digital data, 1:100,000, 1981–89;
Universal Transverse Mercator Projection, Zone 10

Geology from C. Wentworth,
U.S. Geological Survey,
written commun., 2003

December 2017

TODD GROUNDWATER

Figure 2-2
Geologic Map

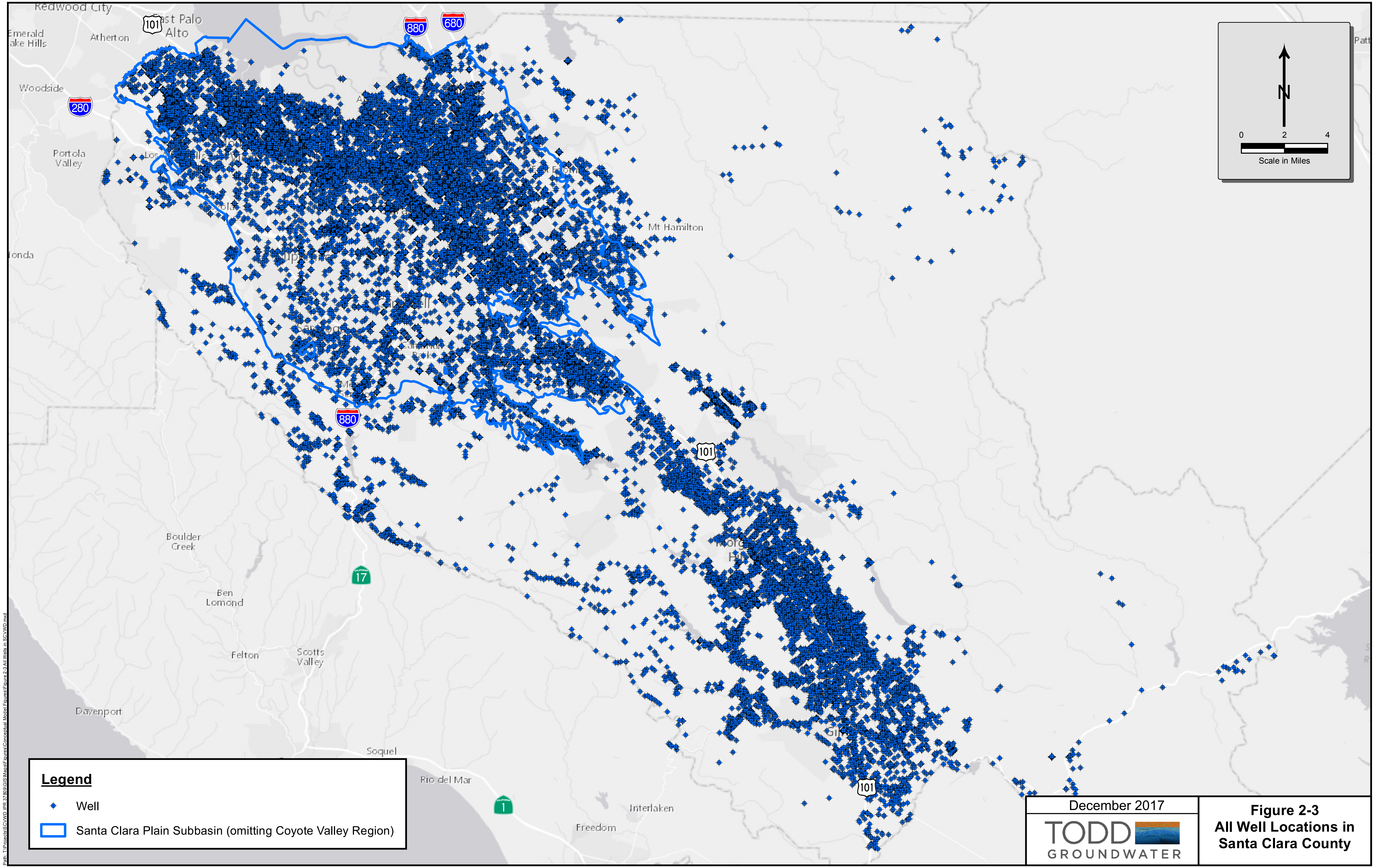

December 2017

Figure 2-3
All Well Locations in
Santa Clara County

Path: T:\Projects\SCVWD IPR 37809\GIS\Maps\Figures\Conceptual Model Figures\Figure 2-3 All Wells in SCVWD.mxd

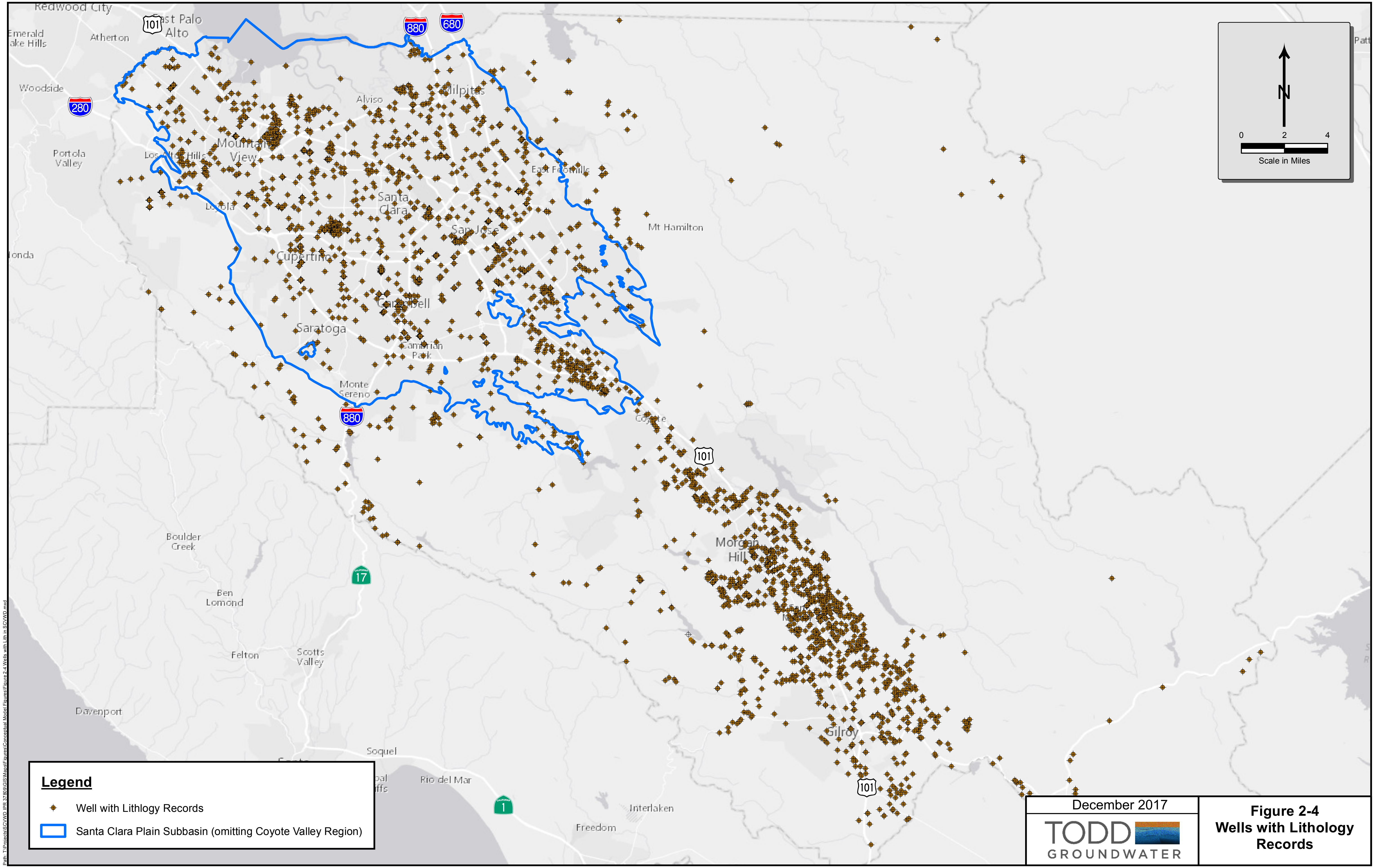

December 2017

Figure 2-4
Wells with Lithology Records

Path: T:\Projects\SCVWD IPR 37809\GIS\Maps\Figures\Conceptual Model Figures\Figure 2-4 Wells with Lith in SCVWD.mxd

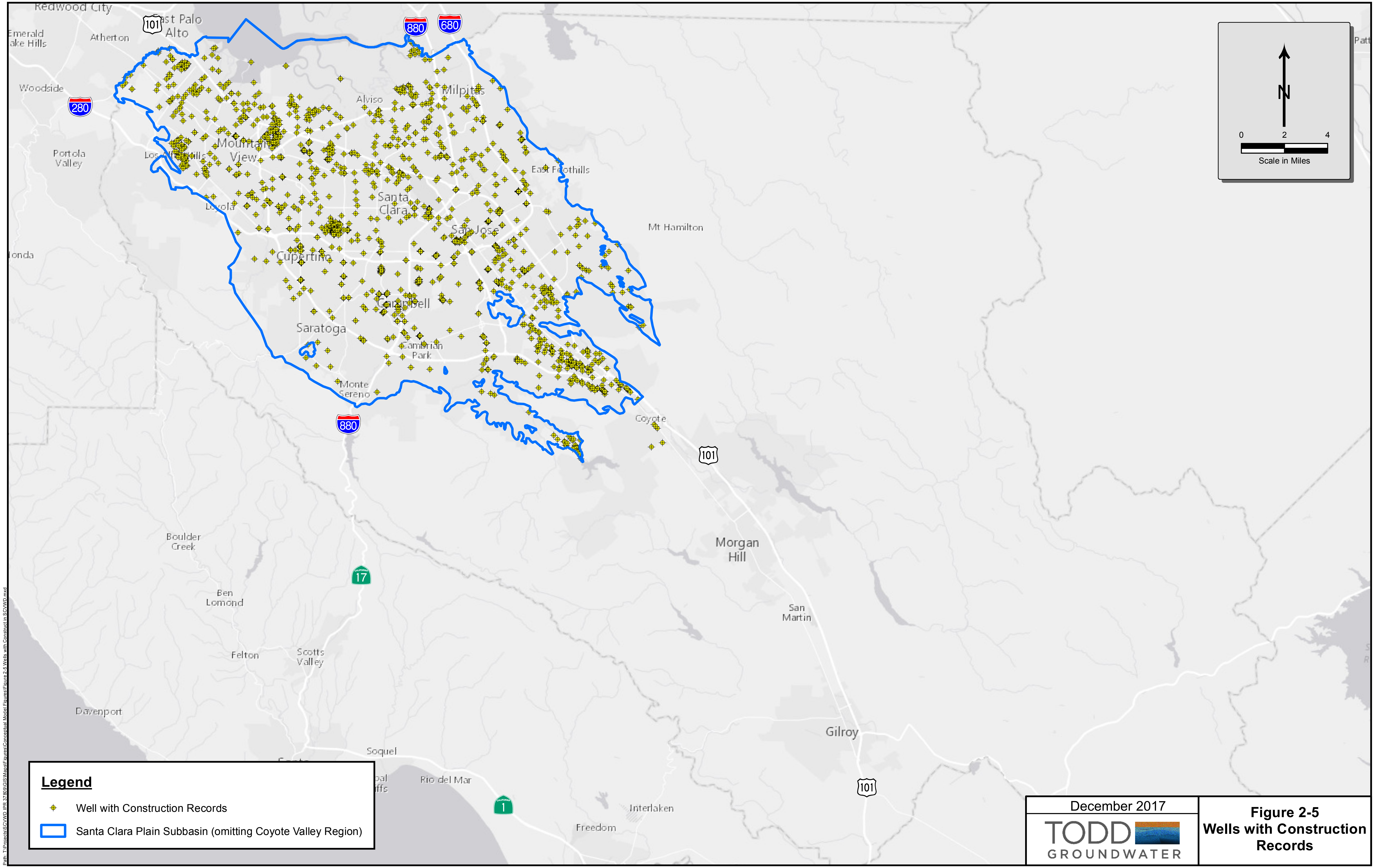

Legend

- ✦ Well with Construction Records
- ▭ Santa Clara Plain Subbasin (omitting Coyote Valley Region)

December 2017

TODD GROUNDWATER

Figure 2-5
Wells with Construction Records

Path: T:\Projects\SCVWD IPR 37809\GIS\Maps\Figures\Conceptual Model Figures\Figure 2-5 Wells with Construct in SCVWD.mxd

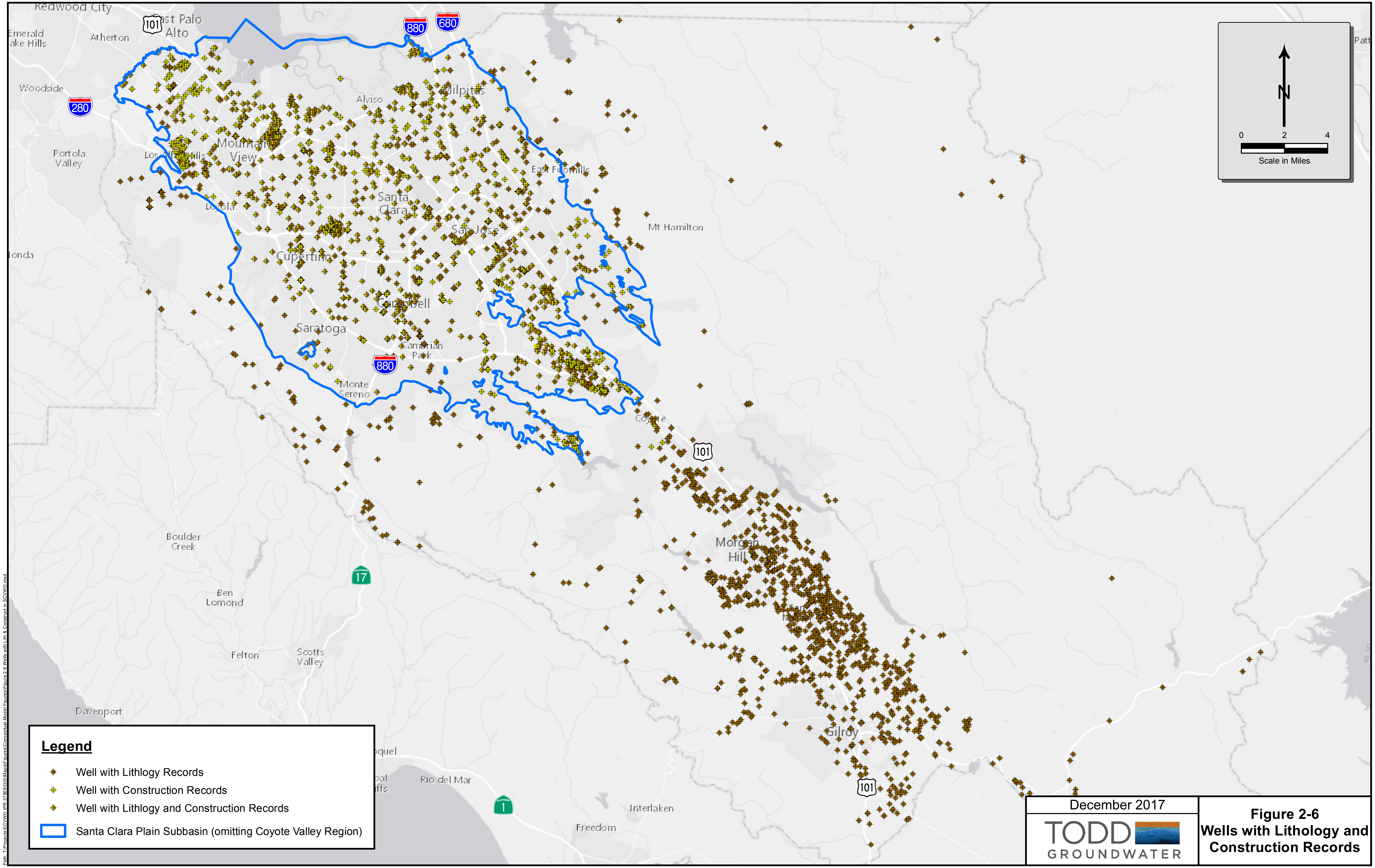

Legend

◆ Well with Lithology Records
◆ Well with Construction Records
◆ Well with Lithology and Construction Records
▭ Santa Clara Plain Subbasin (omitting Coyote Valley Region)

December 2017

TODD GROUNDWATER

Figure 2-6
Wells with Lithology and Construction Records

Path: T:\Projects\SCVWD IPR 37809\GIS\Maps\Figures\Conceptual Model Figures\Figure 2-6 Wells with Lith & Construct in SCVWD.mxd

Path: T:\Projects\SCVWD IPR 37809\GIS\Maps\Figures\Conceptual Model Figures\Figure 2-7 Study Area.mxd

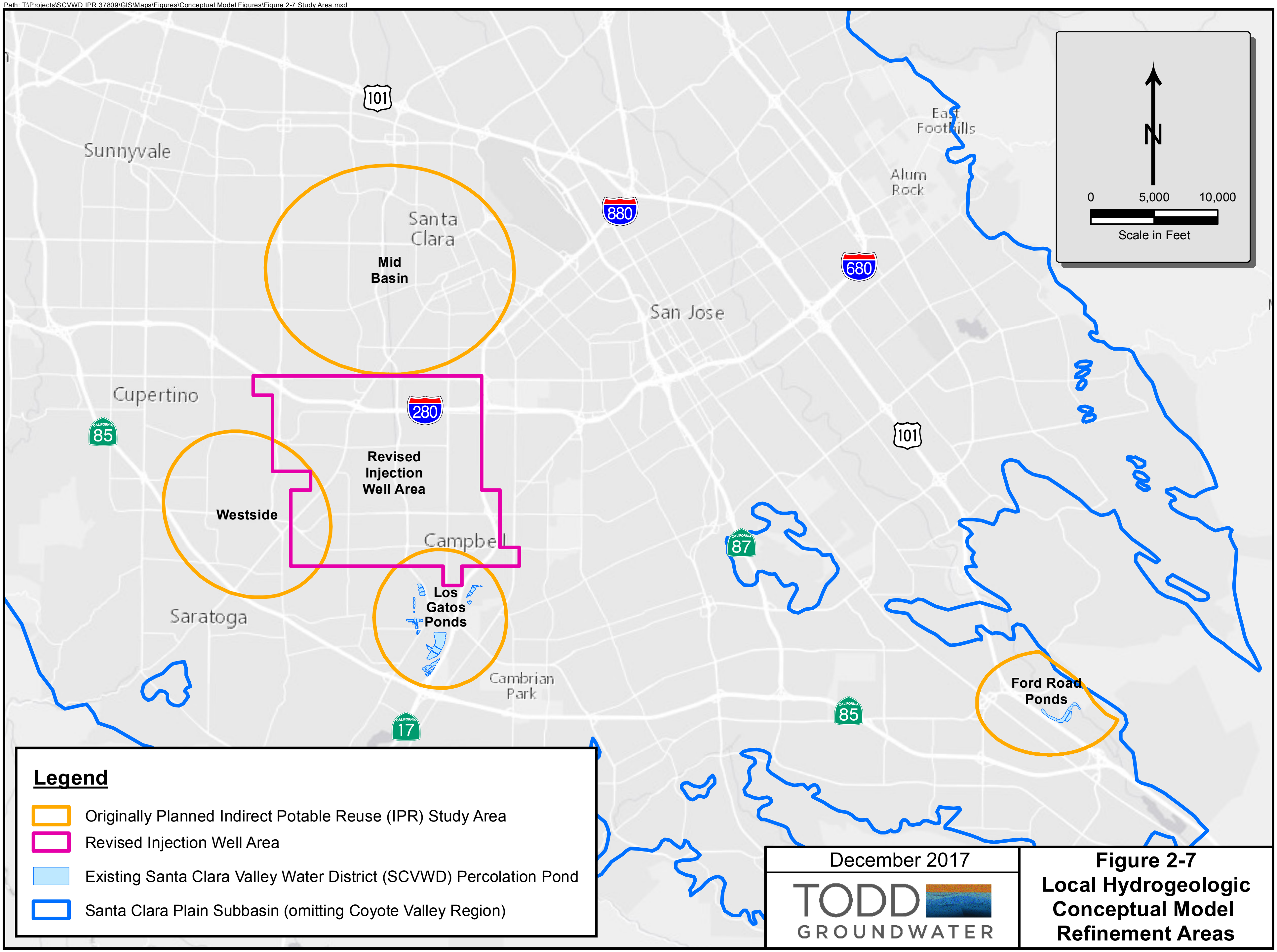

Legend

🟧 Originally Planned Indirect Potable Reuse (IPR) Study Area

🟪 Revised Injection Well Area

🟦 Existing Santa Clara Valley Water District (SCVWD) Percolation Pond

🟦 Santa Clara Plain Subbasin (omitting Coyote Valley Region)

December 2017

TODD GROUNDWATER

Figure 2-7
Local Hydrogeologic Conceptual Model Refinement Areas

Path: T:\Projects\SCVWD IPR 37809\GIS\Maps\Figures\Conceptual Model Figures\Figure 2-8 XS Locations and Orientations.mxd

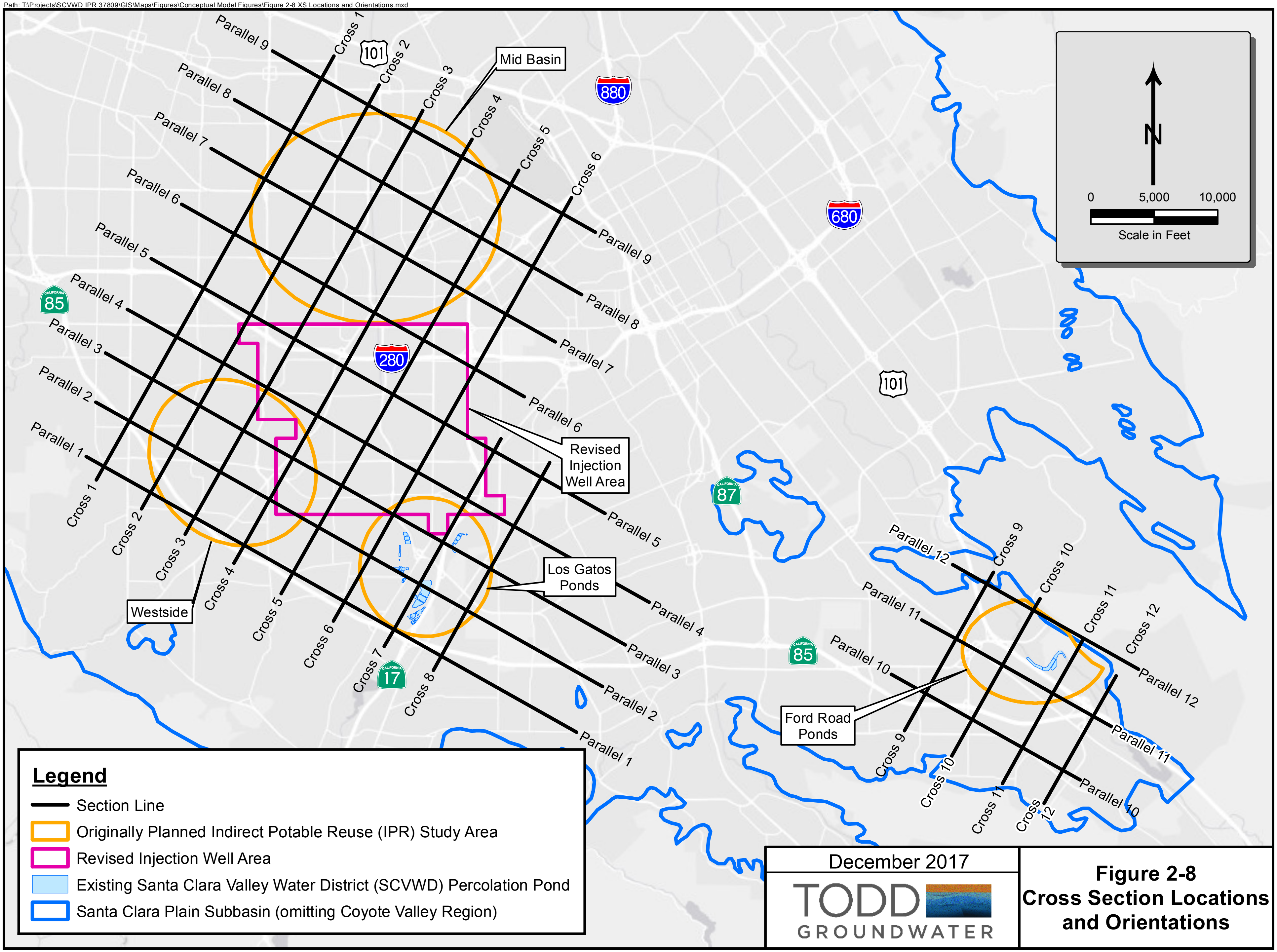

Figure 2-8
Cross Section Locations and Orientations

Path: T:\Projects\SCVWD IPR 37809\GIS\Maps\Figures\Conceptual Model Figures\Figure 2-9 Cross Section Locations w Wells.mxd

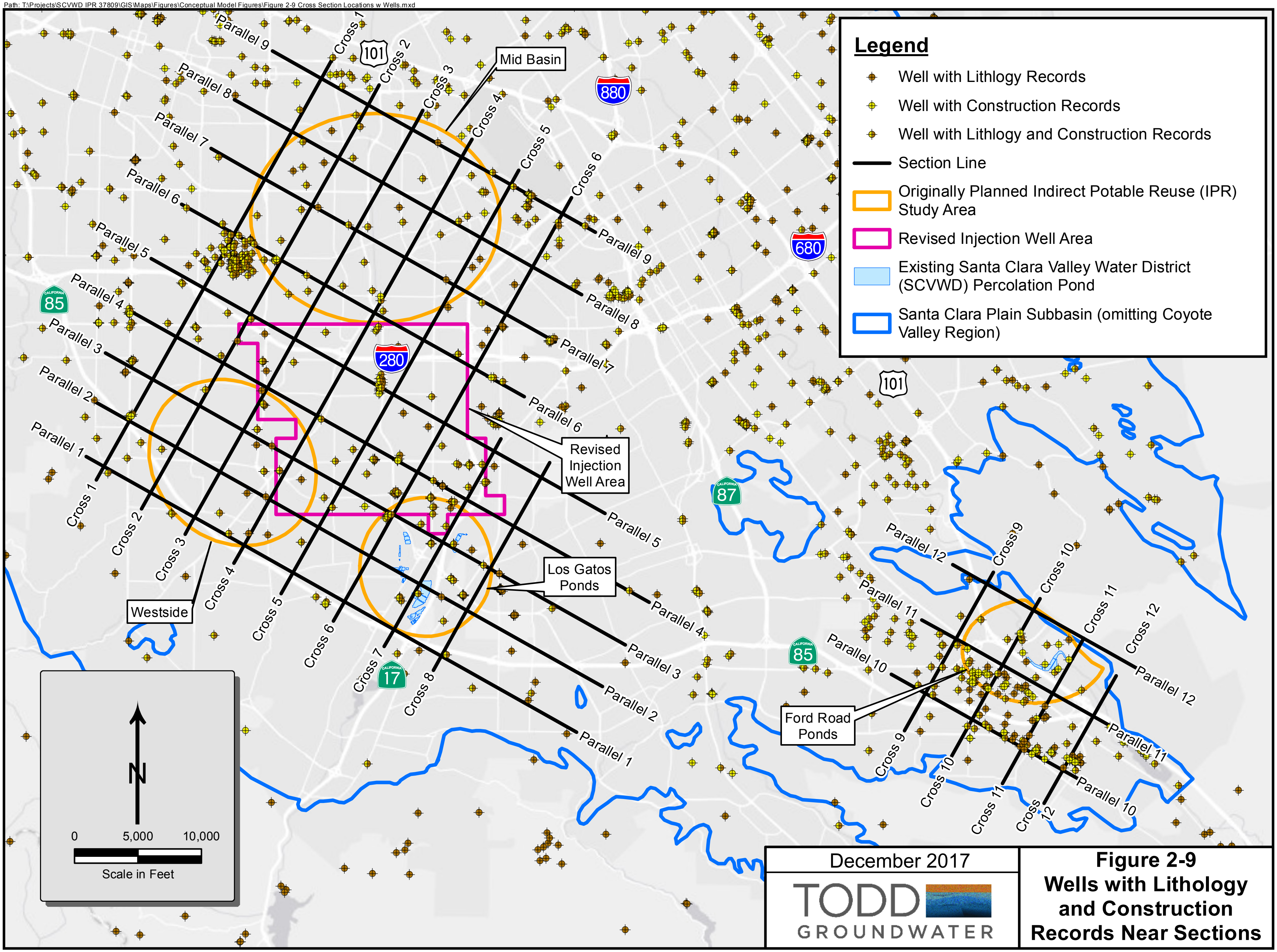

Legend

⌖	Well with Lithology Records
⌖	Well with Construction Records
⌖	Well with Lithology and Construction Records
—	Section Line
▭	Originally Planned Indirect Potable Reuse (IPR) Study Area
▭	Revised Injection Well Area
▭	Existing Santa Clara Valley Water District (SCVWD) Percolation Pond
▭	Santa Clara Plain Subbasin (omitting Coyote Valley Region)

December 2017

TODD GROUNDWATER

Figure 2-9
Wells with Lithology and Construction Records Near Sections

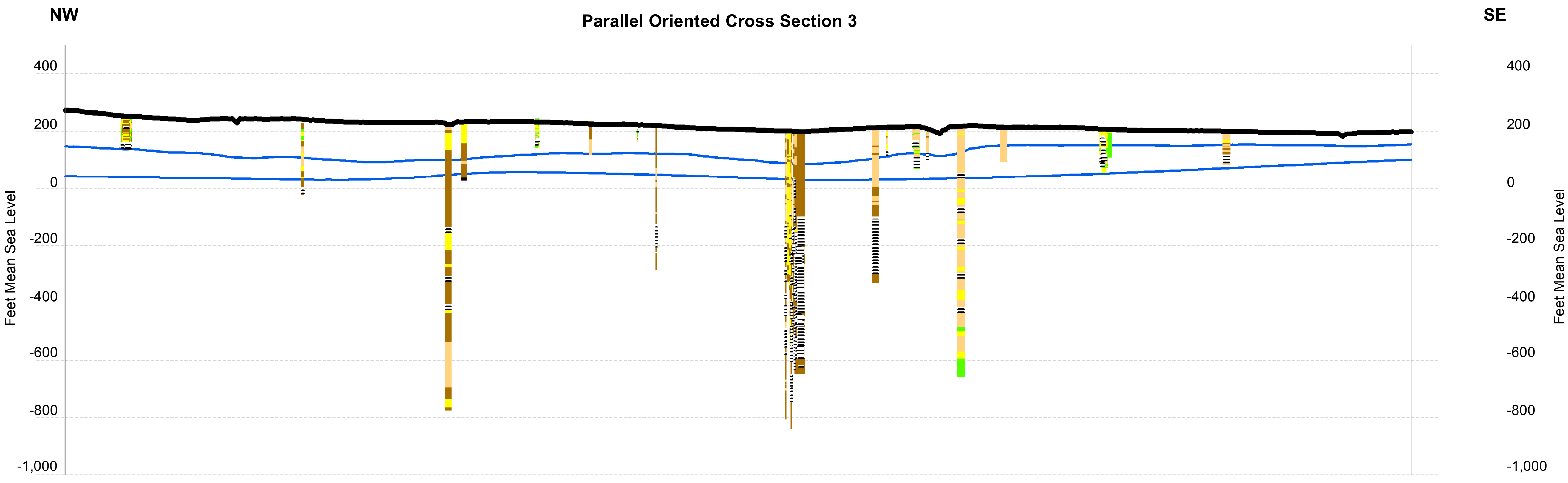

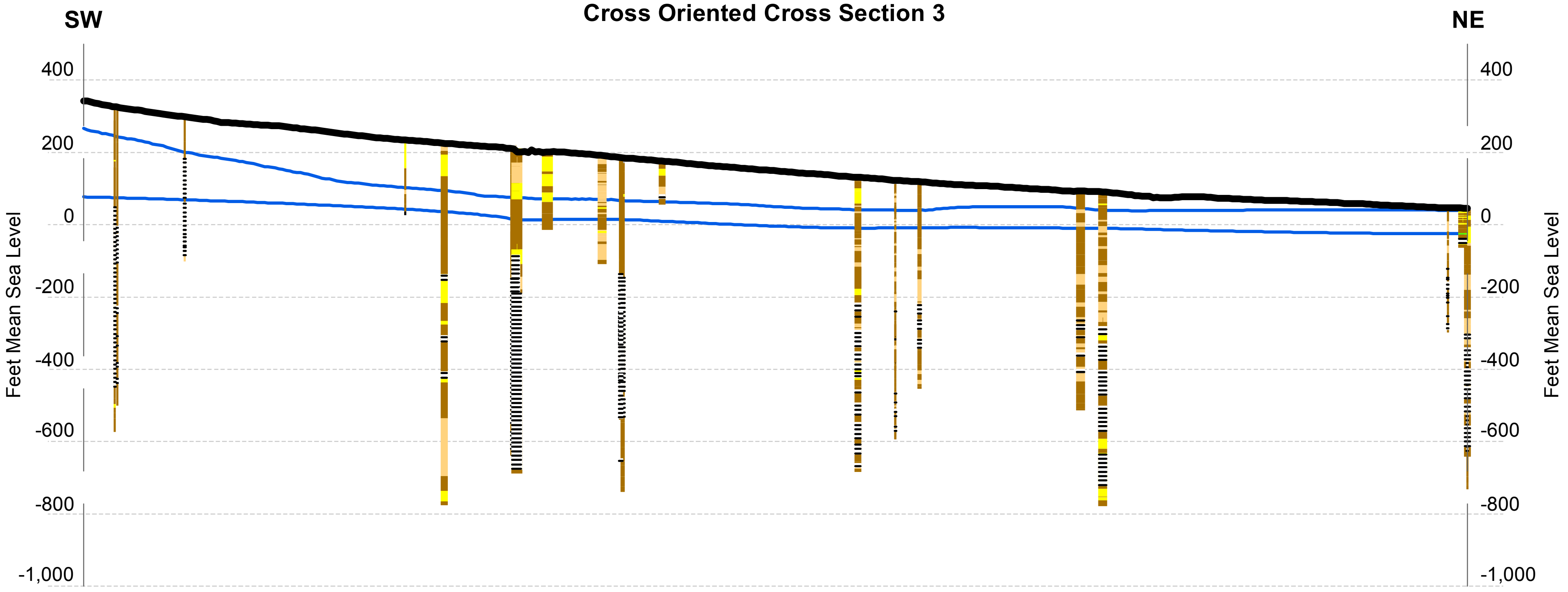

Legend

▬ Ground Surface

— High (yr) and Low (yr) Groundwater Elevations

IIIIIIIII Perforated Well Interval

Lithology

- ▬ Topsoil
- ▬ Fill
- ▬ Boulders / Cobbles
- ▬ Gravel
- ▬ Sand
- ▬ Silt
- ▬ Clay
- ▬ Bedrock

0 2,000 4,000
Scale in Feet
10 X Vertical Exaggeration

Note:
The thickness of the lithology and perforated interval lines for wells and boreholes is a function of the distance of the point from the section line. The closer the point, the wider the line is shown on the section.

December 2017

TODD GROUNDWATER

Figure 2-10
Example Cross Sections with Lithology and Screens

Path: T:\Projects\SCVWD IPR 37809\GIS\Maps\Figures\Conceptual Model Figures\Figure 2-10 Example Sections Lith & Screens.mxd

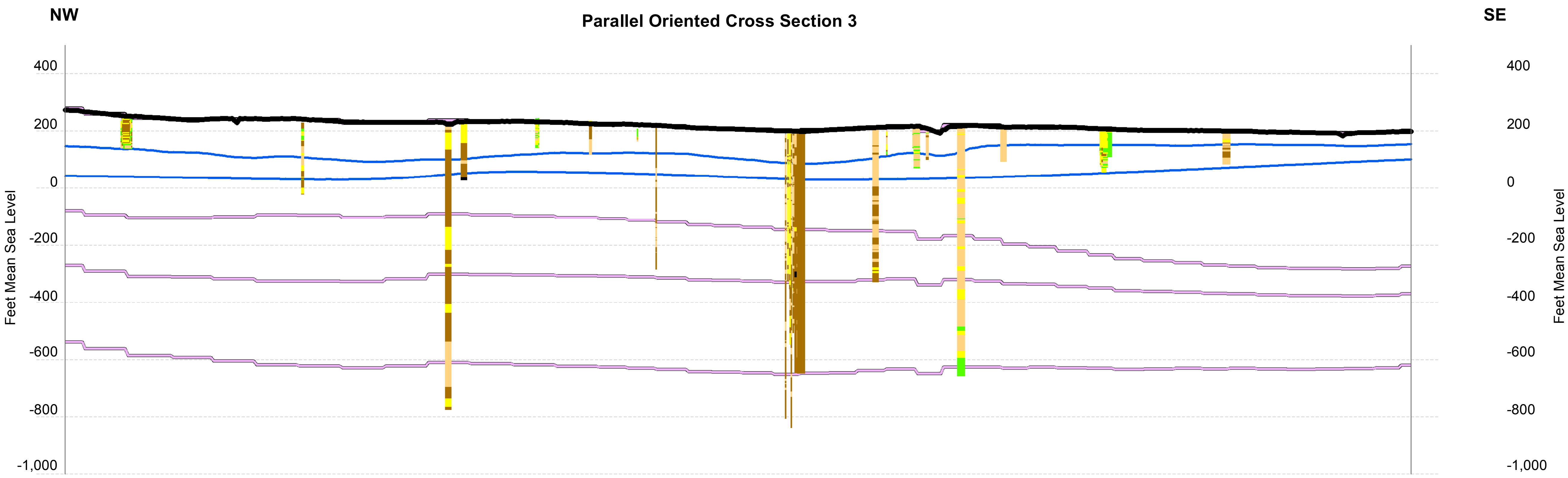

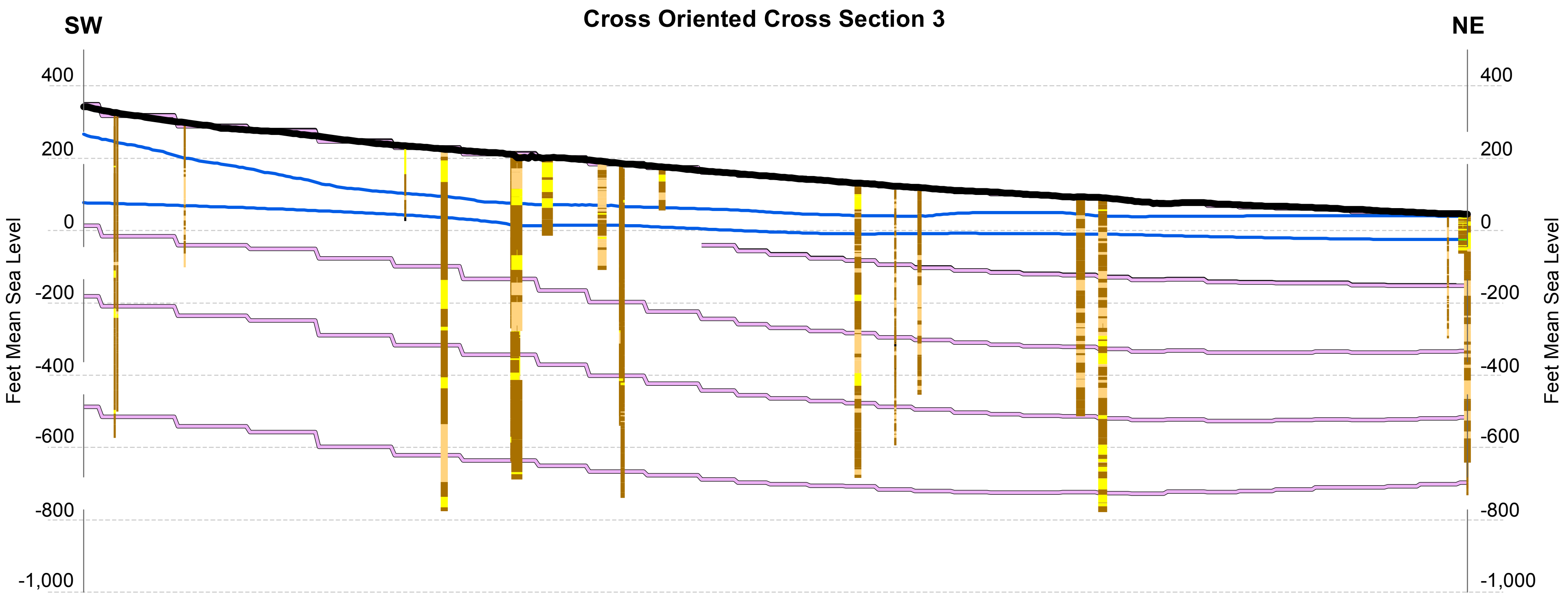

Legend

▬	Ground Surface	▬	Topsoil
▬	High (yr) and Low (yr) Groundwater Elevations	▬	Fill
▬	GMOD and XMOD Model Layers	▬	Boulders / Cobbles
		▬	Gravel
		▬	Sand
		▬	Silt
		▬	Clay
		▬	Bedrock

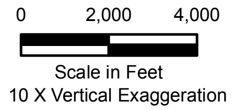

Note:
The thickness of the lithology lines for wells and boreholes is a function of the distance of the point from the section line. The closer the point, the wider the line is shown on the section.

December 2017

TODD
GROUNDWATER

Figure 2-11
Example Cross Sections with Lithology and GMOD and XMOD Model Layers

Path: T:\Projects\SCVWD IPR 37809\GIS\Maps\Figures\Conceptual Model Figures\Figure 2-11 Example Sections GMOD, Lith, Screens.mxd

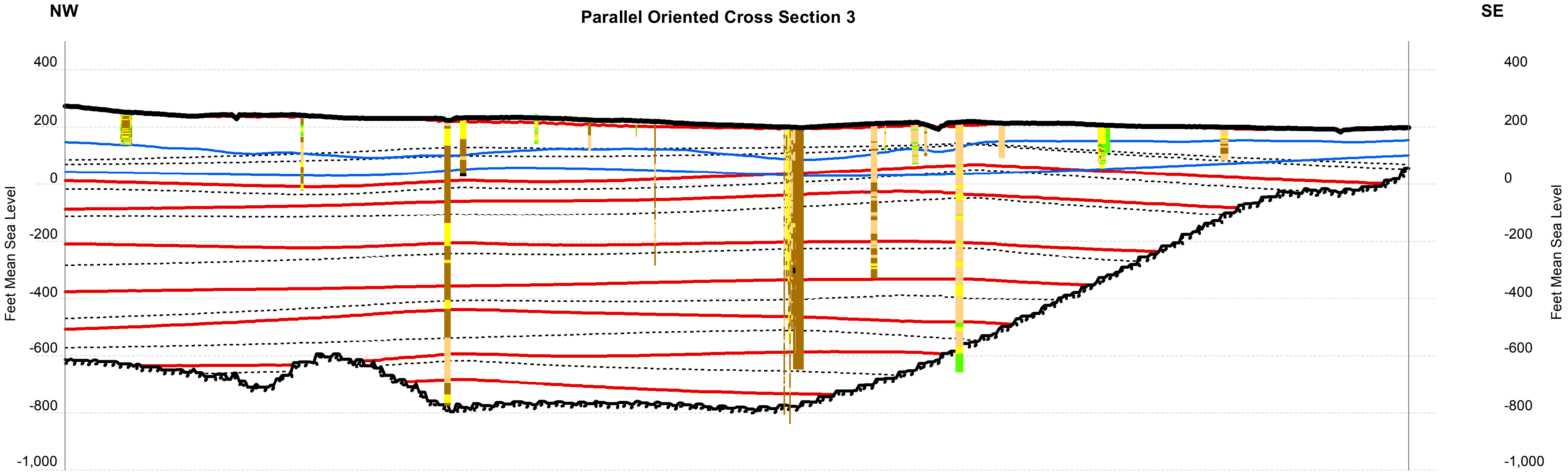

Parallel Oriented Cross Section 3

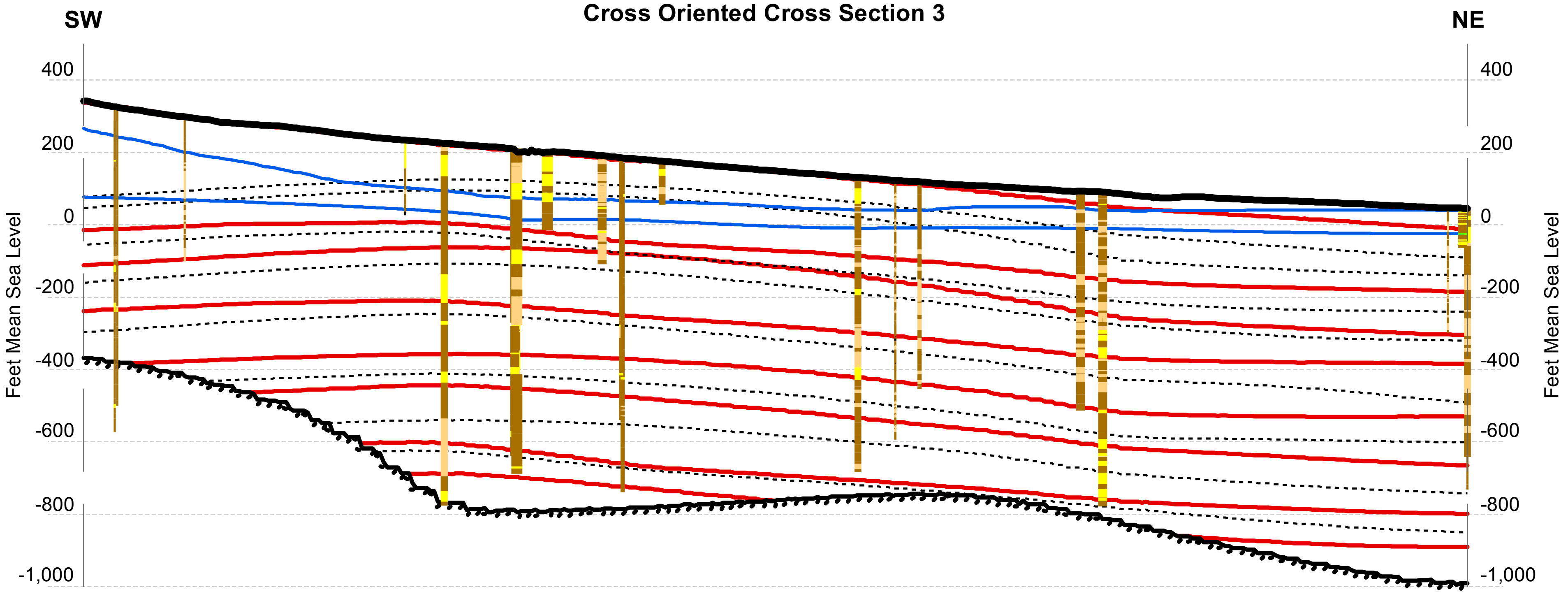

Cross Oriented Cross Section 3

Legend

▬	Ground Surface	▬	Topsoil
―	High (yr) and Low (yr) Groundwater Elevations	▬	Fill
―	Wentworth Cycle Boundaries	▬	Boulders / Cobbles
┄	Wentworth Inter-Cycle Contacts	▬	Gravel
┼┼┼	Wentworth Bedrock	▬	Sand
		▬	Silt
		▬	Clay
		▬	Bedrock

0 2,000 4,000
Scale in Feet
10 X Vertical Exaggeration

Note:
The thickness of the lithology lines for wells and boreholes is a function of the distance of the point from the section line. The closer the point, the wider the line is shown on the section.

December 2017

TODD
GROUNDWATER

Figure 2-12
Example Cross Sections with Wentworth Interpretations and Lithology

Path: T:\Projects\SCVWD IPR 37809\GIS\Maps\Figures\Conceptual Model Figures\Figure 2-12 Example Sections WW, Lith, Screens.mxd

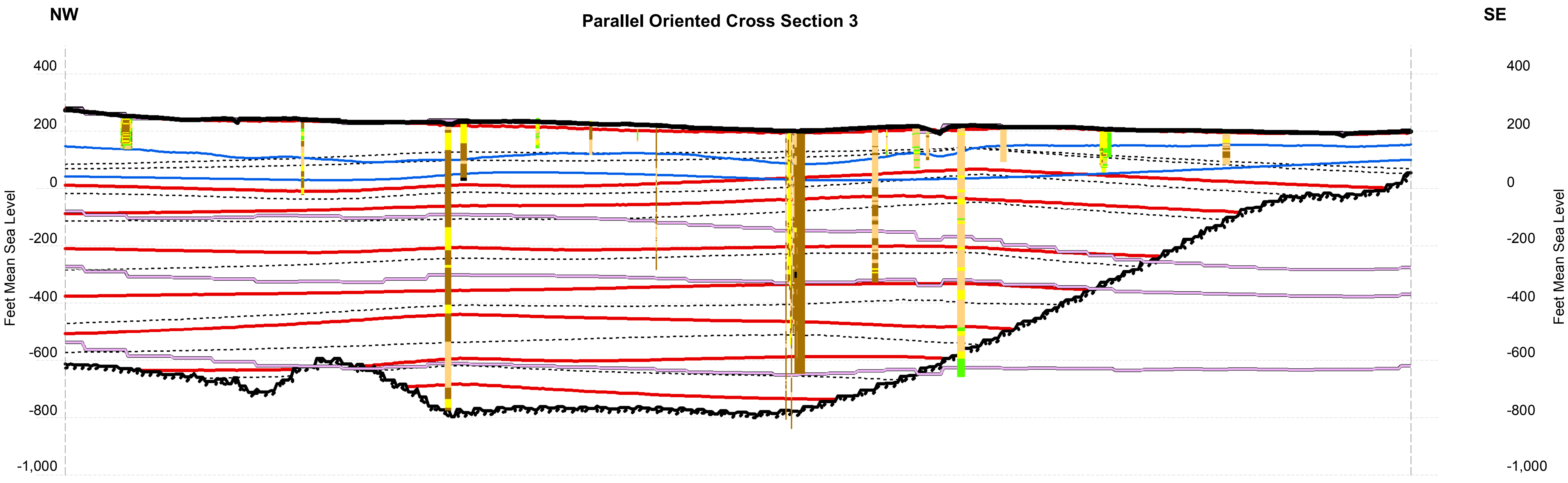

Parallel Oriented Cross Section 3

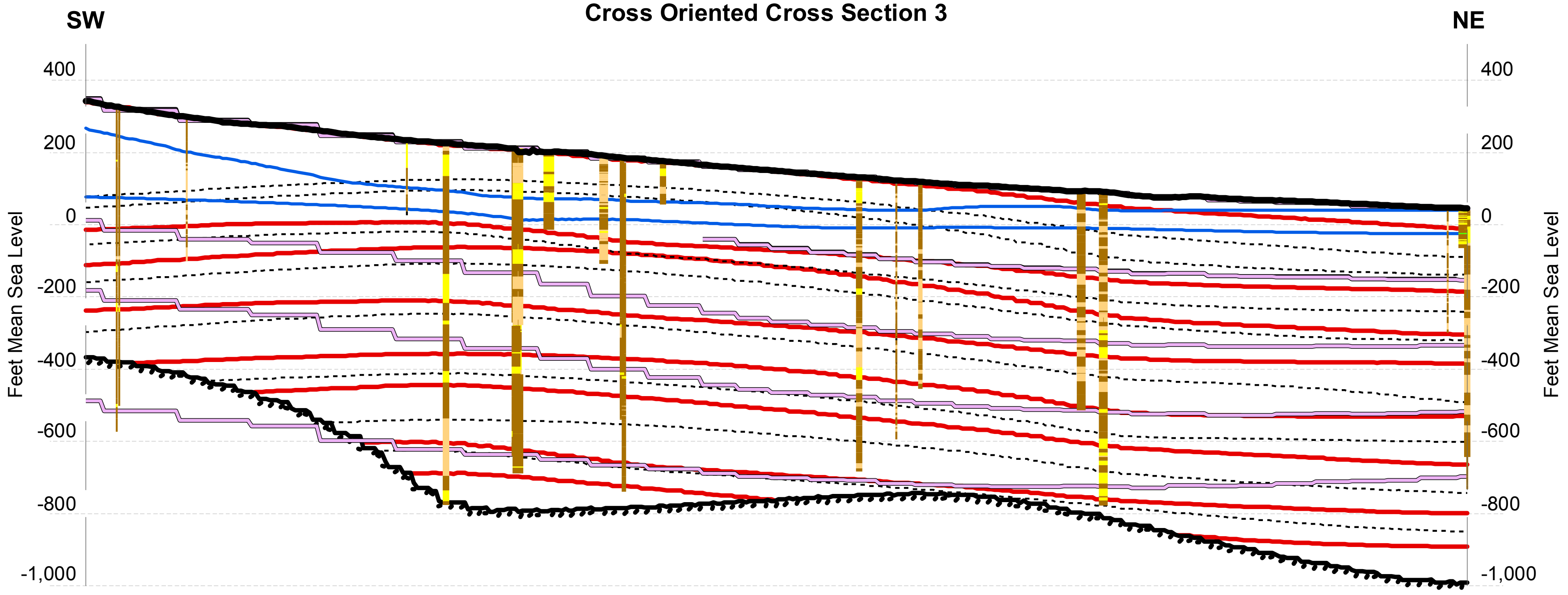

Cross Oriented Cross Section 3

Legend

- Ground Surface
- High (yr) and Low (yr) Groundwater Elevations
- GMOD and XMOD Model Layers
- Wentworth Cycle Boundaries
- Wentworth Inter-Cycle Contacts
- Wentworth Bedrock
- Topsoil
- Fill
- Boulders / Cobbles
- Gravel
- Sand
- Silt
- Clay
- Bedrock

0 2,000 4,000
Scale in Feet
10 X Vertical Exaggeration

Note:
The thickness of the lithology lines for wells and boreholes is a function of the distance of the point from the section line. The closer the point, the wider the line is shown on the section.

December 2017

TODD GROUNDWATER

Figure 2-13
Example Cross Sections Showing All Data

Path: T:\Projects\SCVWD IPR 37809\GIS\Maps\Figures\Conceptual Model Figures\Figure 2-13 Example Sections All Data.mxd

Path: T:\Projects\SCVWD IPR 37809\GIS\Maps\Figures\Conceptual Model Figures\Figure 2-14 Cross Section Locations w Geophysical Wells.mxd

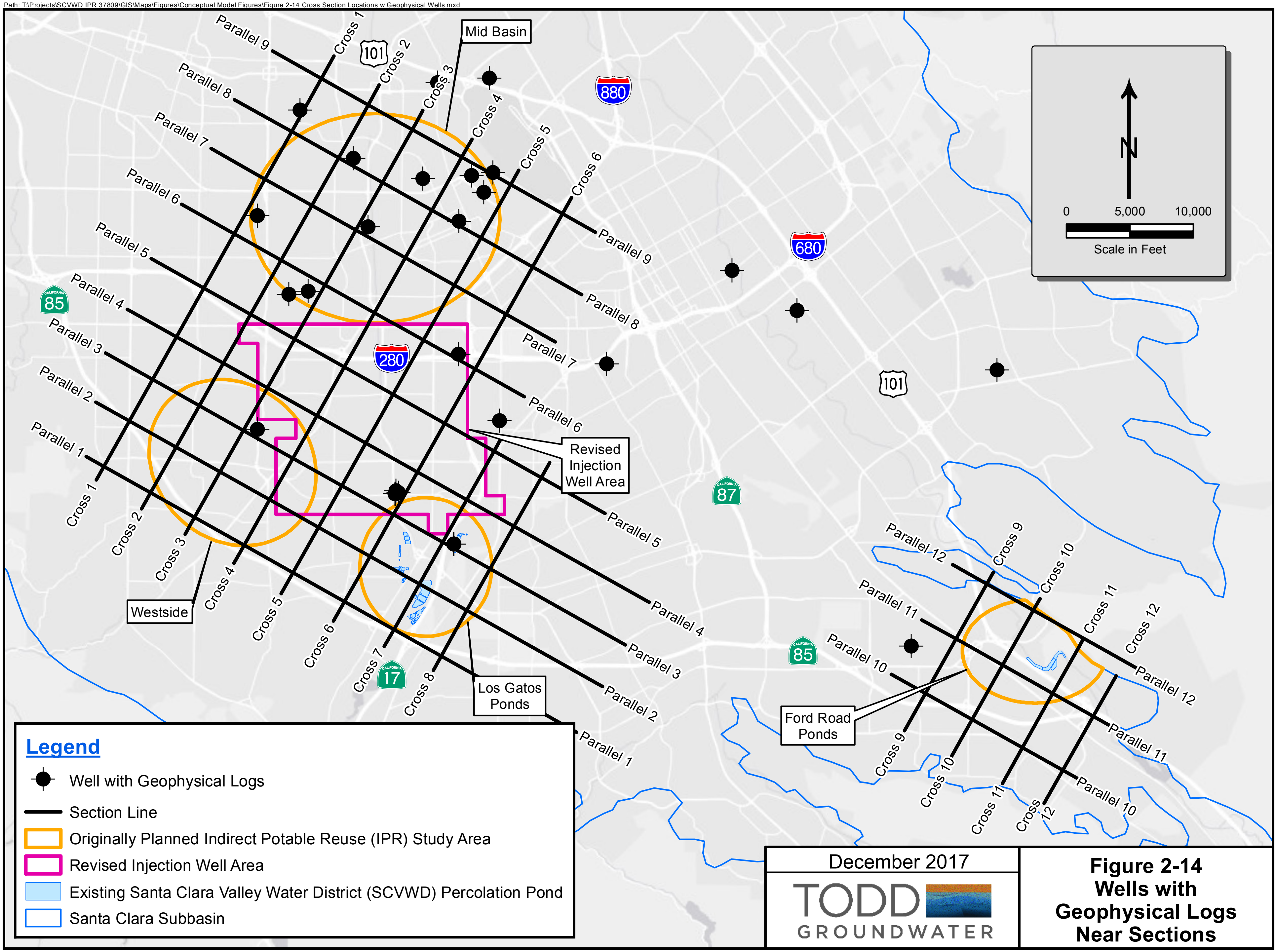

Legend

● Well with Geophysical Logs

— Section Line

🟧 Originally Planned Indirect Potable Reuse (IPR) Study Area

🟪 Revised Injection Well Area

🟦 Existing Santa Clara Valley Water District (SCVWD) Percolation Pond

☐ Santa Clara Subbasin

December 2017

TODD GROUNDWATER

Figure 2-14
Wells with Geophysical Logs Near Sections

Path: T:\Projects\SCVWD IPR 37809\GIS\Maps\Figures\Conceptual Model Figures\Figure 2-15 Cross Section Locations w Multi-Completion Wells.mxd

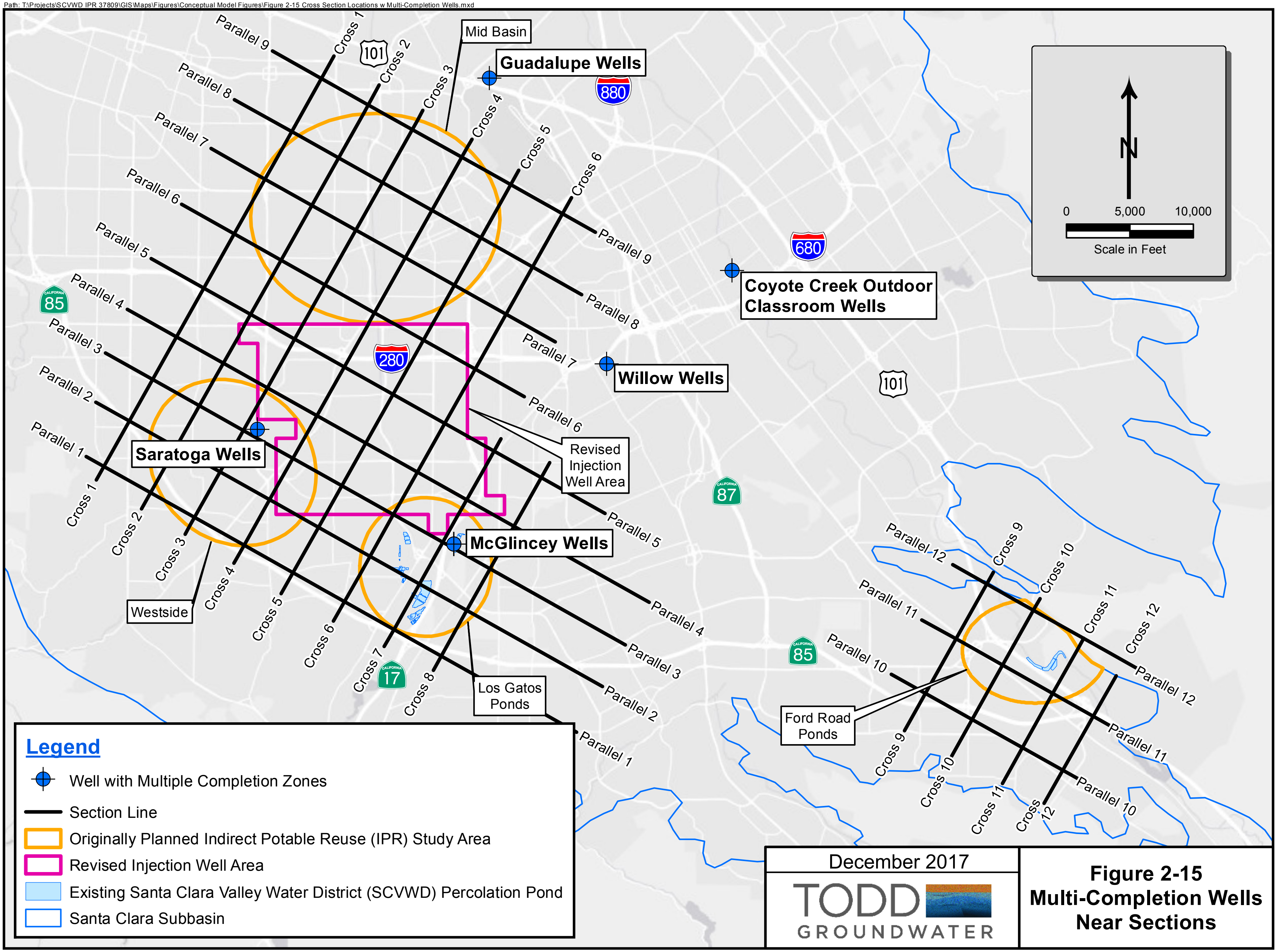

December 2017

TODD GROUNDWATER

Figure 2-15
Multi-Completion Wells Near Sections

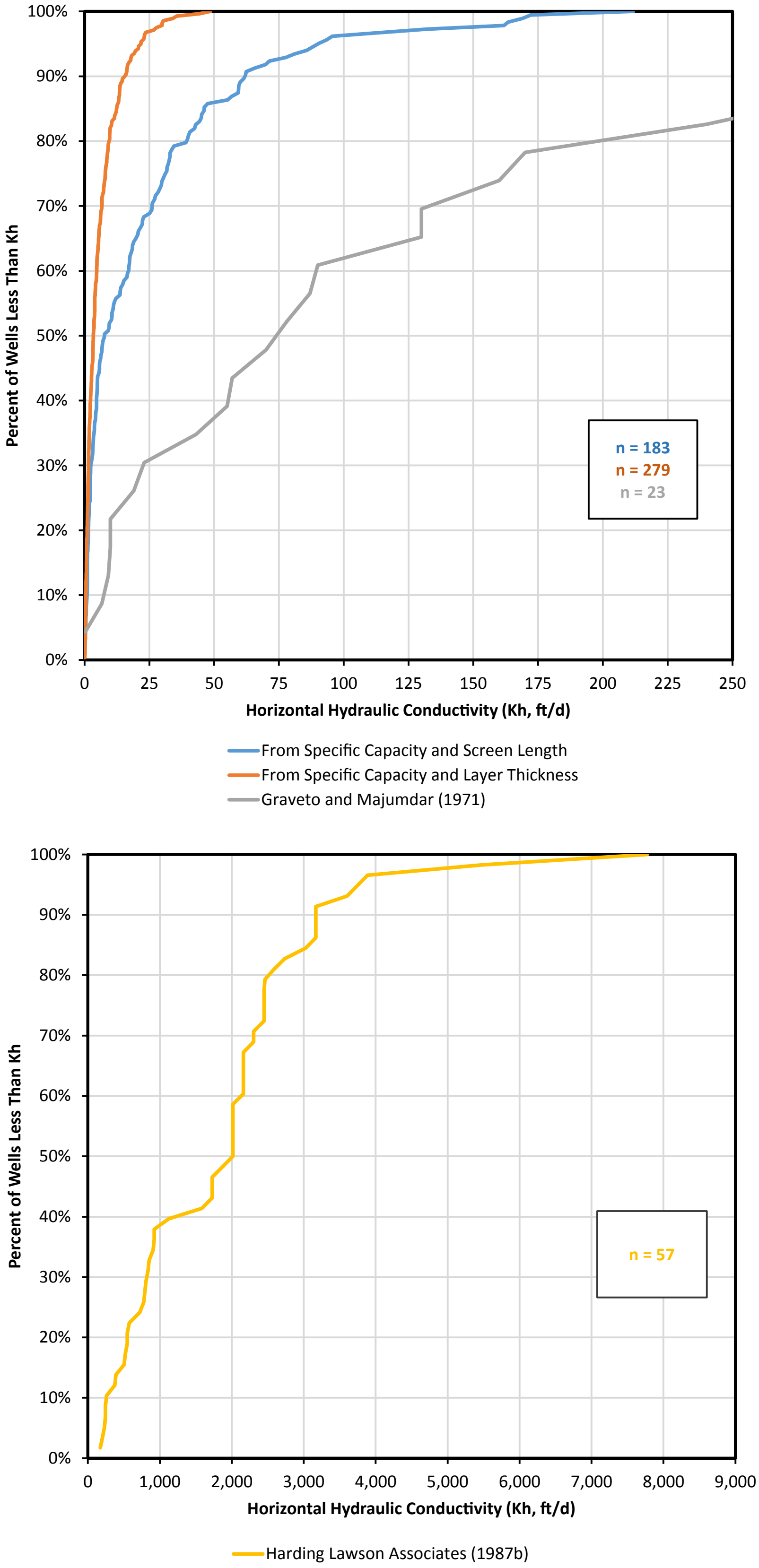

December 2017

TODD GROUNDWATER

Figure 2-16
Frequency Distribution of Horizontal Hydraulic Conductivity Estimated from Well Tests

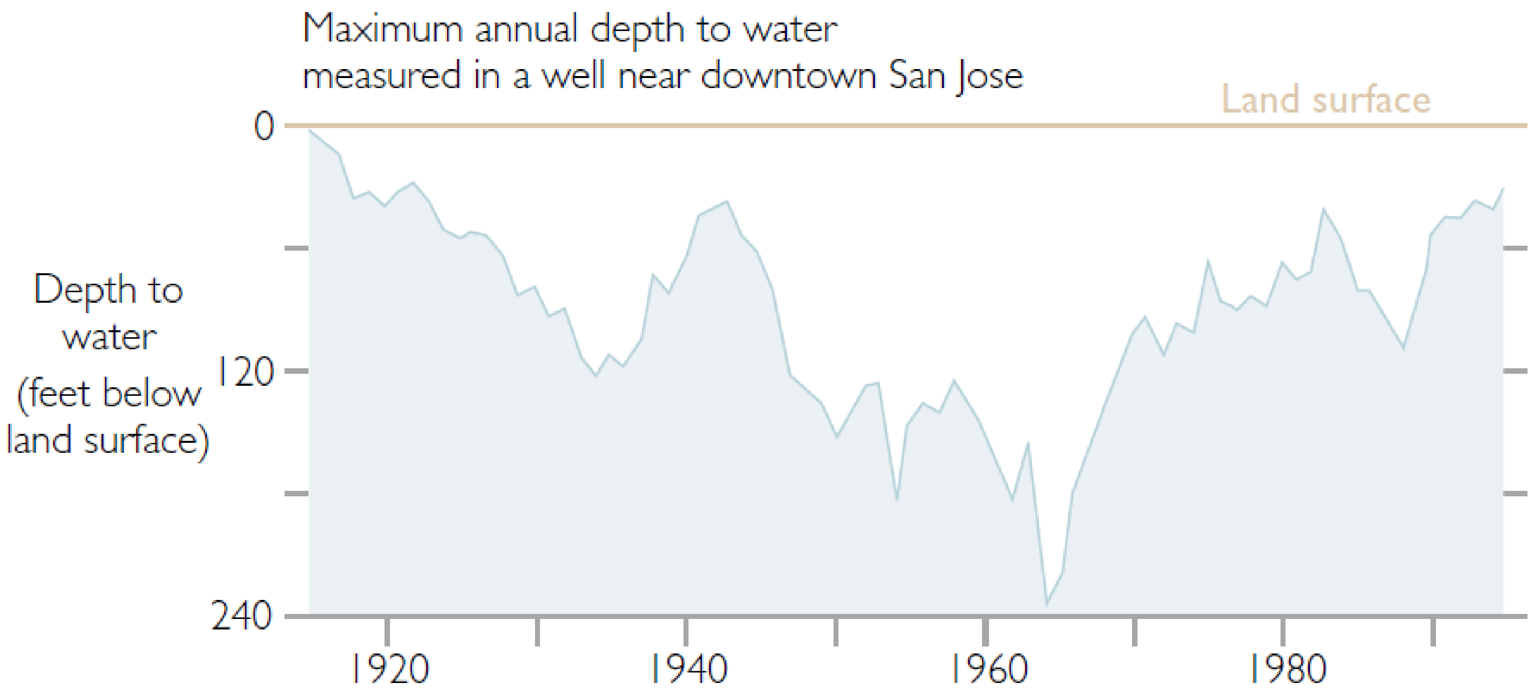

Source: Ingebritsen and Jones, 1999.

December 2017

TODD GROUNDWATER

Figure 2-17
Water Level Hydrograph at a Well near Downtown San Jose, 1915-1995

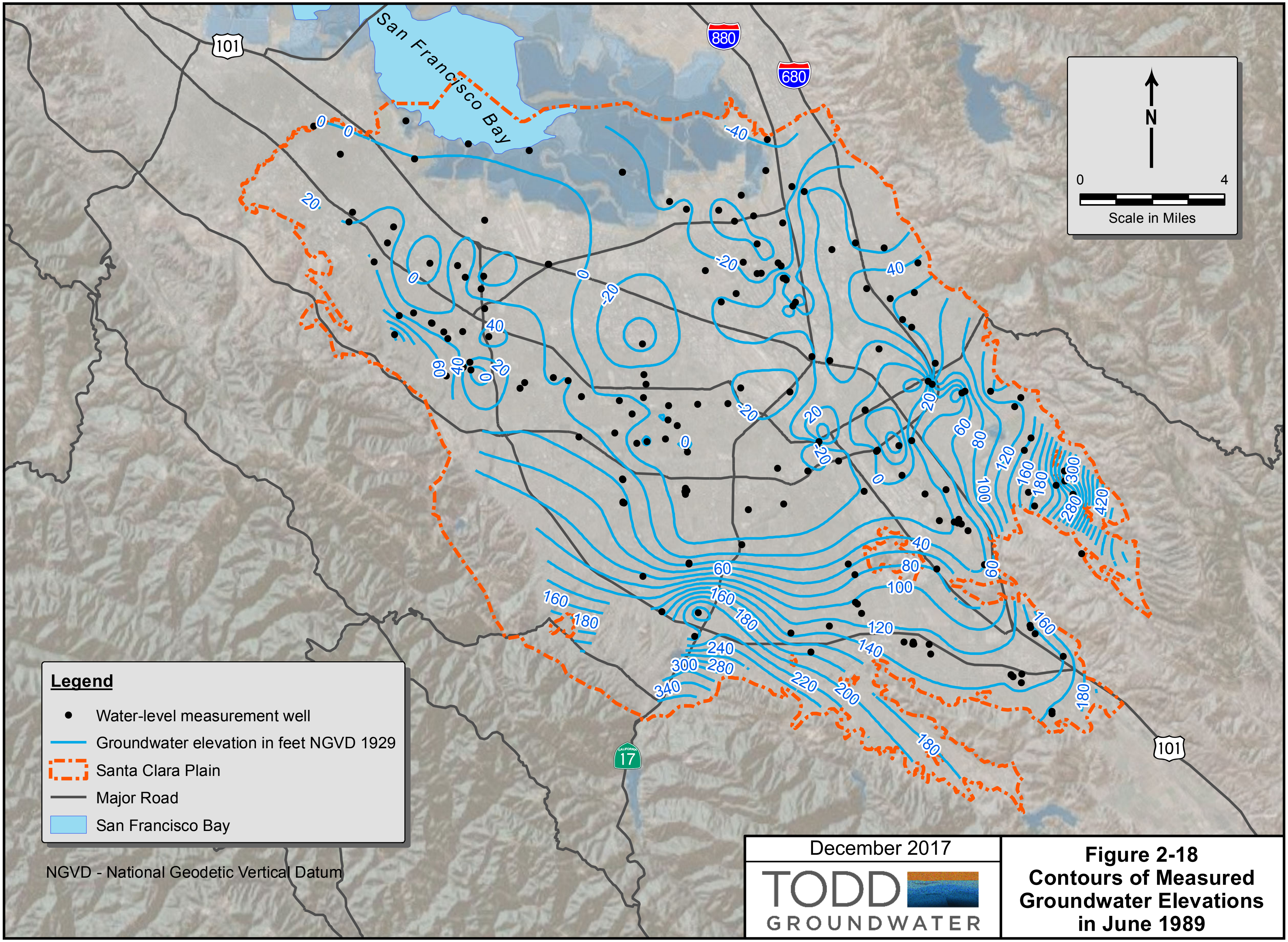

December 2017

TODD GROUNDWATER

Figure 2-18
Contours of Measured Groundwater Elevations in June 1989

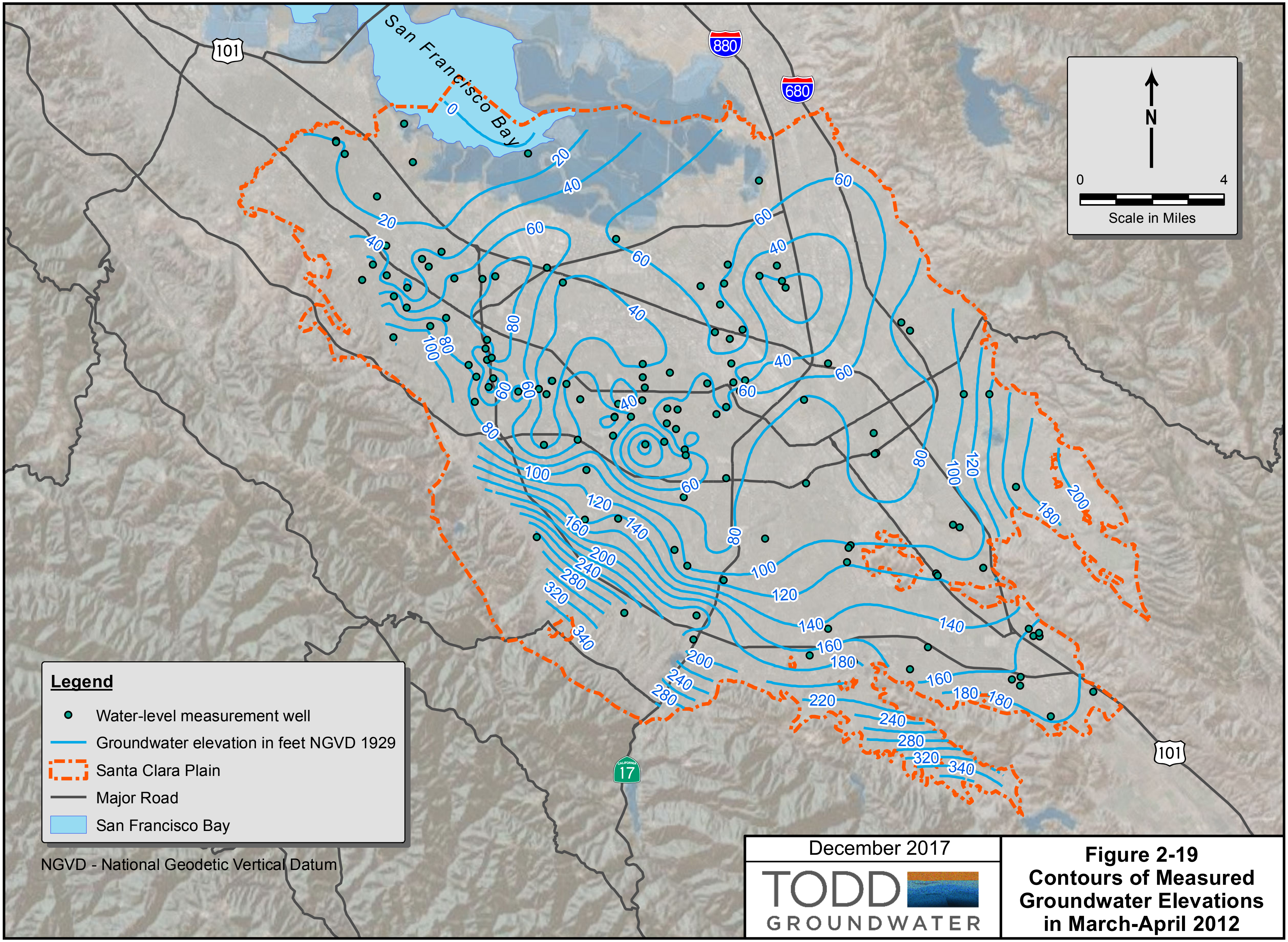

December 2017

TODD GROUNDWATER

Figure 2-19
Contours of Measured Groundwater Elevations in March-April 2012

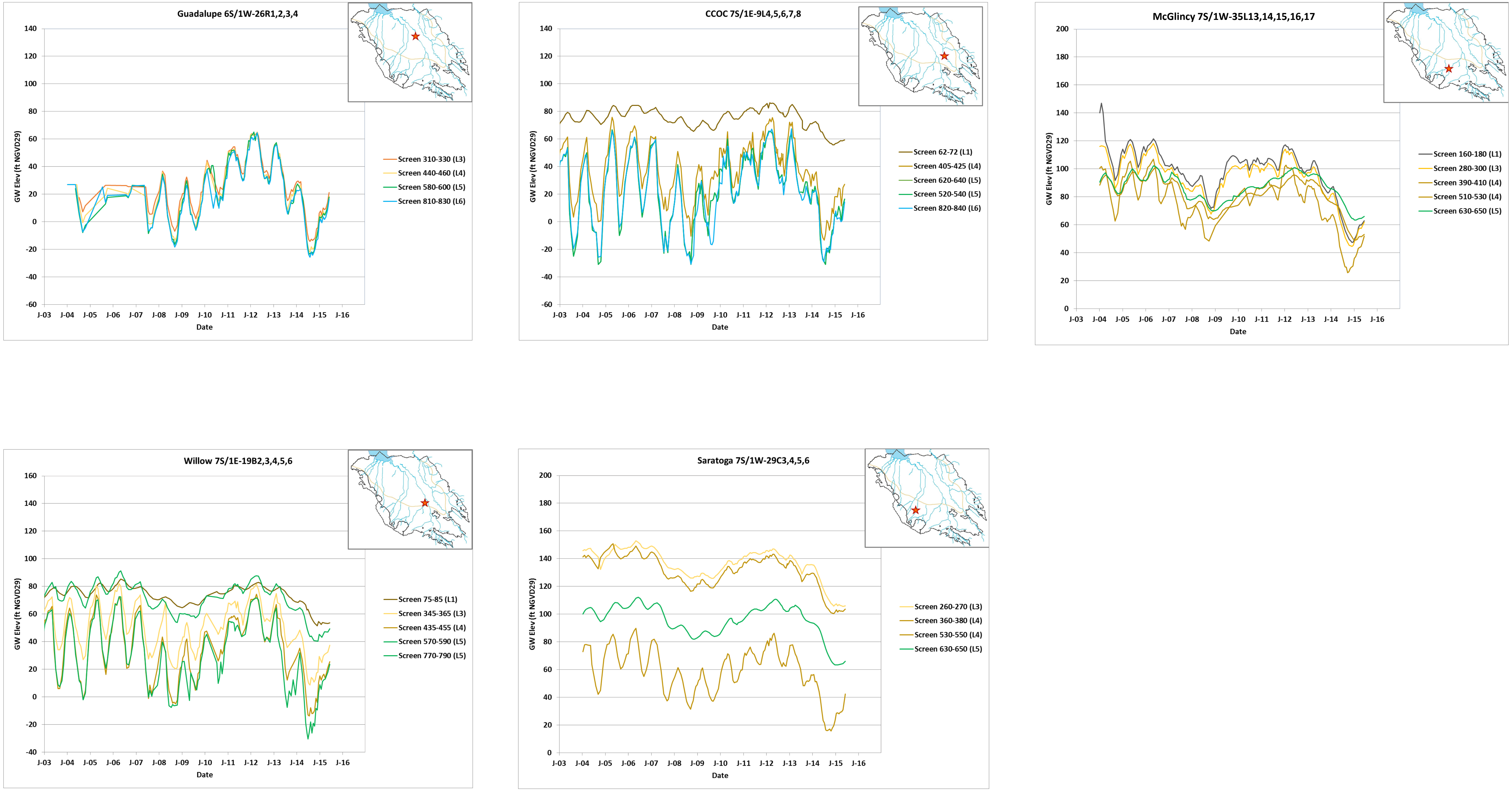

December 2017

TODD GROUNDWATER

Figure 2-20
Hydrographs of Measured Water Levels at Multiple Depth Monitoring Well Clusters

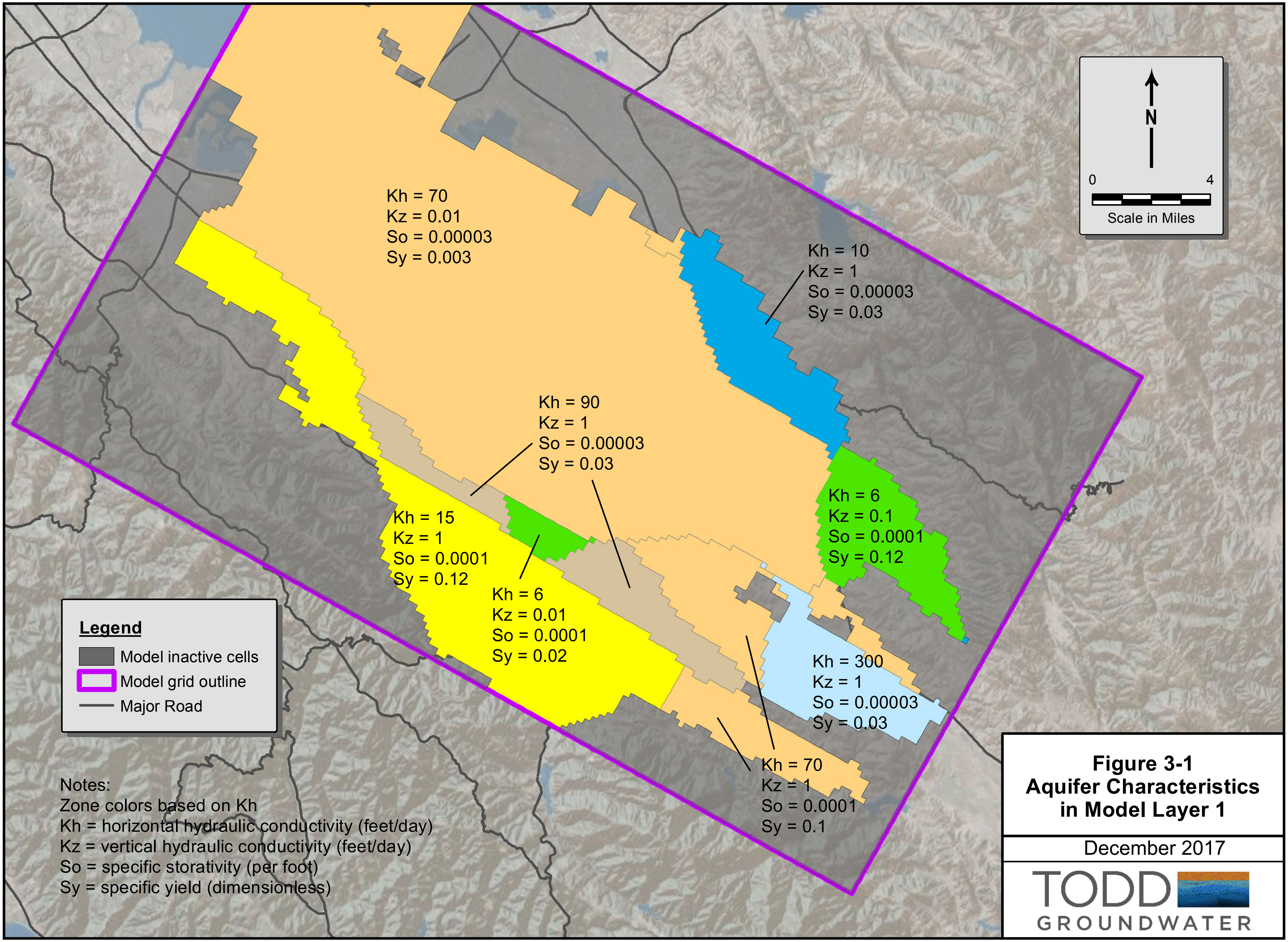

Notes:
Zone colors based on Kh
Kh = horizontal hydraulic conductivity (feet/day)
Kz = vertical hydraulic conductivity (feet/day)
So = specific storativity (per foot)
Sy = specific yield (dimensionless)

Figure 3-1
Aquifer Characteristics in Model Layer 1

December 2017

TODD GROUNDWATER

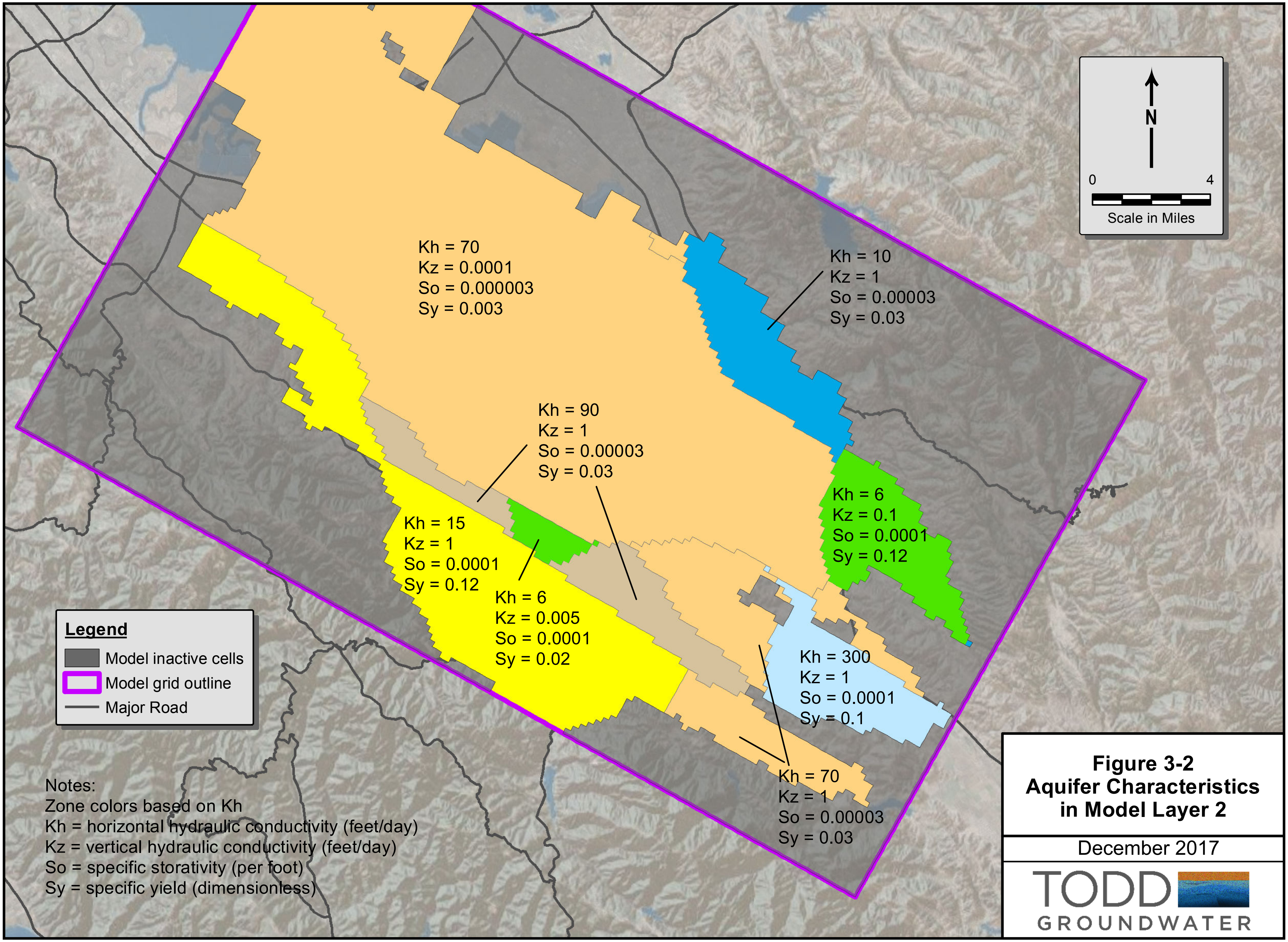

Notes:
Zone colors based on Kh
Kh = horizontal hydraulic conductivity (feet/day)
Kz = vertical hydraulic conductivity (feet/day)
So = specific storativity (per foot)
Sy = specific yield (dimensionless)

Figure 3-2
Aquifer Characteristics in Model Layer 2

December 2017

TODD GROUNDWATER

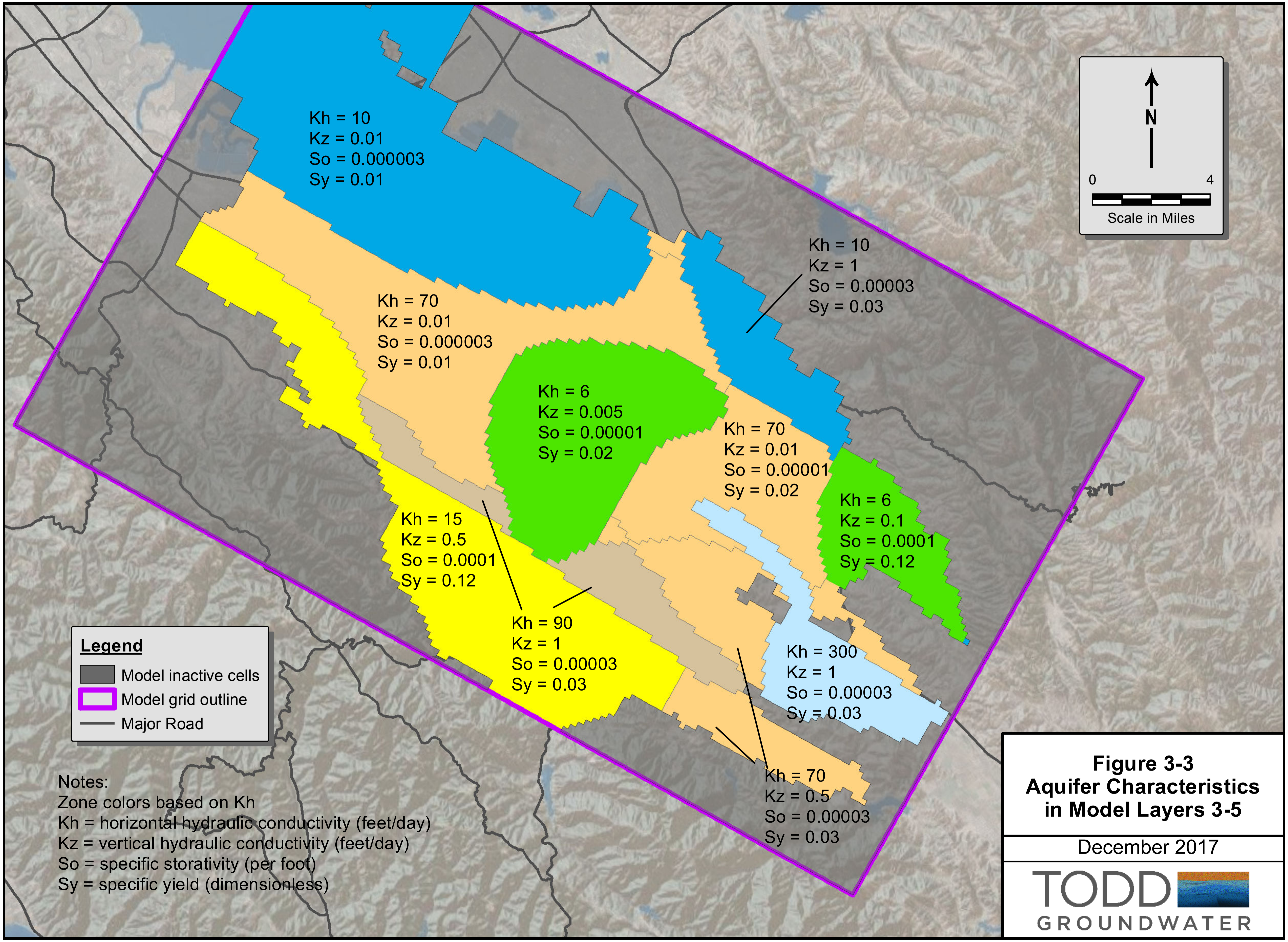

Notes:
Zone colors based on Kh
Kh = horizontal hydraulic conductivity (feet/day)
Kz = vertical hydraulic conductivity (feet/day)
So = specific storativity (per foot)
Sy = specific yield (dimensionless)

Figure 3-3
Aquifer Characteristics
in Model Layers 3-5

December 2017

TODD
GROUNDWATER

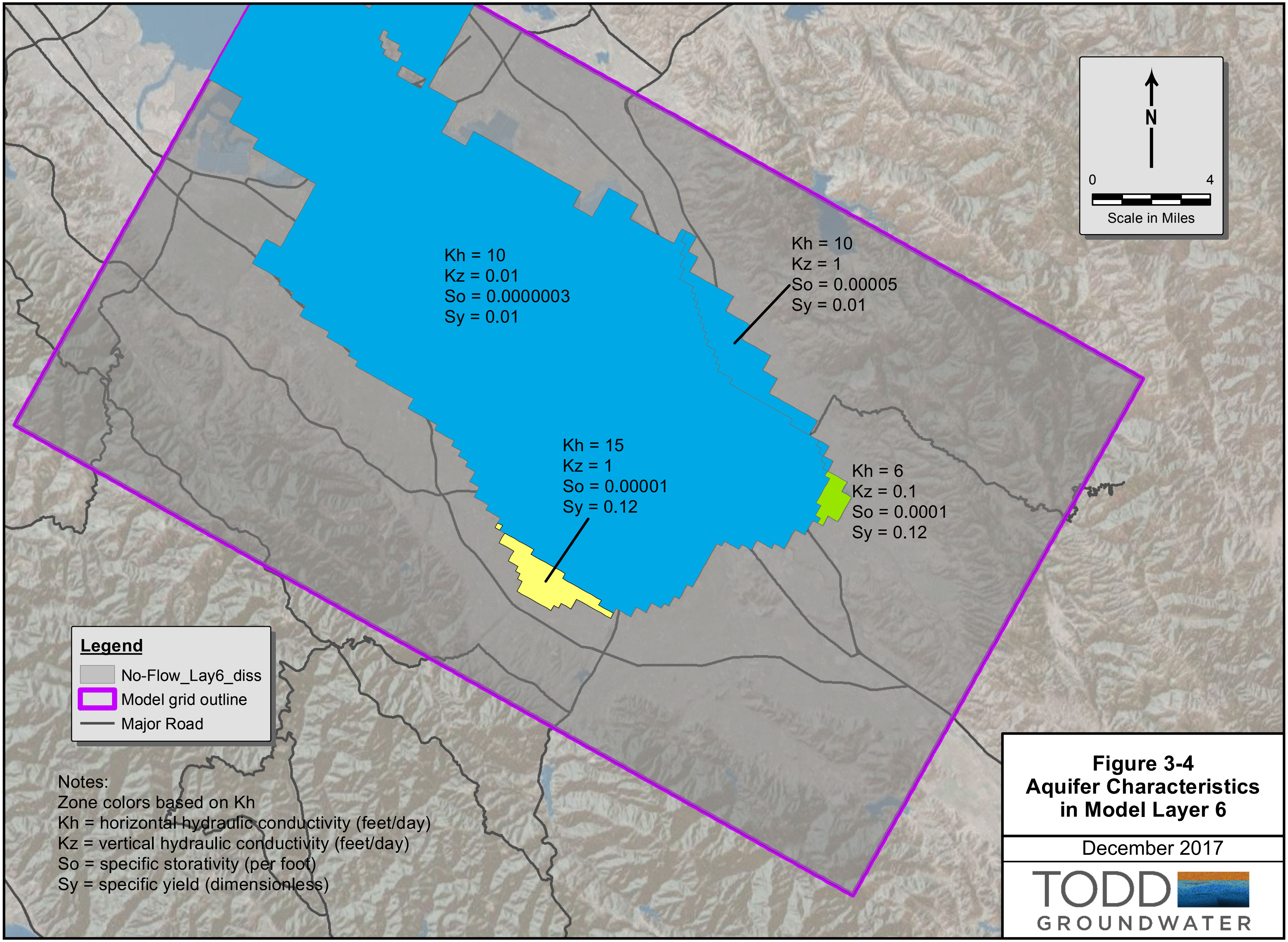

Notes:
Zone colors based on Kh
Kh = horizontal hydraulic conductivity (feet/day)
Kz = vertical hydraulic conductivity (feet/day)
So = specific storativity (per foot)
Sy = specific yield (dimensionless)

Figure 3-4
Aquifer Characteristics in Model Layer 6

December 2017

TODD GROUNDWATER

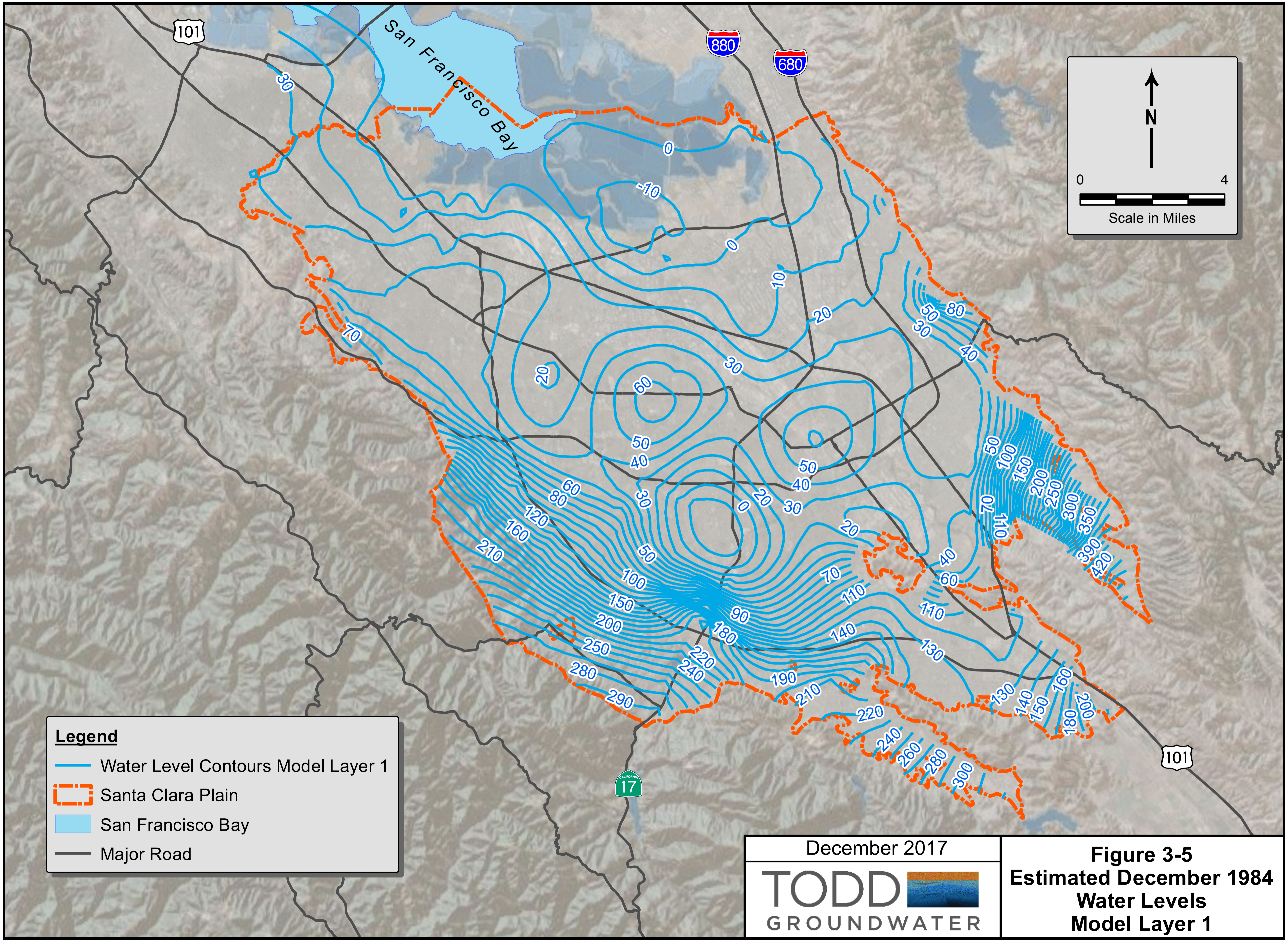

December 2017

TODD GROUNDWATER

Figure 3-5
Estimated December 1984
Water Levels
Model Layer 1

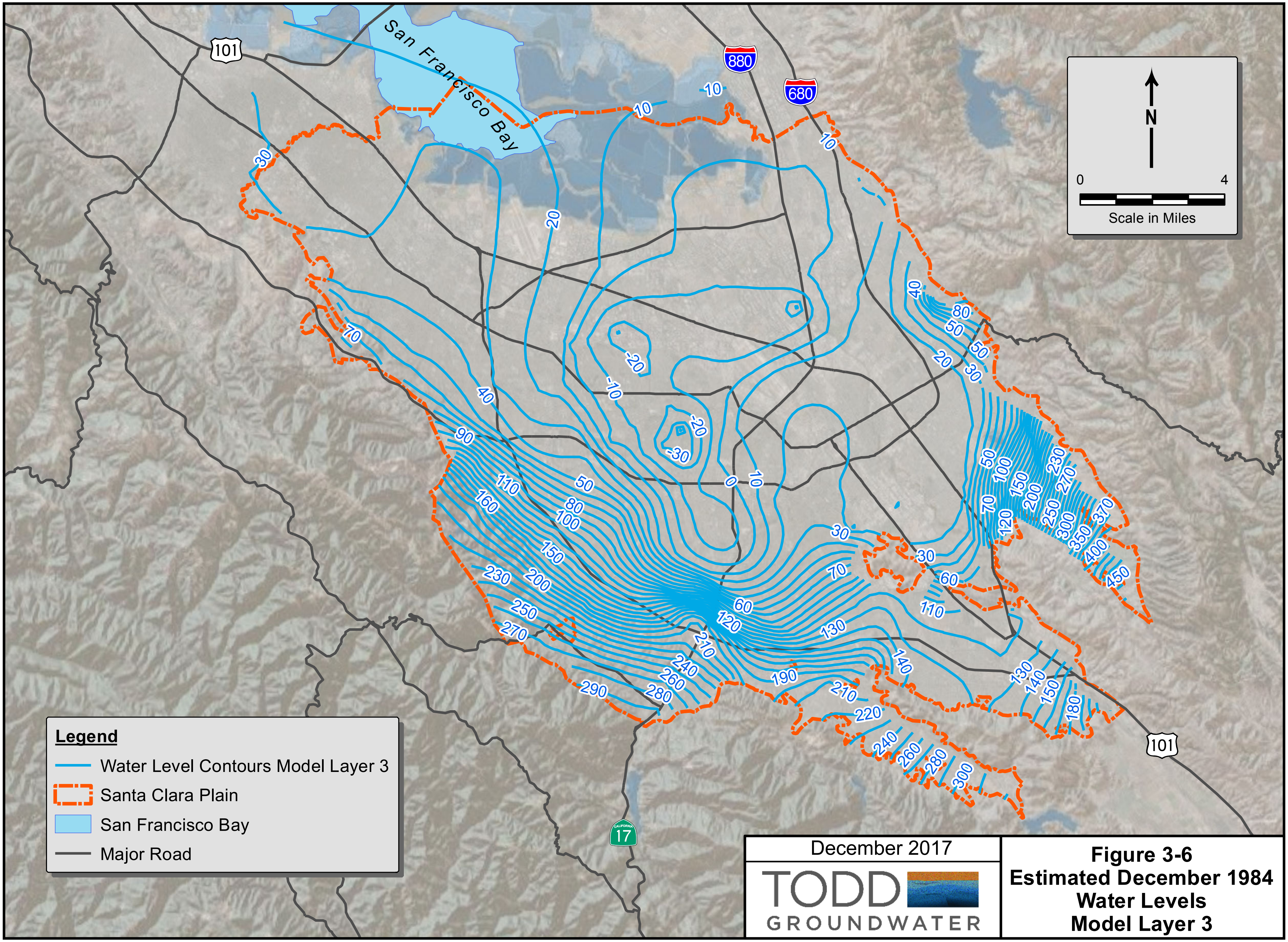

December 2017

TODD GROUNDWATER

Figure 3-6
Estimated December 1984
Water Levels
Model Layer 3

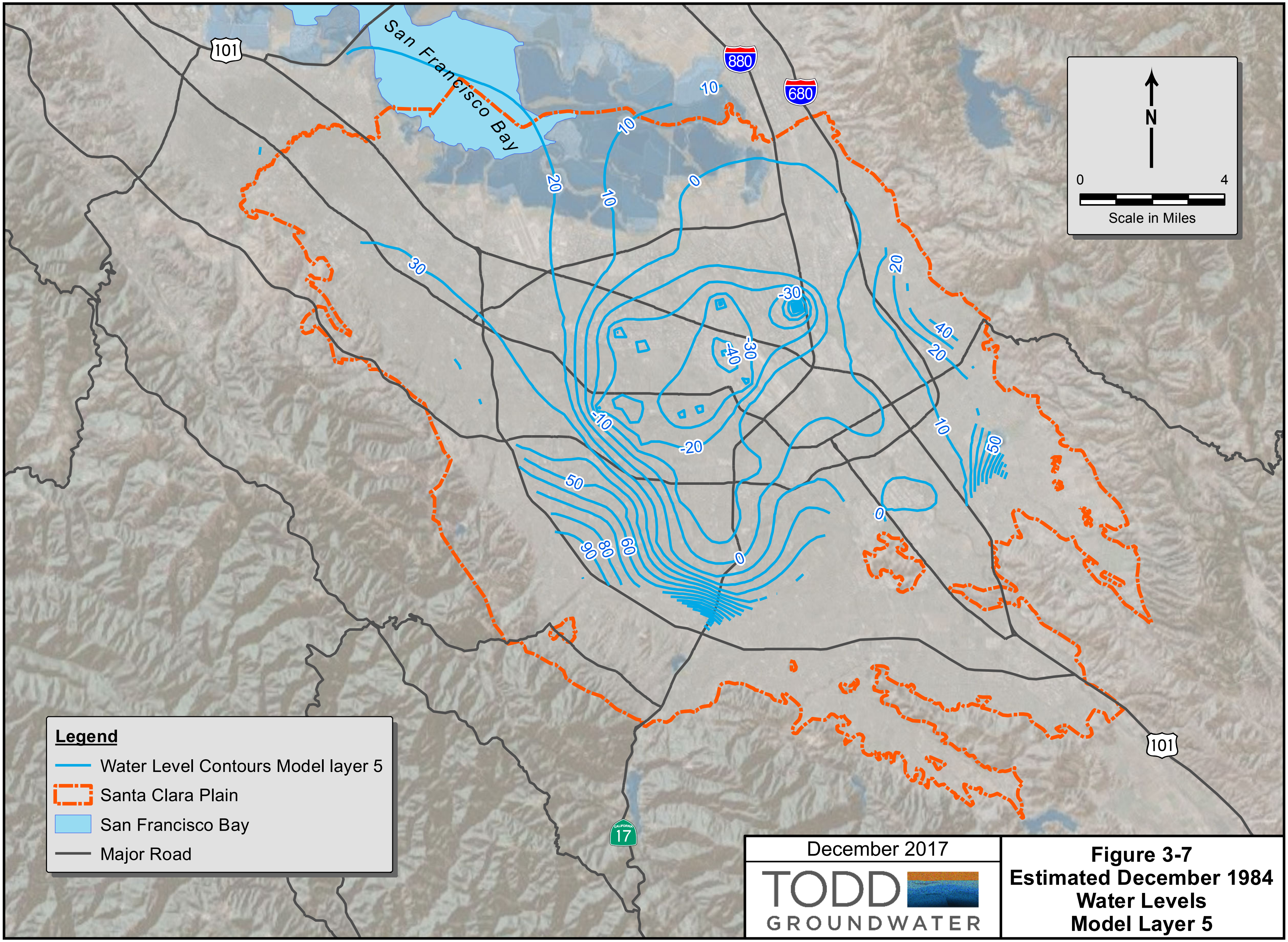

December 2017

TODD GROUNDWATER

Figure 3-7
Estimated December 1984
Water Levels
Model Layer 5

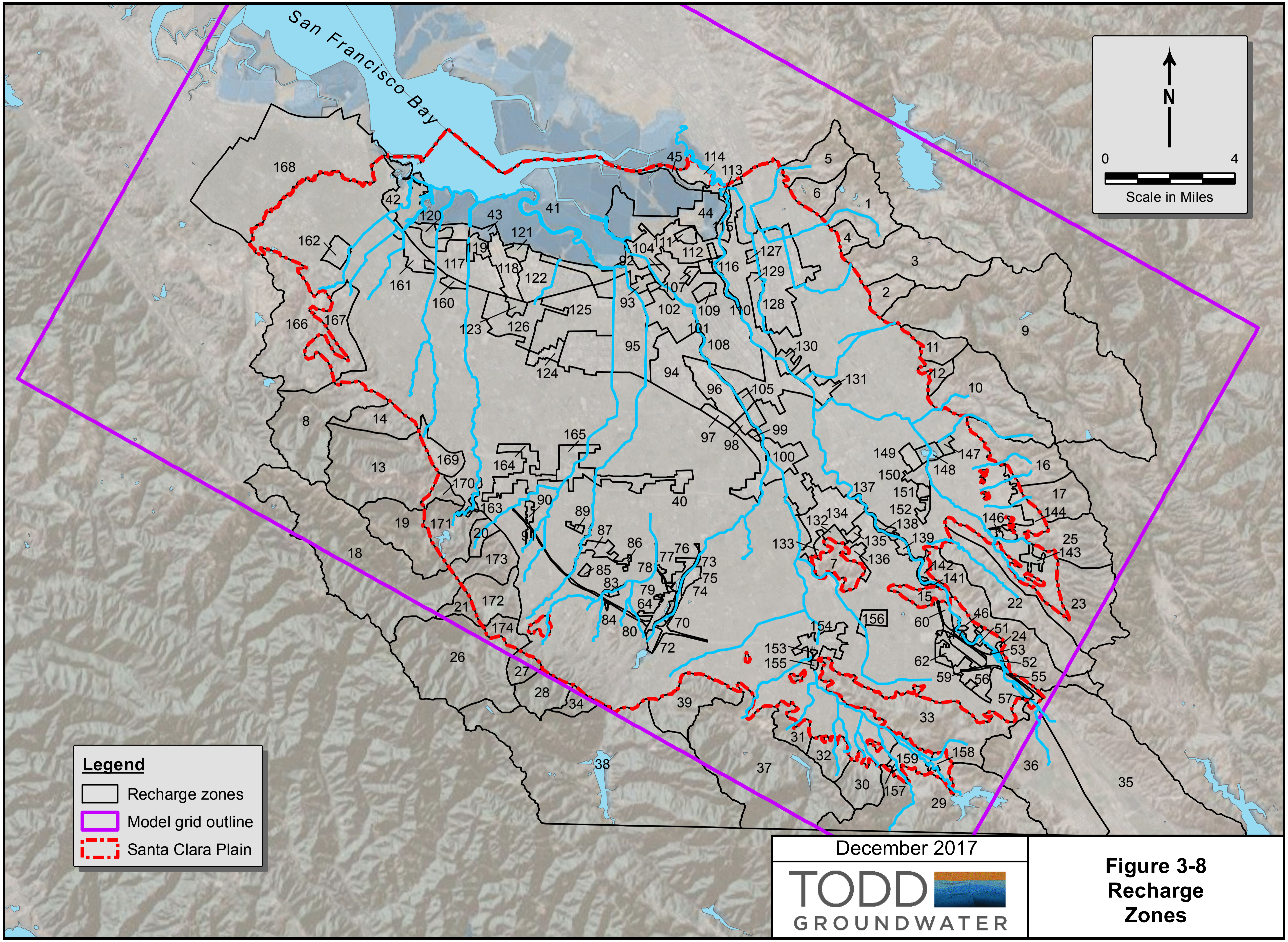

December 2017

TODD GROUNDWATER

Figure 3-8 Recharge Zones

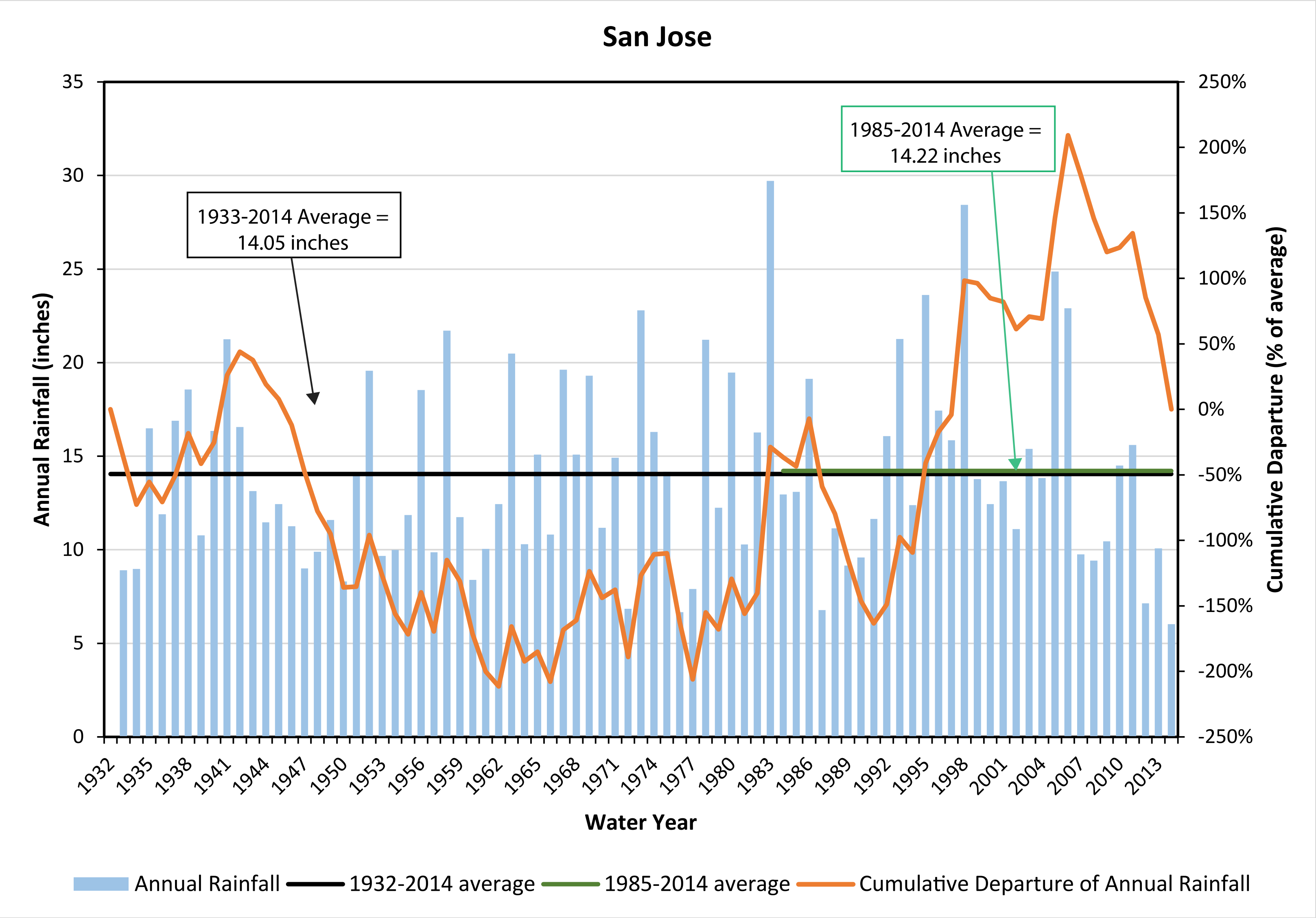

December 2017

TODD GROUNDWATER

Figure 3-9
Cumulative Departure of Annual Precipitation

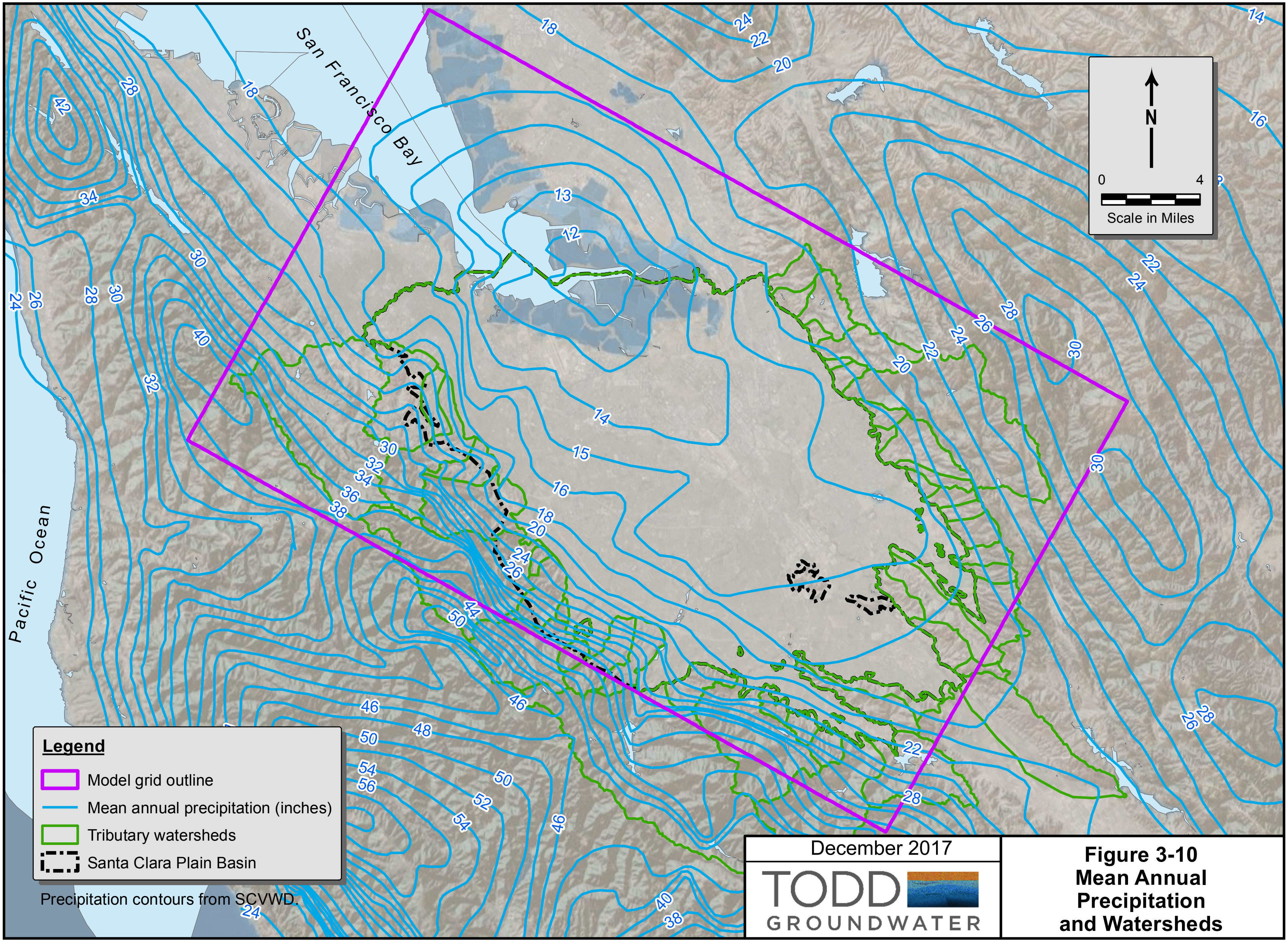

Precipitation contours from SCVWD.

December 2017

TODD GROUNDWATER

Figure 3-10
Mean Annual Precipitation and Watersheds

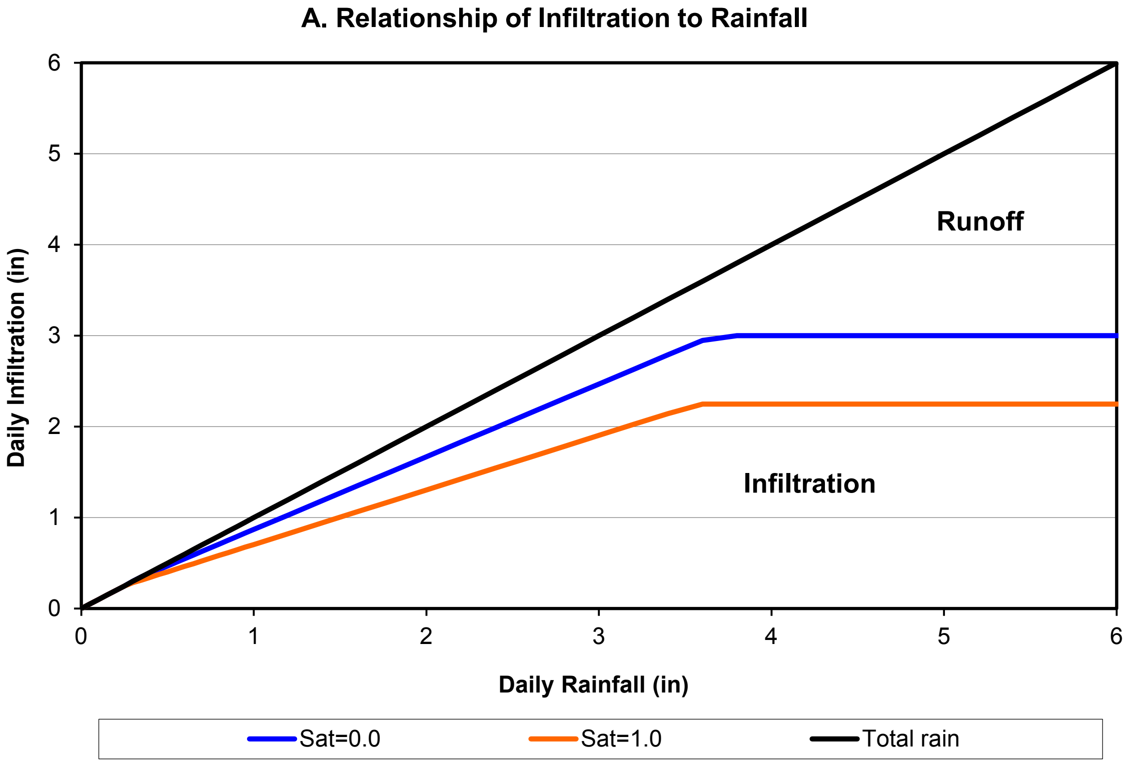

A. Relationship of Infiltration to Rainfall

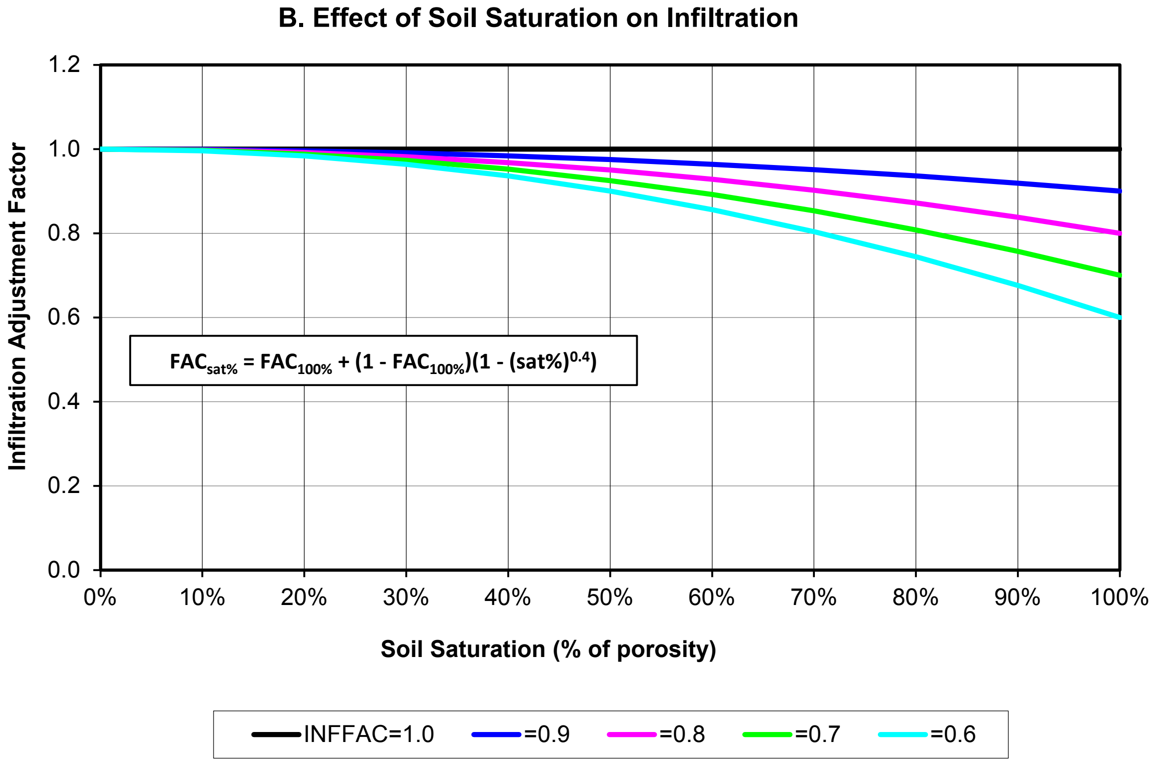

B. Effect of Soil Saturation on Infiltration

December 2017

TODD GROUNDWATER

Figure 3-11
Generalized Relationship of Daily Infiltration to Rainfall

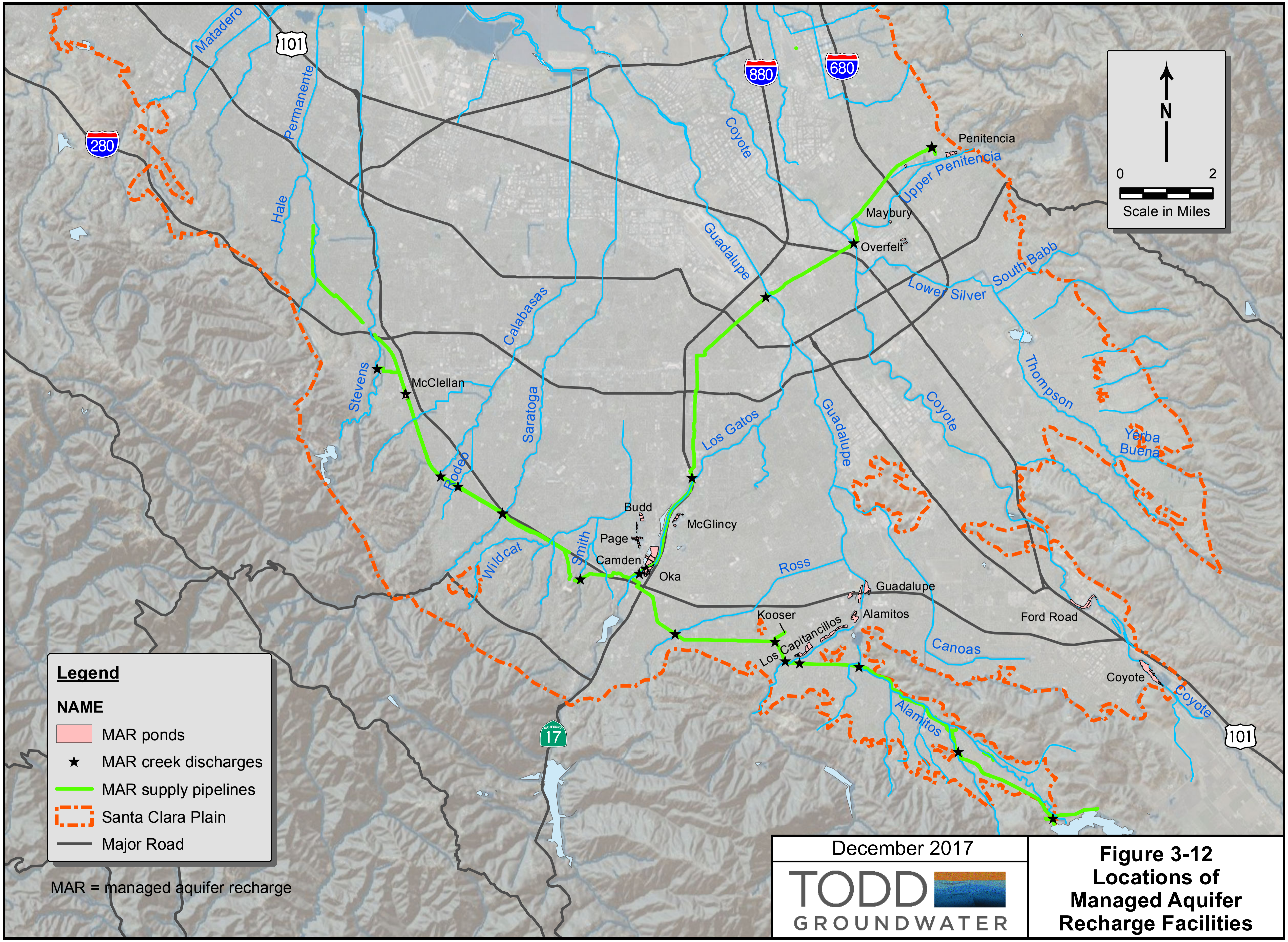

December 2017

TODD GROUNDWATER

Figure 3-12 Locations of Managed Aquifer Recharge Facilities

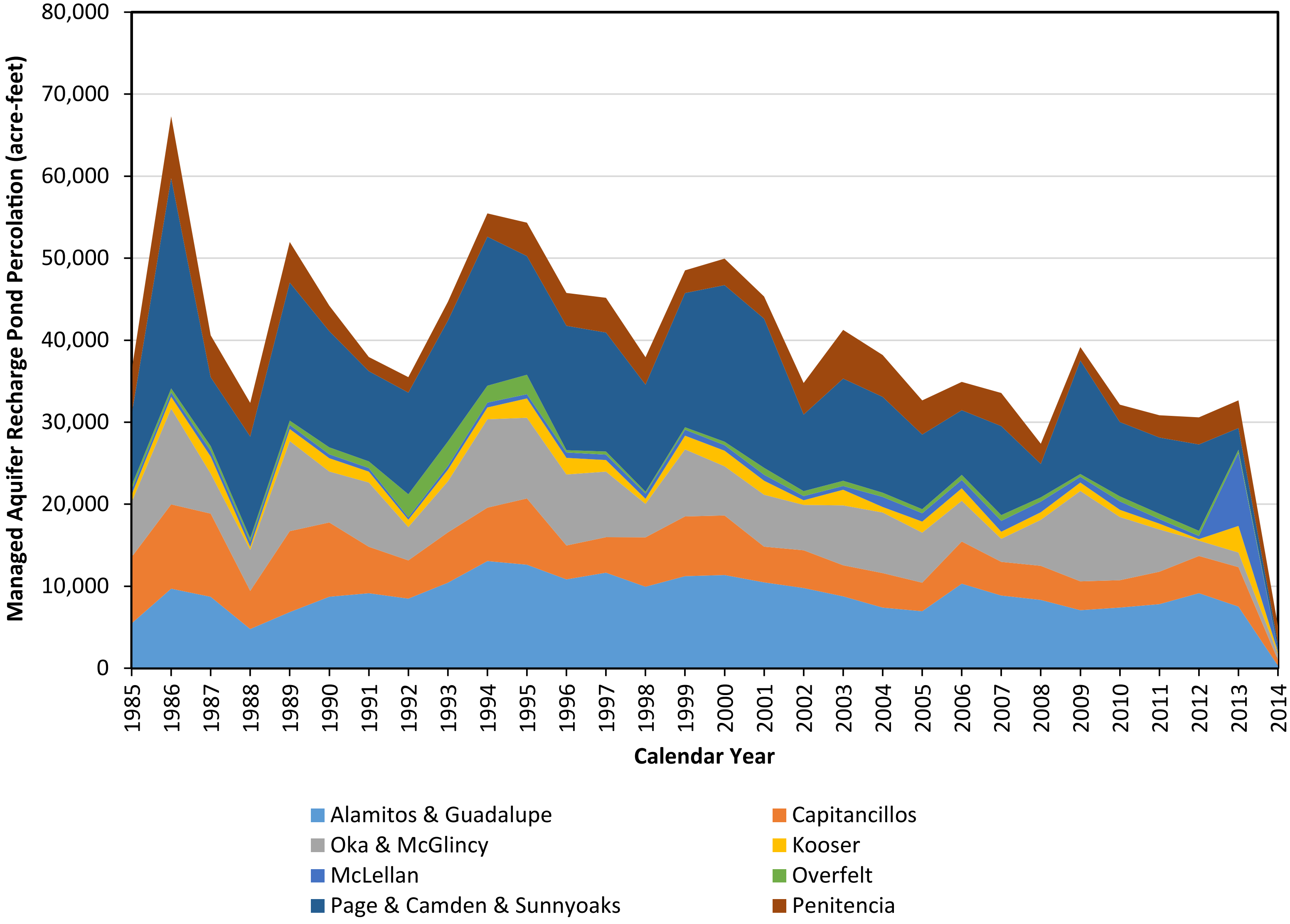

MAR = managed aquifer recharge

December 2017

TODD GROUNDWATER

Figure 3-13
MAR Pond
Percolation
1985 - 2014

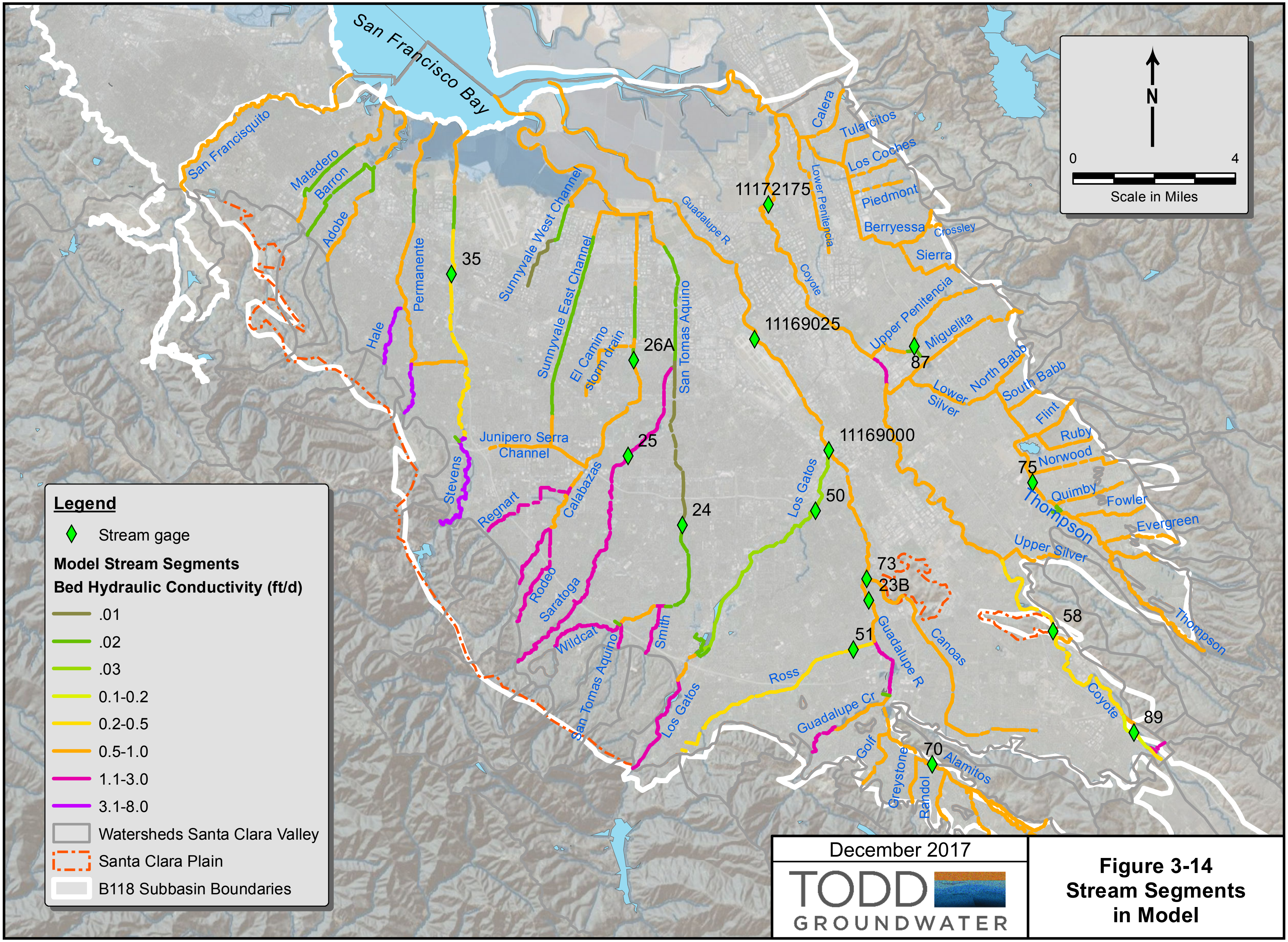

December 2017

TODD GROUNDWATER

Figure 3-14
Stream Segments in Model

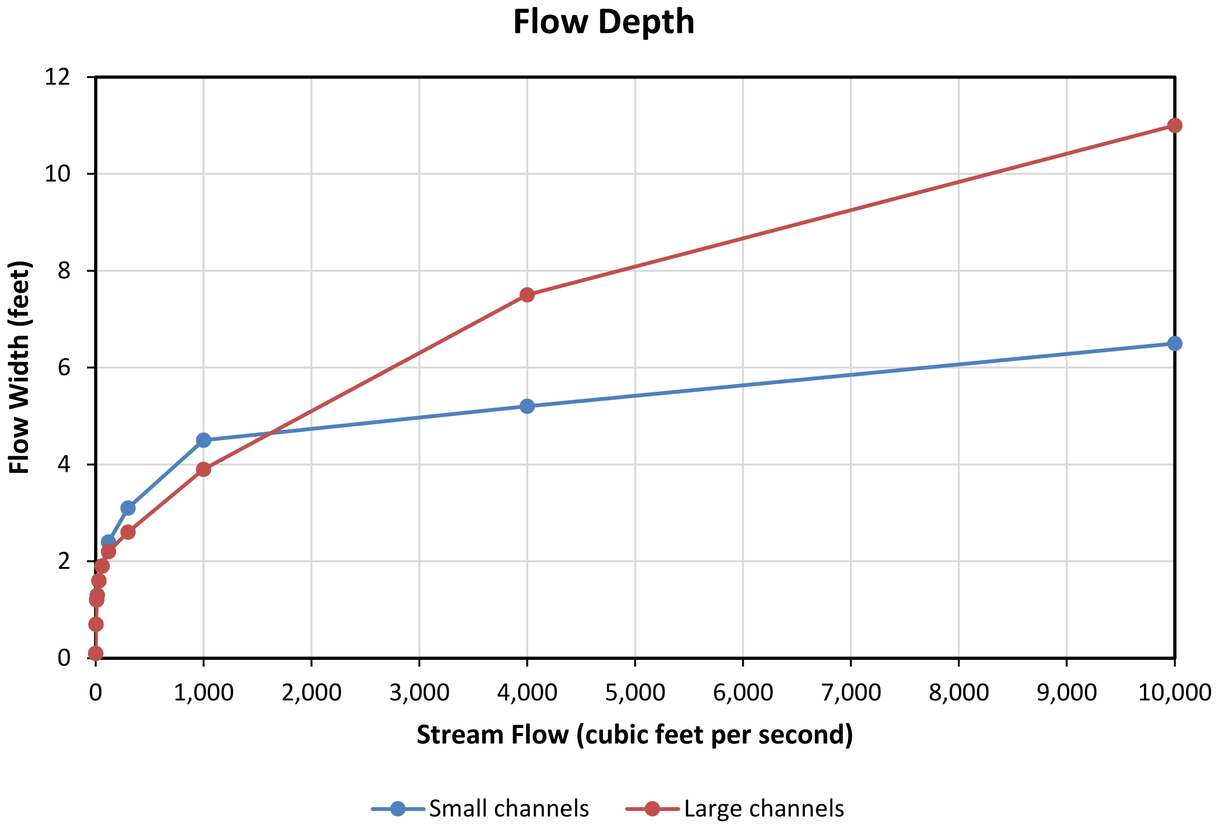

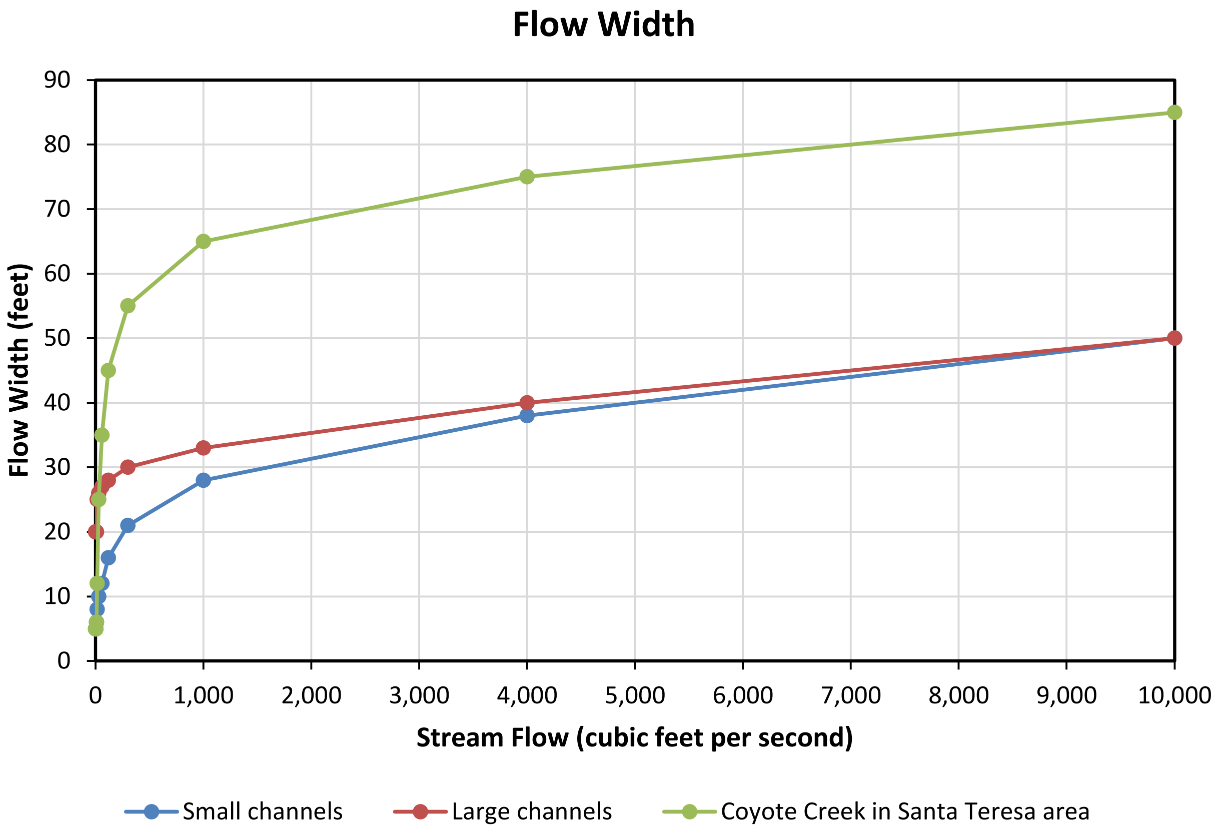

December 2017

TODD GROUNDWATER

Figure 3-15
Stream Channel
Depth and Width
Functions

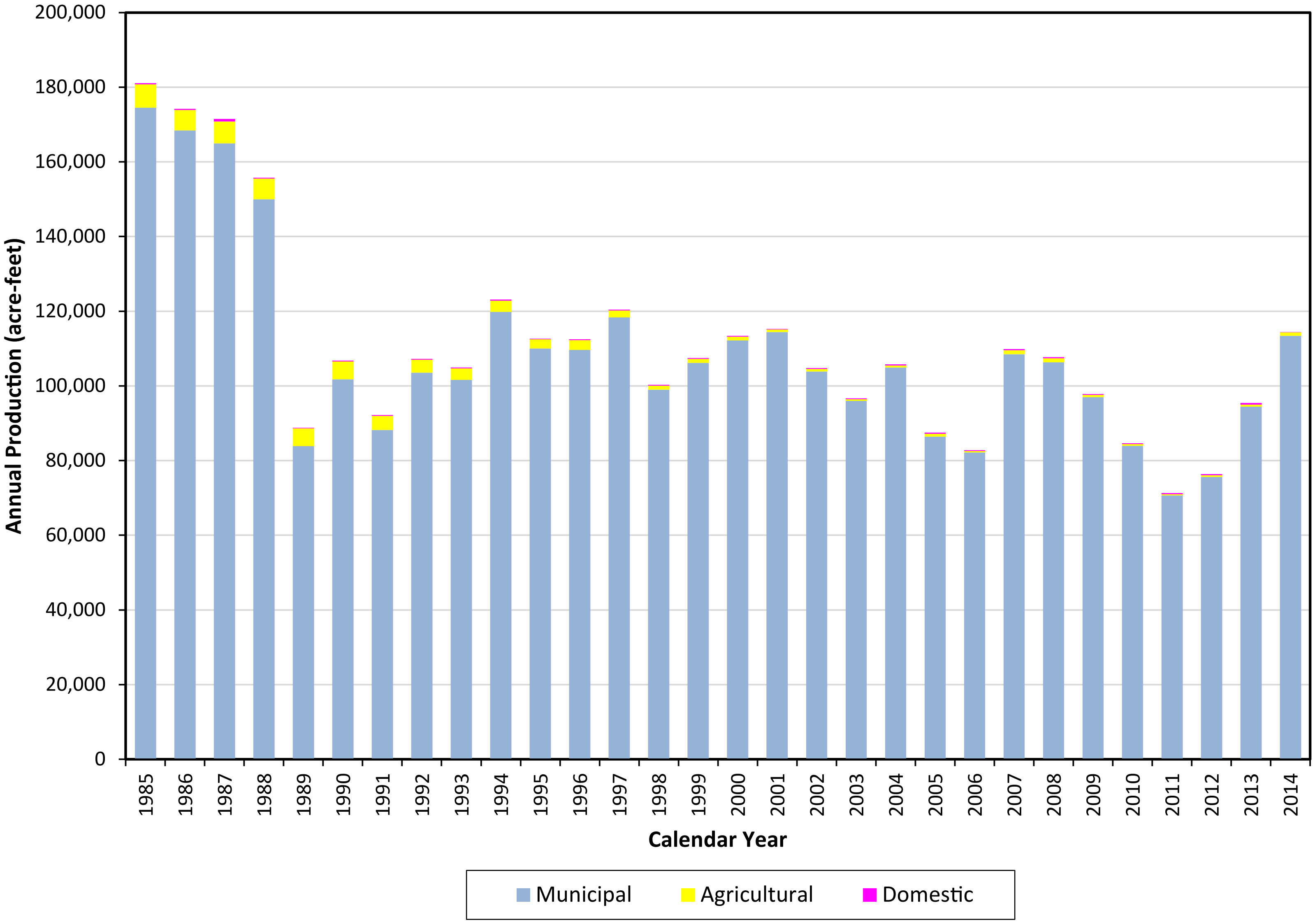

December 2017

TODD GROUNDWATER

Figure 3-16
Annual
Groundwater Production
1985 - 2014

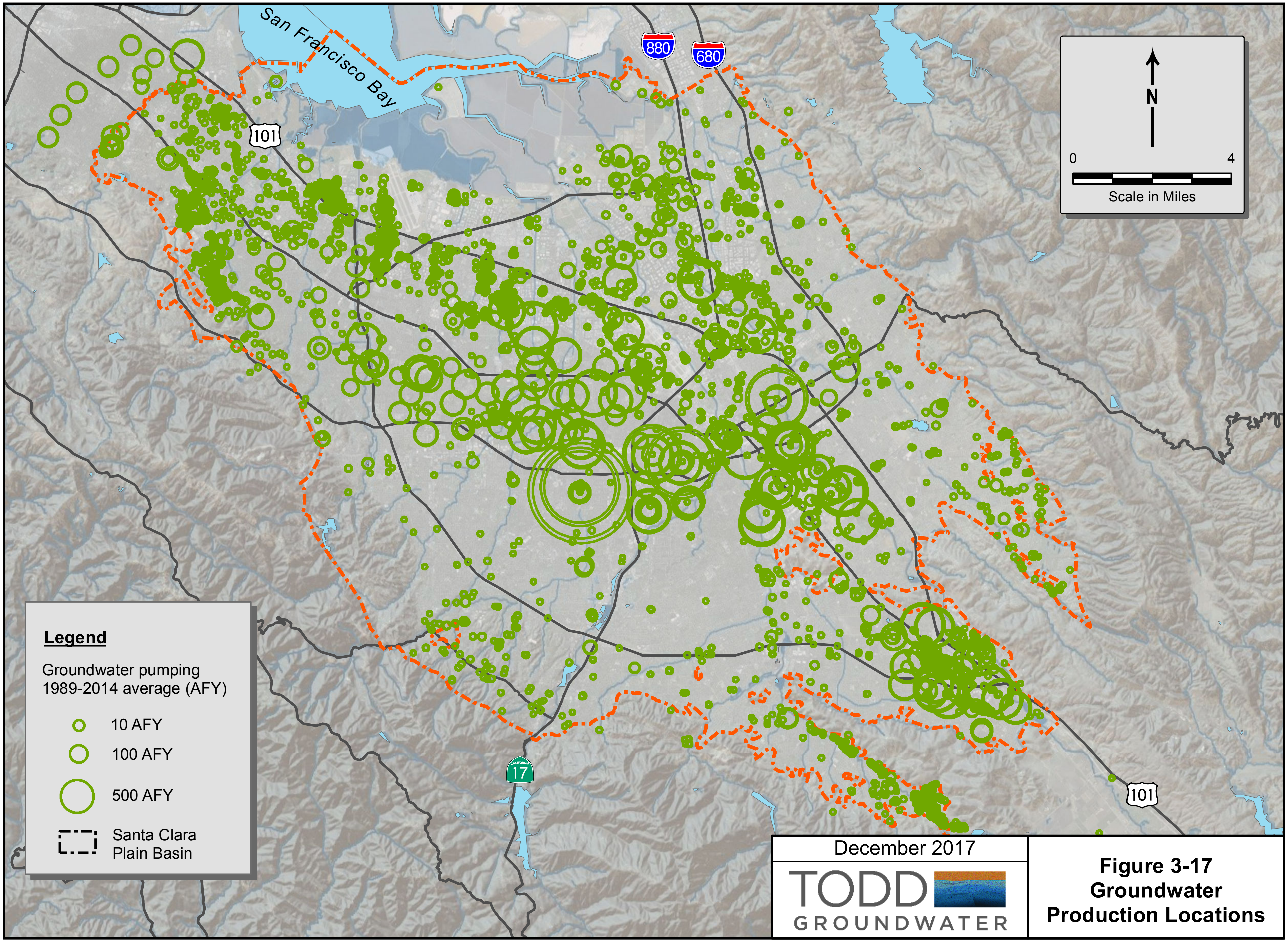

December 2017

TODD GROUNDWATER

Figure 3-17
Groundwater
Production Locations

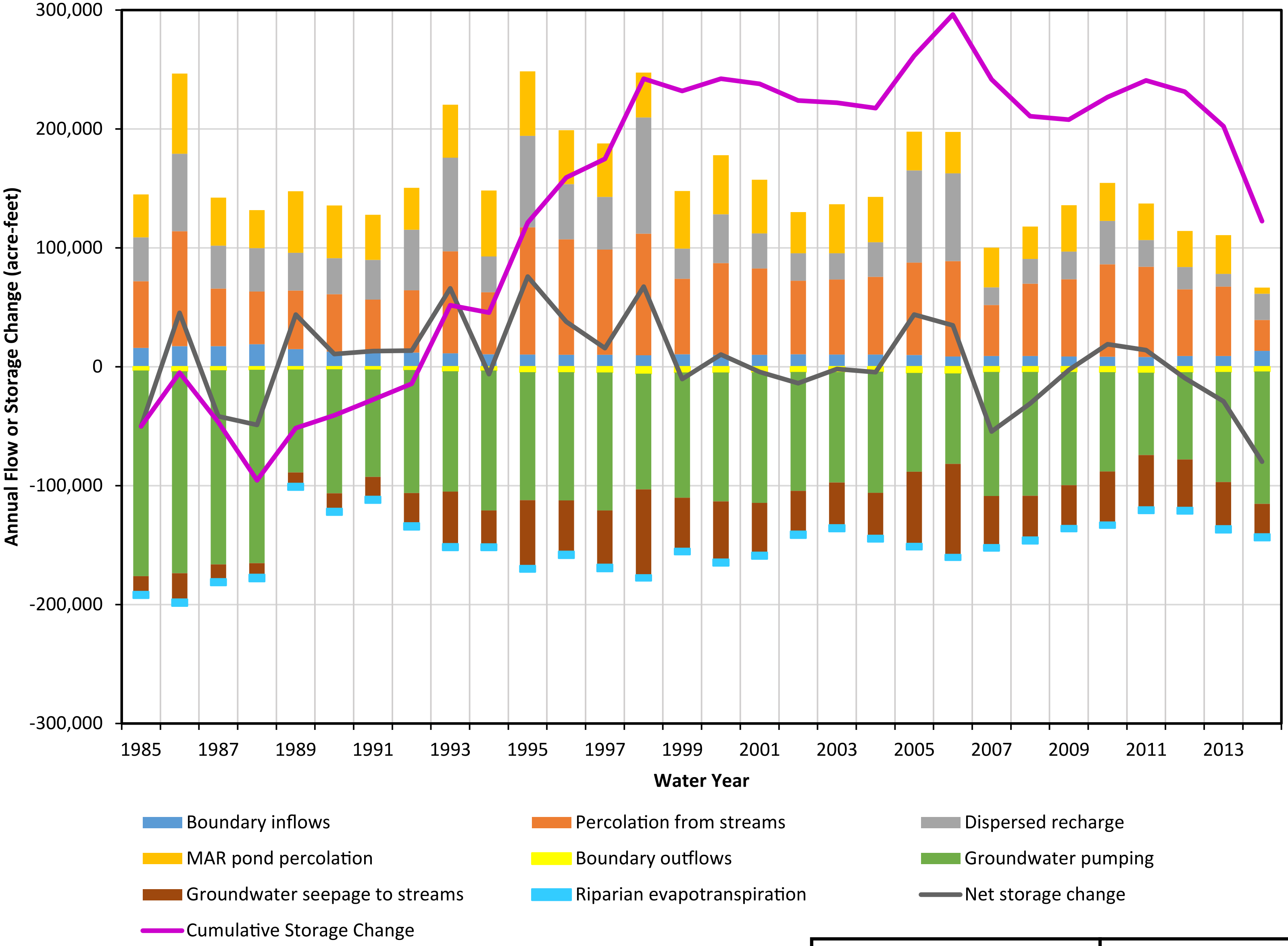

Note: Excludes the San Mateo County Subarea.

December 2017

TODD GROUNDWATER

Figure 3-18
Annual Groundwater Balances 1985 - 2014

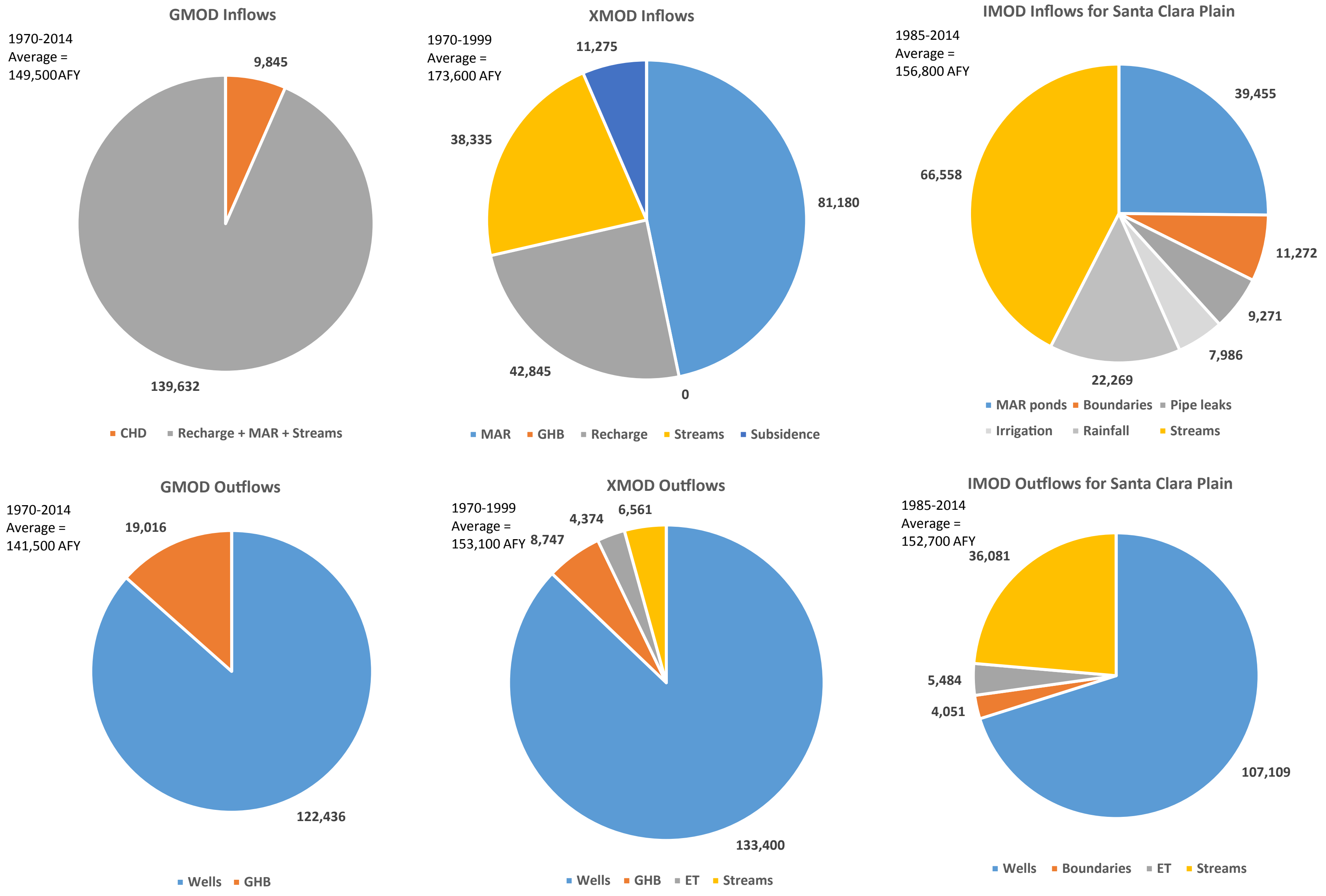

Notes: CHD = constant head boundary, MAR = managed aquifer recharge, GHB = general-head boundary, ET = riparian evapotranspiration, AFY = acre-feet per year

December 2017

TODD GROUNDWATER

Figure 3-19
Water Balance
Comparison with
GMOD and XMOD

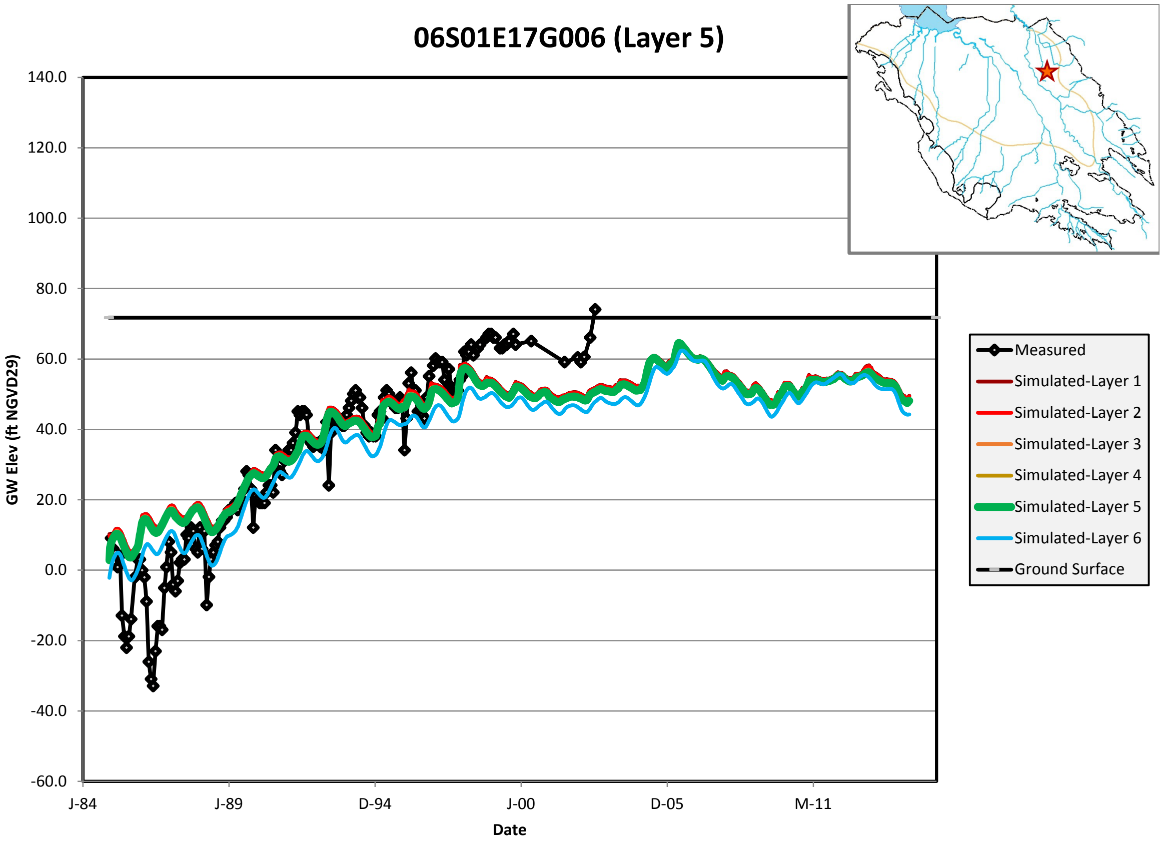

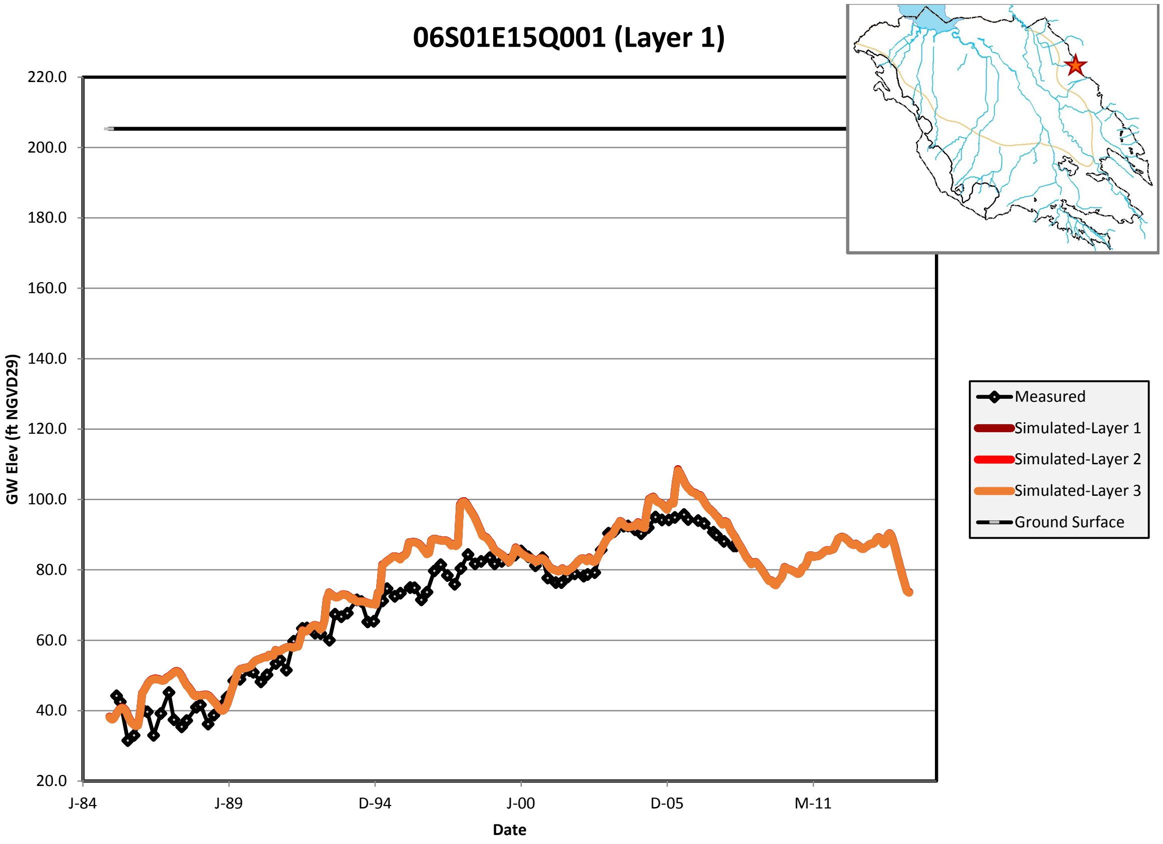

December 2017

TODD GROUNDWATER

Figure 4-1
Hydrographs of Measured and Simulated Groundwater Levels Northeast Subbasin Margin

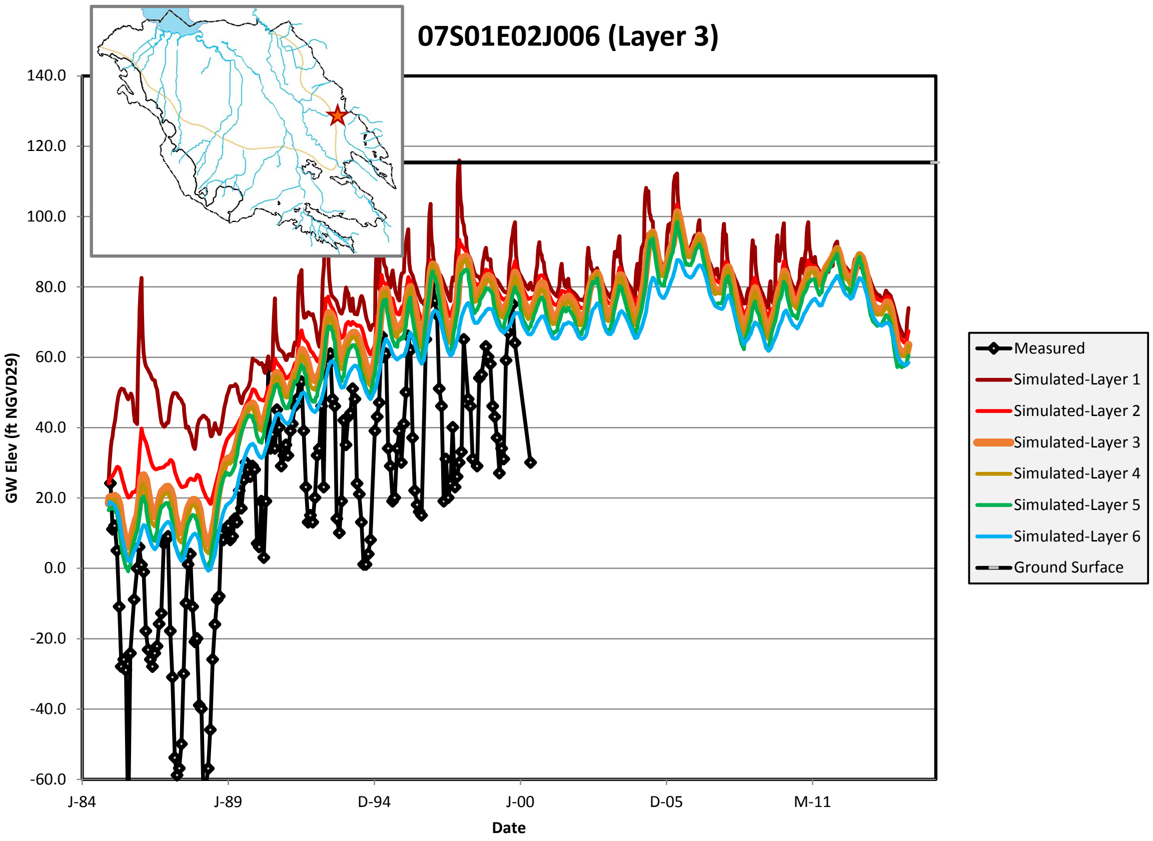

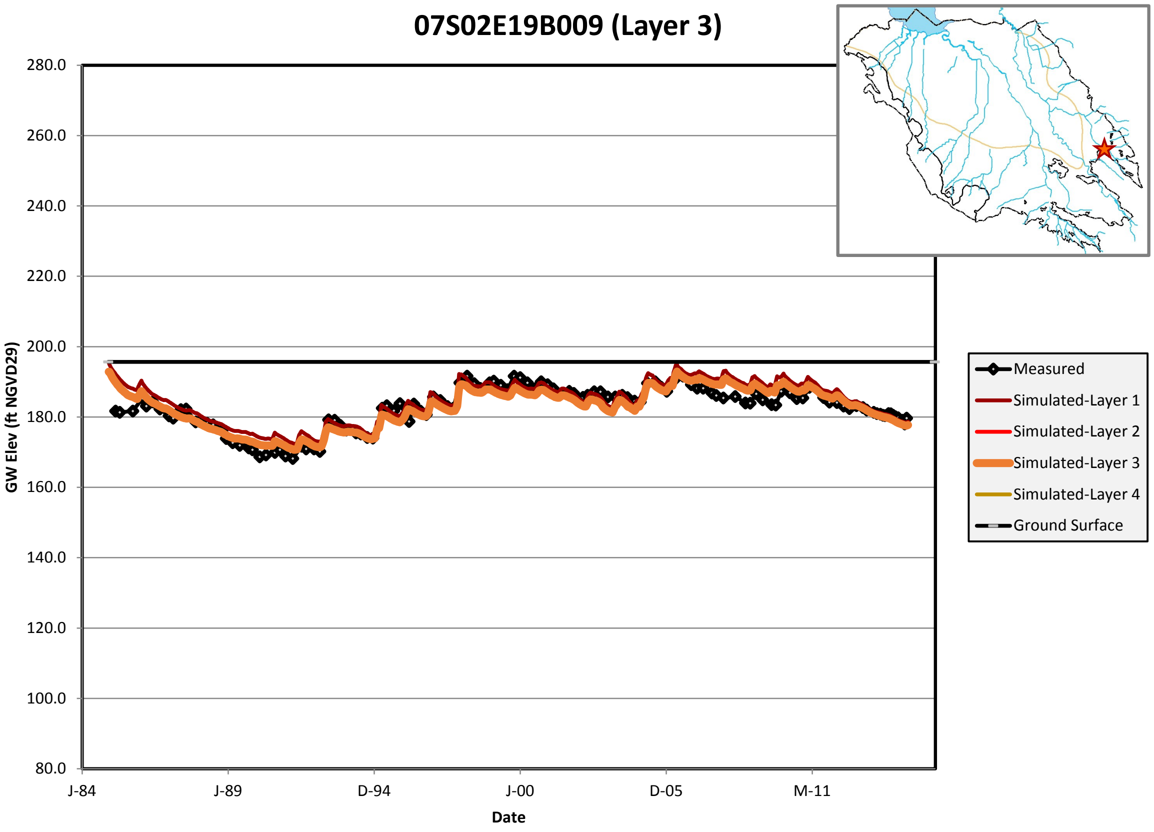

December 2017

TODD GROUNDWATER

Figure 4-2
Hydrographs of Measured and Simulated Groundwater Levels Southeast Subbasin Margin

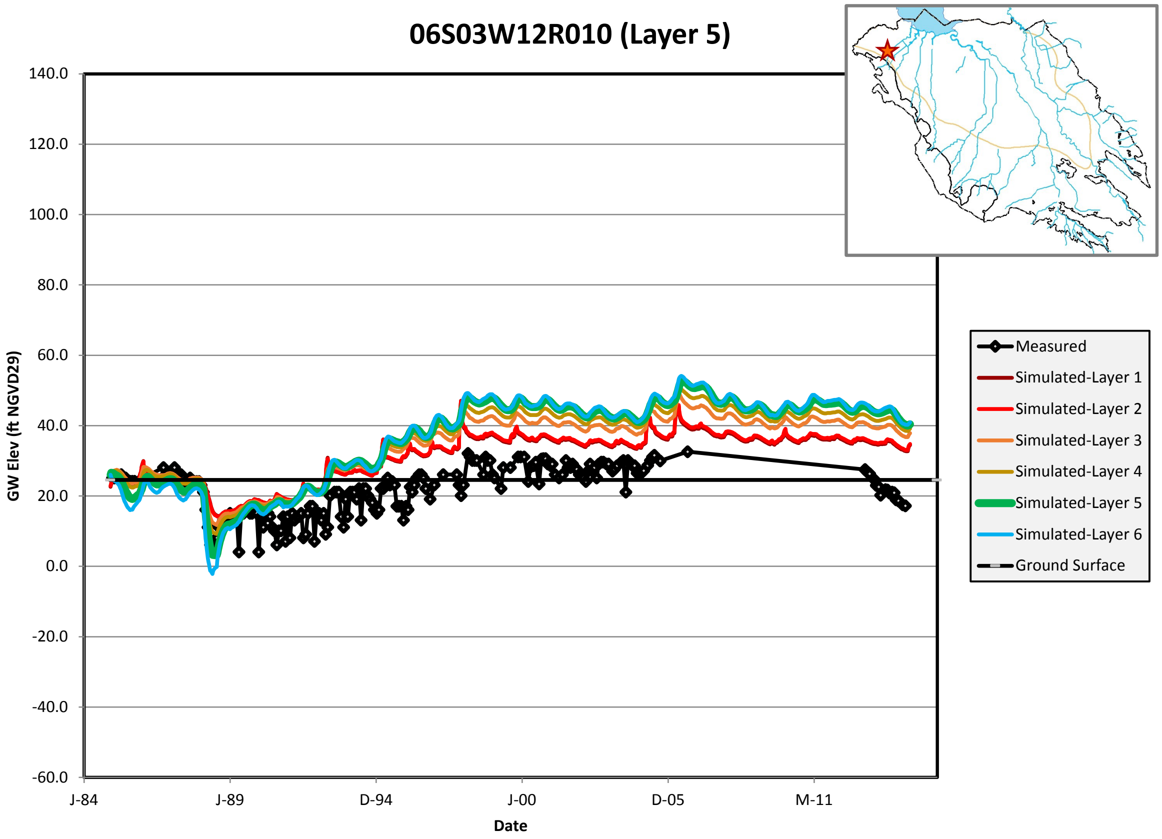

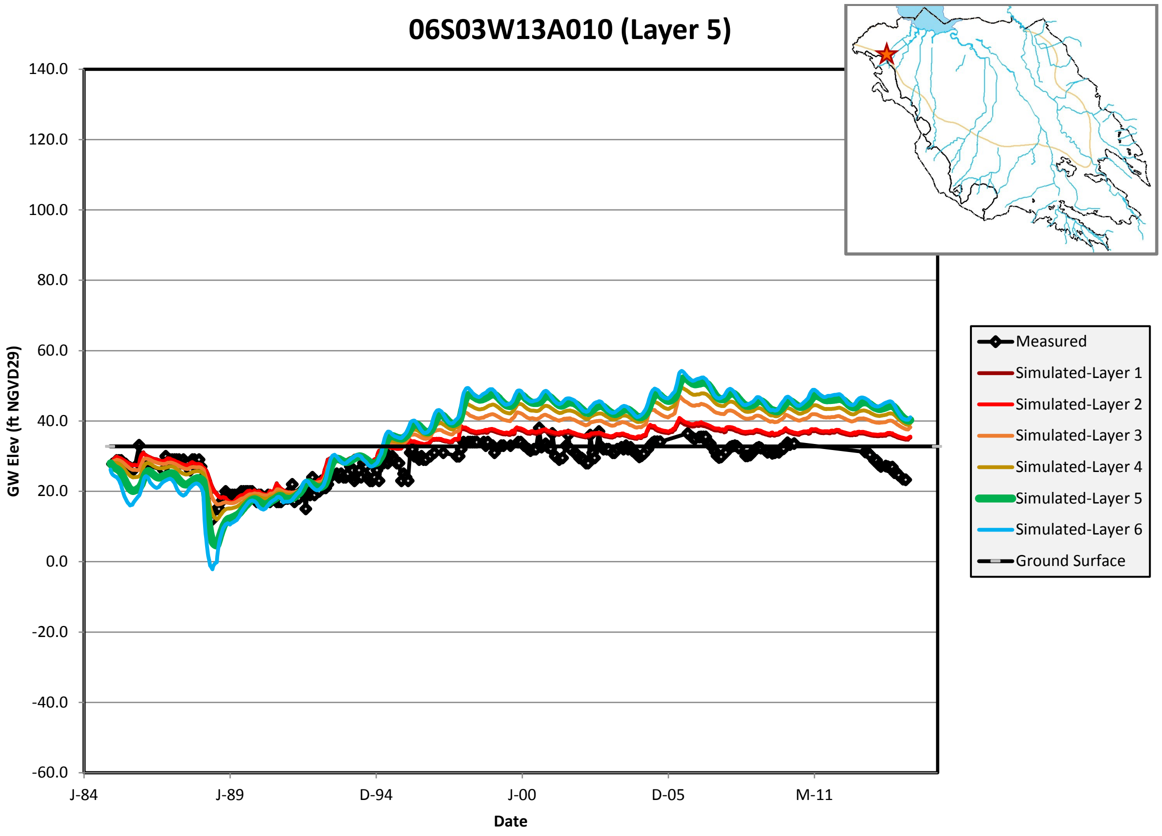

December 2017

TODD GROUNDWATER

Figure 4-3a
Hydrographs of Measured and Simulated Groundwater Levels Northwest Subbasin Margin

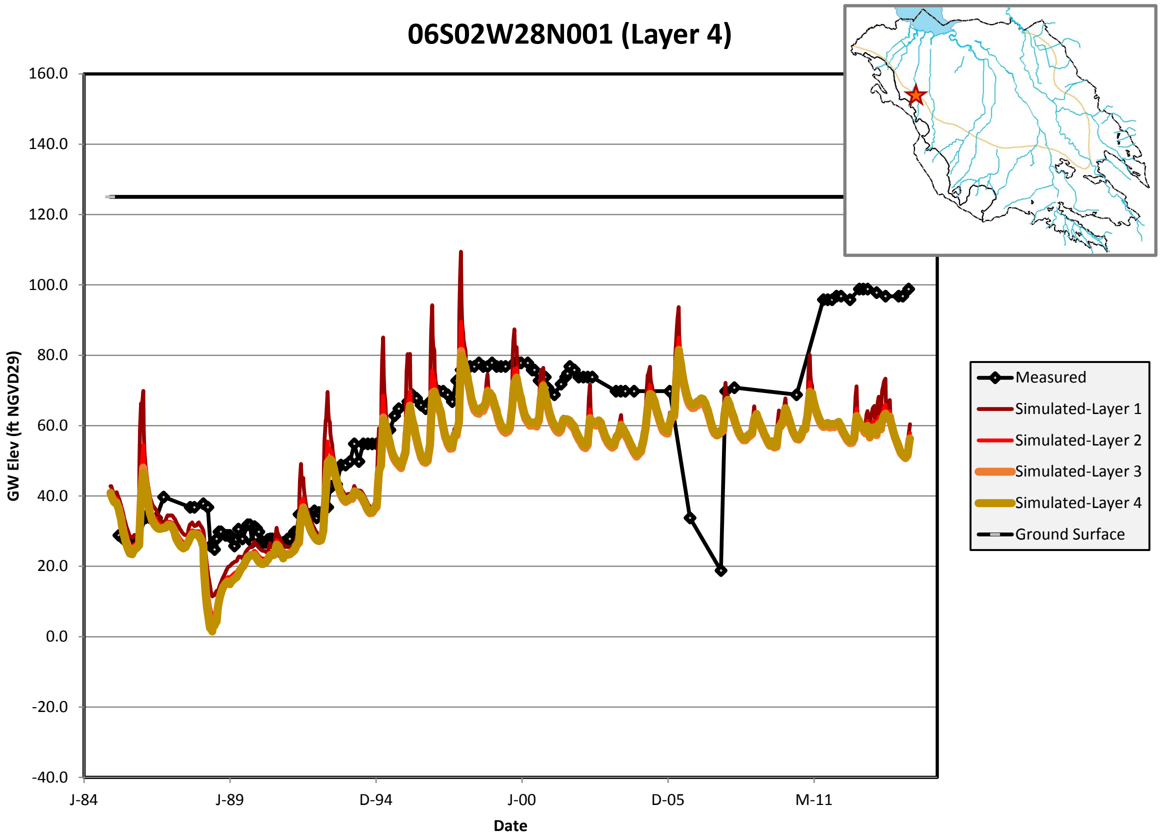
06S02W28N001 (Layer 4)

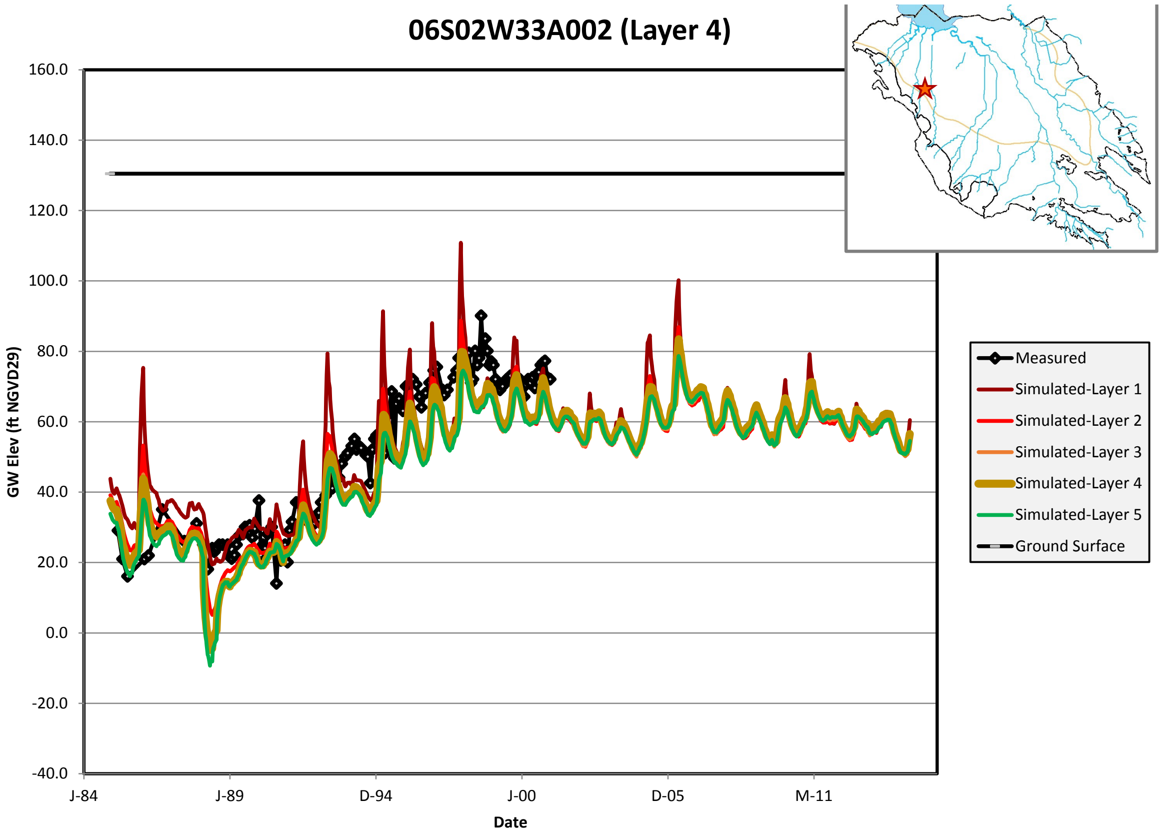
06S02W33A002 (Layer 4)

December 2017

TODD GROUNDWATER

Figure 4-3b
Hydrographs of Measured and Simulated Groundwater Levels Northwest Subbasin Margin

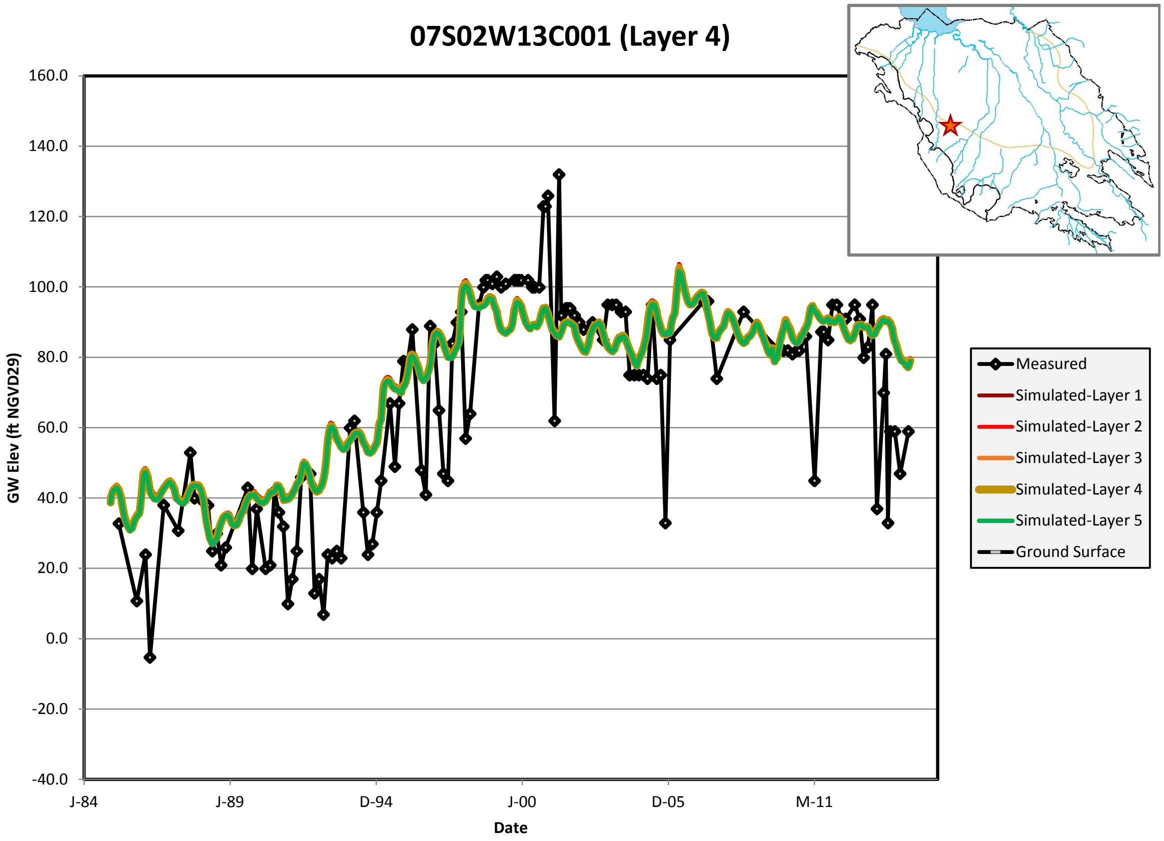

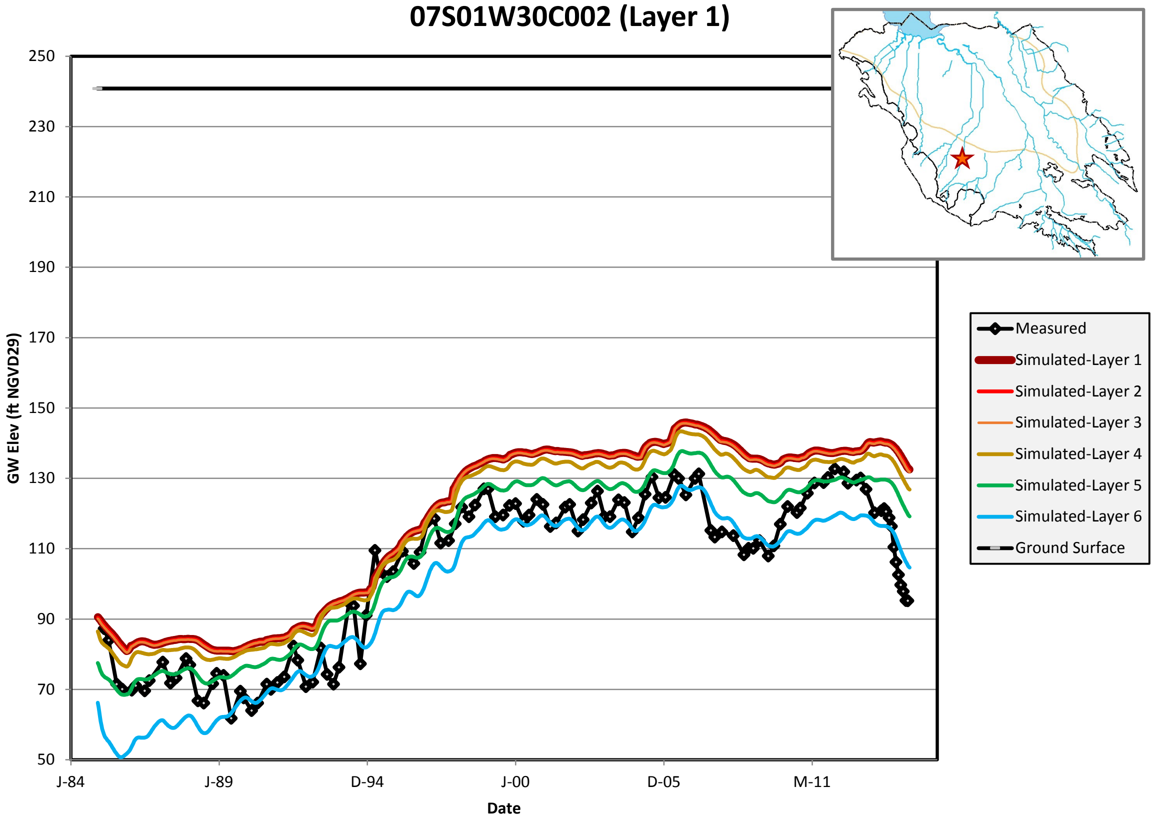

December 2017

TODD GROUNDWATER

Figure 4-4a
Hydrographs of Measured and Simulated Groundwater Levels Southwest Subbasin Margin

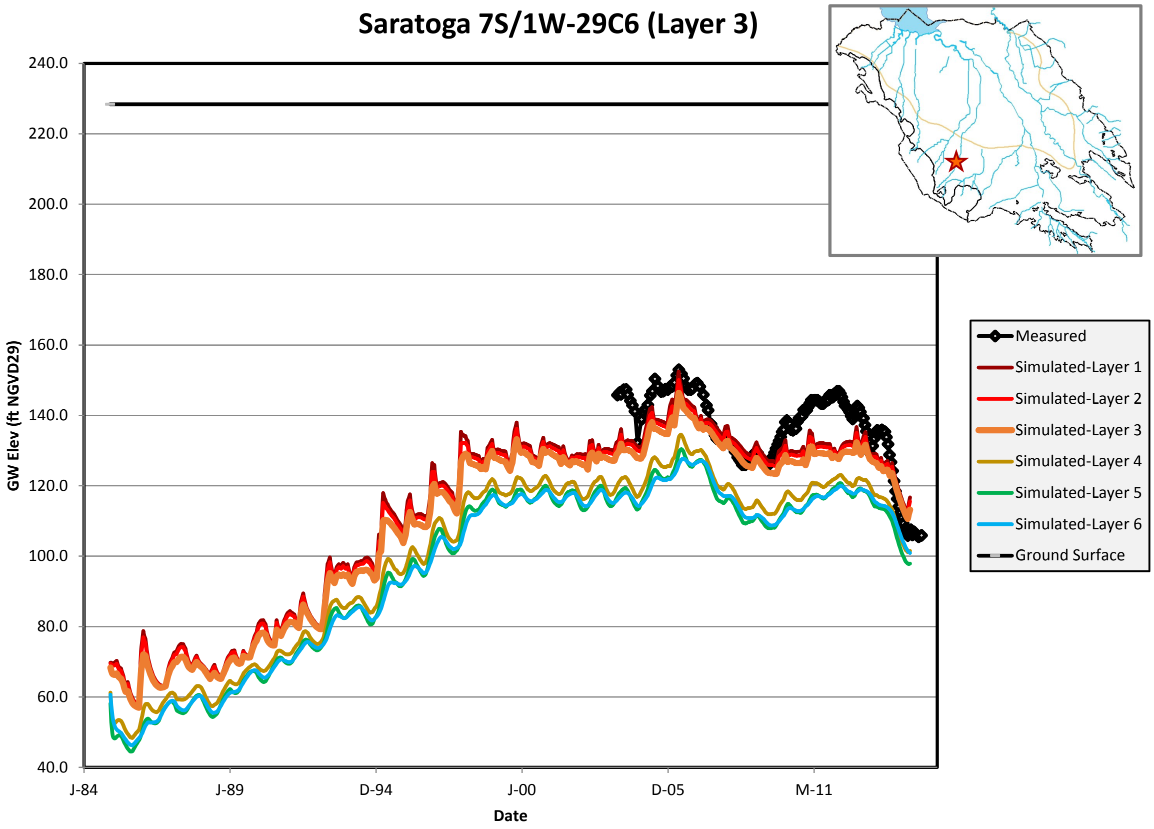
Saratoga 7S/1W-29C6 (Layer 3)

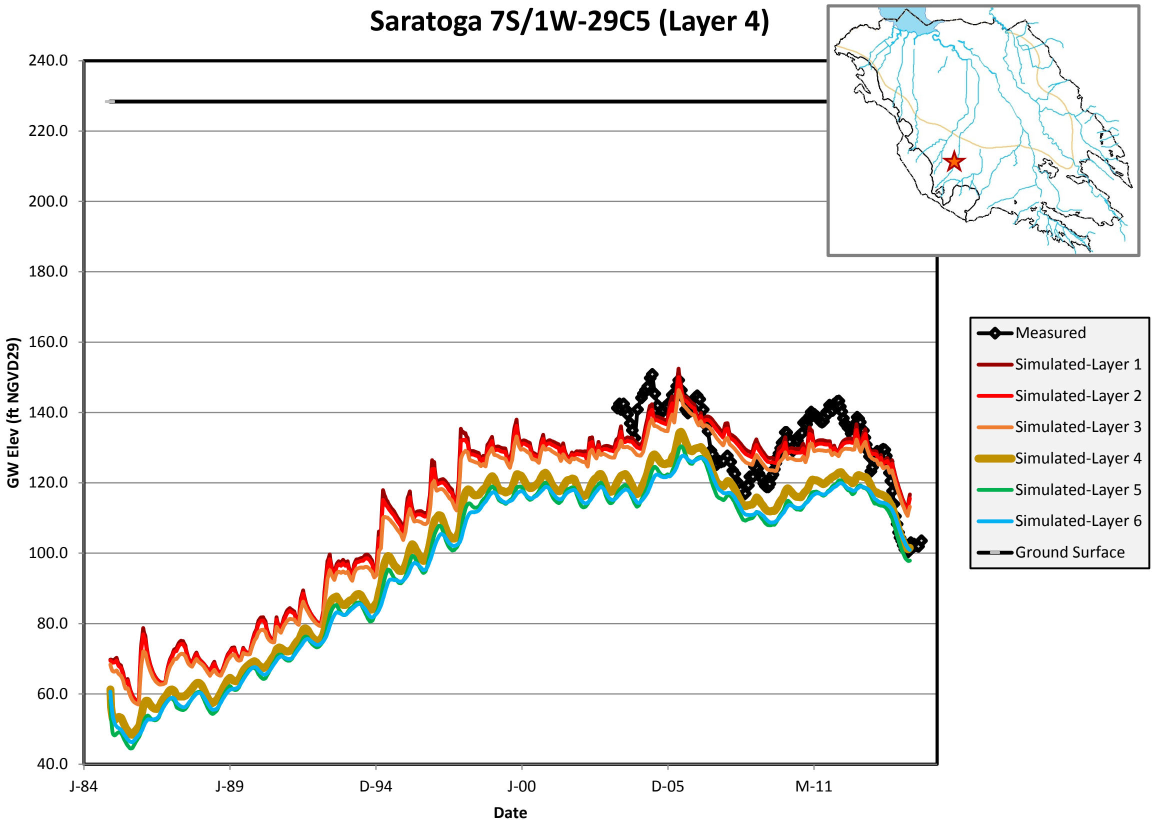
Saratoga 7S/1W-29C5 (Layer 4)

December 2017

TODD GROUNDWATER

Figure 4-4b
Hydrographs of Measured and Simulated Groundwater Levels Southwest Subbasin Margin

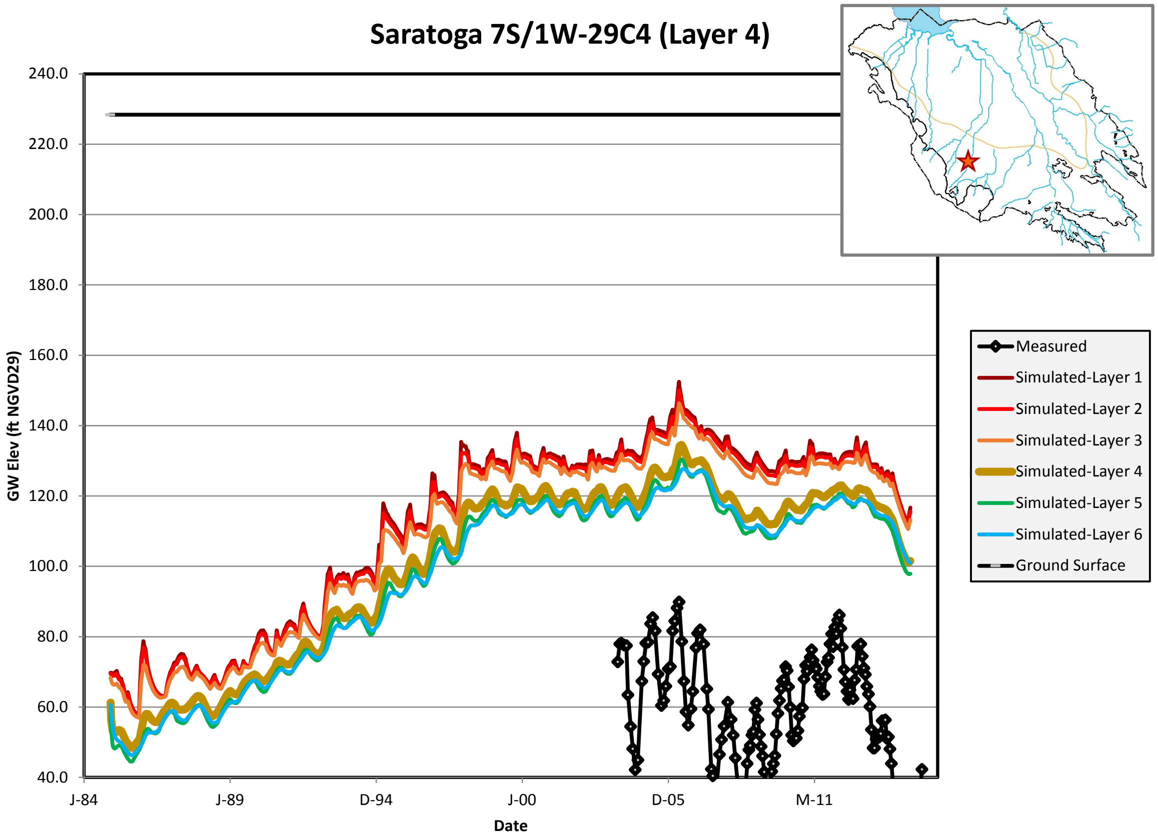

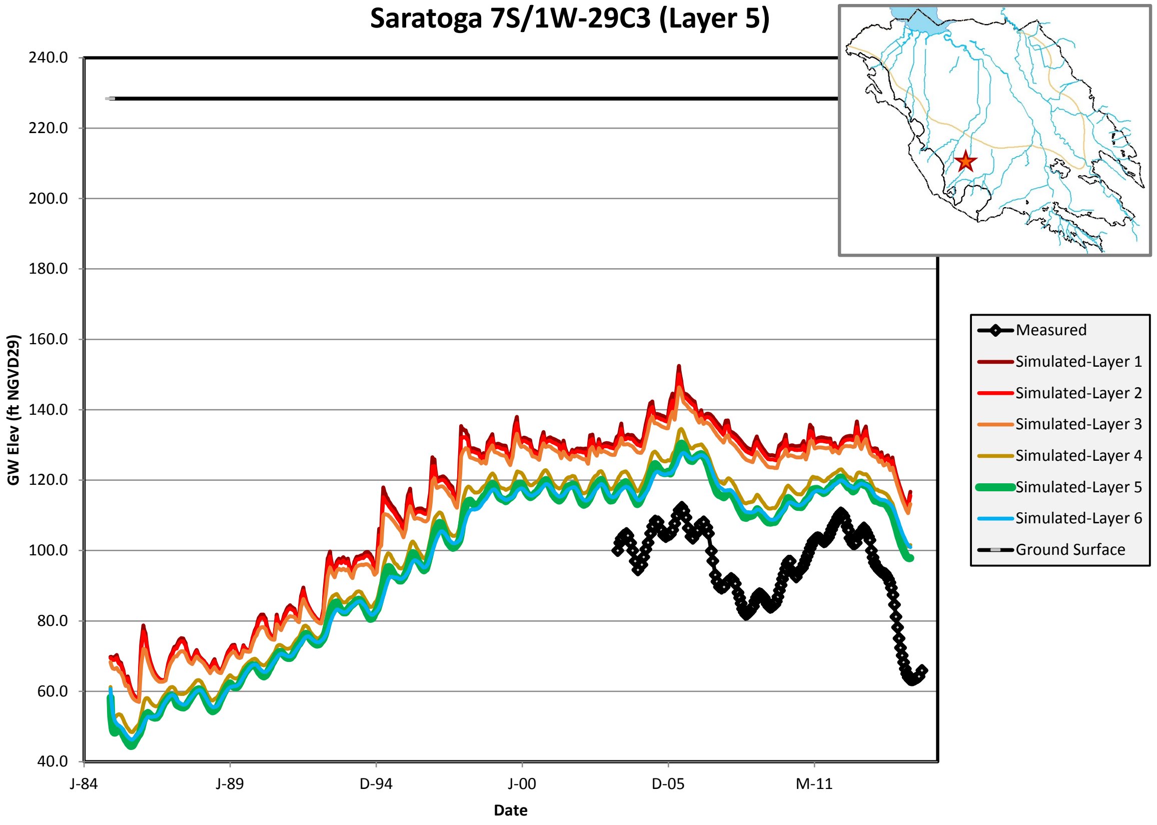

December 2017

TODD GROUNDWATER

Figure 4-4c
Hydrographs of Measured and Simulated Groundwater Levels Southwest Subbasin Margin

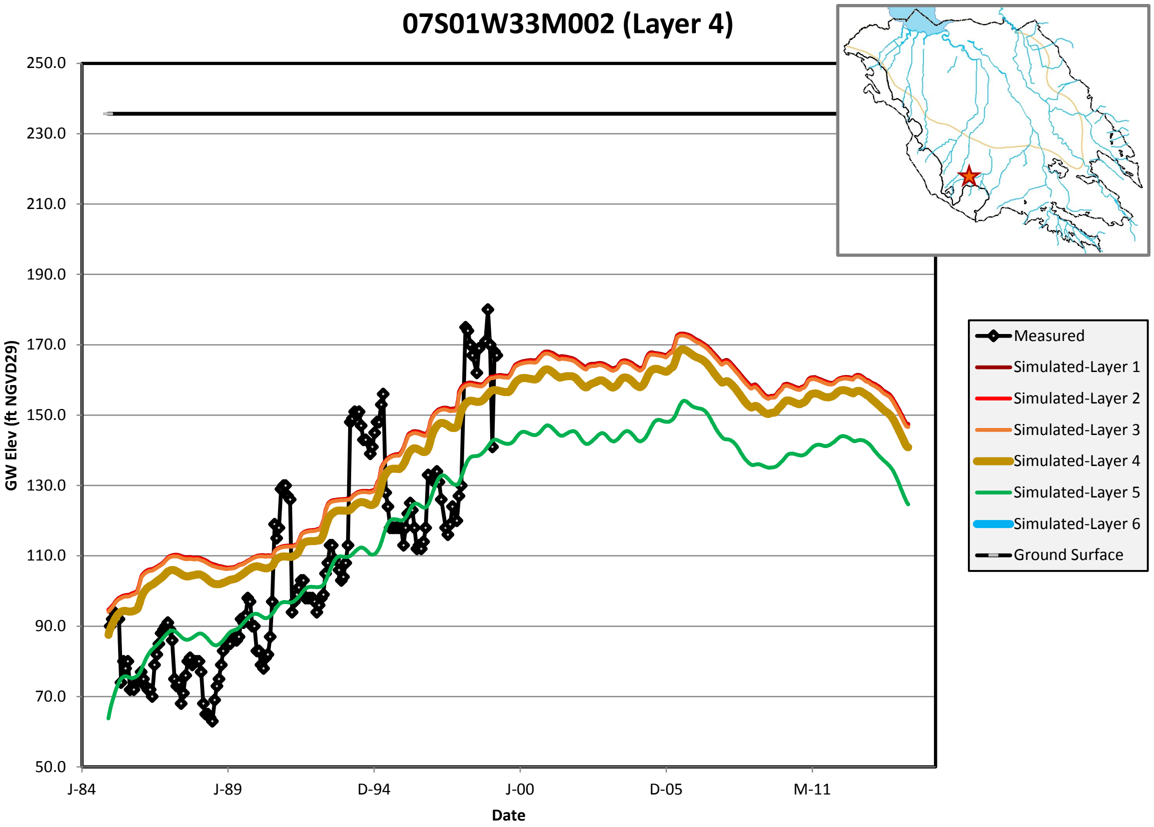
07S01W33M002 (Layer 4)

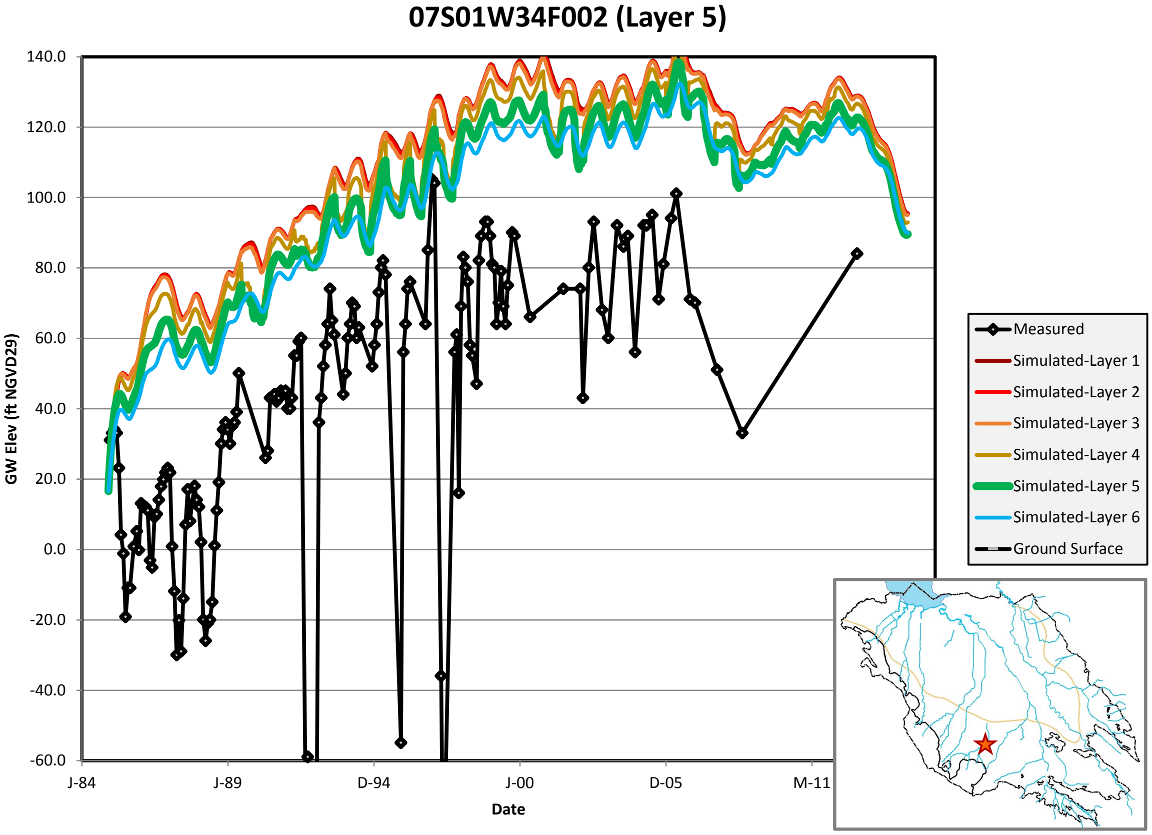
07S01W34F002 (Layer 5)

December 2017

TODD GROUNDWATER

Figure 4-4d
Hydrographs of Measured and Simulated Groundwater Levels Southwest Subbasin Margin

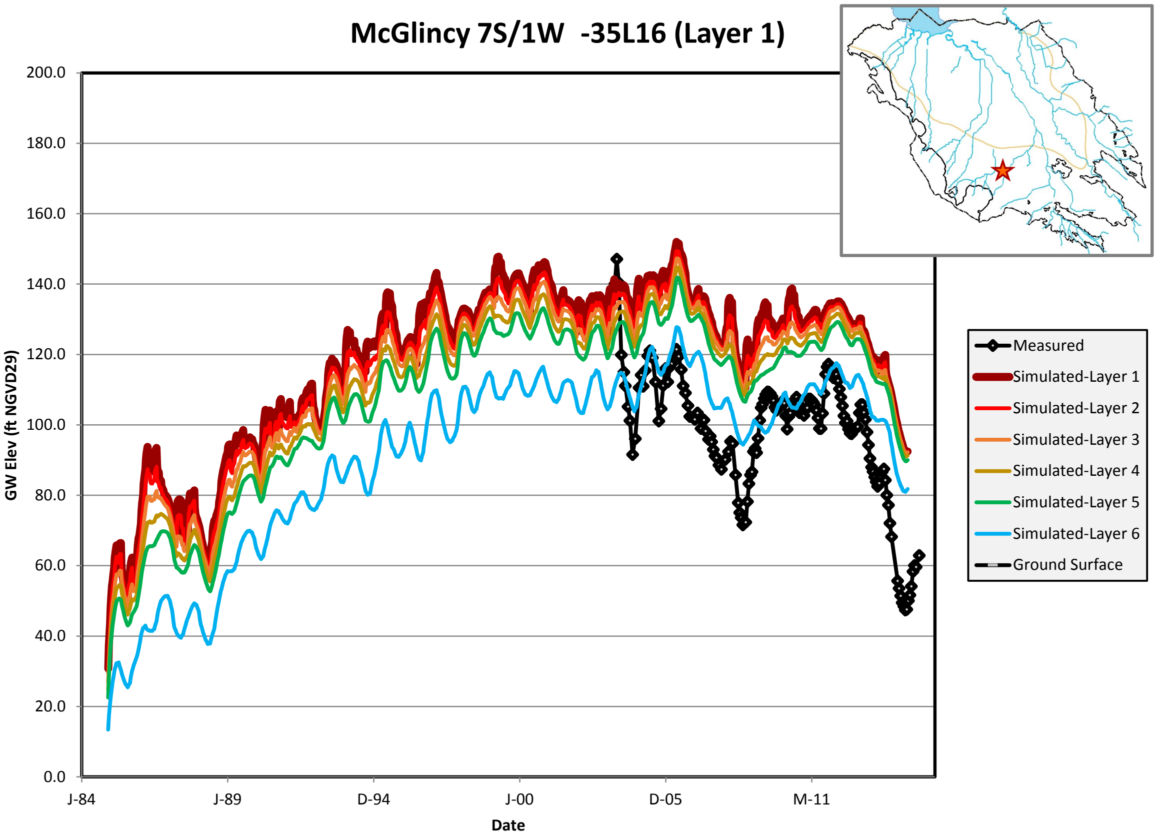

McGlincy 7S/1W -35L16 (Layer 1)

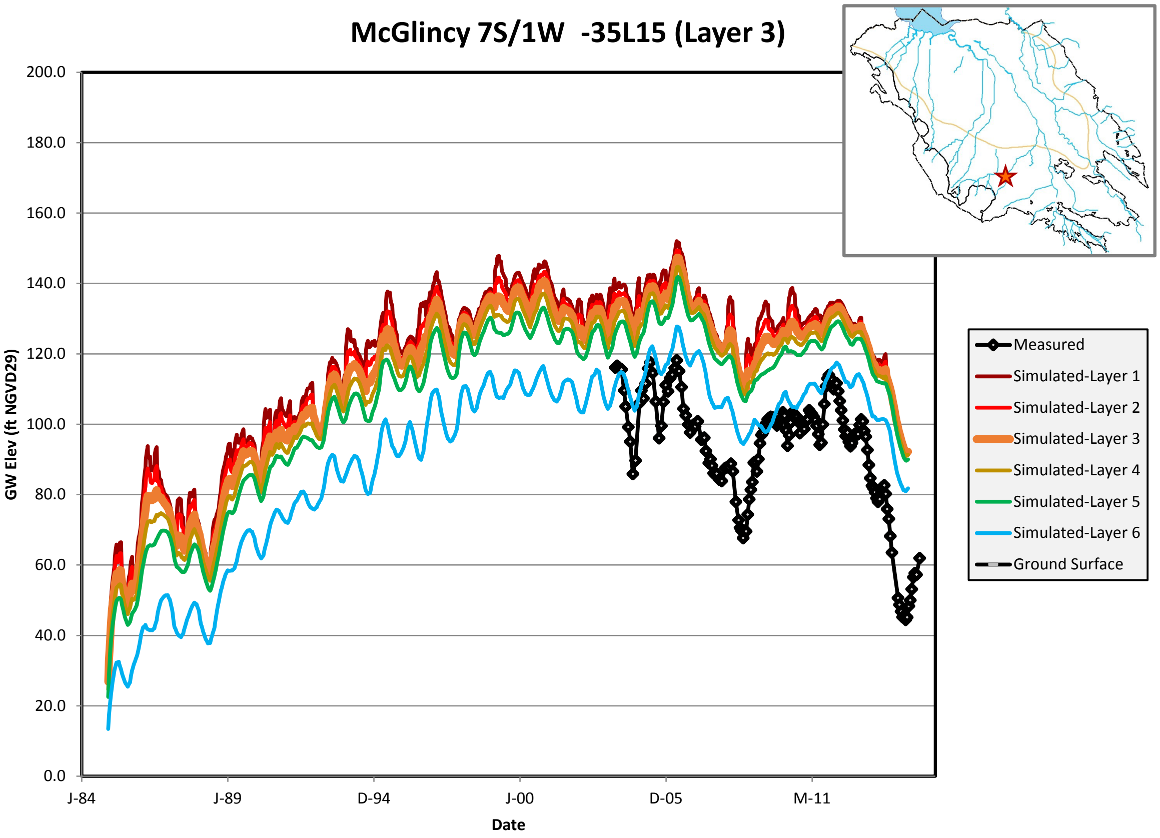

McGlincy 7S/1W -35L15 (Layer 3)

December 2017

TODD GROUNDWATER

Figure 4-4e
Hydrographs of Measured and Simulated Groundwater Levels Southwest Subbasin Margin

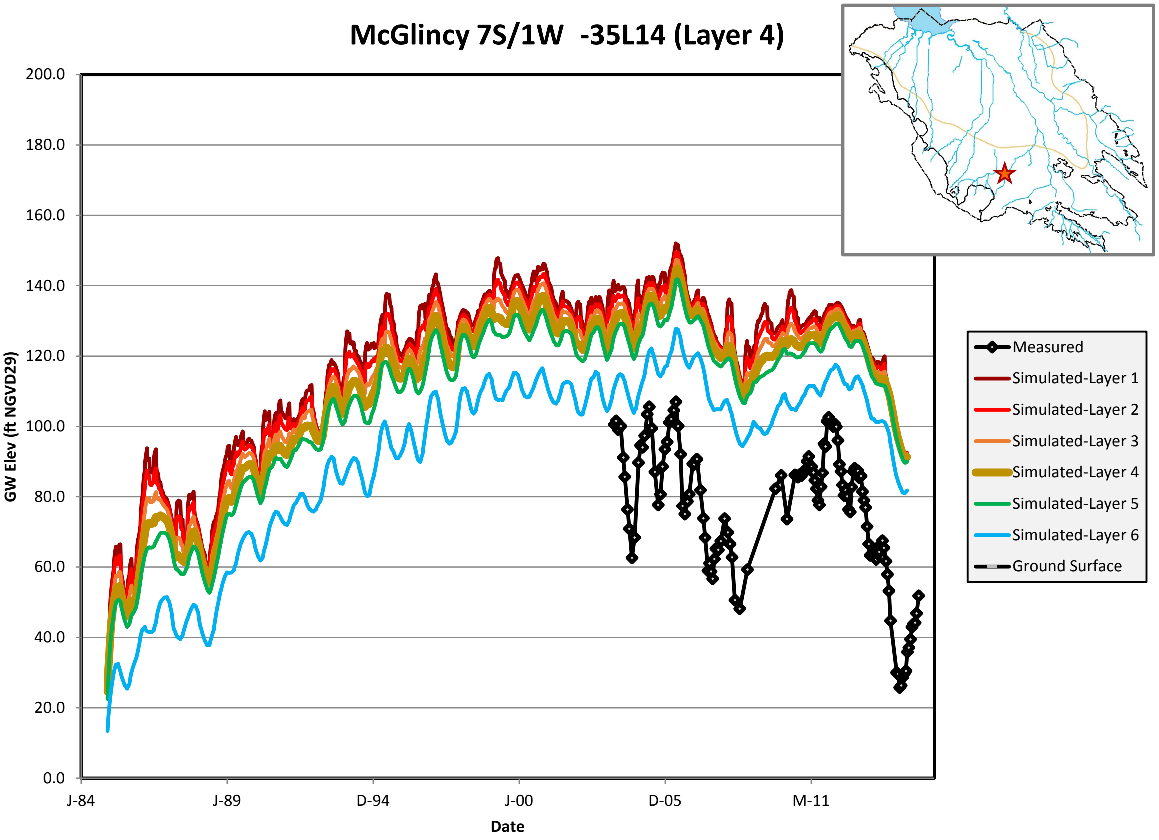

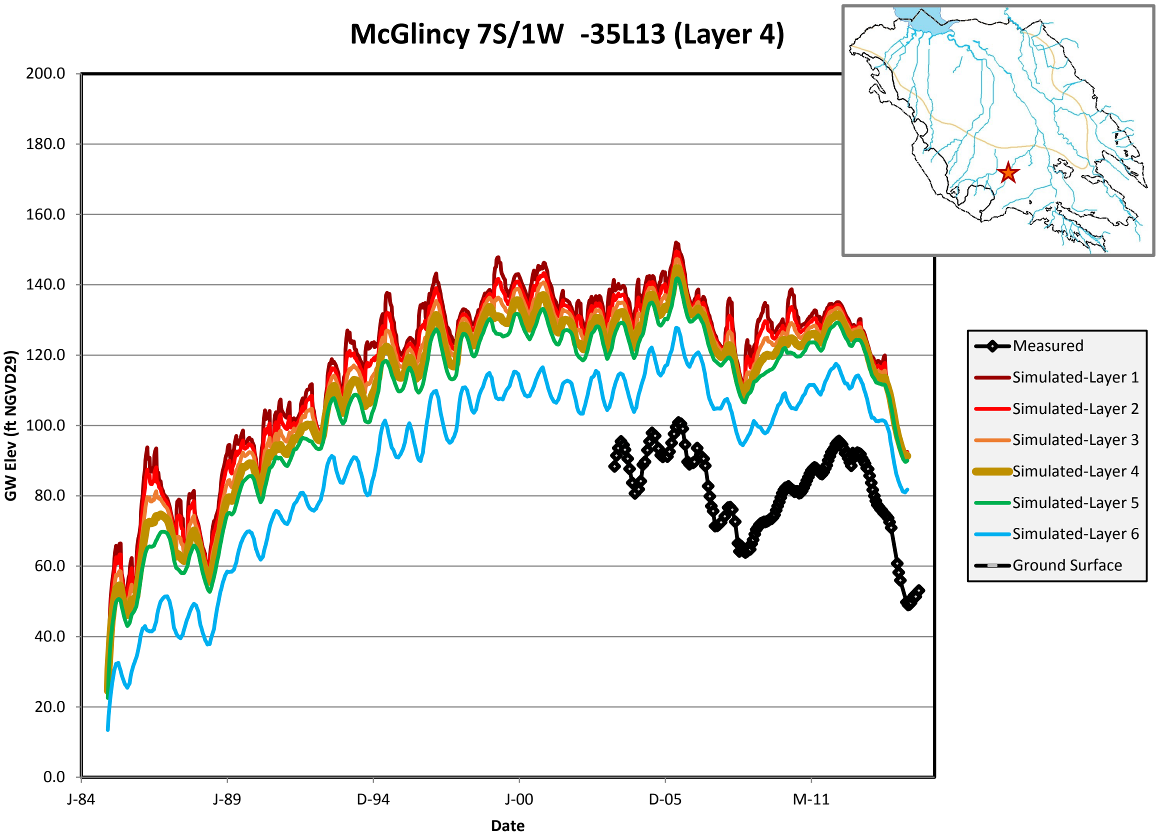

December 2017

TODD GROUNDWATER

Figure 4-4f
Hydrographs of Measured and Simulated Groundwater Levels Southwest Subbasin Margin

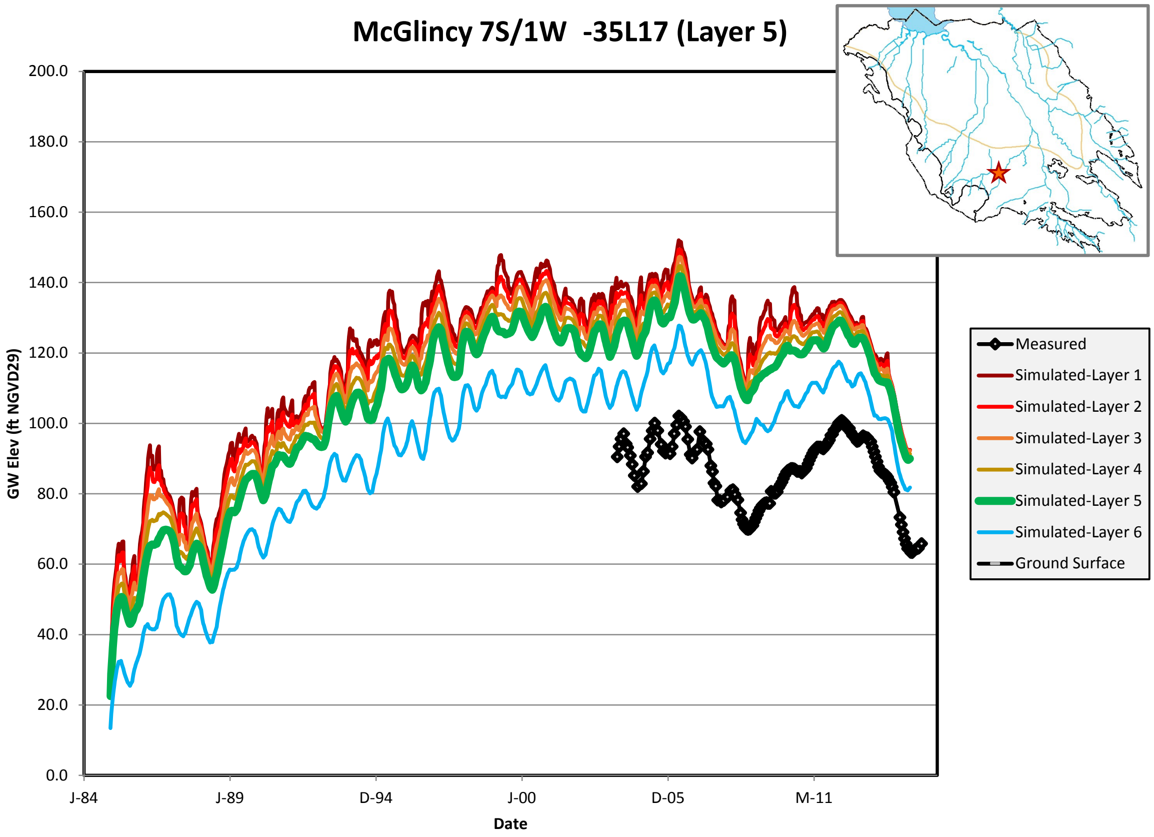

McGlincy 7S/1W -35L17 (Layer 5)

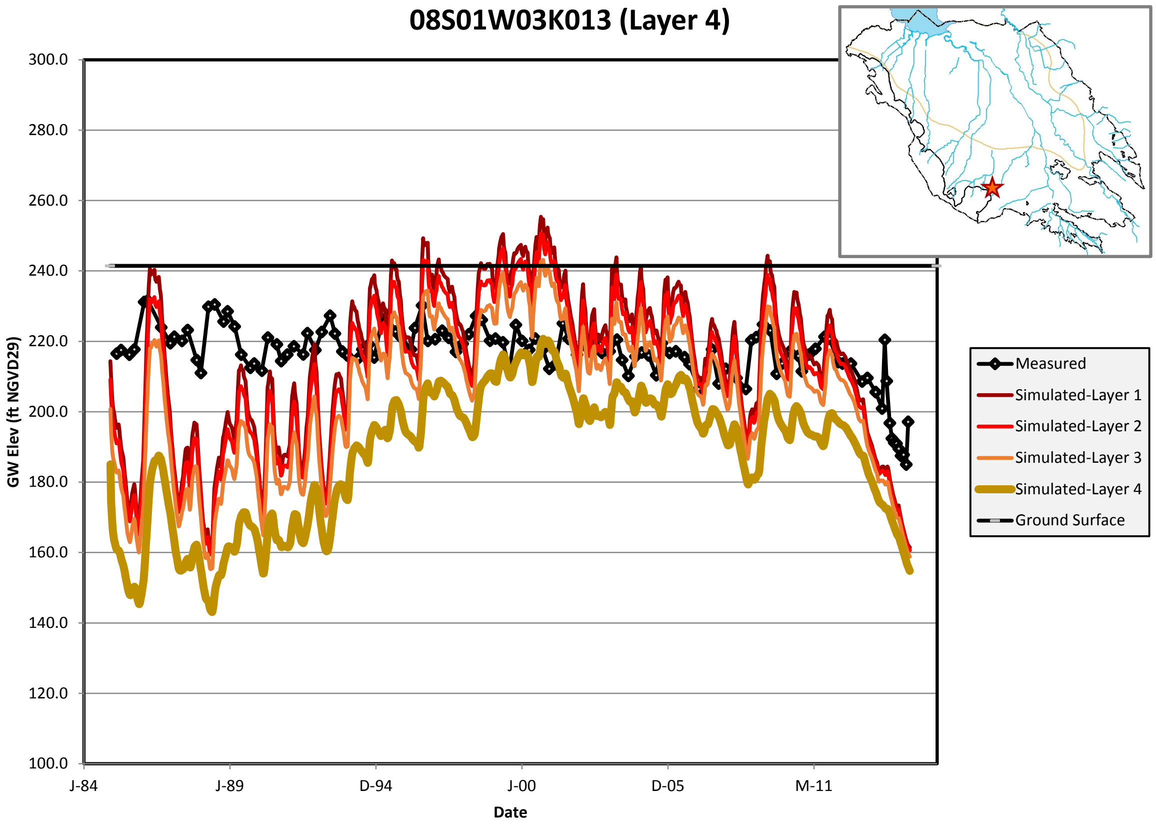

08S01W03K013 (Layer 4)

December 2017

TODD GROUNDWATER

Figure 4-4g
Hydrographs of Measured and Simulated Groundwater Levels Southwest Subbasin Margin

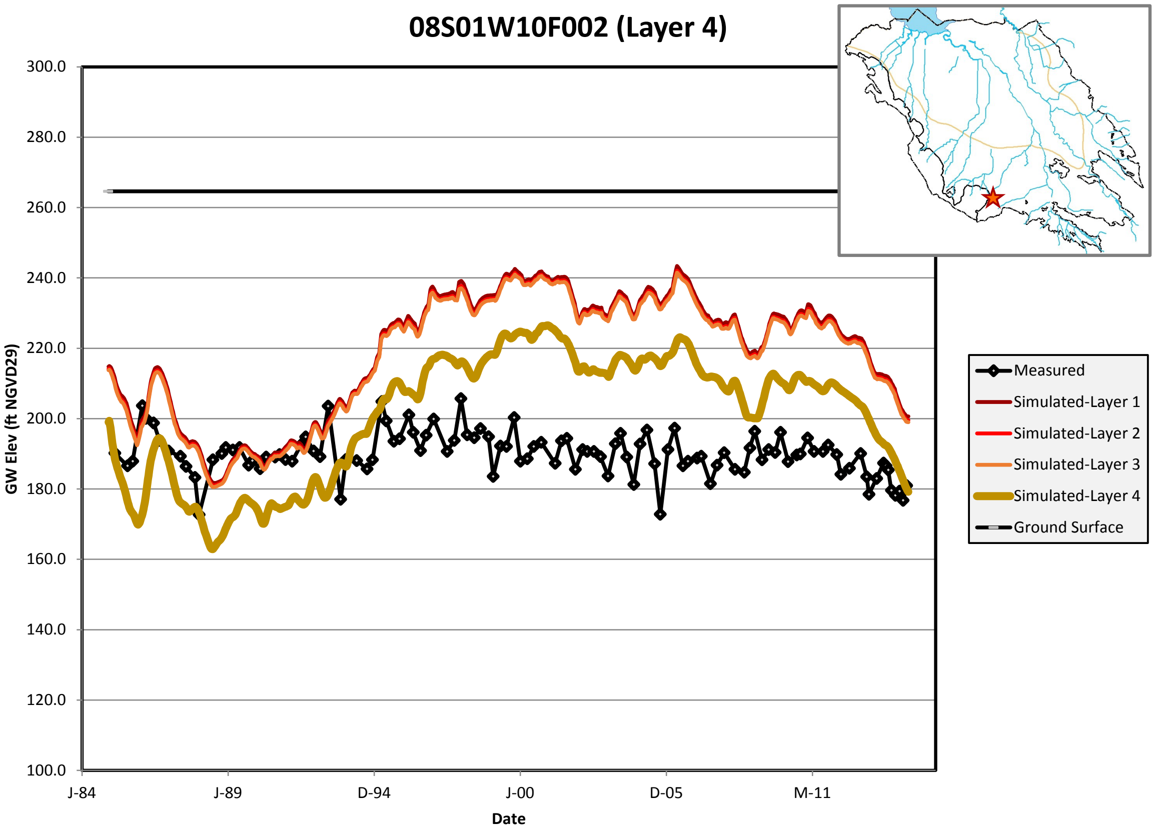

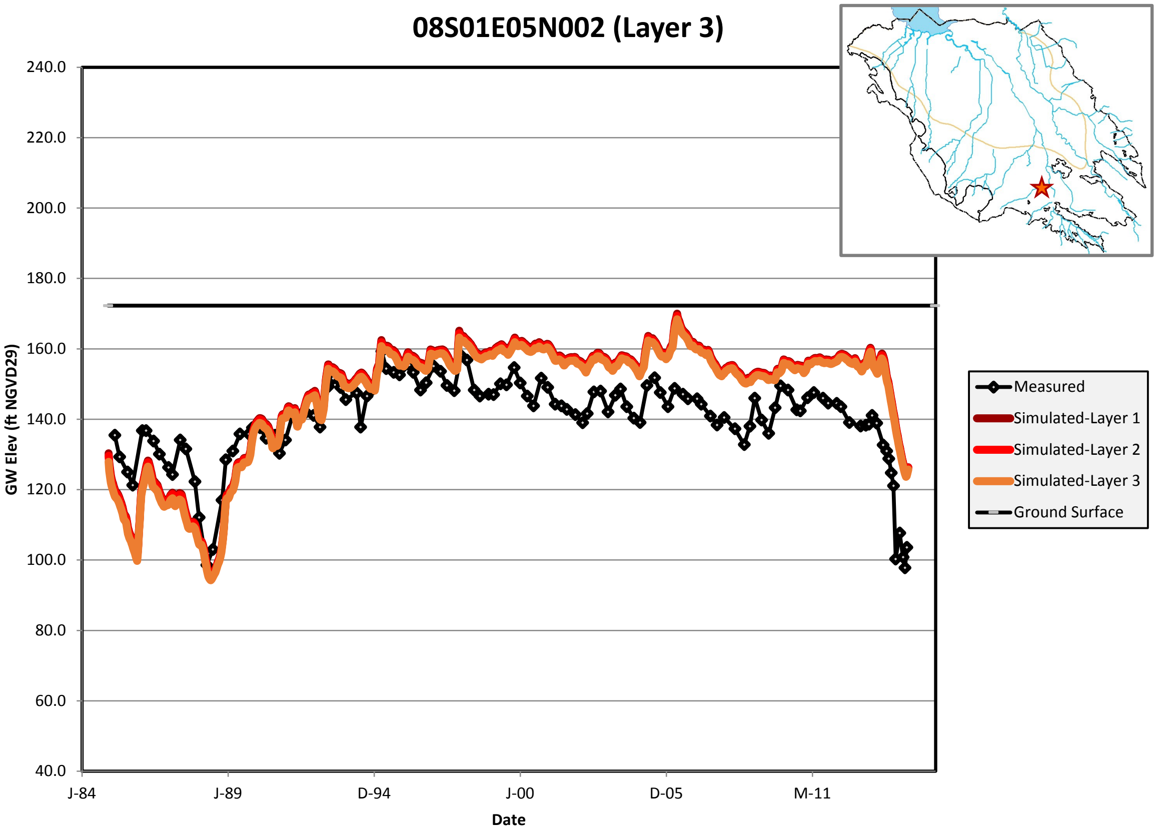

December 2017

TODD GROUNDWATER

Figure 4-4h
Hydrographs of Measured and Simulated Groundwater Levels Southwest Subbasin Margin

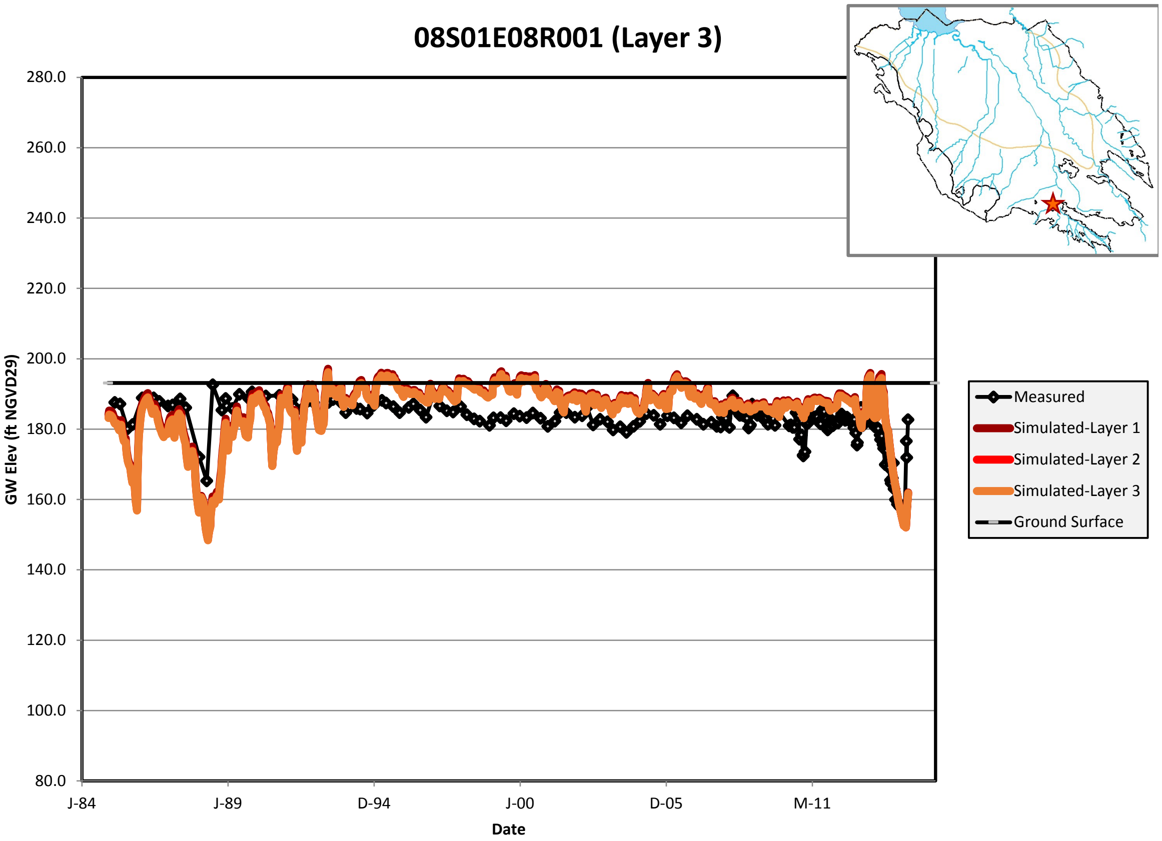

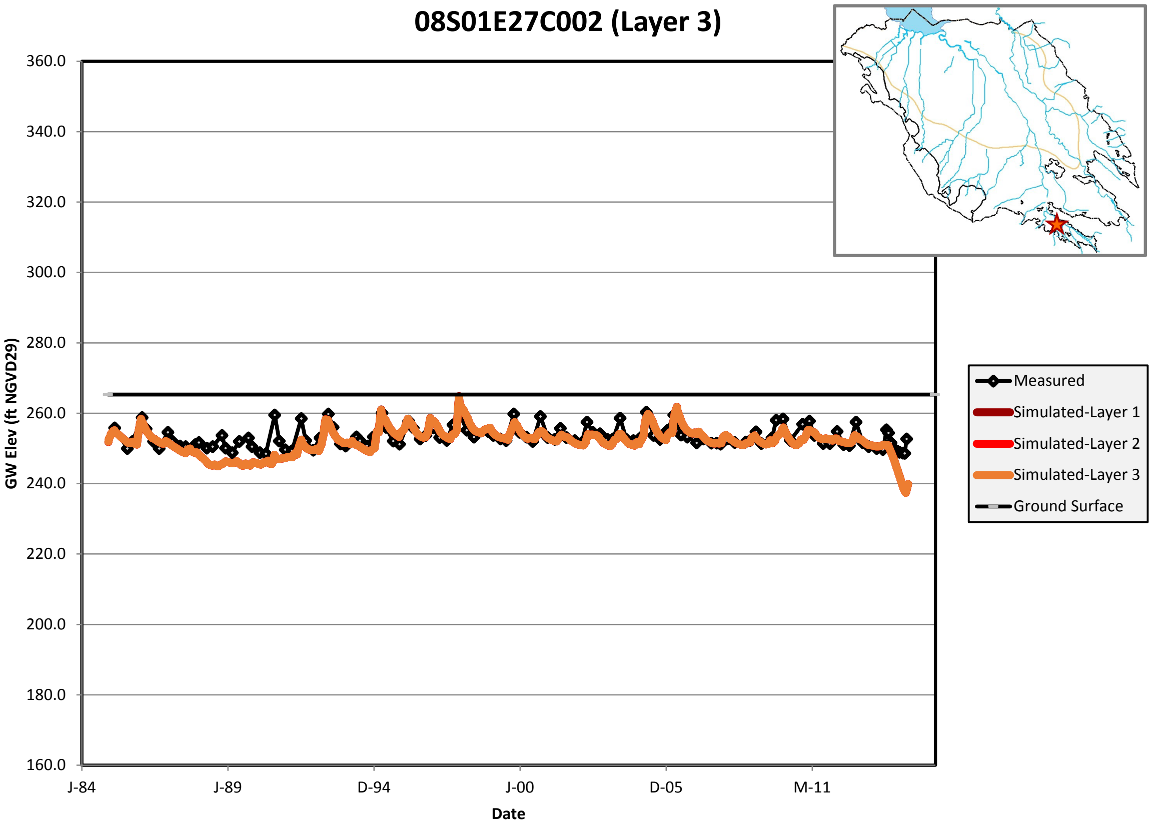

December 2017

TODD GROUNDWATER

Figure 4-4i
Hydrographs of Measured and Simulated Groundwater Levels Southwest Subbasin Margin

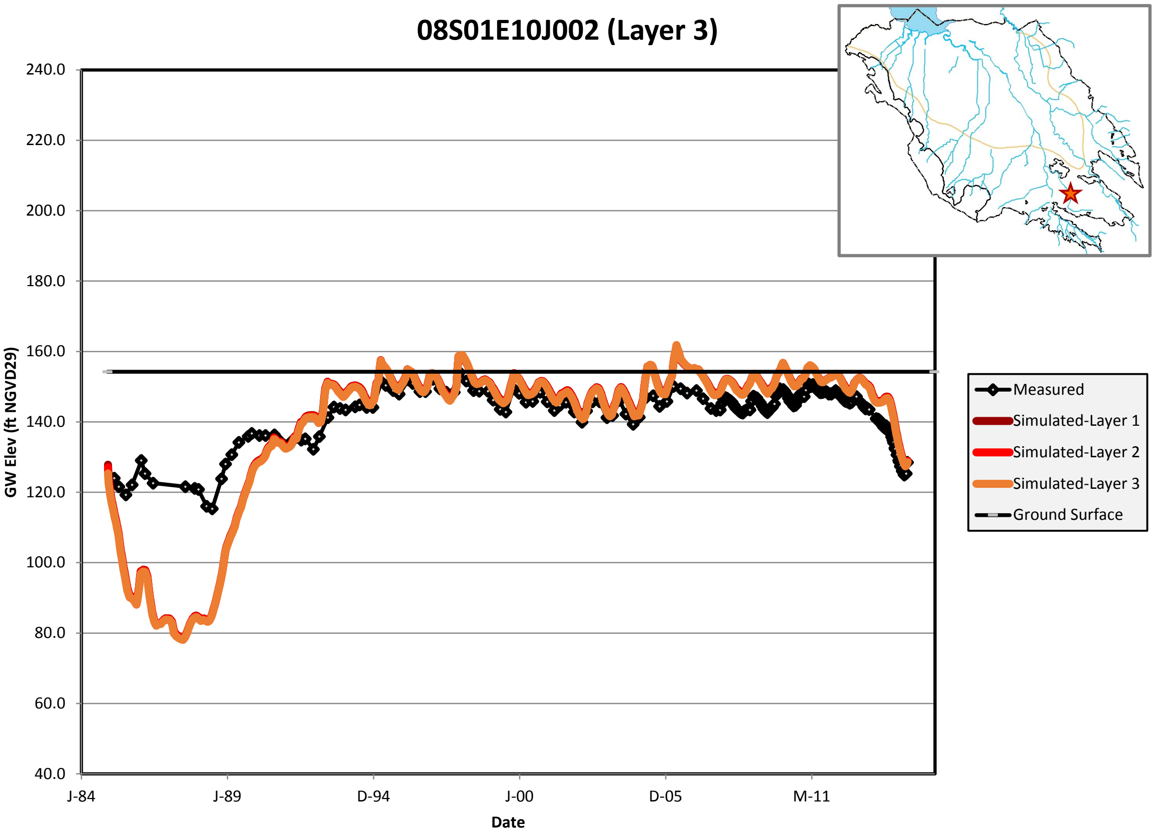

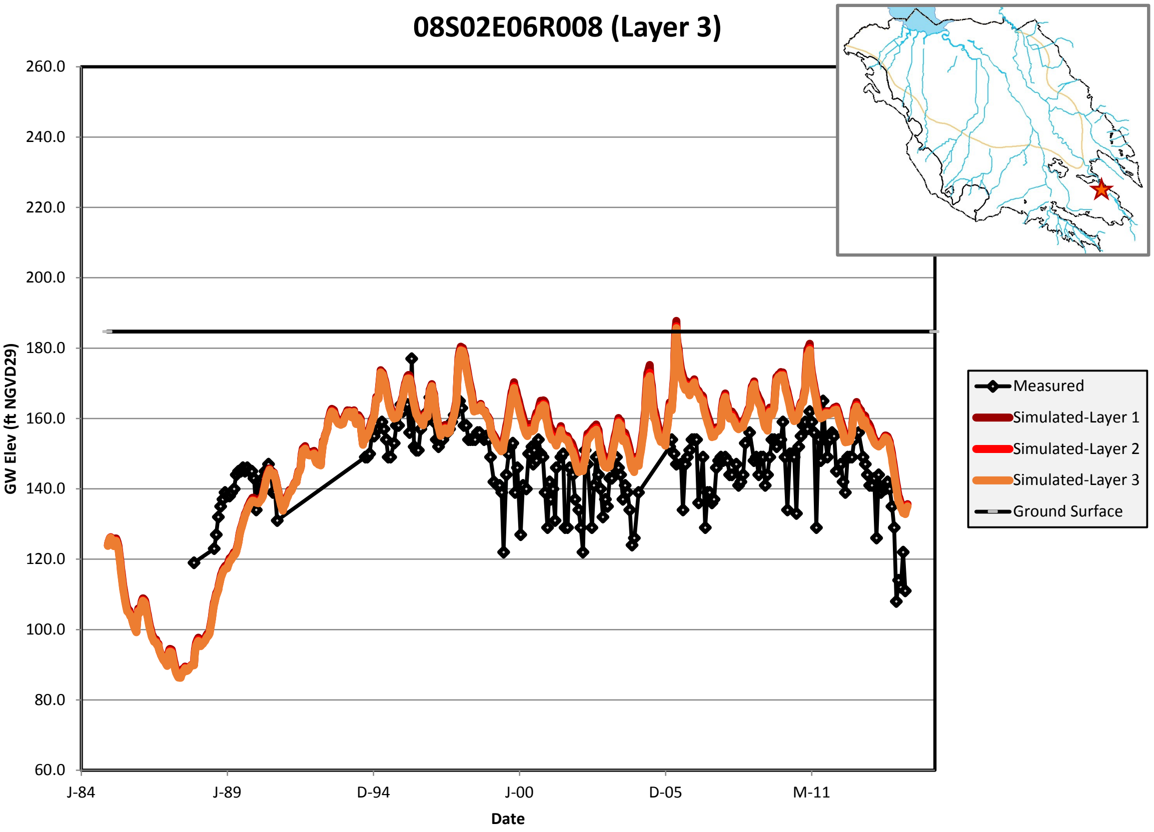

December 2017

TODD GROUNDWATER

Figure 4-5a
Hydrographs of Measured and Simulated Groundwater Levels Santa Teresa Area

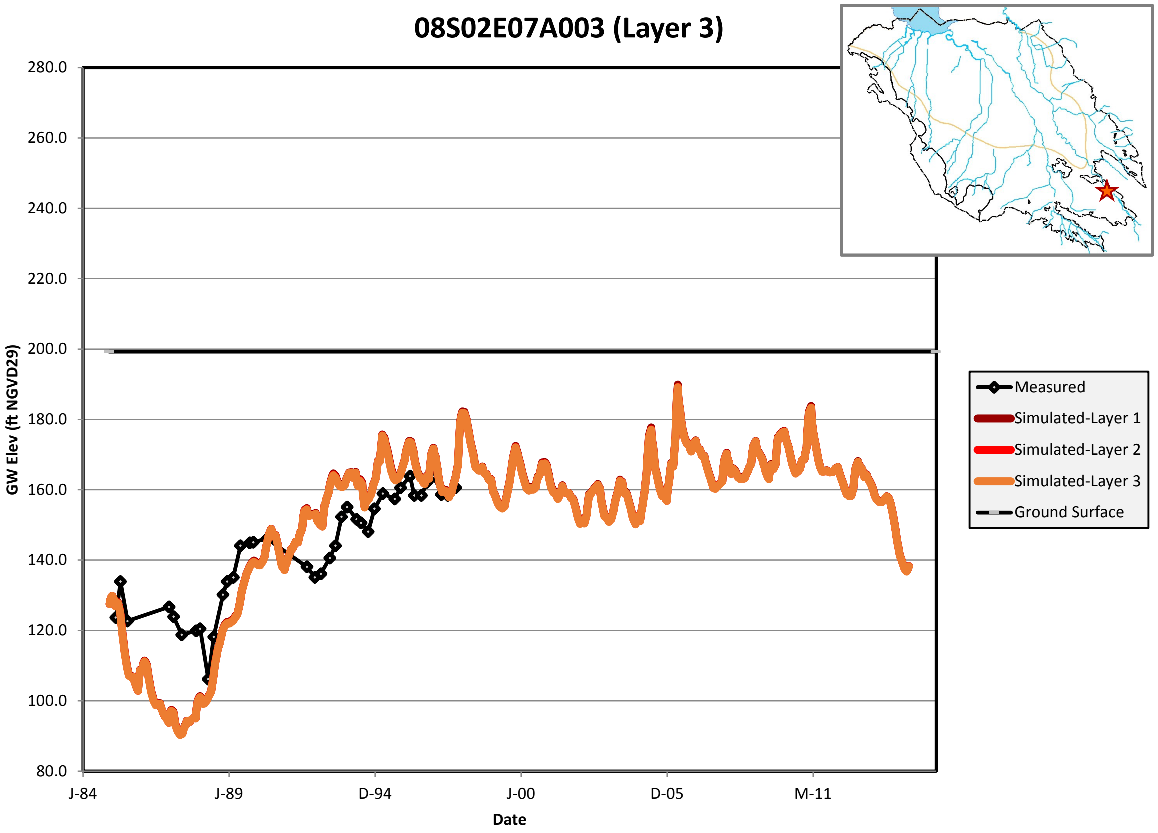
08S02E07A003 (Layer 3)

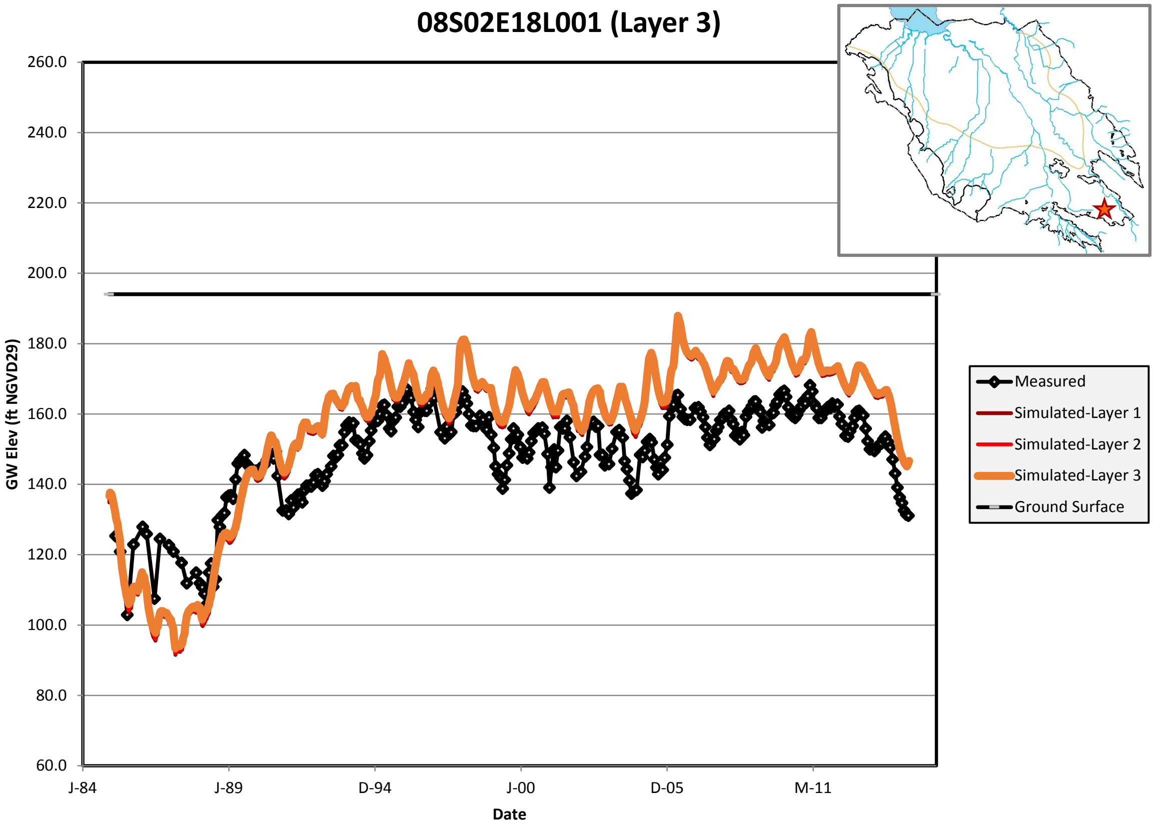
08S02E18L001 (Layer 3)

December 2017

TODD GROUNDWATER

Figure 4-5b
Hydrographs of Measured and Simulated Groundwater Levels Santa Teresa Area

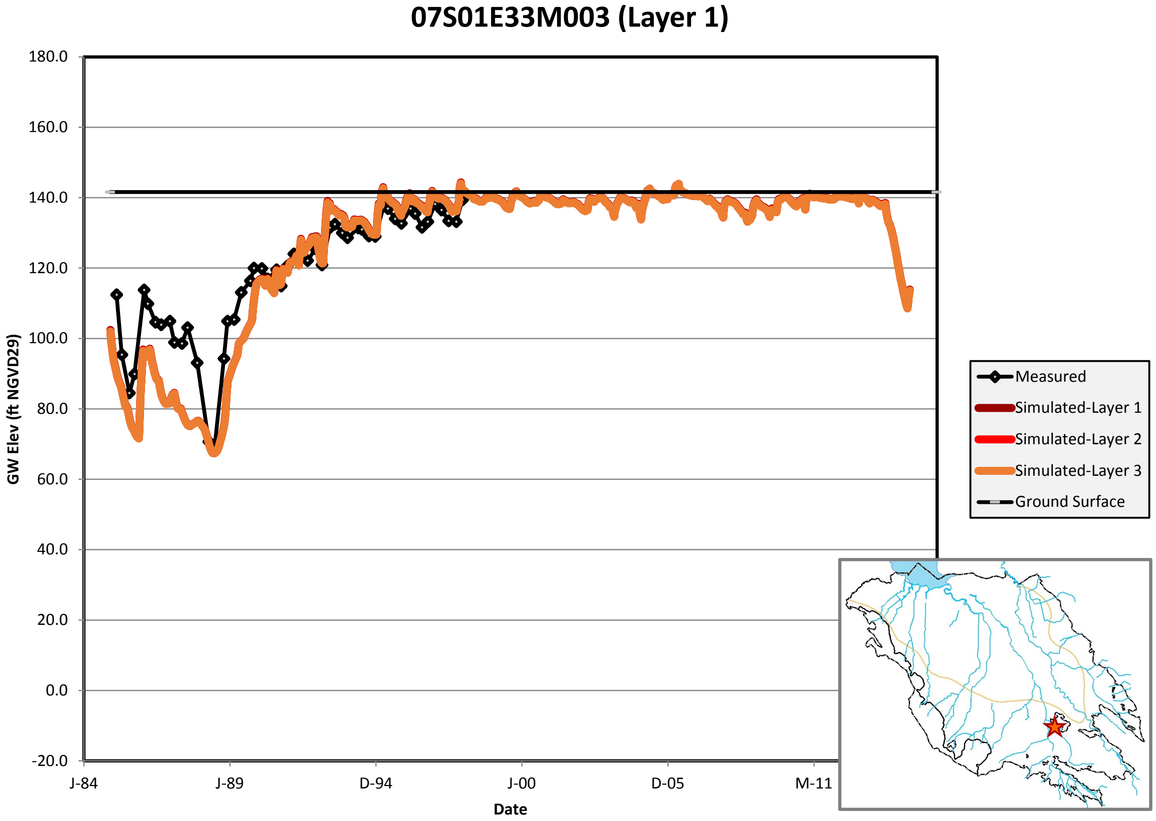

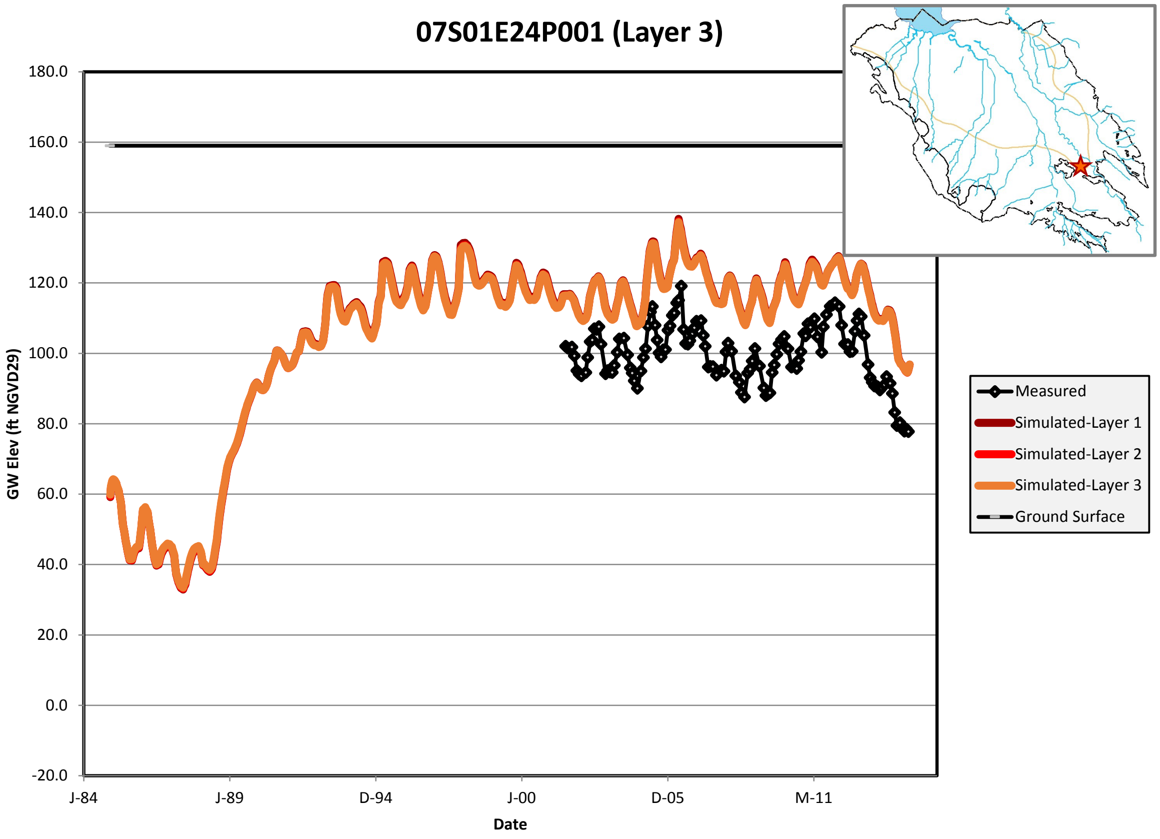

December 2017

TODD GROUNDWATER

Figure 4-6a
Hydrographs of Measured and Simulated Groundwater Levels Southeast-Central Area

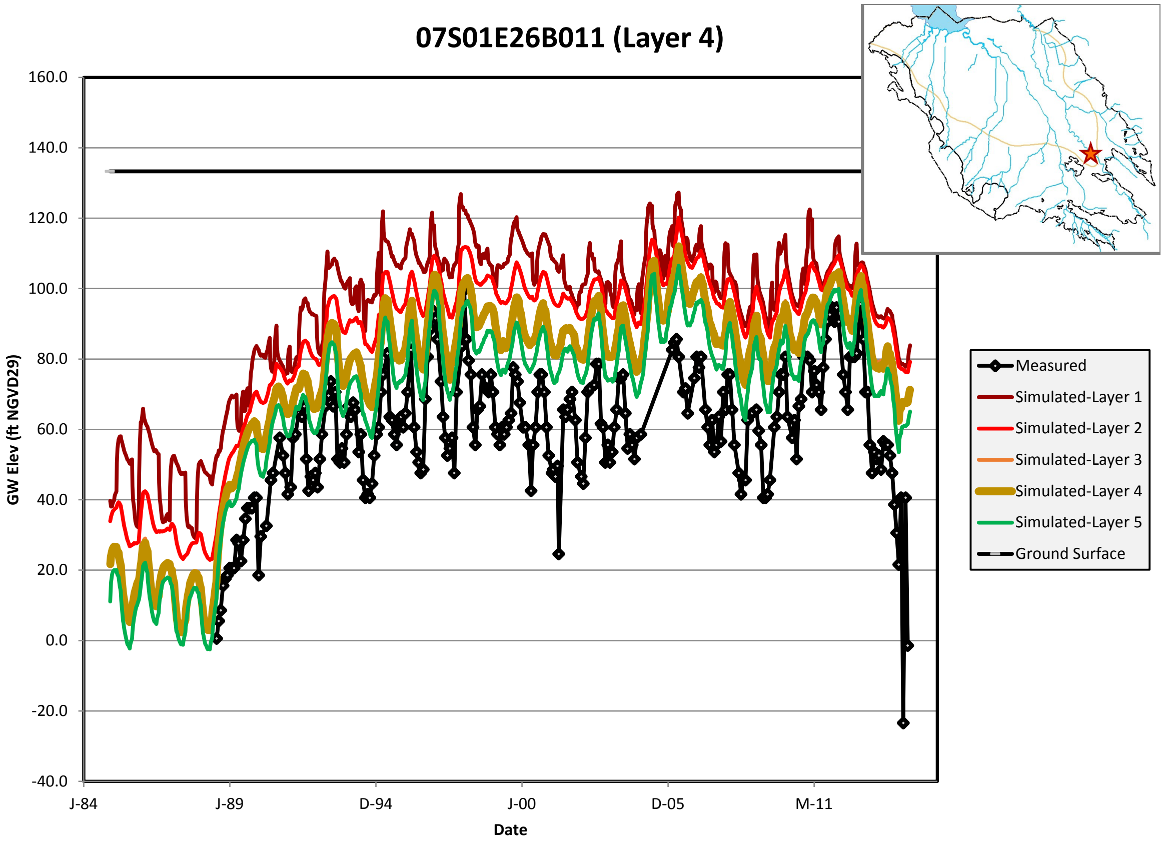

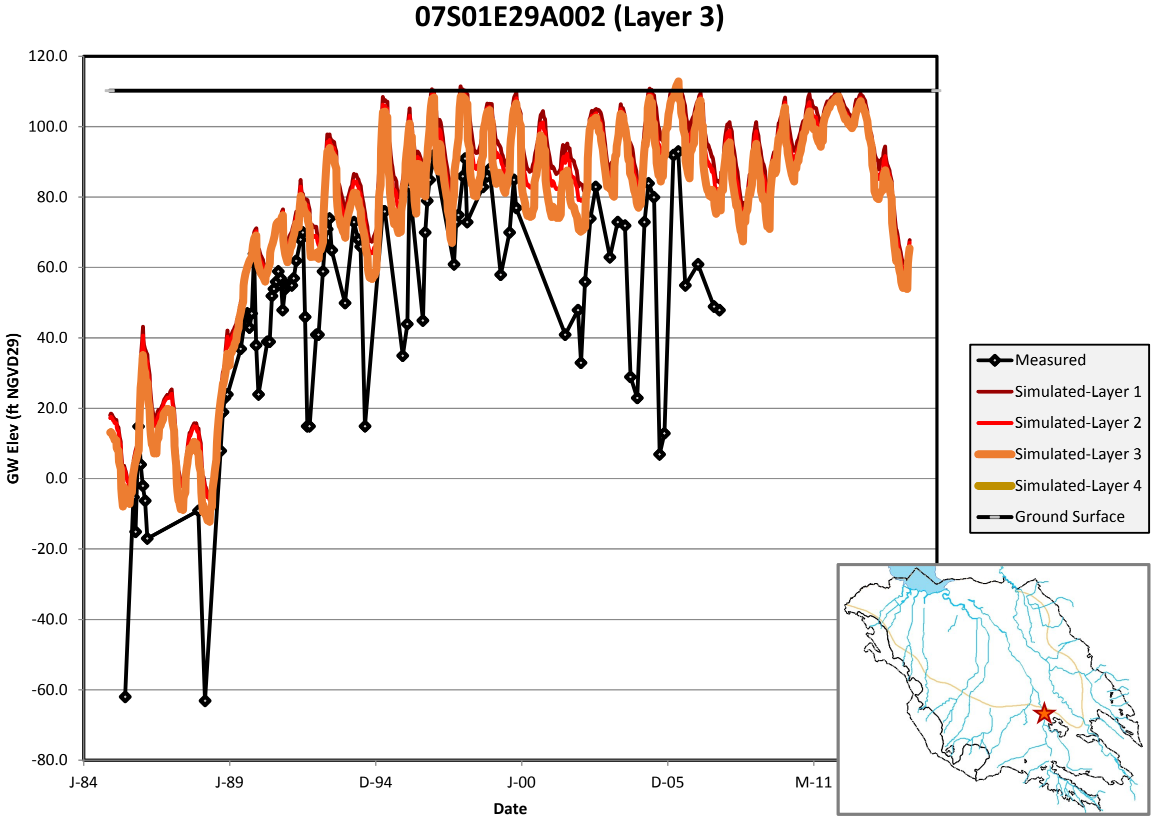

December 2017

TODD GROUNDWATER

Figure 4-6b

Hydrographs of Measured and Simulated Groundwater Levels Southeast-Central Area

07S01W24H004 (Layer 1)

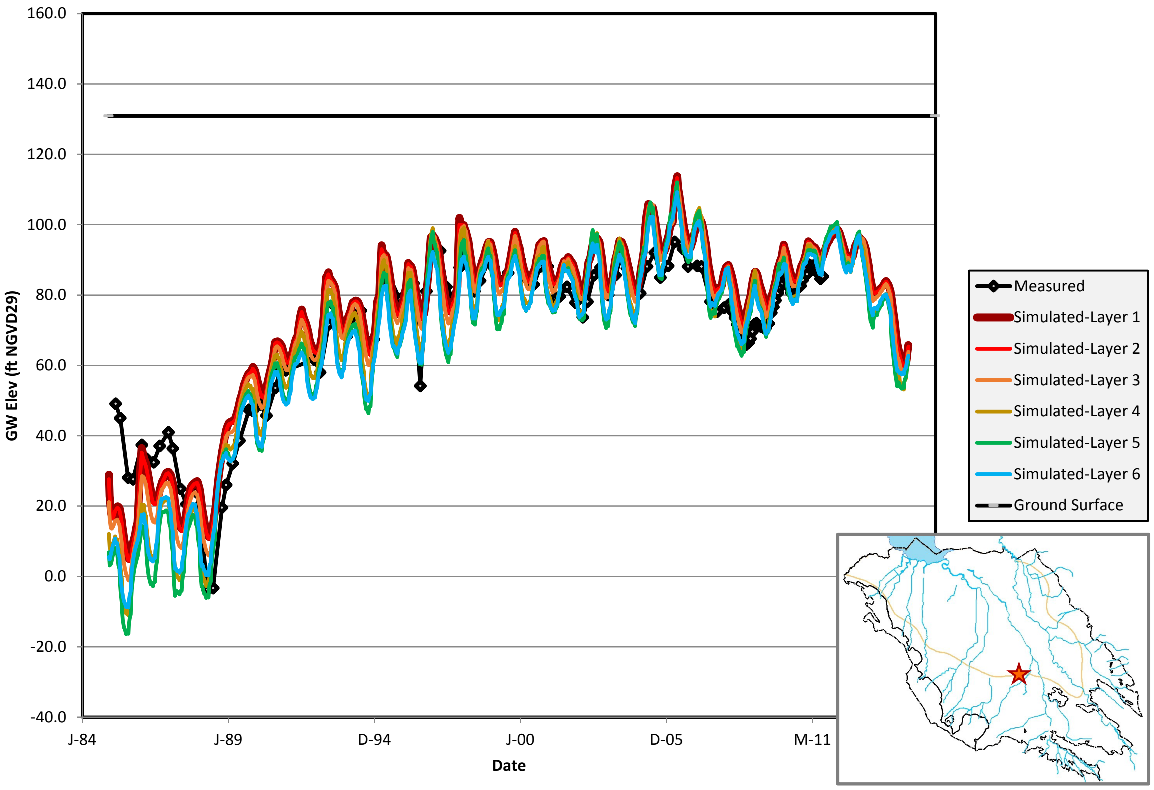

Willow 7S/1E-19B2 (Layer 1)

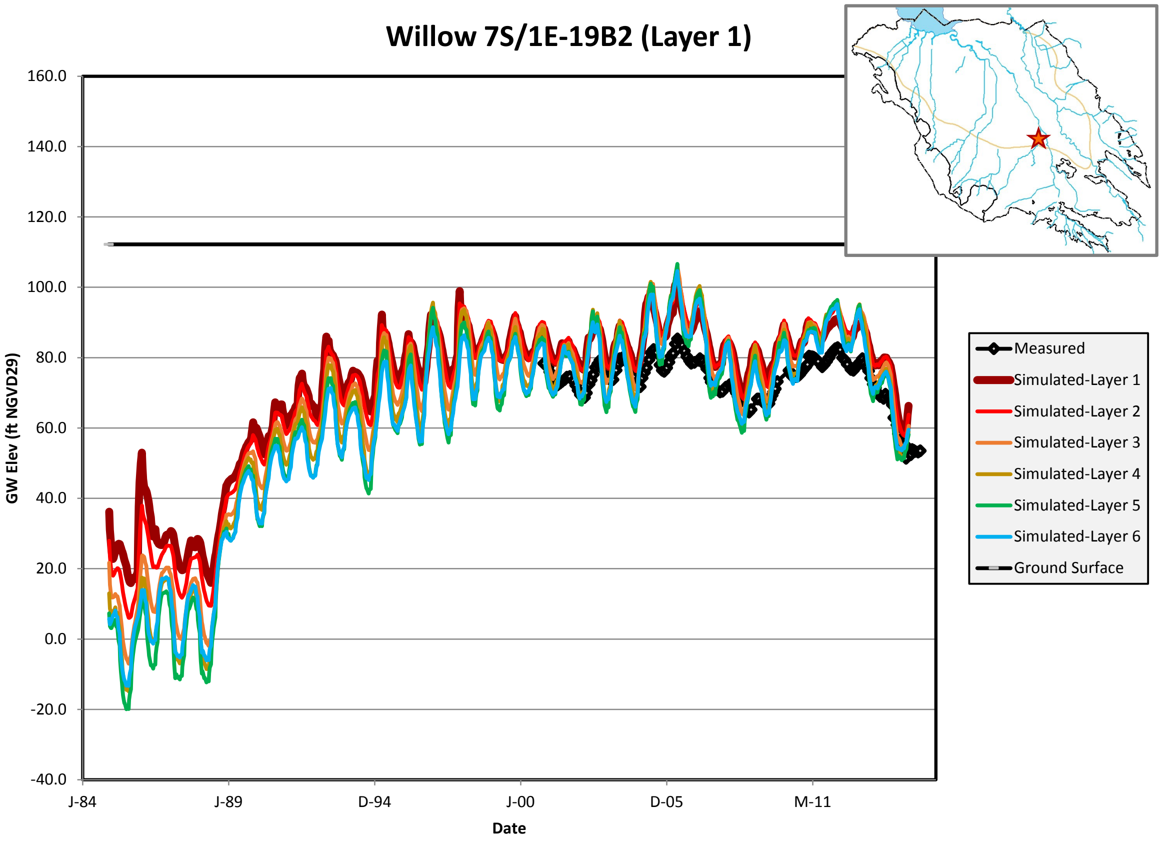

December 2017

TODD GROUNDWATER

Figure 4-6c
Hydrographs of Measured and Simulated Groundwater Levels Southeast-Central Area

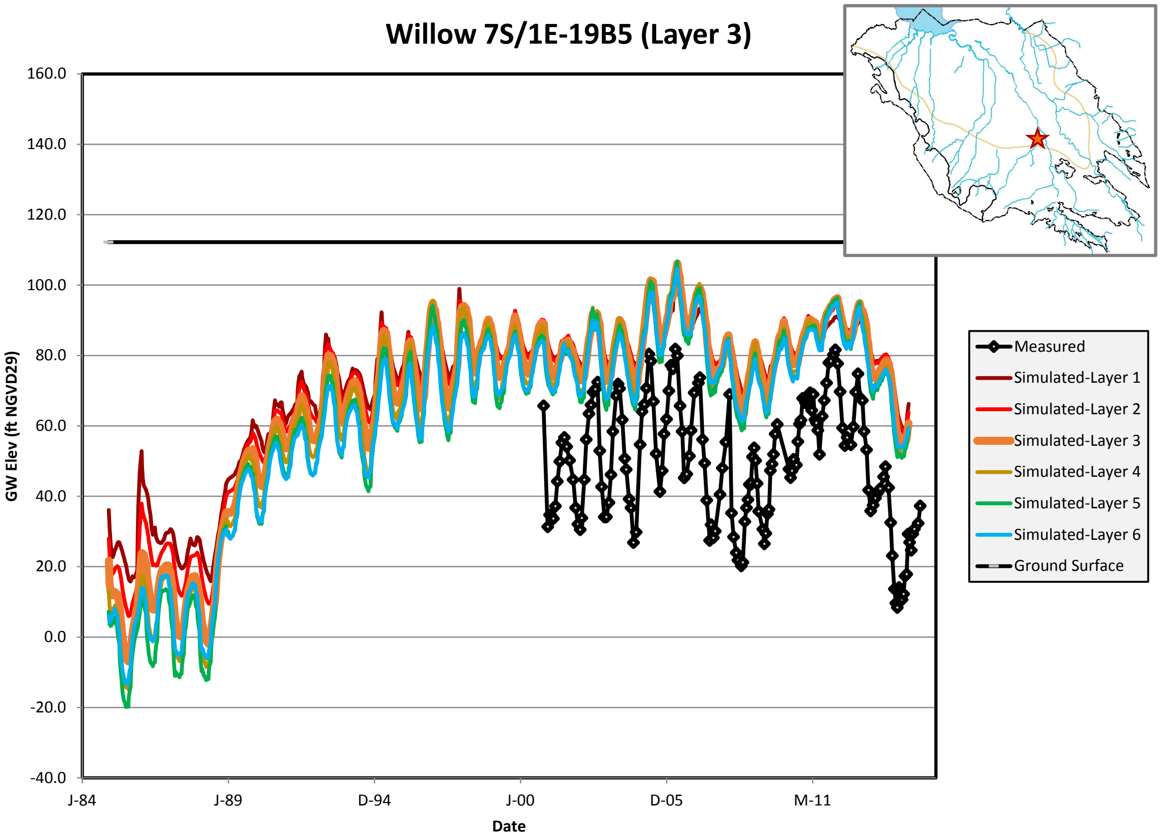

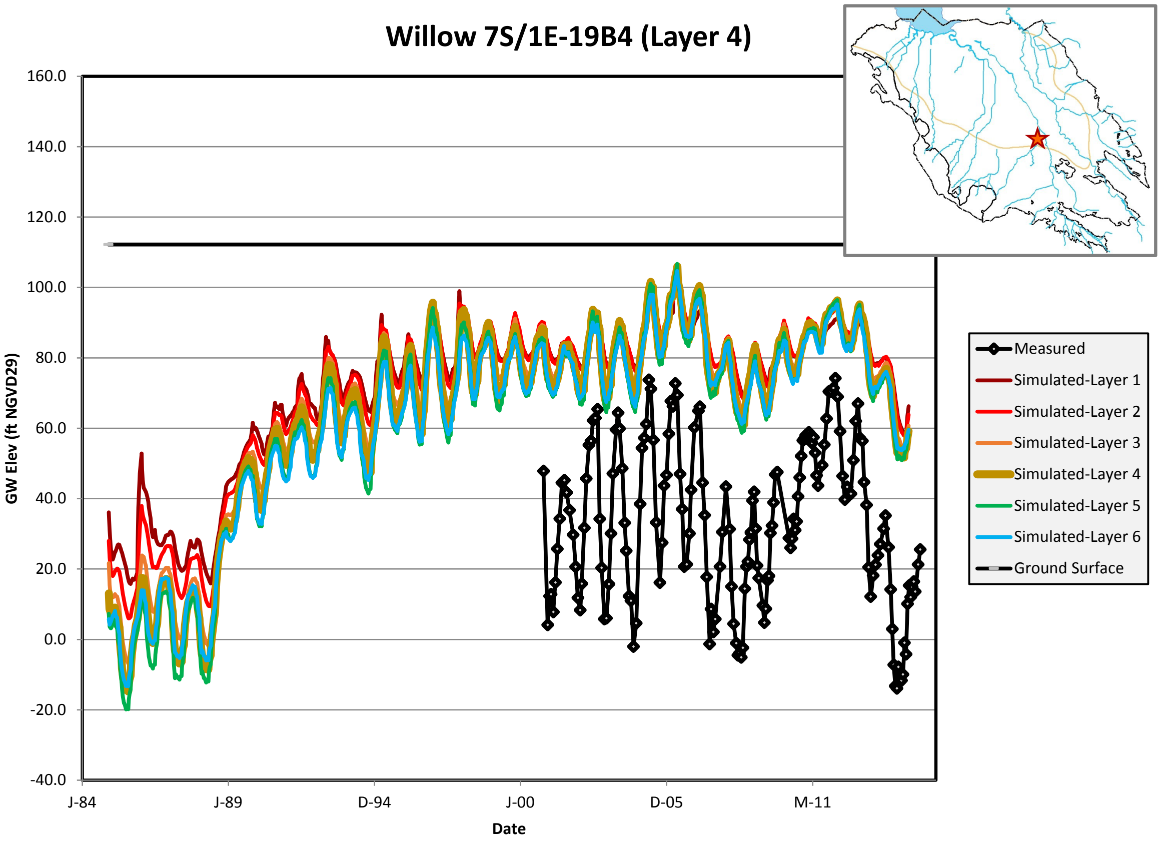

December 2017

TODD GROUNDWATER

Figure 4-6d
Hydrographs of Measured and Simulated Groundwater Levels Southeast-Central Area

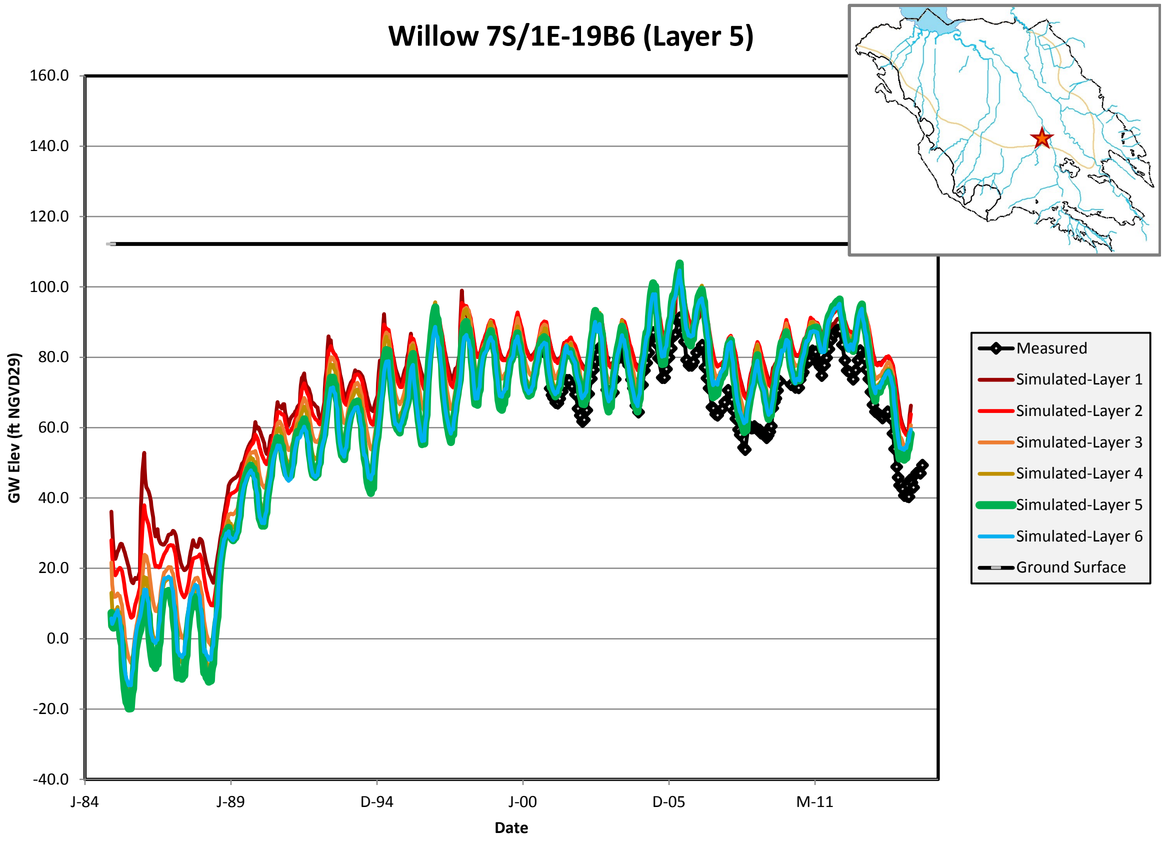

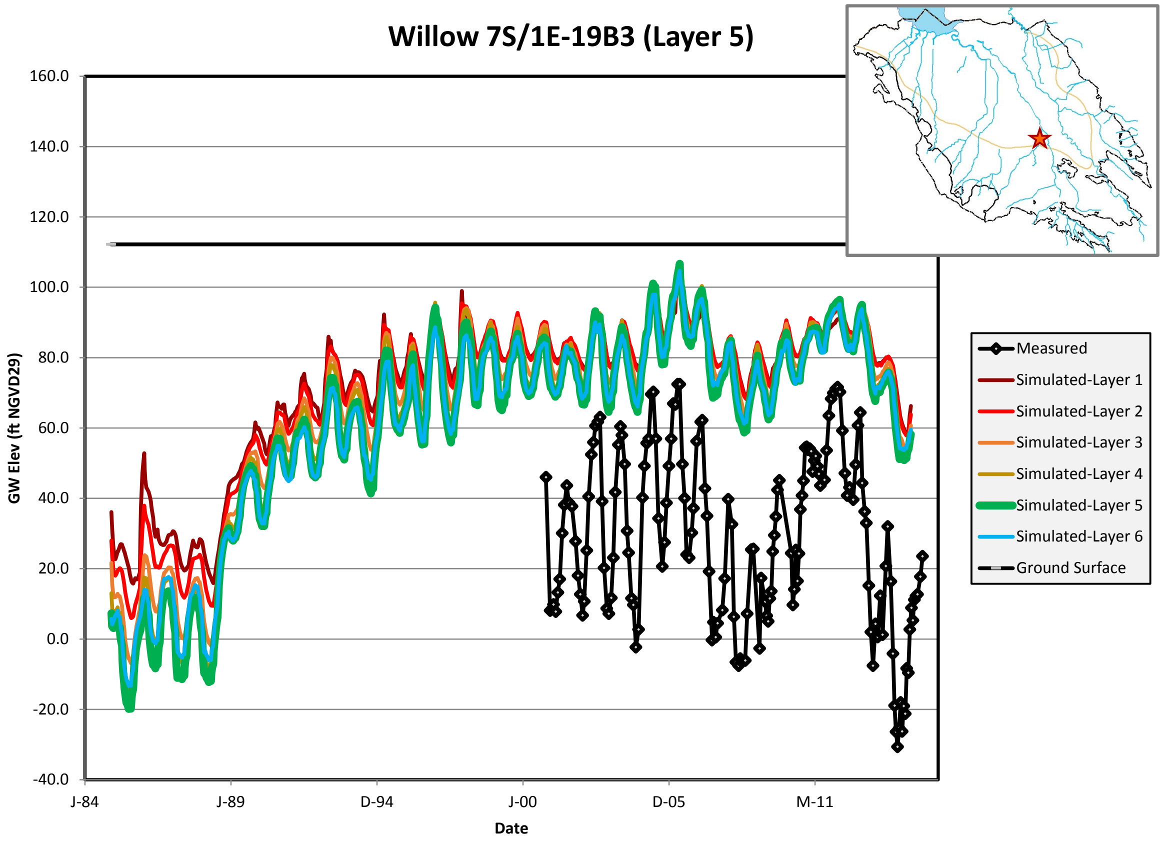

December 2017

TODD GROUNDWATER

Figure 4-6e
Hydrographs of Measured and Simulated Groundwater Levels Southeast-Central Area

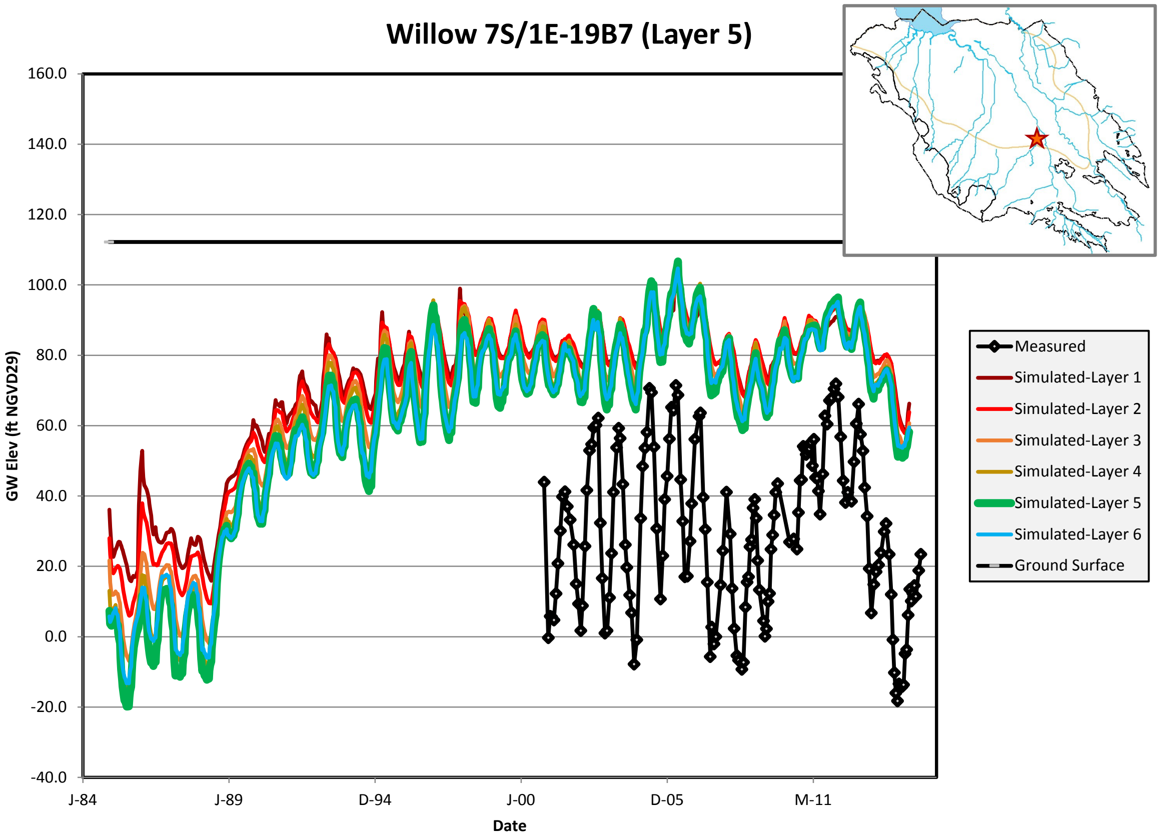
Willow 7S/1E-19B7 (Layer 5)

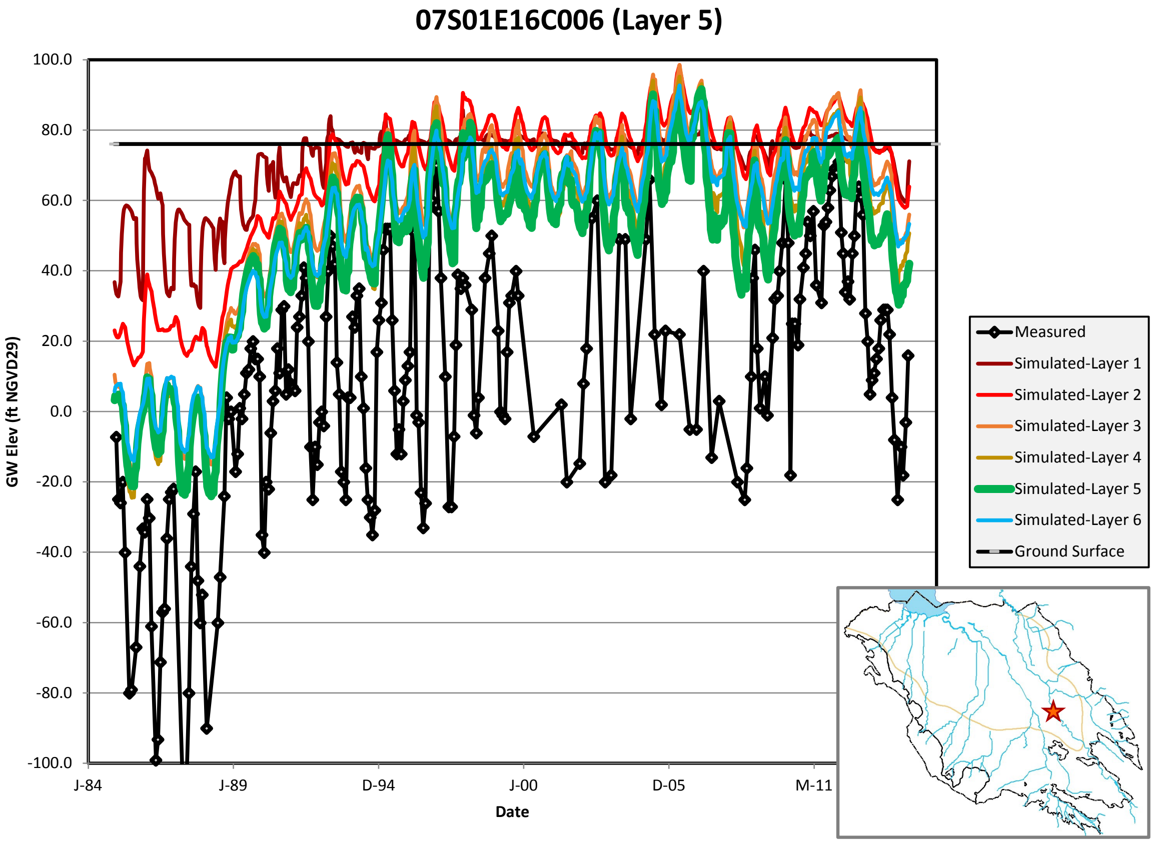
07S01E16C006 (Layer 5)

December 2017

TODD GROUNDWATER

Figure 4-6f
Hydrographs of Measured and Simulated Groundwater Levels Southeast-Central Area

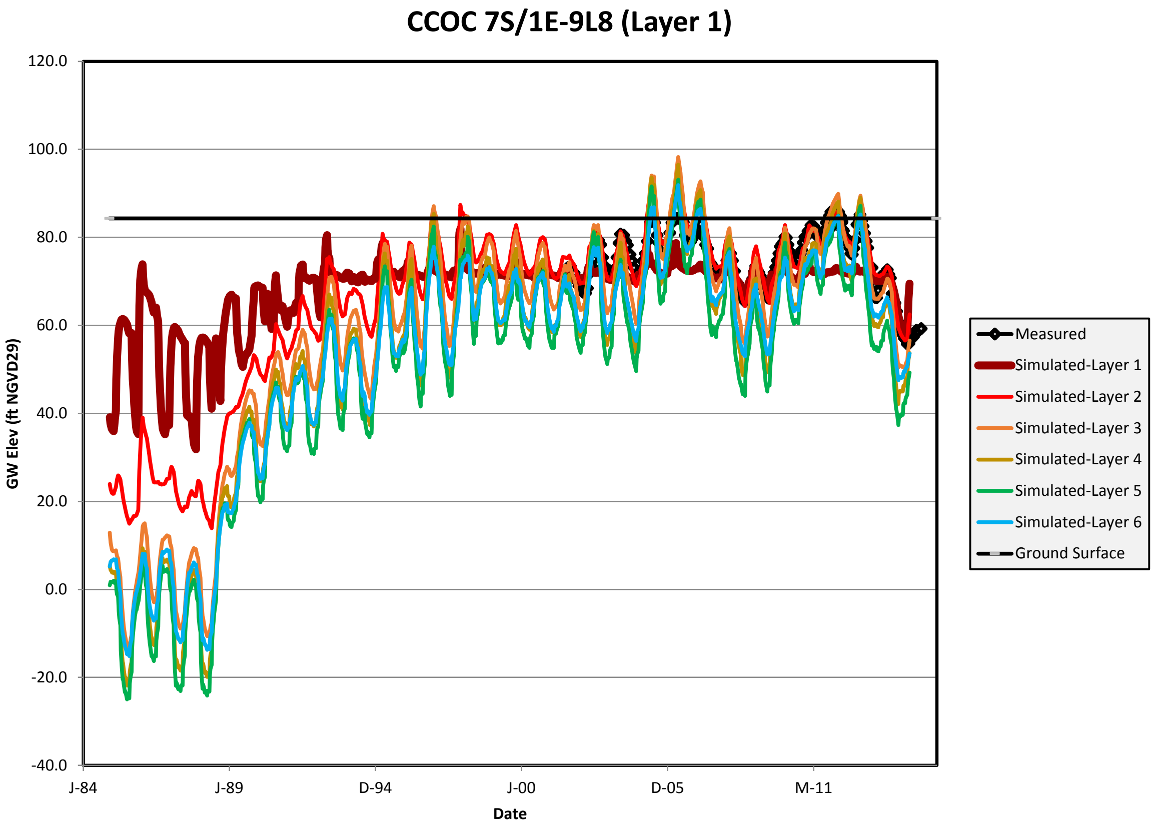

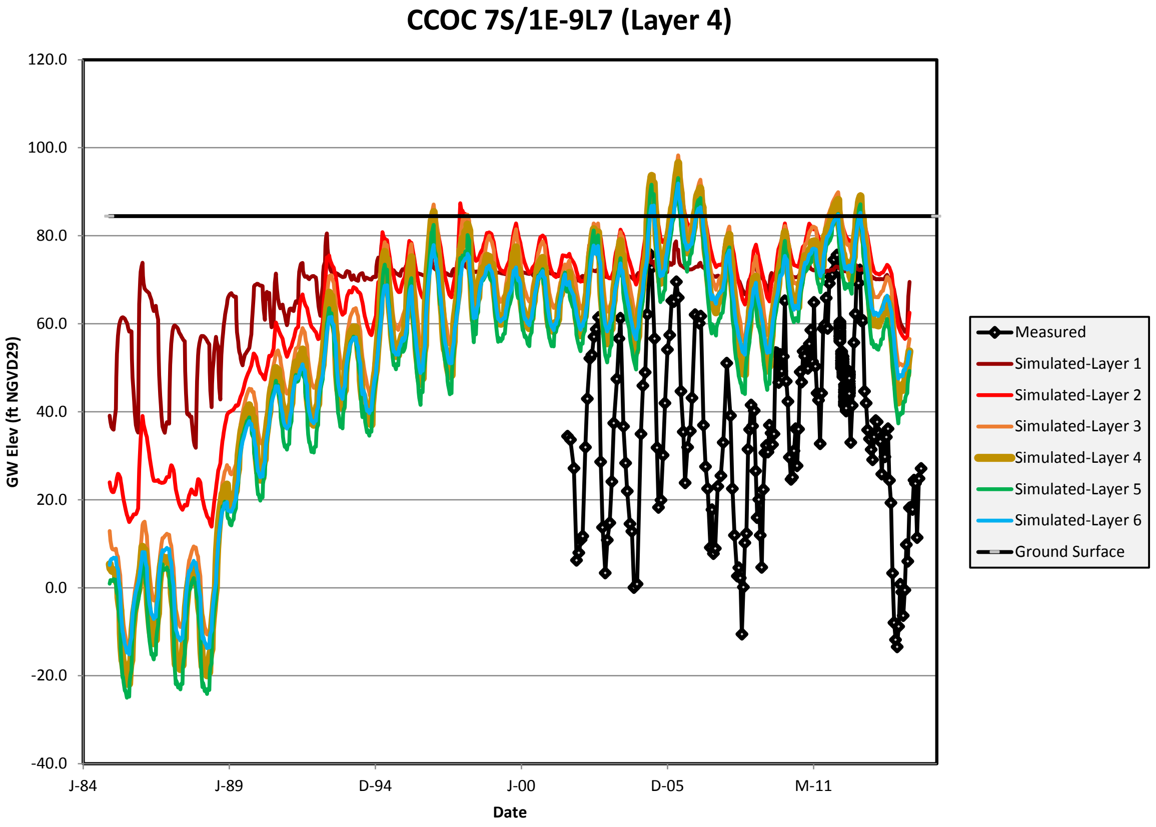

December 2017

TODD GROUNDWATER

Figure 4-6g
Hydrographs of Measured and Simulated Groundwater Levels Southeast-Central Area

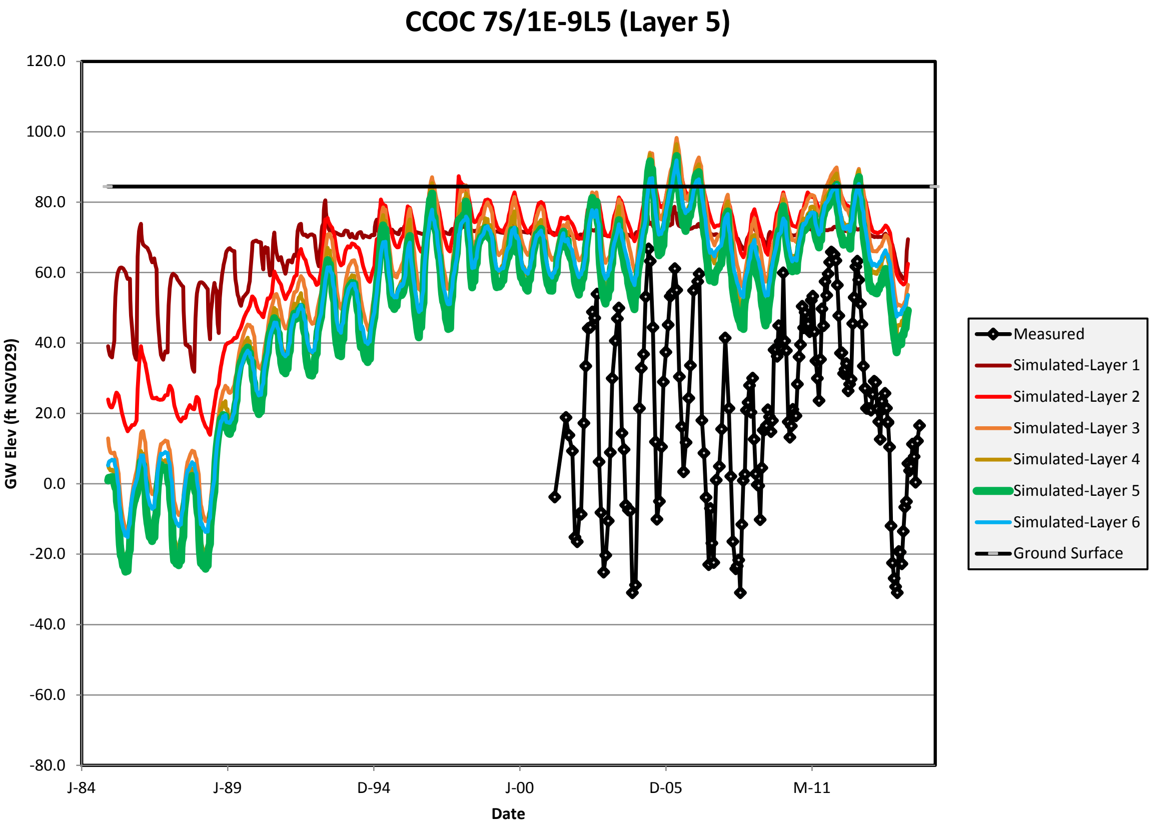

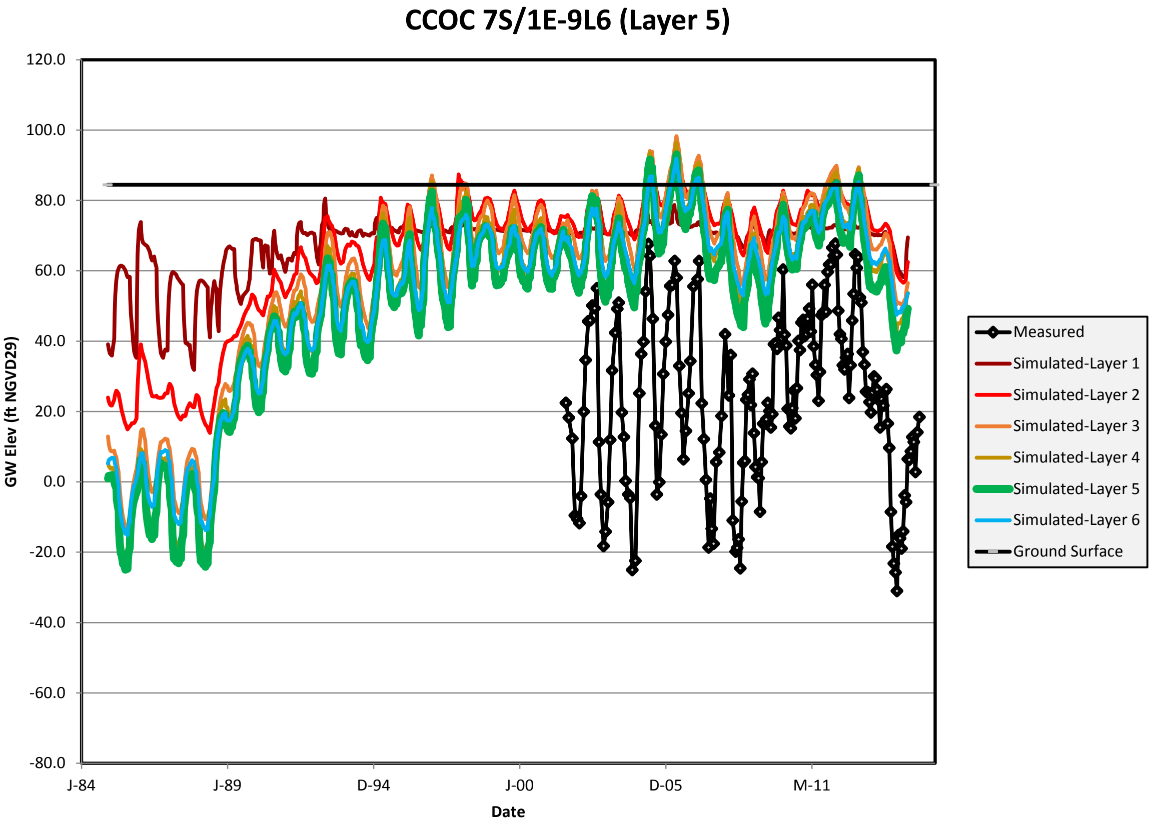

December 2017

TODD GROUNDWATER

Figure 4-6h
Hydrographs of Measured and Simulated Groundwater Levels Southeast-Central Area

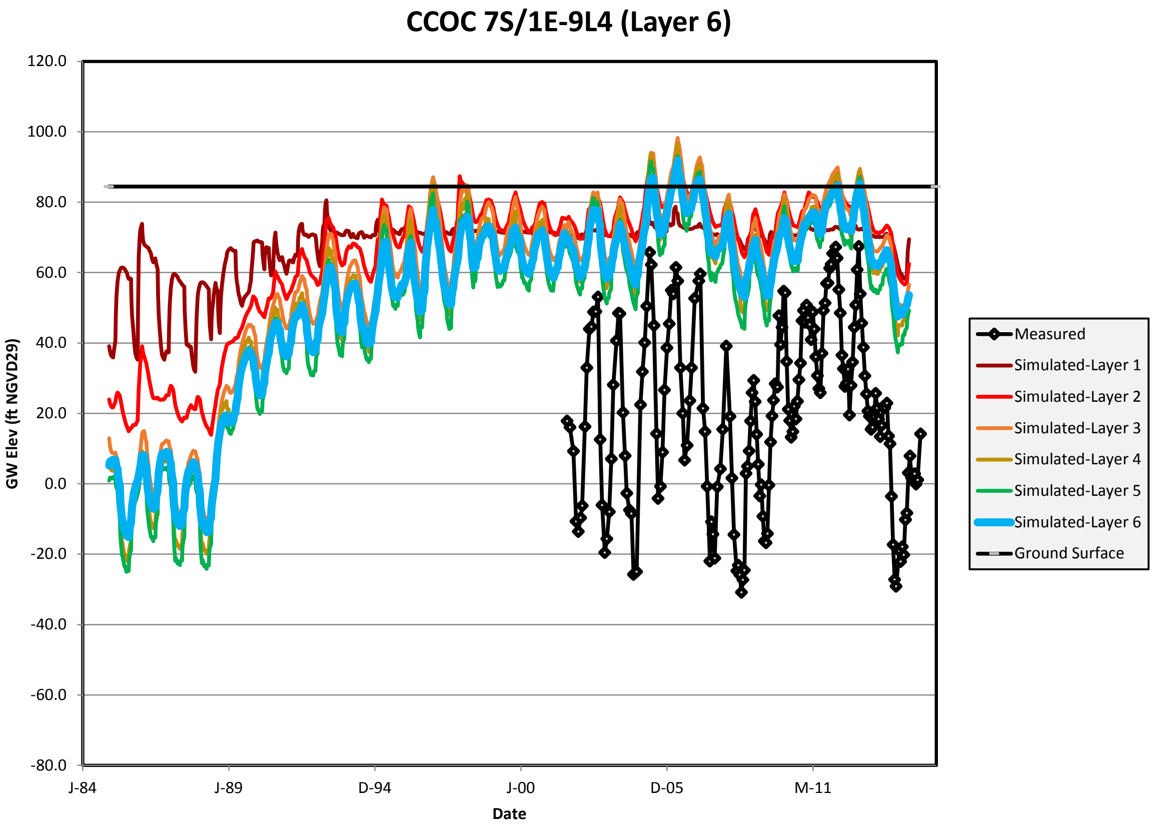

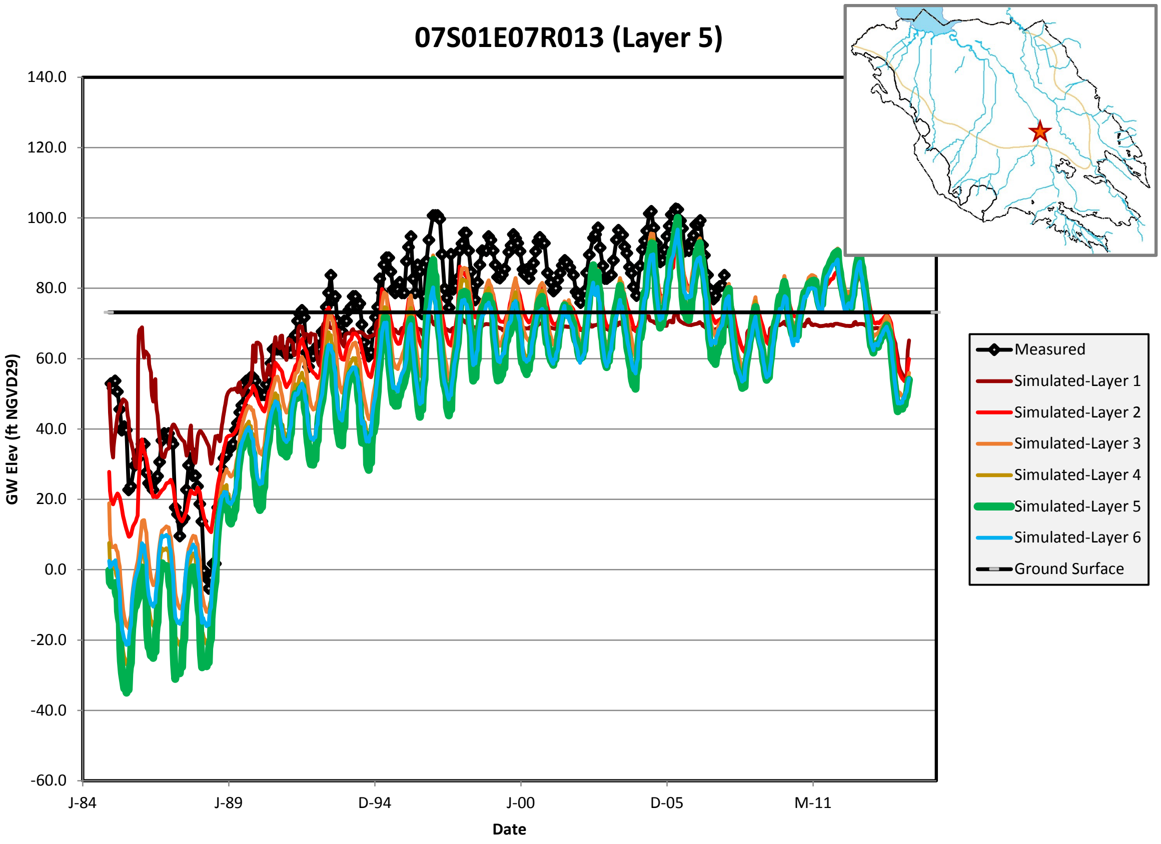

December 2017

TODD GROUNDWATER

Figure 4-6i
Hydrographs of Measured and Simulated Groundwater Levels Southeast-Central Area

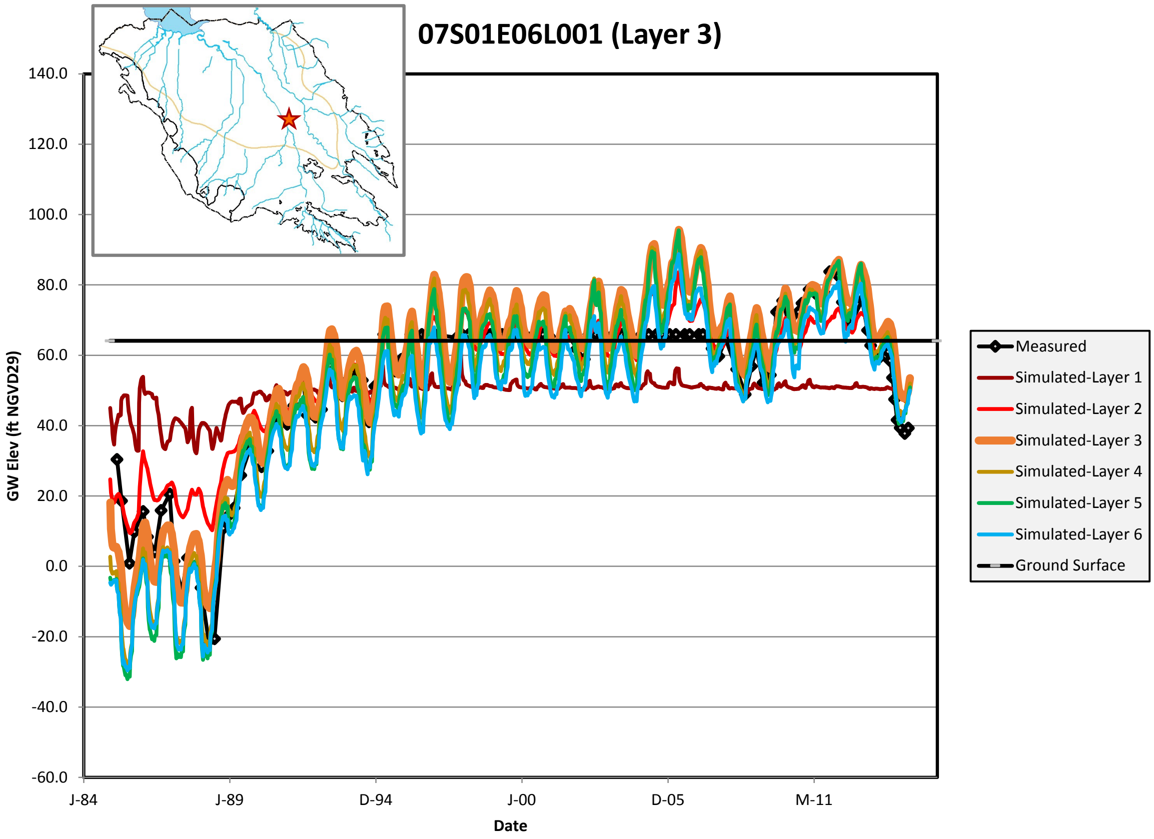

December 2017

TODD GROUNDWATER

Figure 4-6j
Hydrographs of Measured and Simulated Groundwater Levels Southeast-Central Area

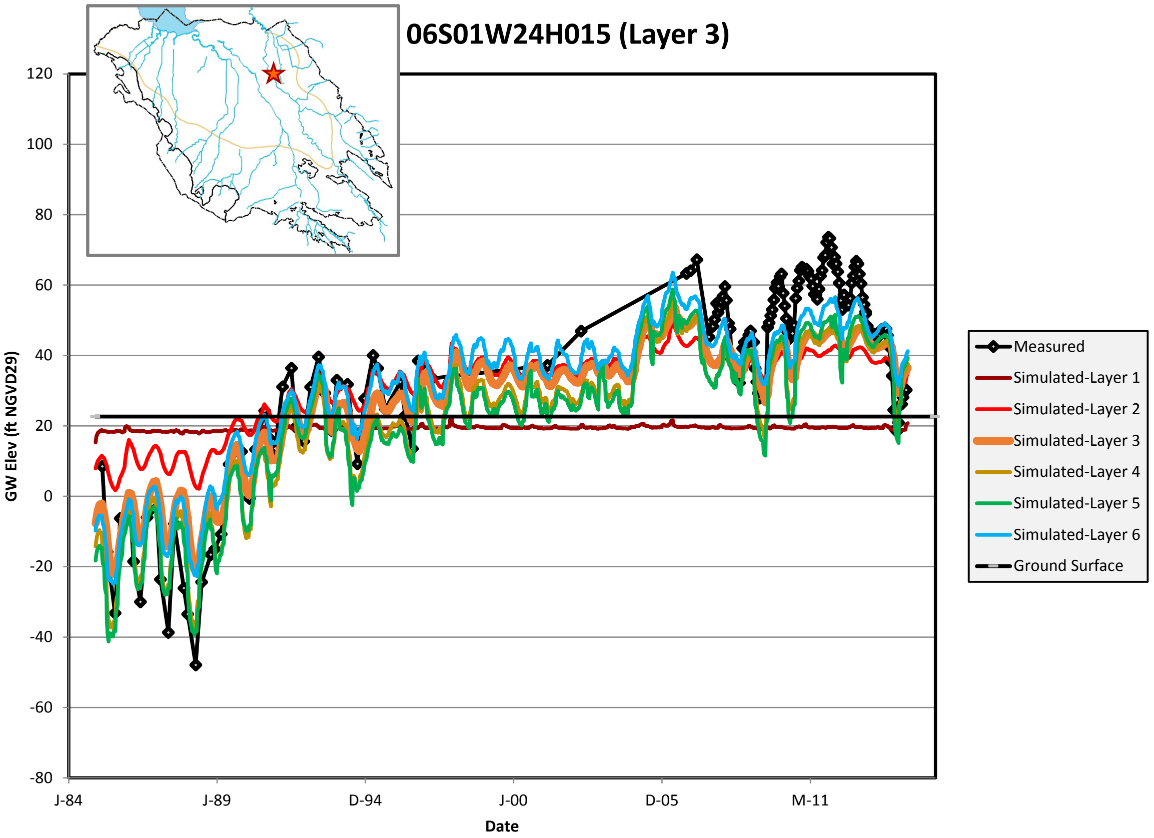

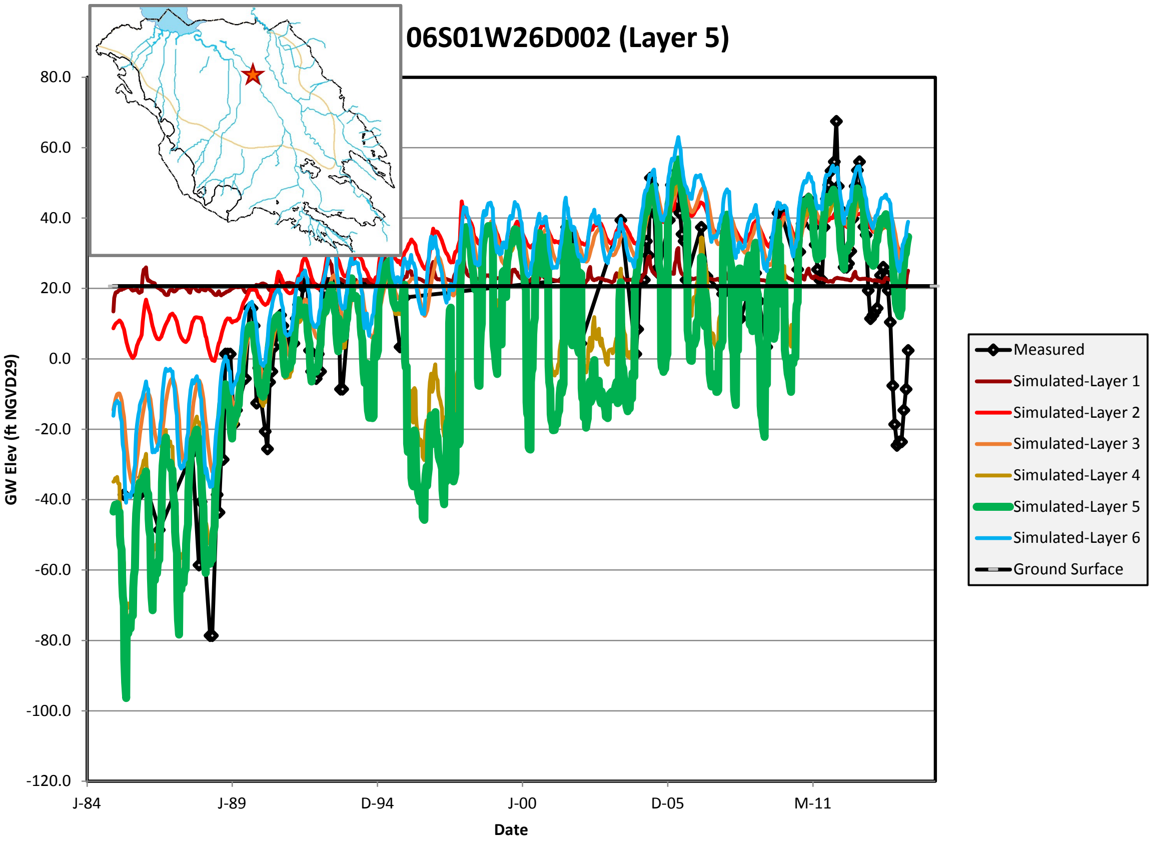

December 2017

TODD GROUNDWATER

Figure 4-7a
Hydrographs of Measured and Simulated Groundwater Levels Central Low-K Zone

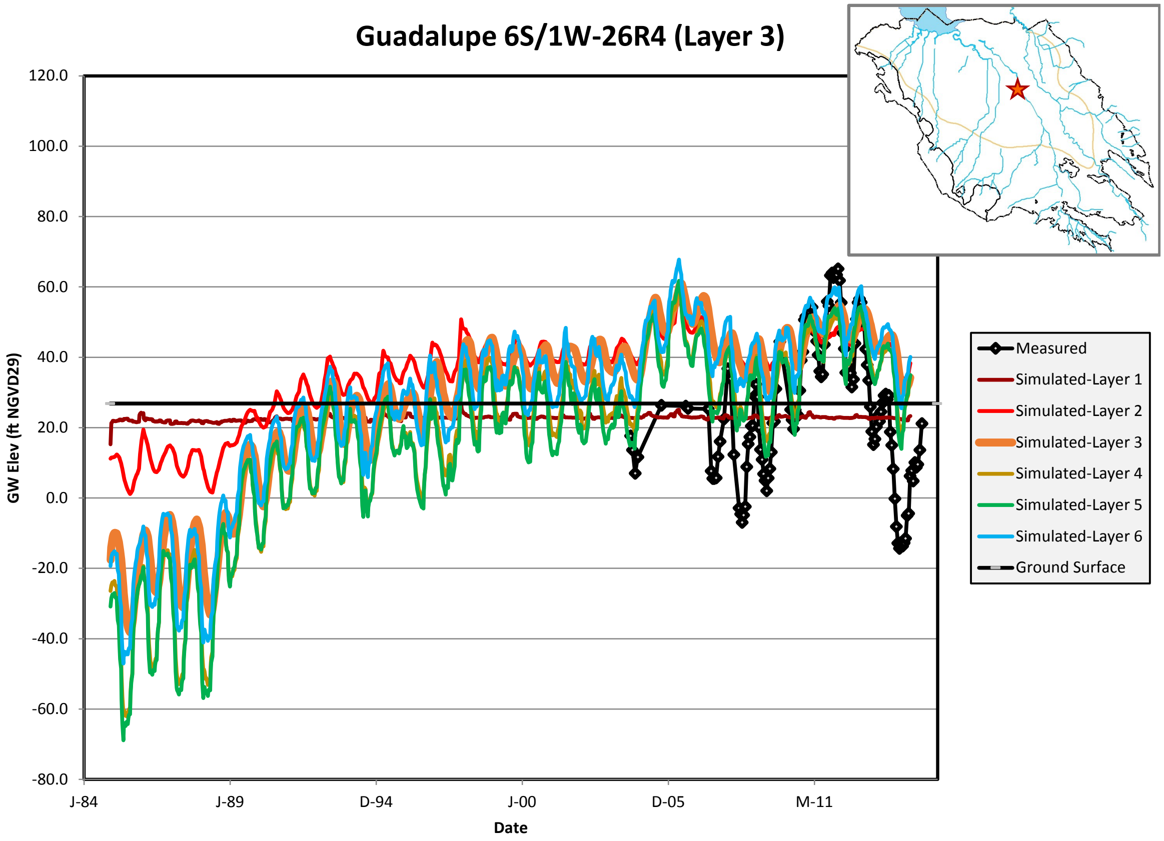
Guadalupe 6S/1W-26R4 (Layer 3)

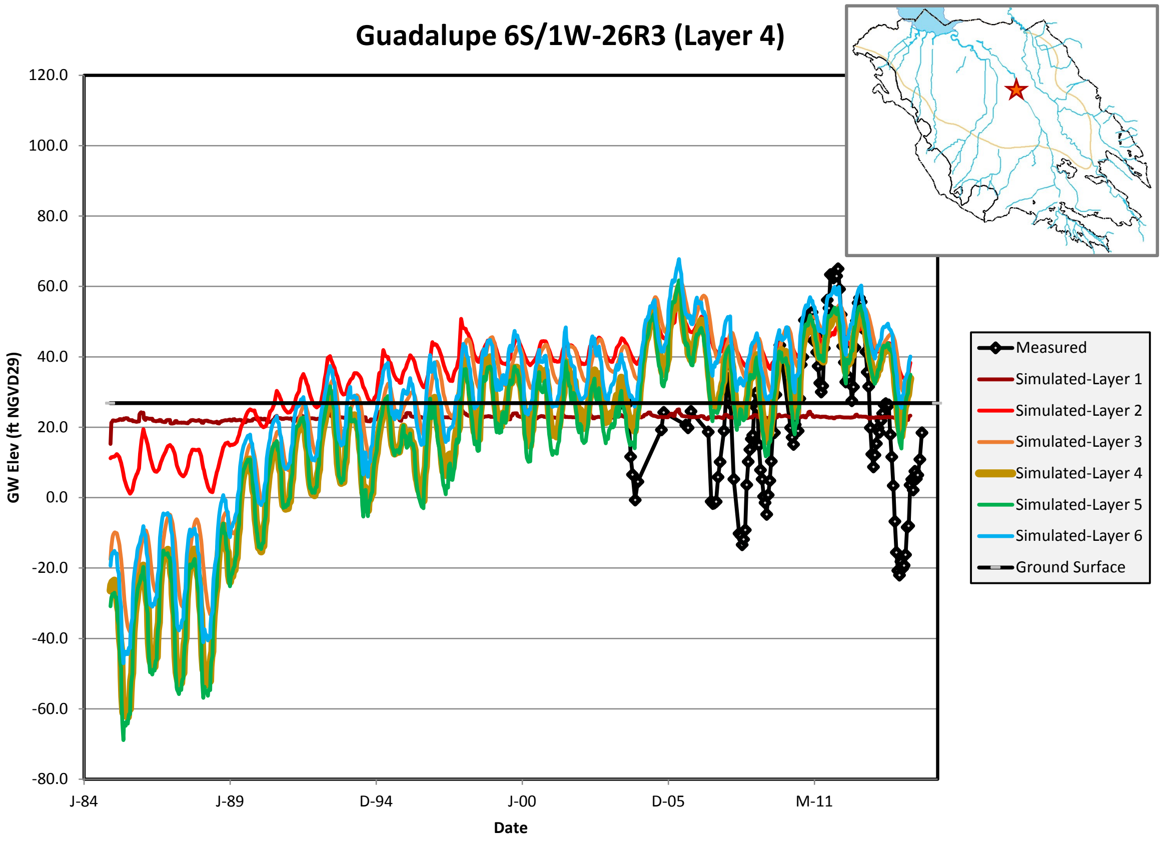
Guadalupe 6S/1W-26R3 (Layer 4)

December 2017

TODD GROUNDWATER

Figure 4-7b
Hydrographs of Measured and Simulated Groundwater Levels Central Low-K Zone

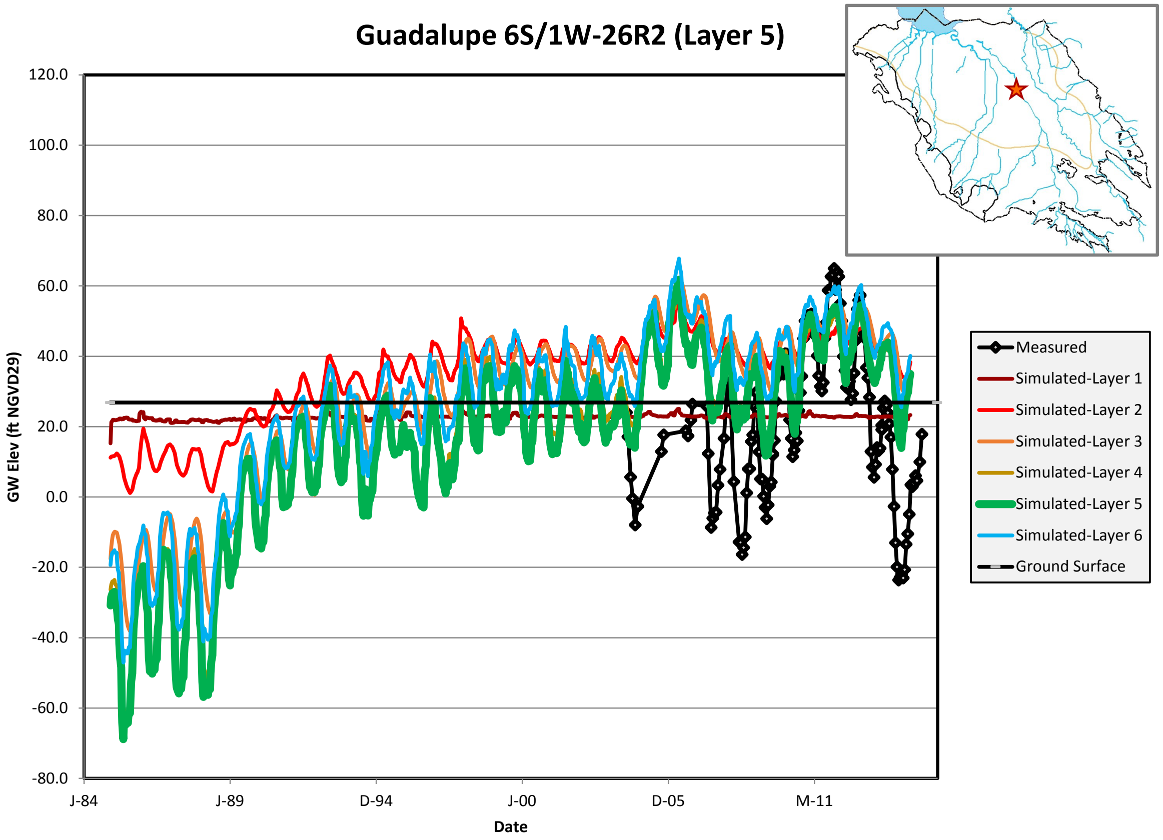
Guadalupe 6S/1W-26R2 (Layer 5)

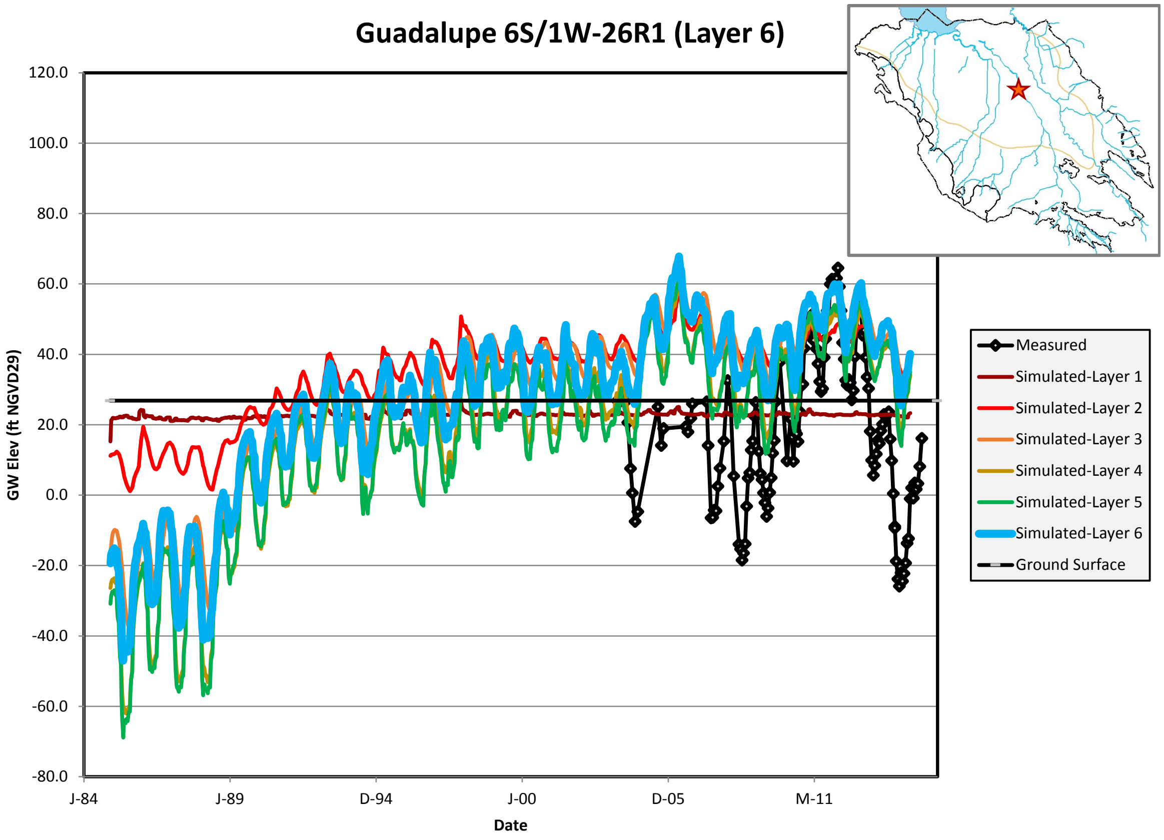
Guadalupe 6S/1W-26R1 (Layer 6)

December 2017

TODD GROUNDWATER

Figure 4-7c
Hydrographs of Measured and Simulated Groundwater Levels Central Low-K Zone

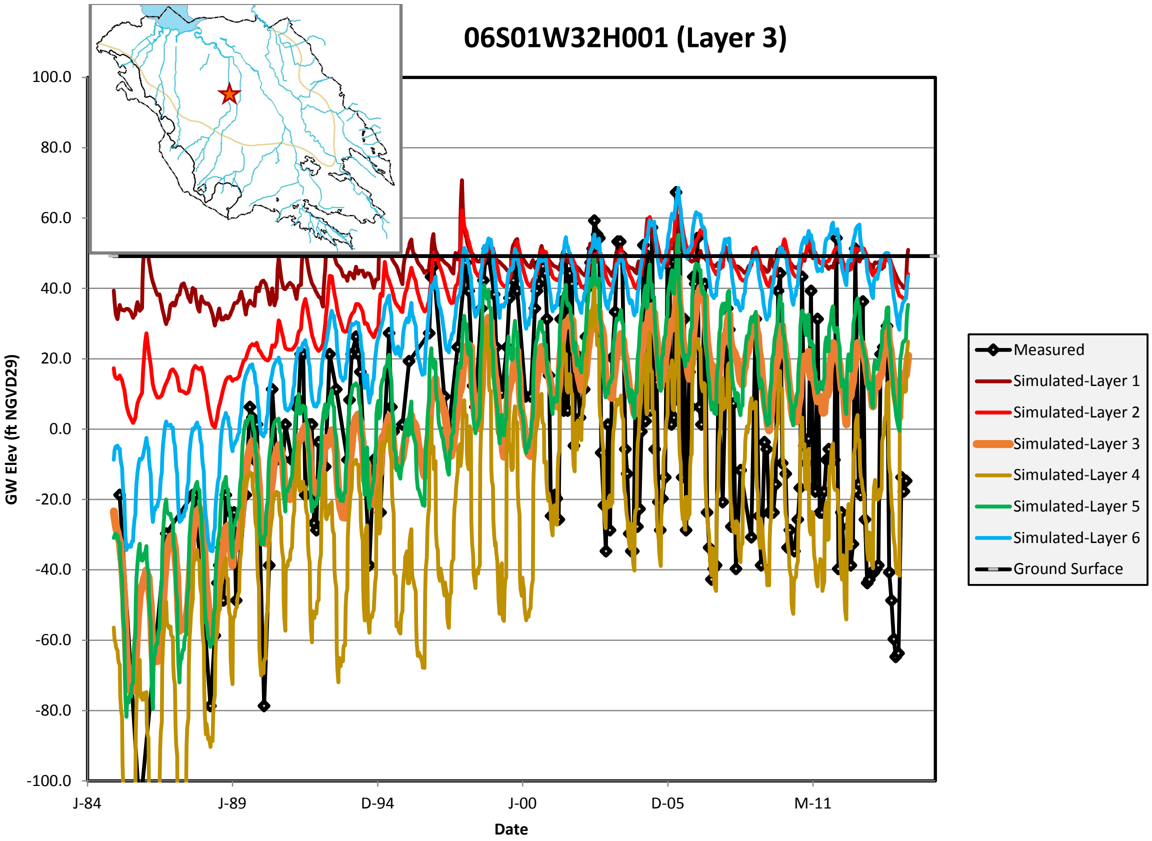

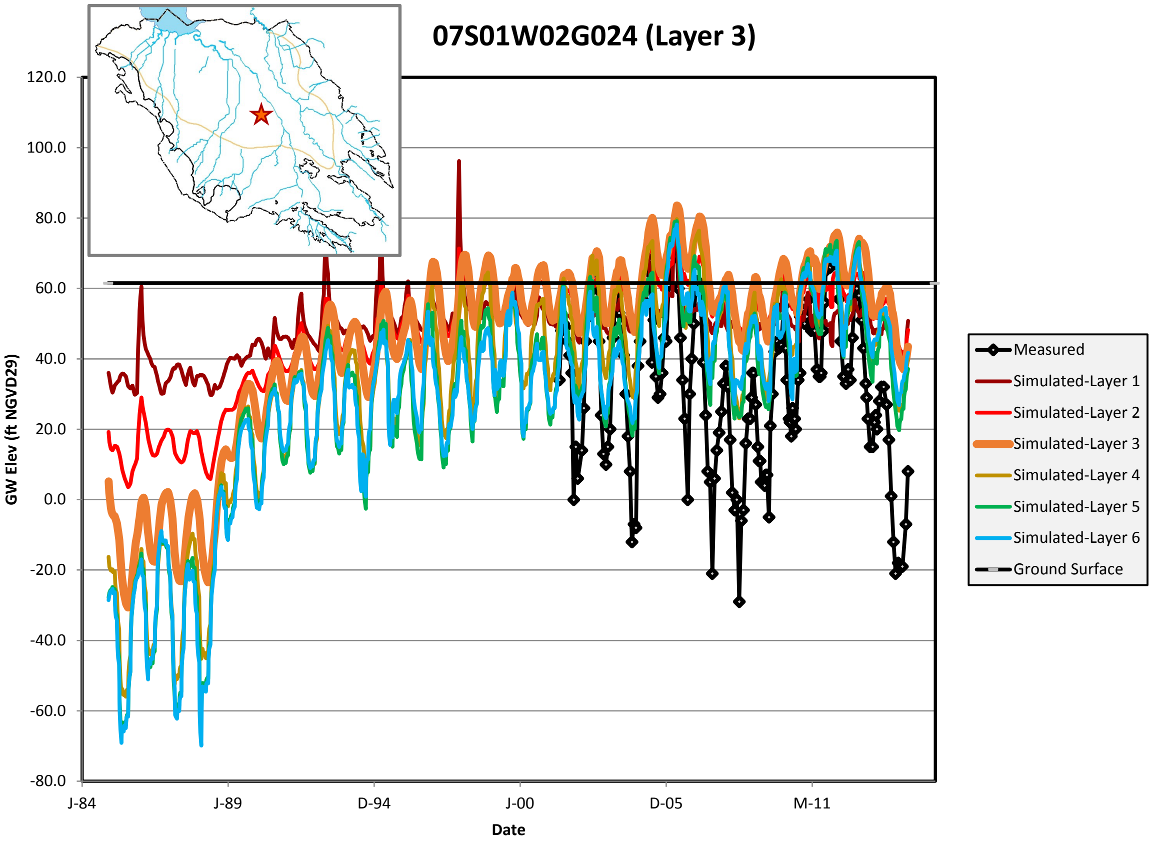

December 2017

TODD GROUNDWATER

Figure 4-7d
Hydrographs of Measured and Simulated Groundwater Levels Central Low-K Zone

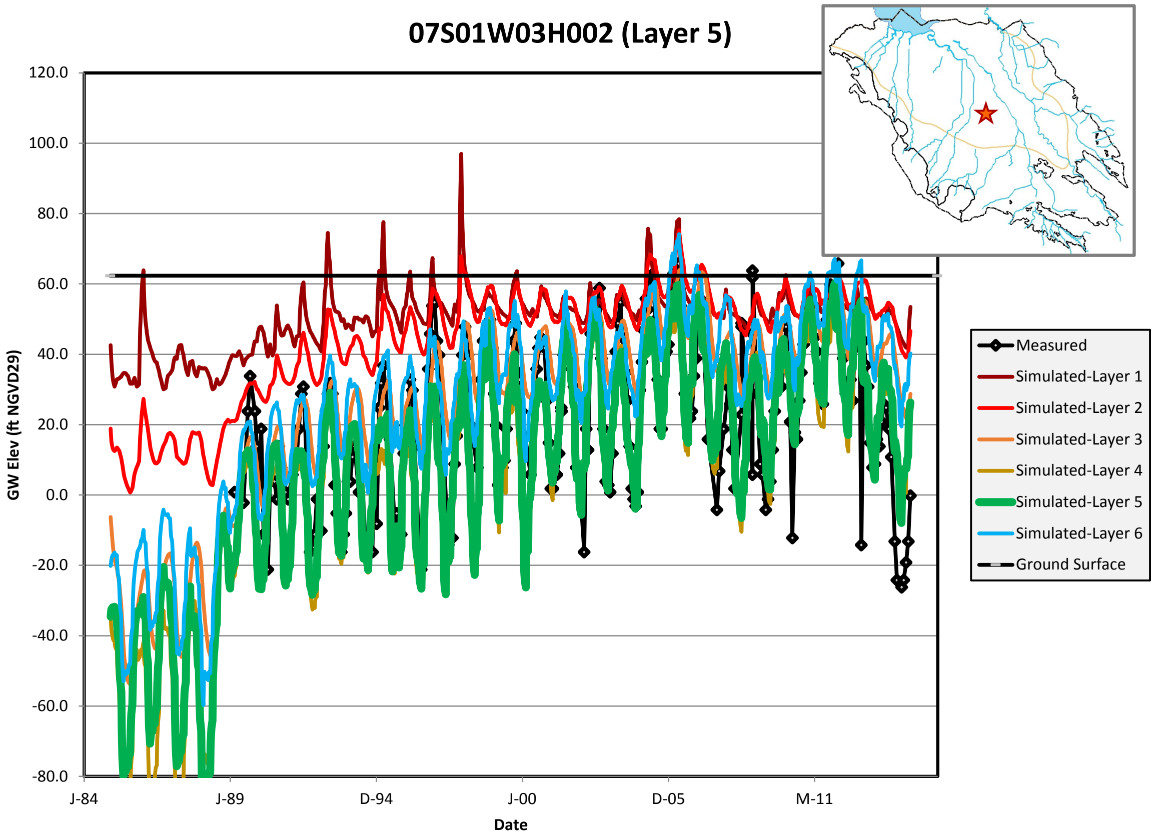

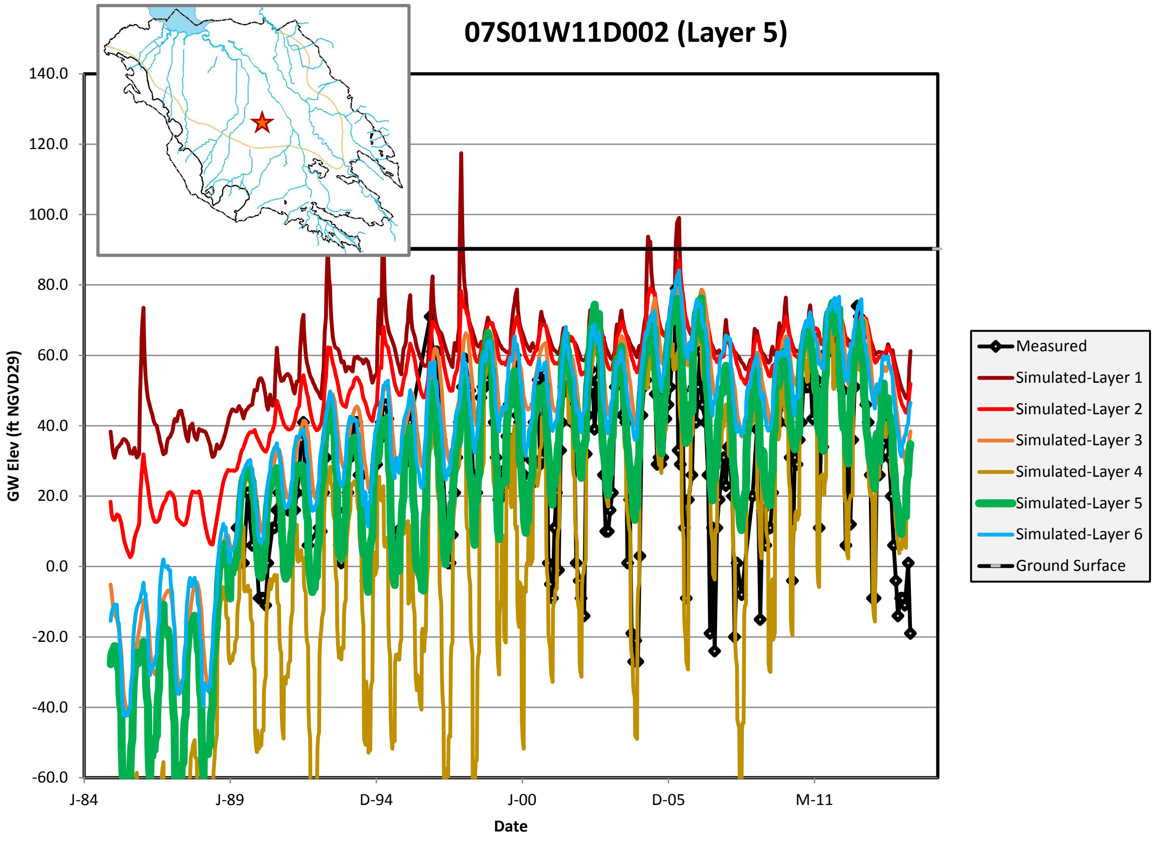

December 2017

TODD GROUNDWATER

Figure 4-7e
Hydrographs of Measured and Simulated Groundwater Levels Central Low-K Zone

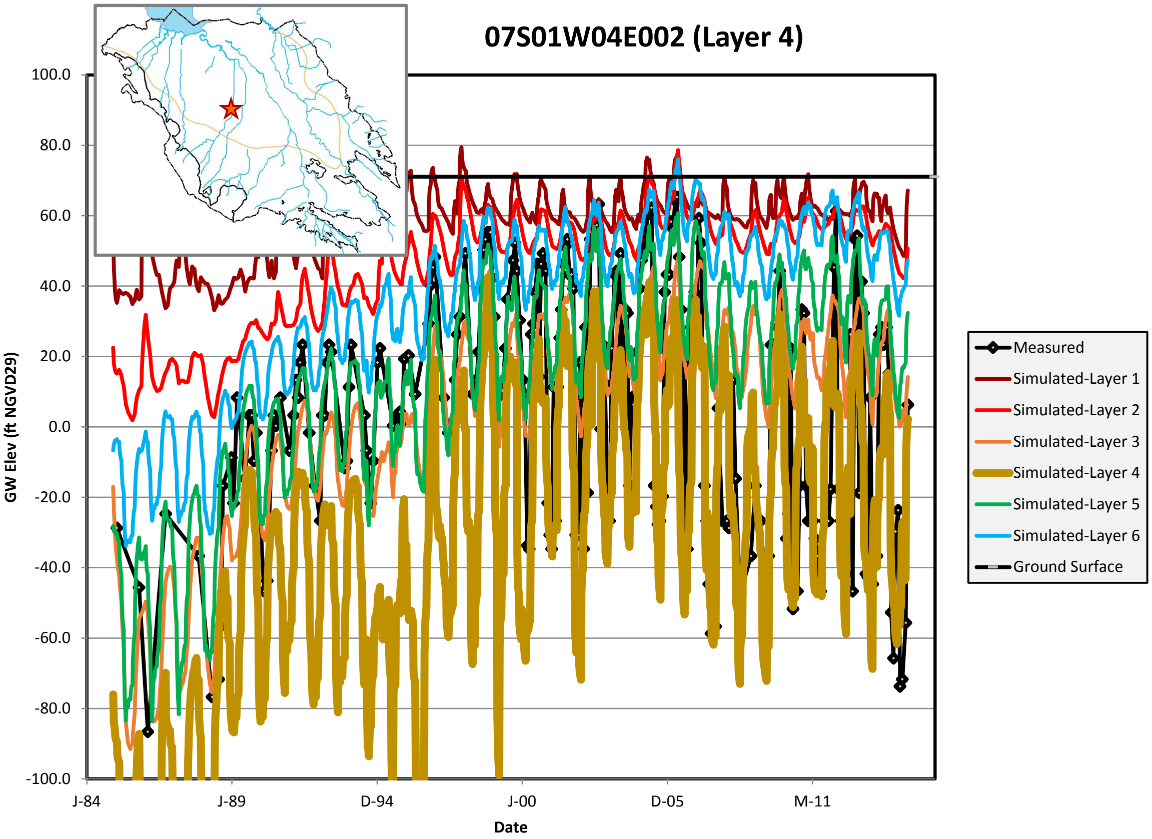

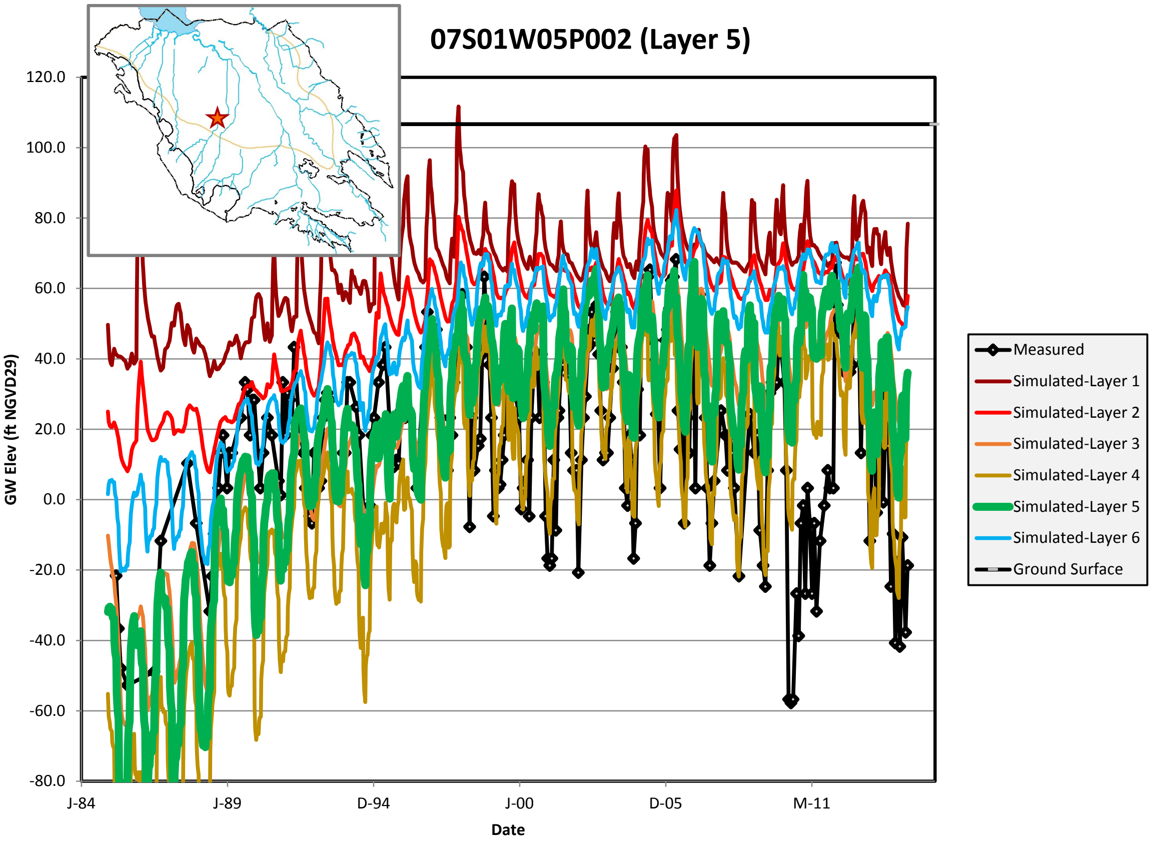

December 2017

TODD GROUNDWATER

Figure 4-7f
Hydrographs of Measured and Simulated Groundwater Levels Central Low-K Zone

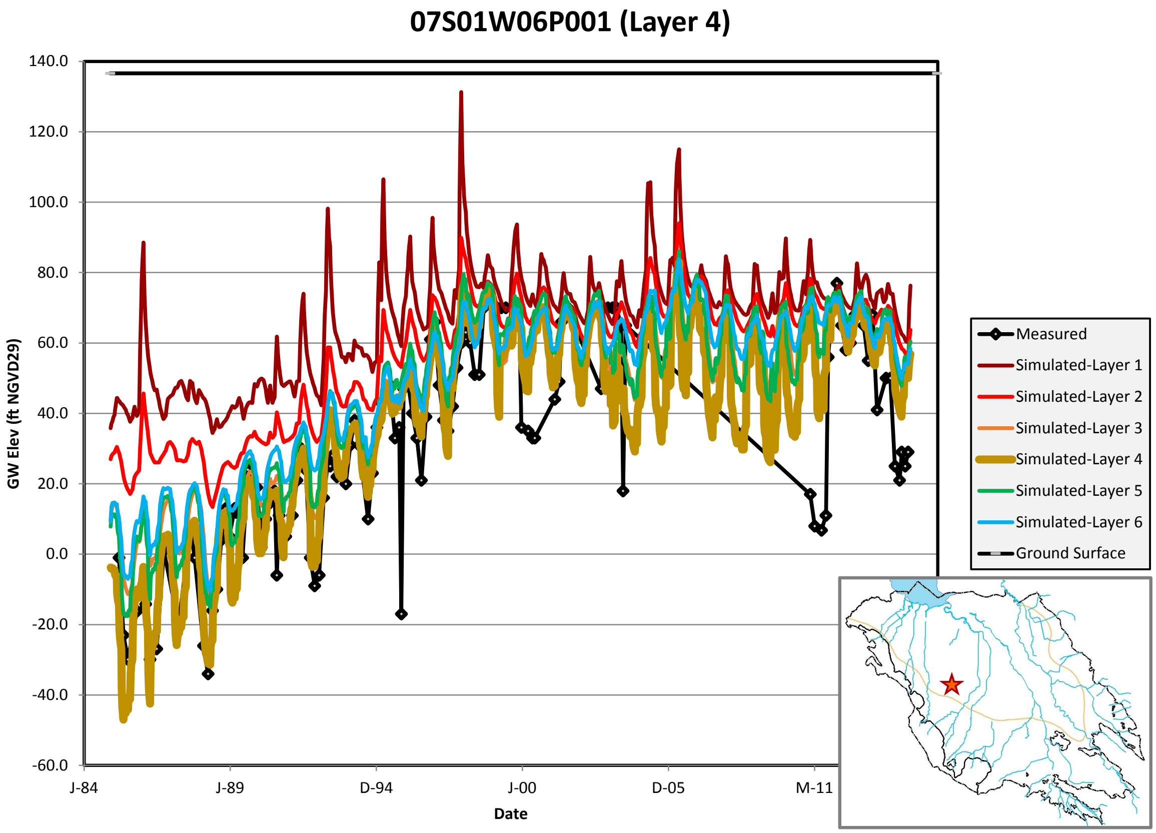

07S01W06P001 (Layer 4)

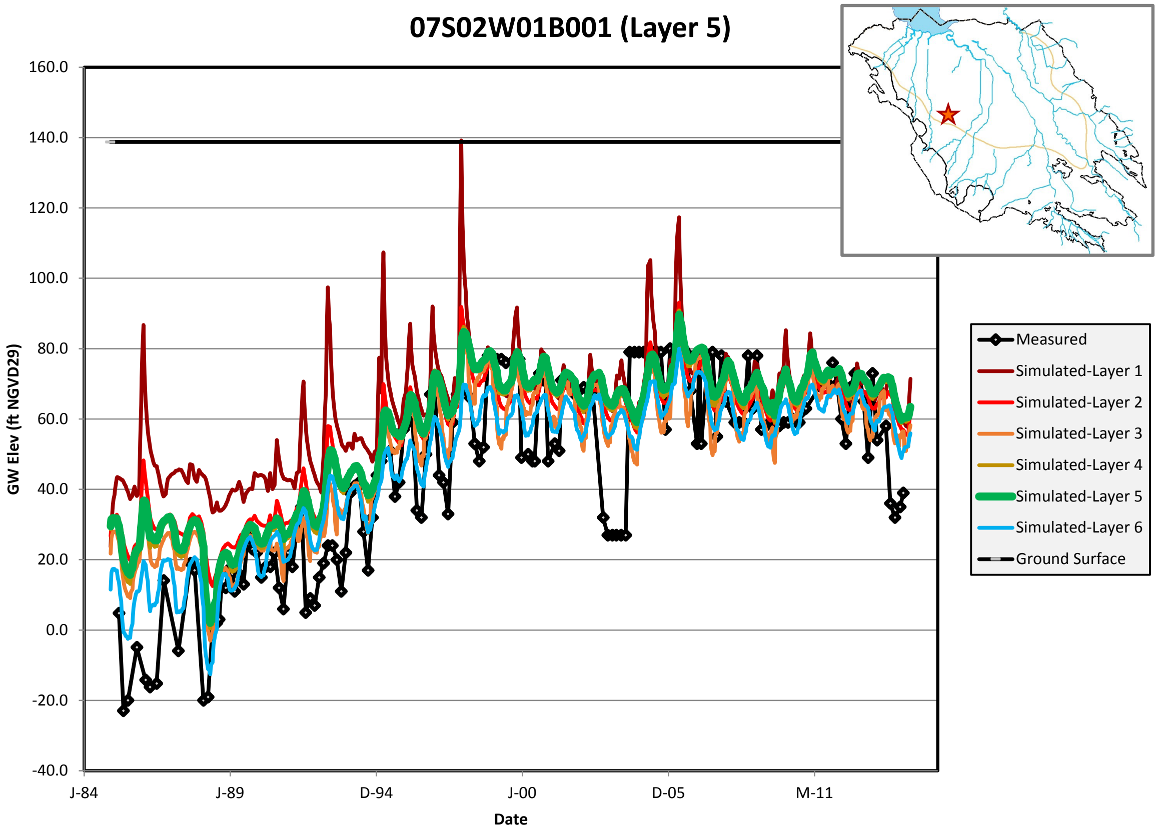

07S02W01B001 (Layer 5)

December 2017

TODD GROUNDWATER

Figure 4-7g
Hydrographs of Measured and Simulated Groundwater Levels
Central Low-K Zone

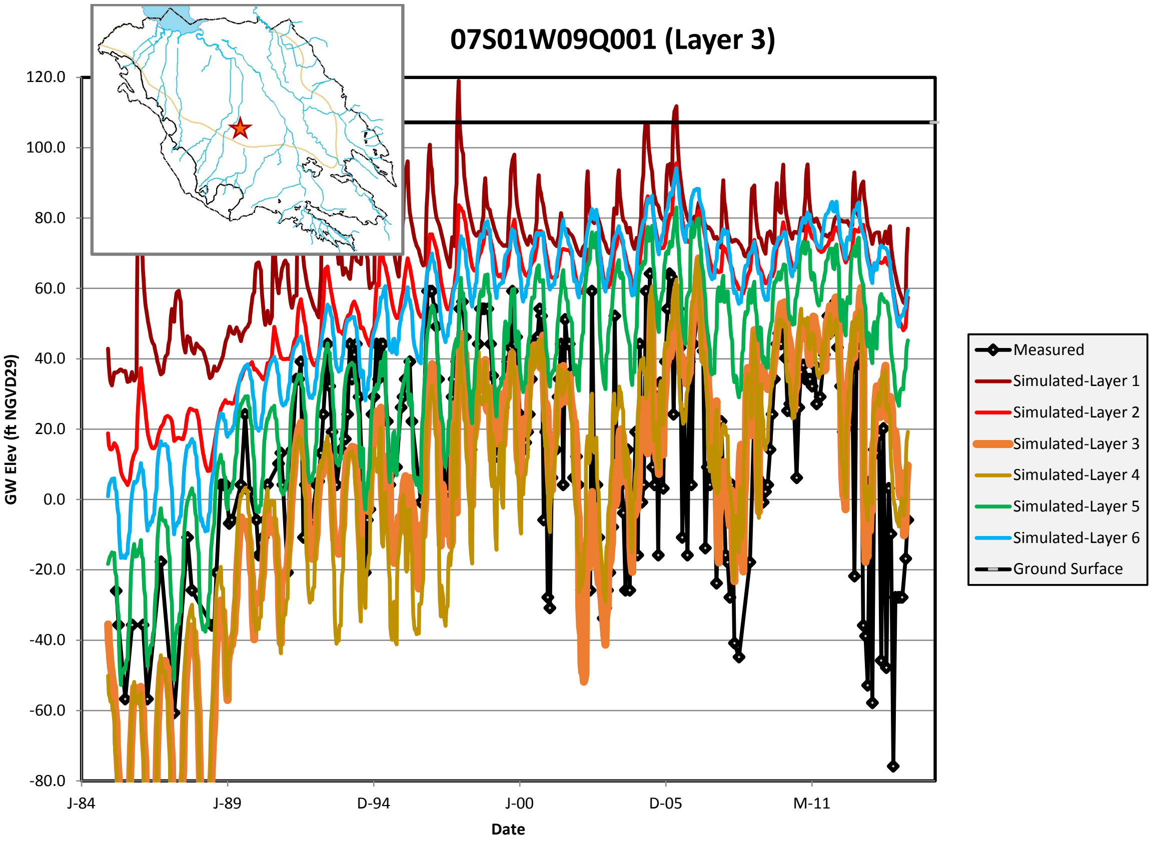

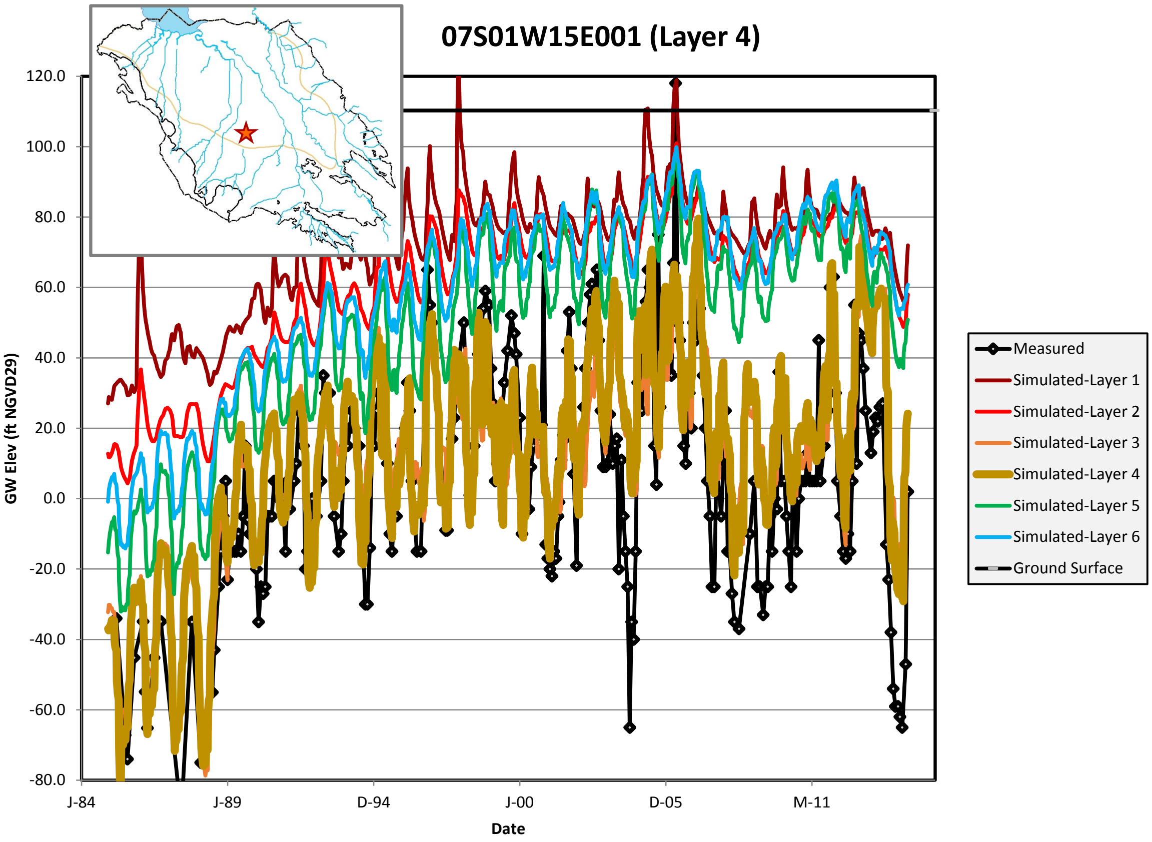

December 2017

TODD GROUNDWATER

Figure 4-7h
Hydrographs of Measured and Simulated Groundwater Levels Central Low-K Zone

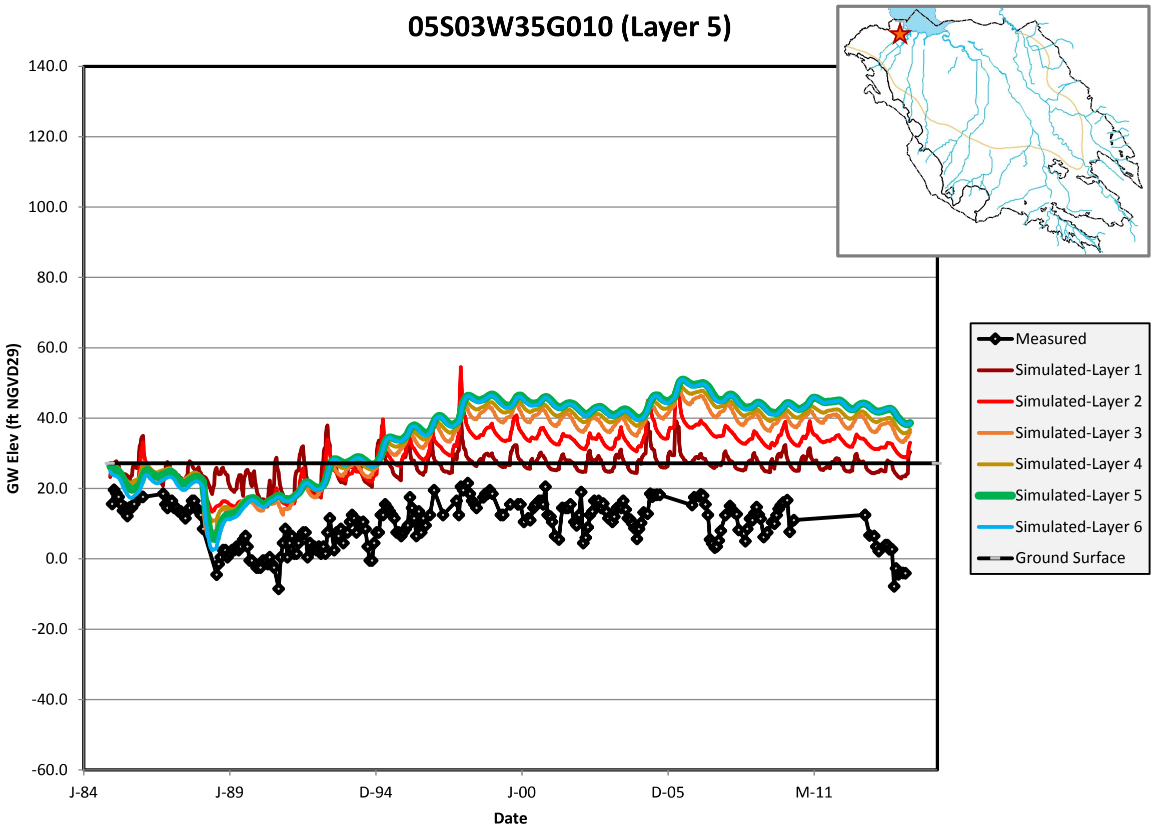
05S03W35G010 (Layer 5)

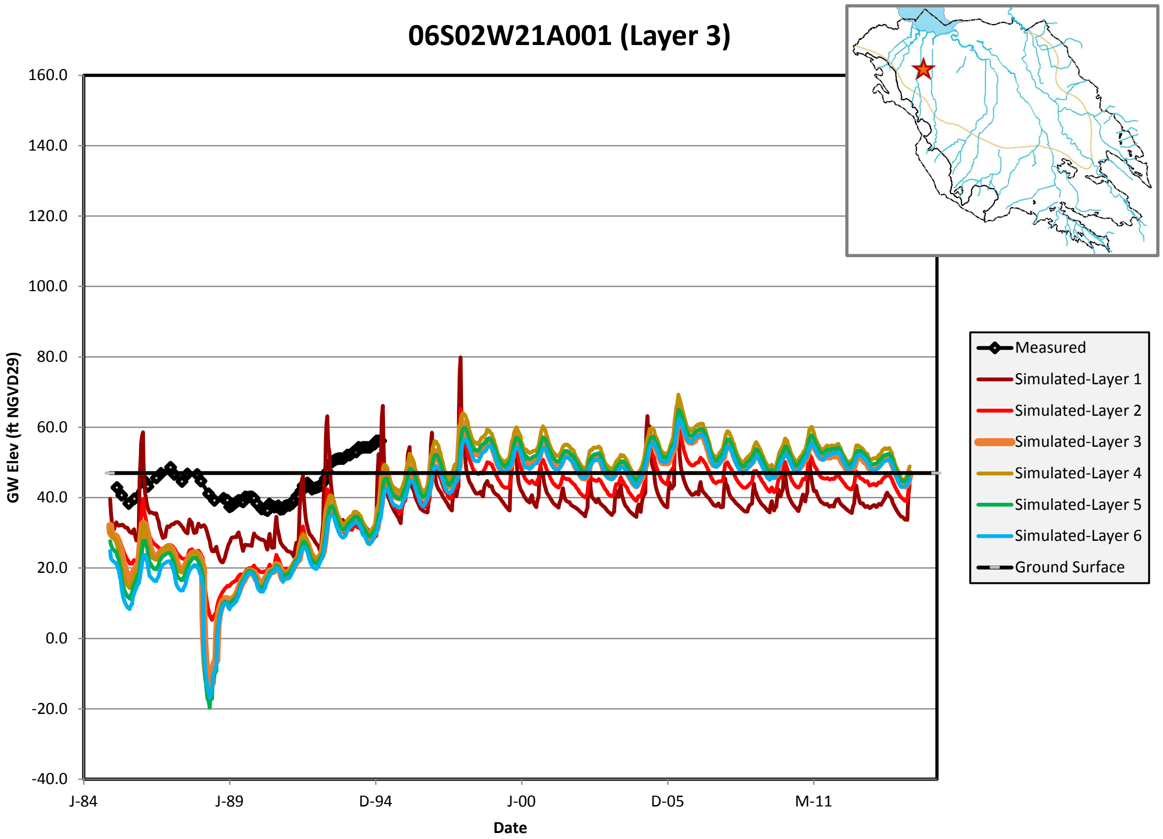
06S02W21A001 (Layer 3)

December 2017

TODD GROUNDWATER

Figure 4-8a
Hydrographs of Measured and Simulated Groundwater Levels San Francisco Bay Margin

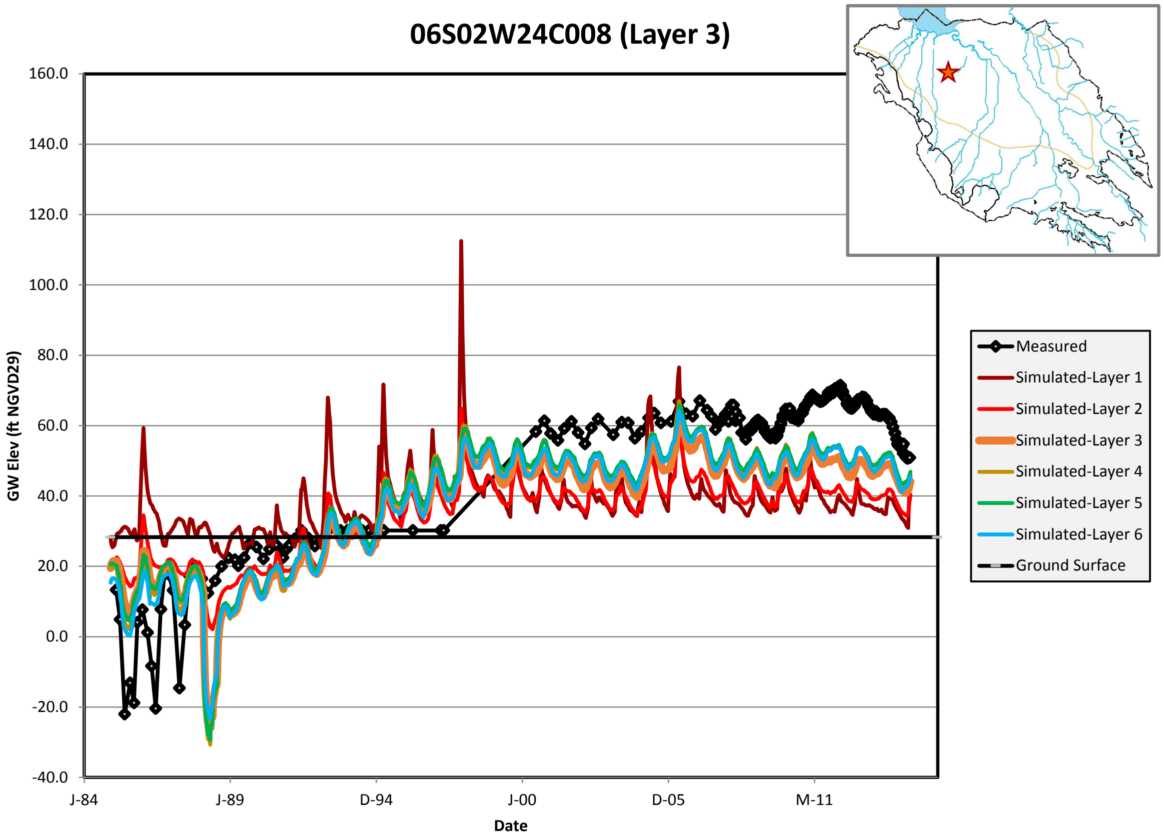
06S02W24C008 (Layer 3)

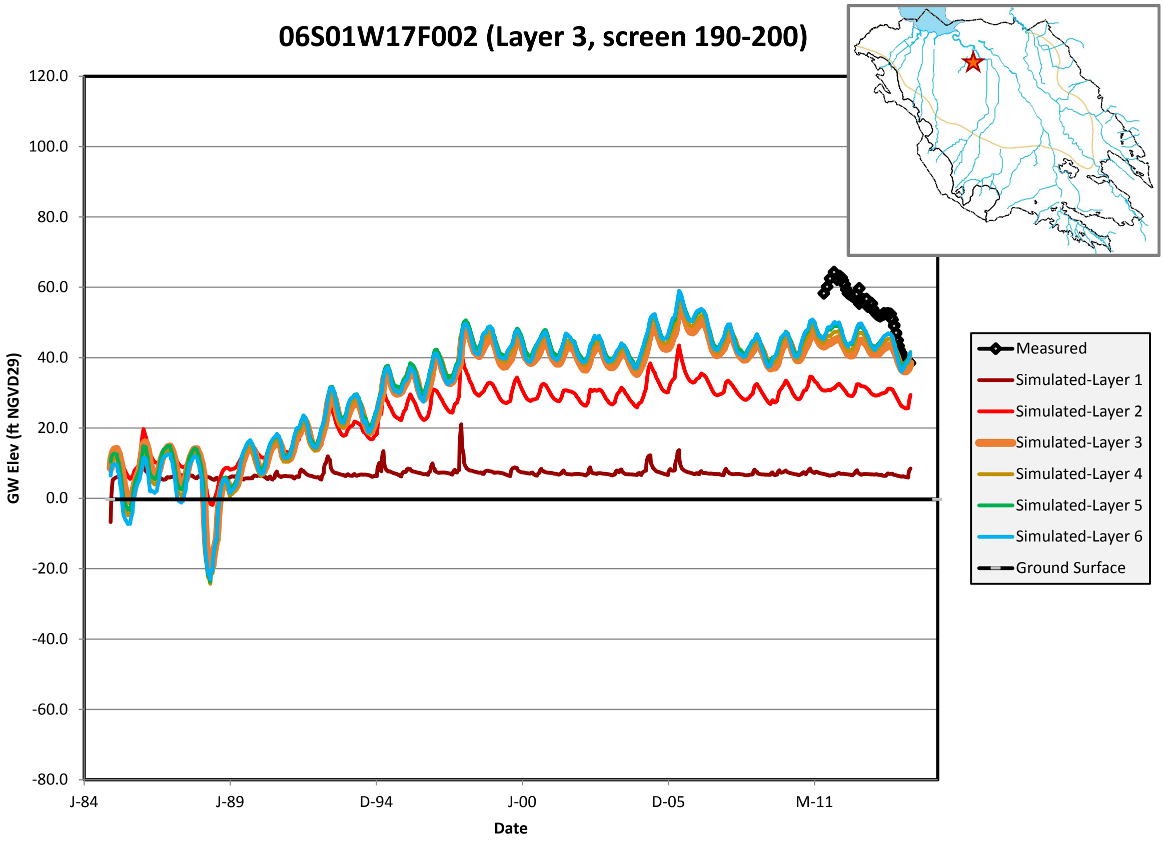
06S01W17F002 (Layer 3, screen 190-200)

December 2017

TODD GROUNDWATER

Figure 4-8b
Hydrographs of Measured and Simulated Groundwater Levels San Francisco Bay Margin

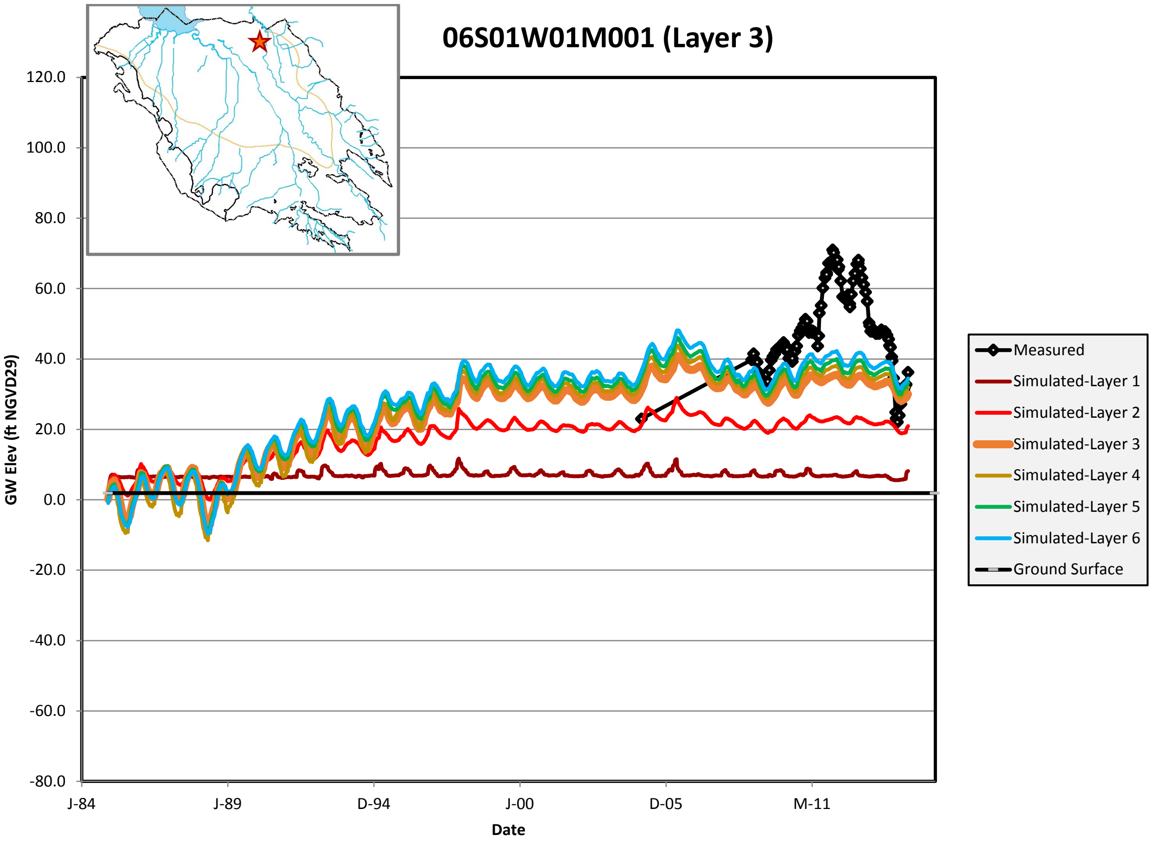

December 2017

TODD GROUNDWATER

Figure 4-8c
Hydrographs of Measured and Simulated Groundwater Levels San Francisco Bay Margin

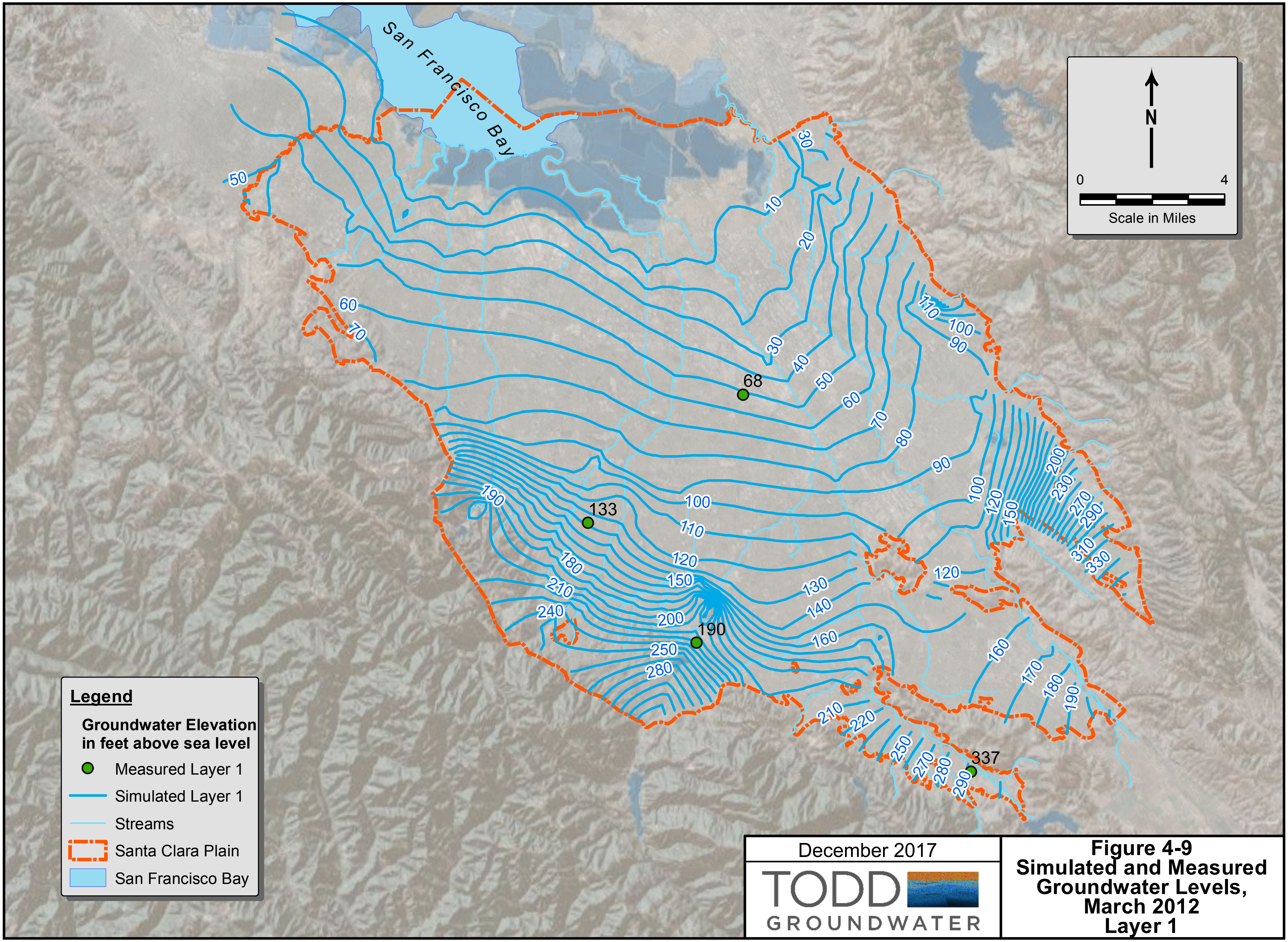

December 2017

TODD GROUNDWATER

Figure 4-9
Simulated and Measured Groundwater Levels, March 2012
Layer 1

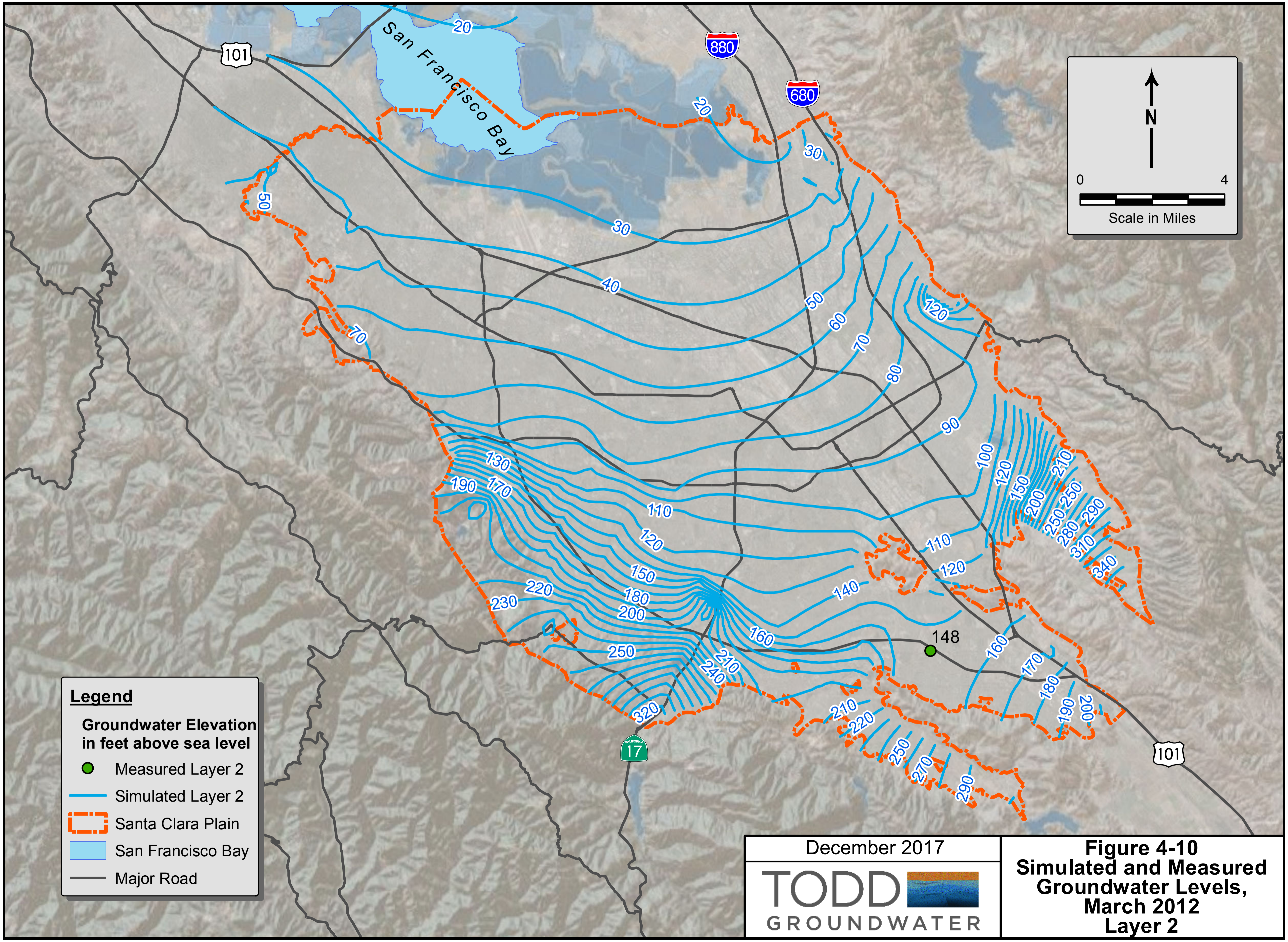

December 2017

TODD GROUNDWATER

Figure 4-10
Simulated and Measured Groundwater Levels, March 2012
Layer 2

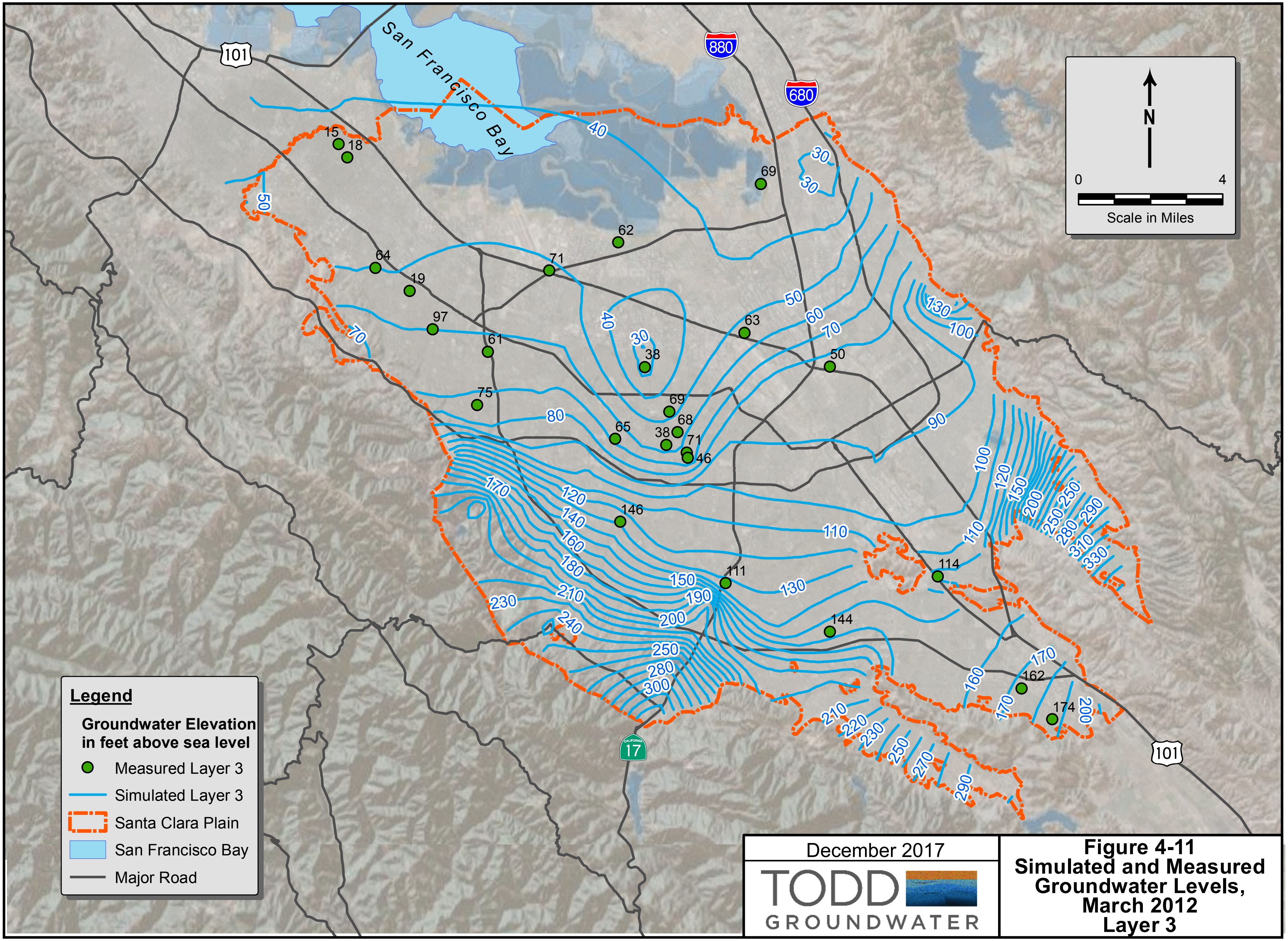

December 2017

TODD GROUNDWATER

Figure 4-11
Simulated and Measured Groundwater Levels, March 2012
Layer 3

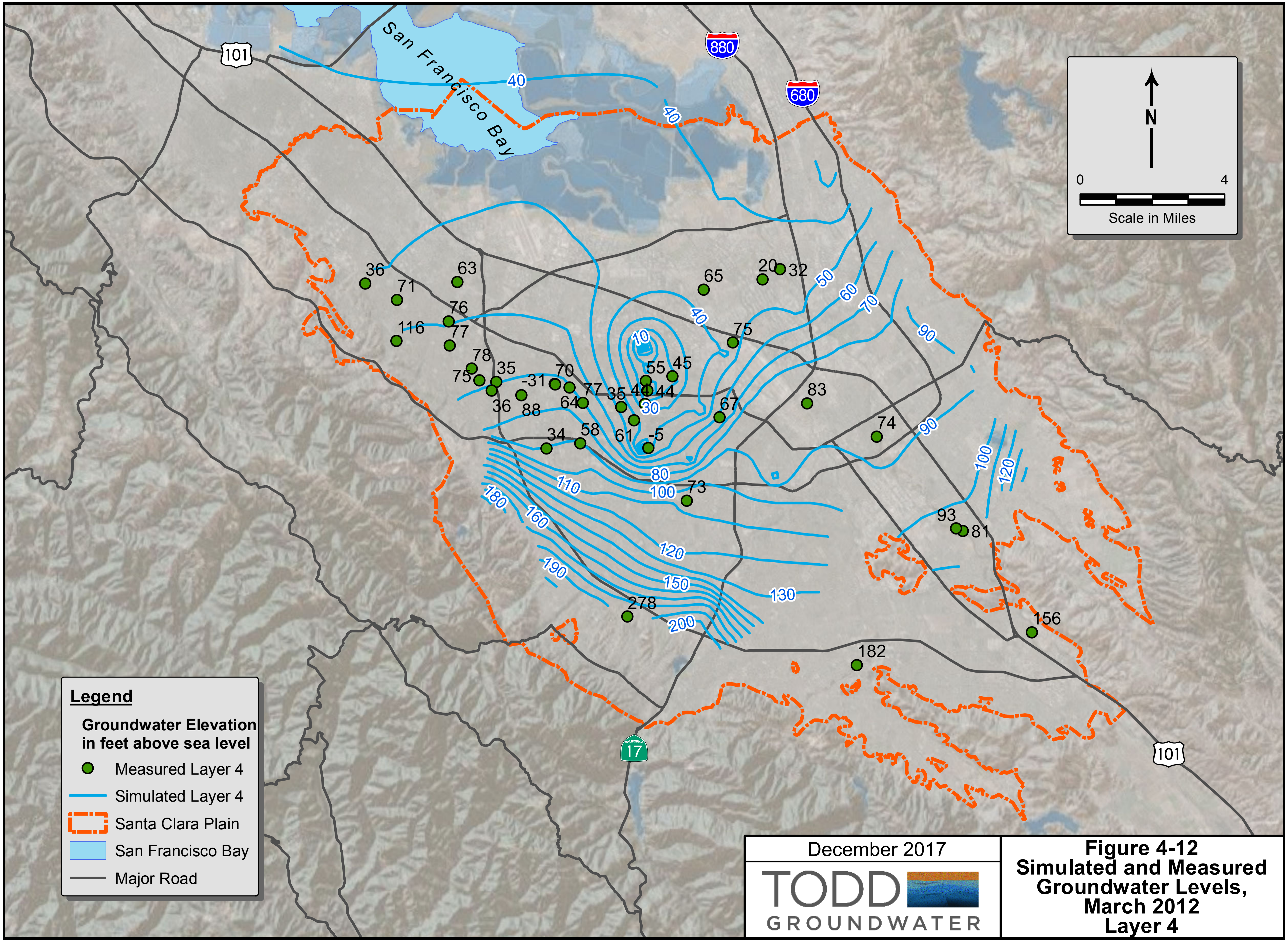

December 2017

TODD GROUNDWATER

Figure 4-12
Simulated and Measured Groundwater Levels, March 2012
Layer 4

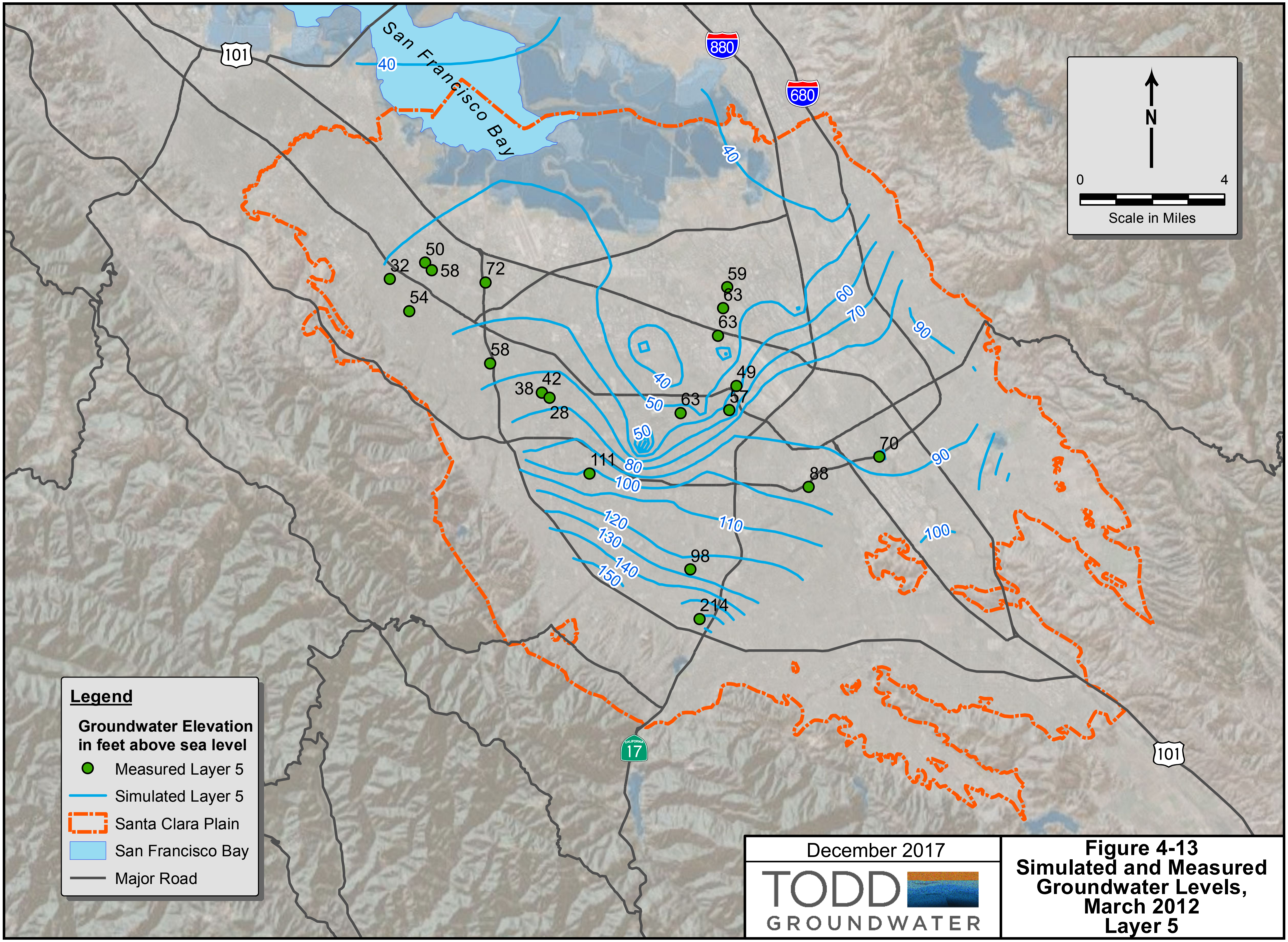

Figure 4-13
Simulated and Measured Groundwater Levels, March 2012 Layer 5

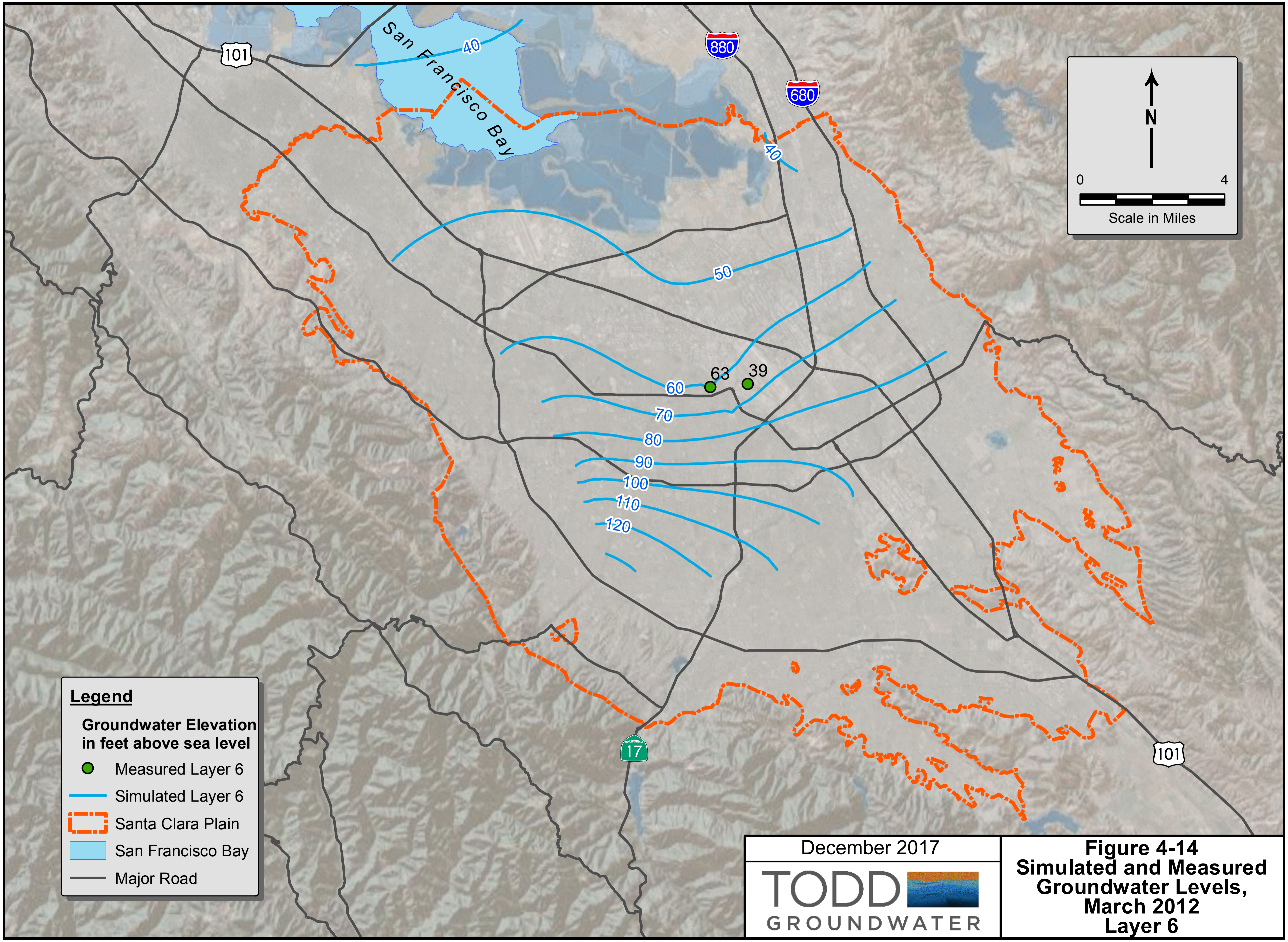

December 2017

TODD GROUNDWATER

Figure 4-14
Simulated and Measured Groundwater Levels, March 2012
Layer 6

A. Simulated Layer 1 Groundwater Levels above Land Surface Elevation in March 2012

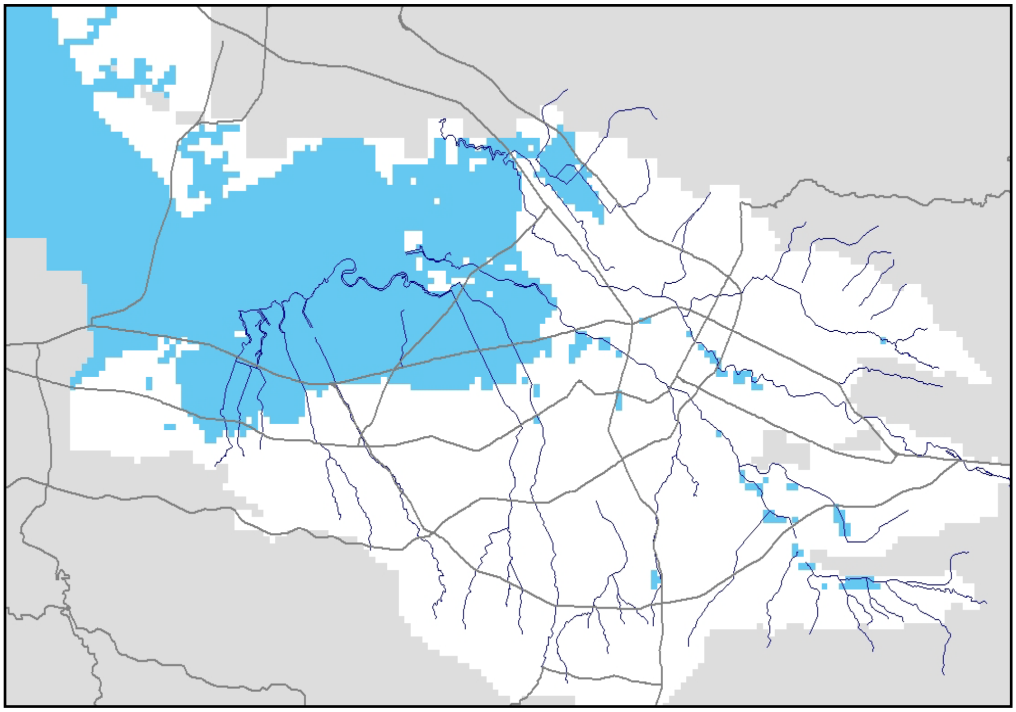

B. Extent of Shallow Groundwater Levels in 2003

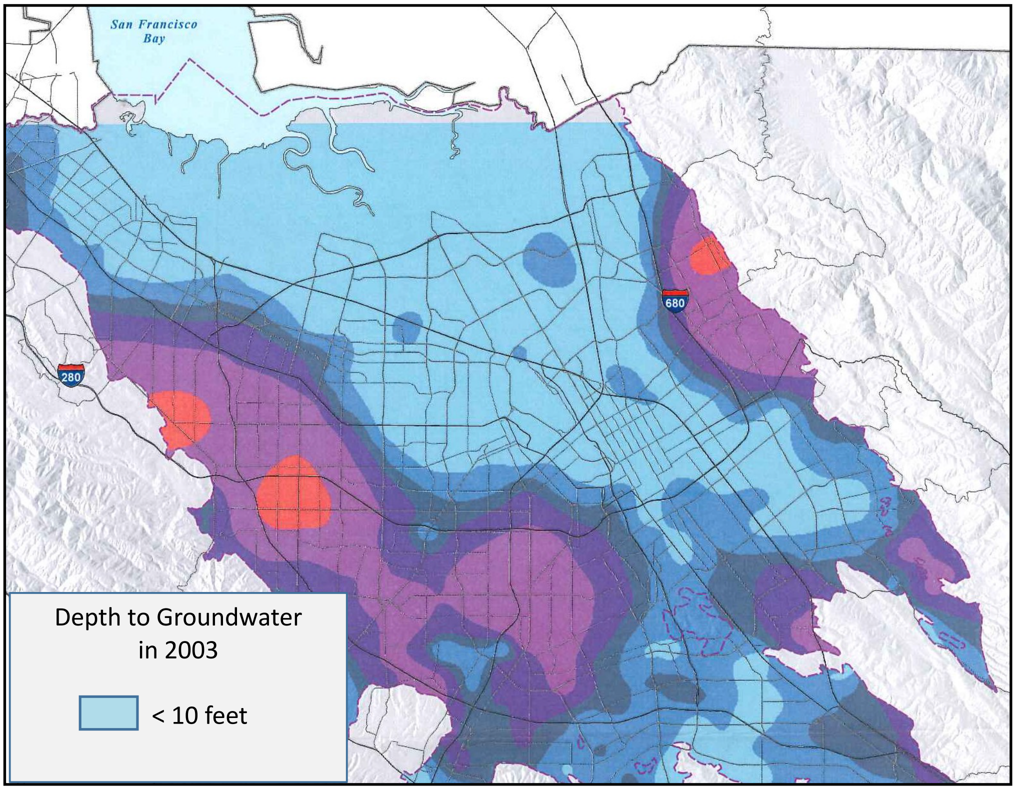

December 2017

TODD GROUNDWATER

Figure 4-15
Simulated and Measured Extent of Shallow Groundwater

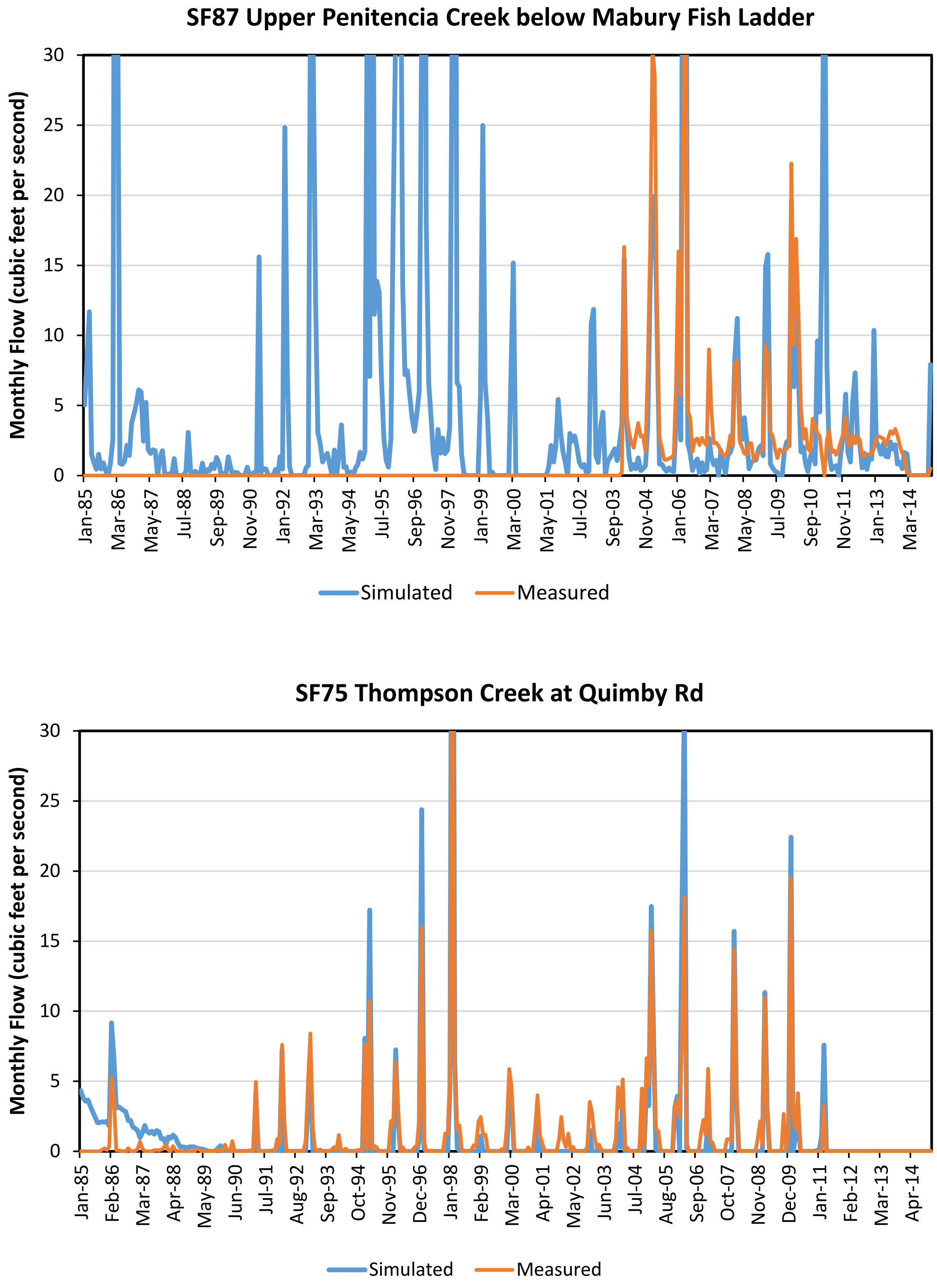

CFS - cubic feet per second

December 2017

TODD GROUNDWATER

Figure 4-16a
Simulated and Measured Streamflow Hydrographs

SF89 Coyote Creek below Percolation Ponds

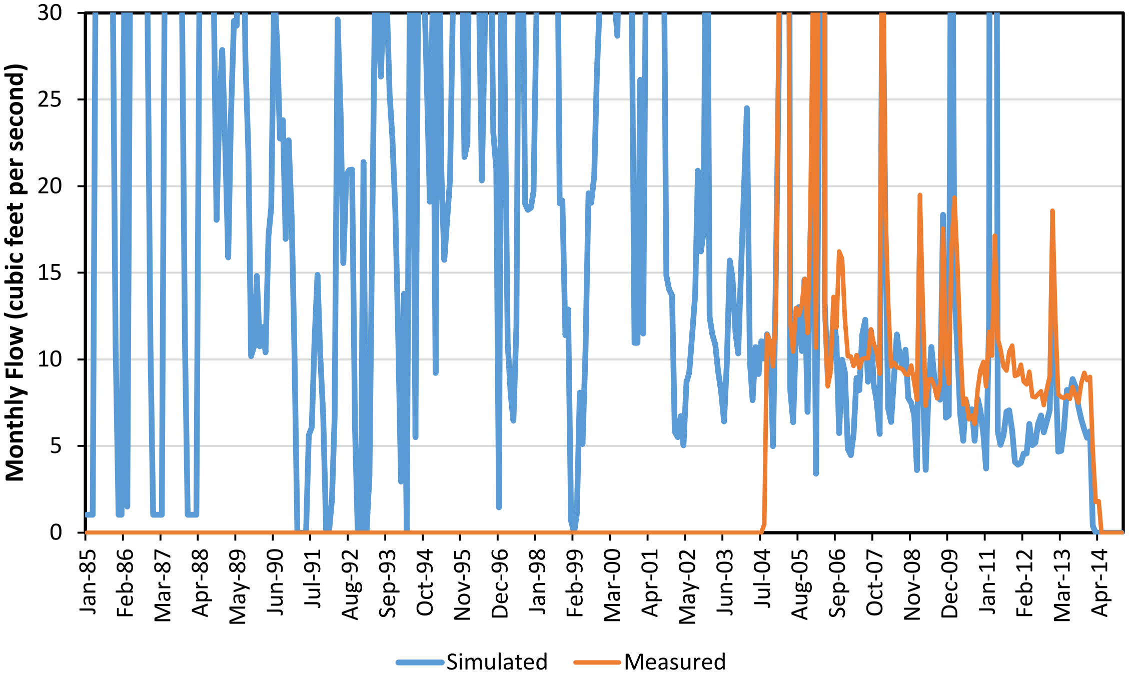

SF58 Coyote Creek at Edenvale Gap

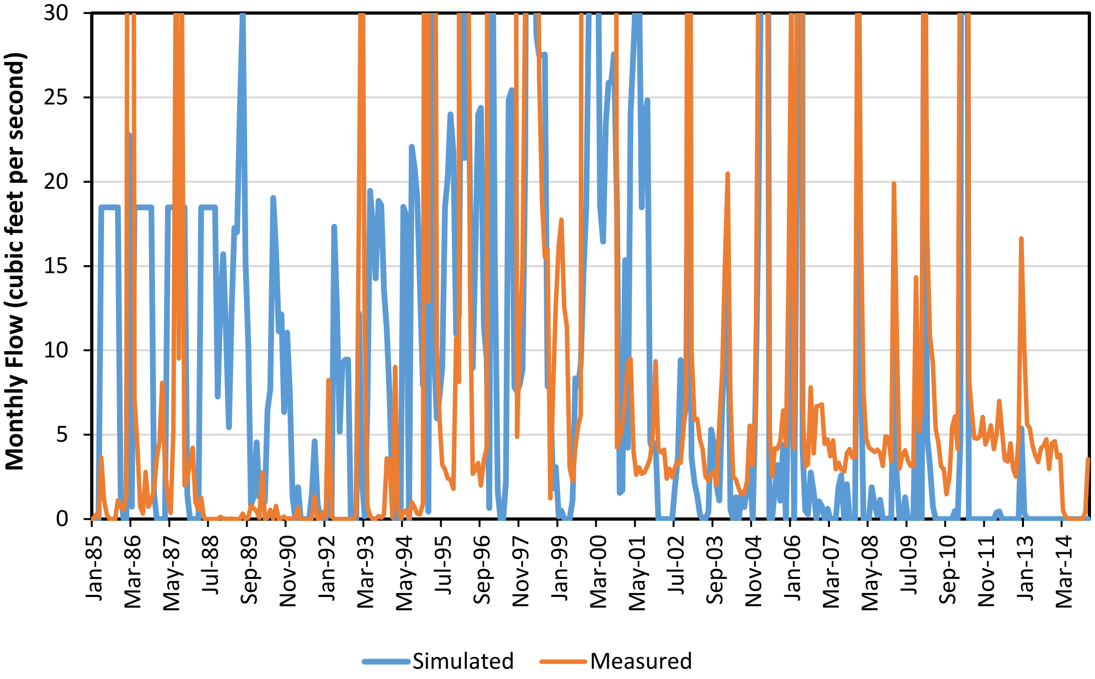

CFS - cubic feet per second

December 2017

TODD GROUNDWATER

Figure 4-16b
Simulated and Measured Streamflow Hydrographs

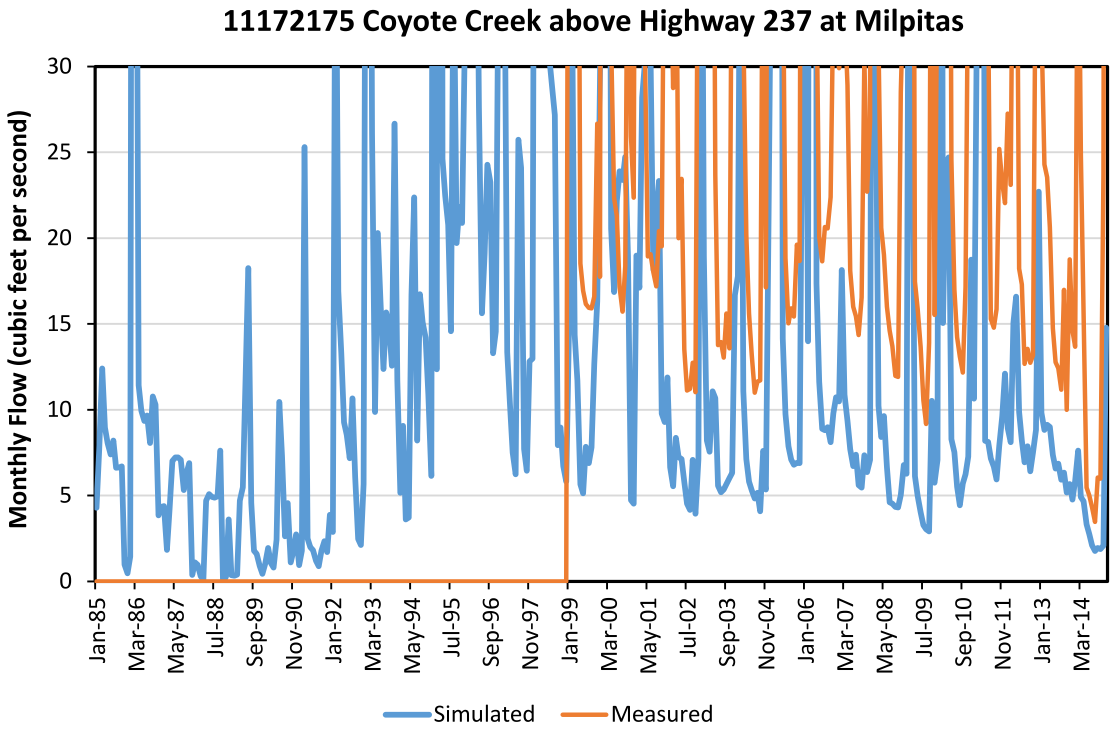
11172175 Coyote Creek above Highway 237 at Milpitas

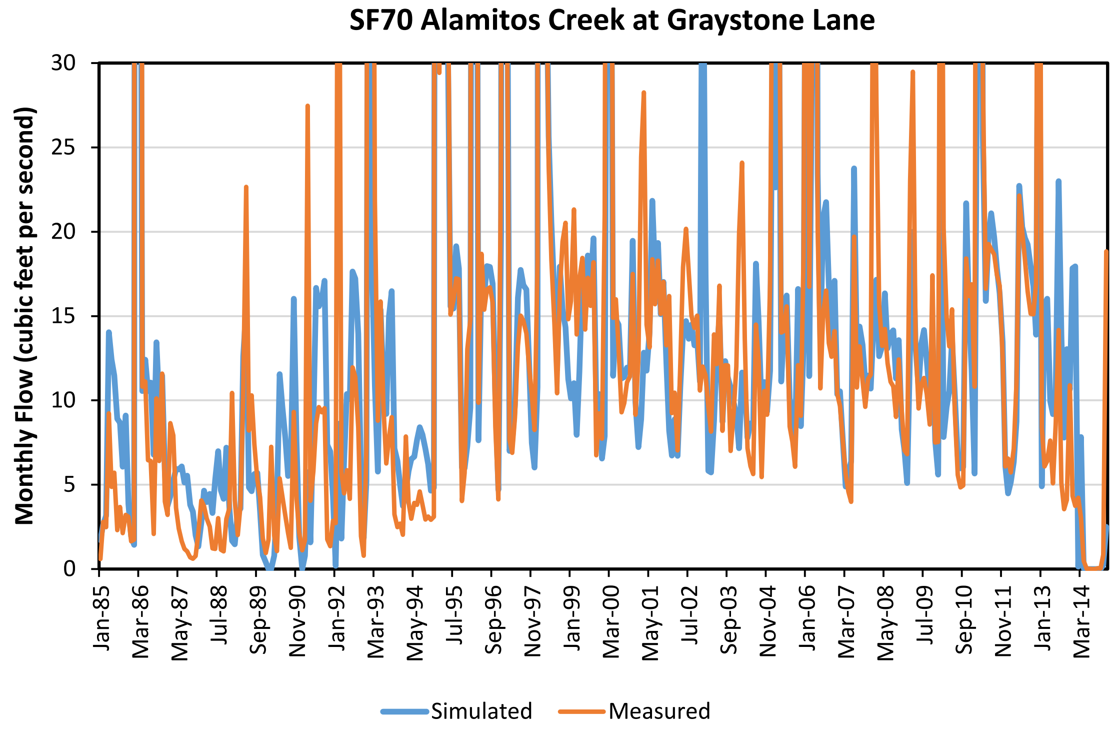
SF70 Alamitos Creek at Graystone Lane

CFS - cubic feet per second

December 2017

TODD GROUNDWATER

Figure 4-16c
Simulated and Measured Streamflow Hydrographs

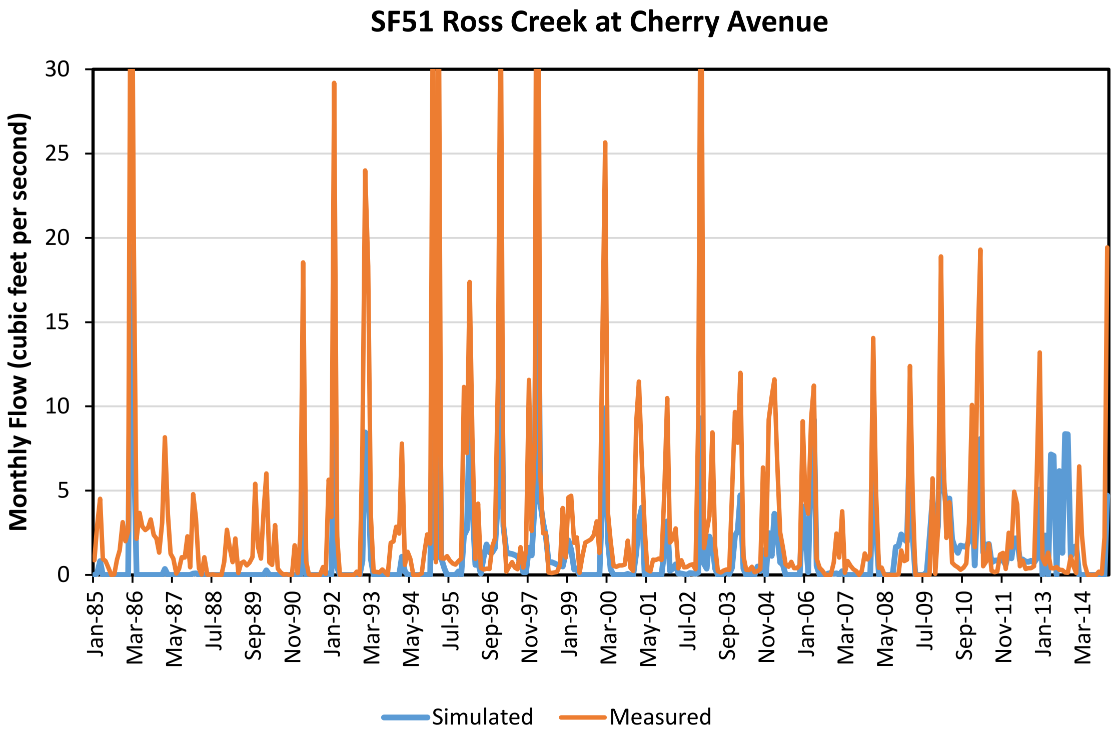

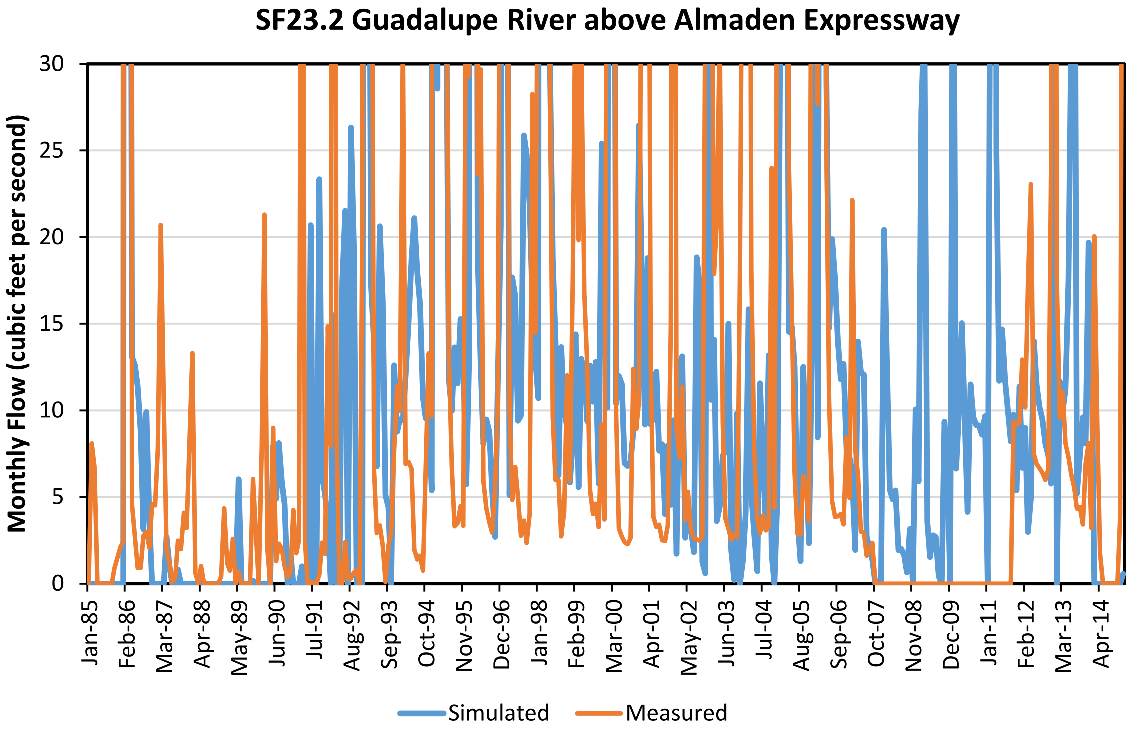

CFS - cubic feet per second

December 2017

TODD GROUNDWATER

Figure 4-16d
Simulated and Measured Streamflow Hydrographs

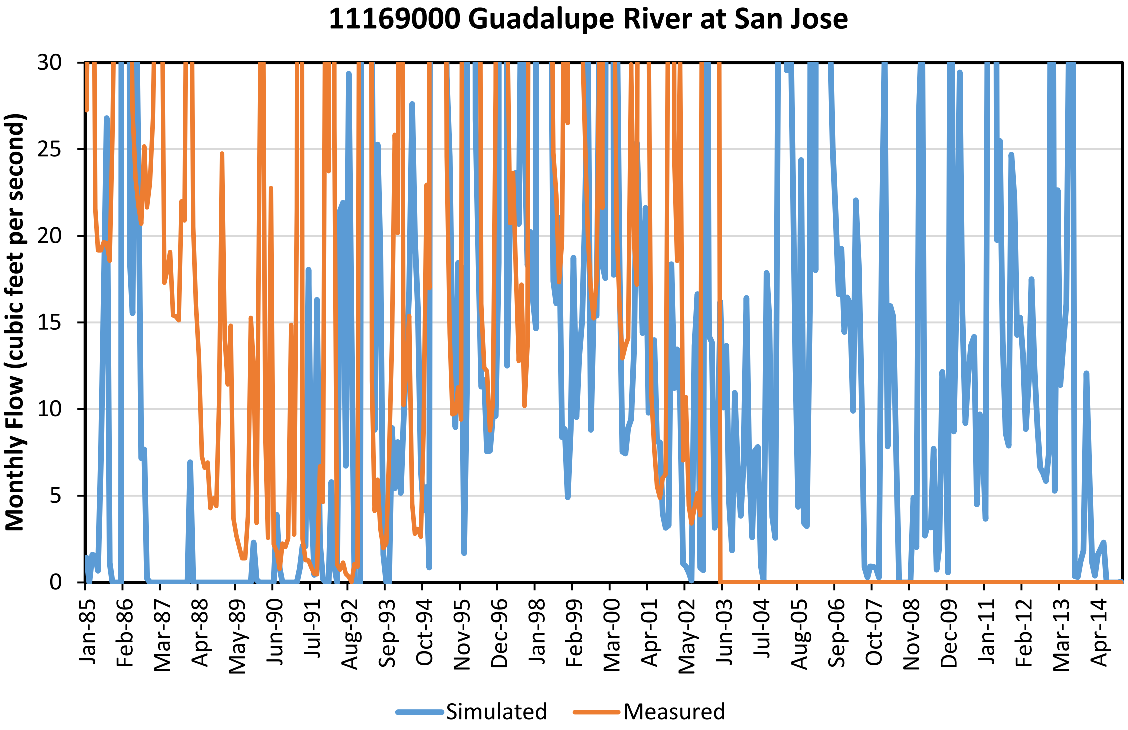

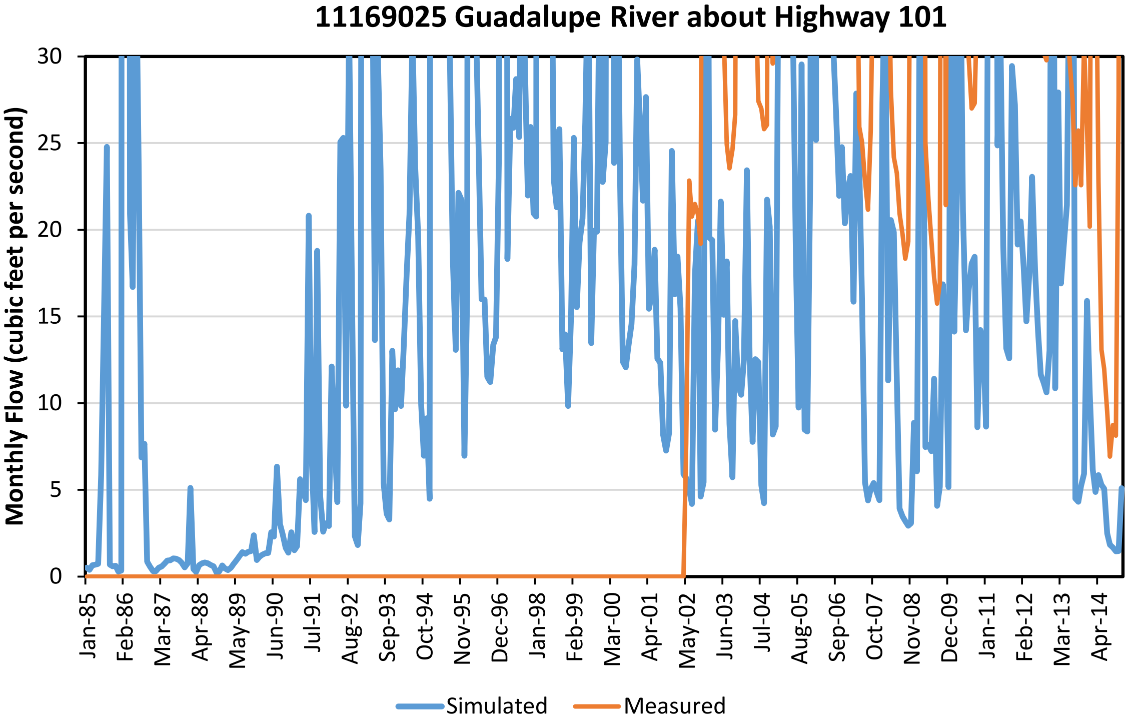

CFS - cubic feet per second

December 2017

TODD GROUNDWATER

Figure 4-16e
Simulated and Measured Streamflow Hydrographs

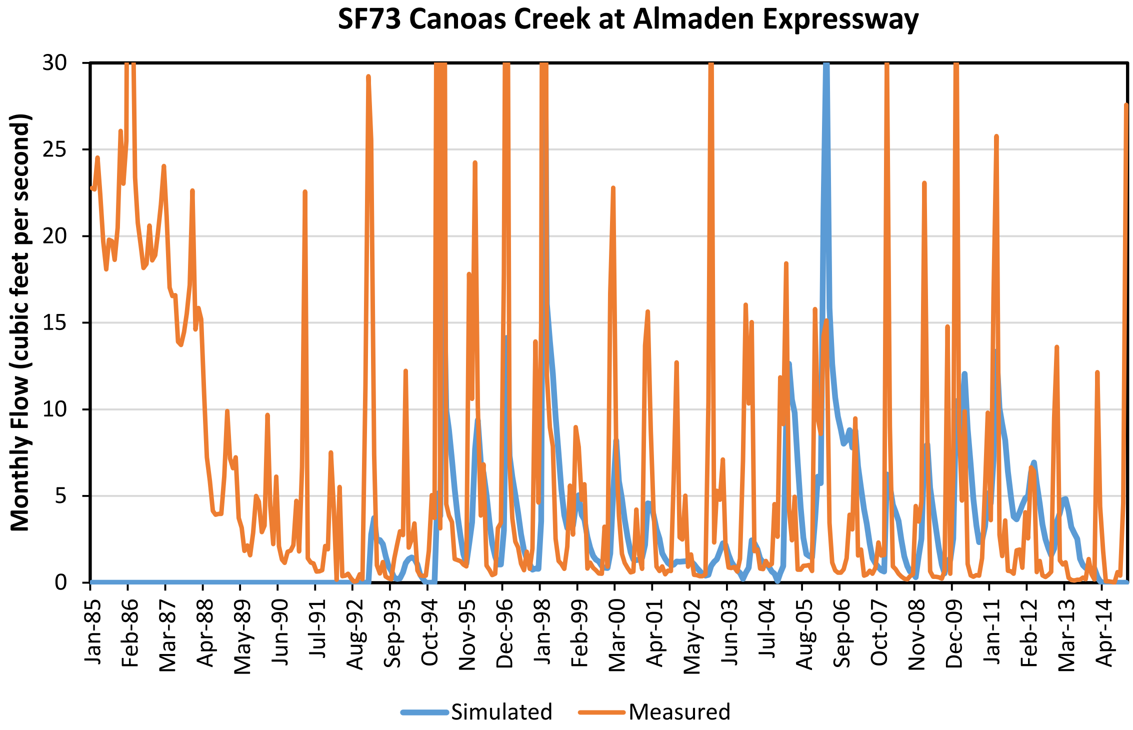

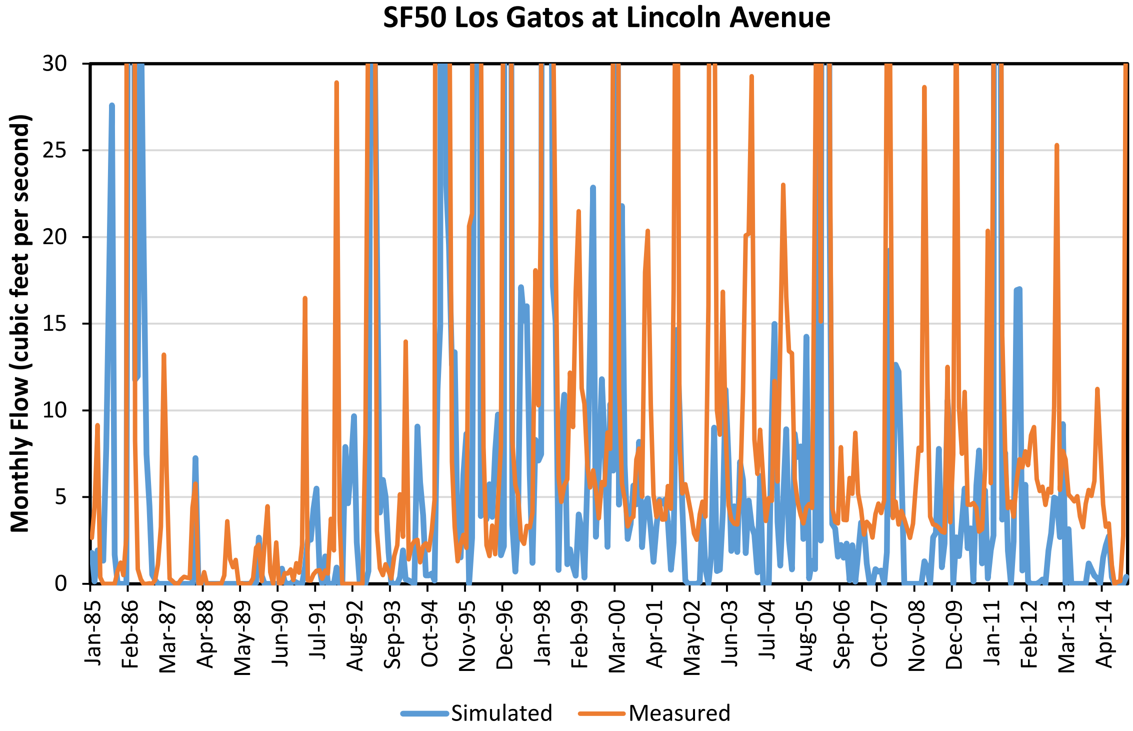

CFS - cubic feet per second

December 2017

TODD GROUNDWATER

Figure 4-16f
Simulated and Measured Streamflow Hydrographs

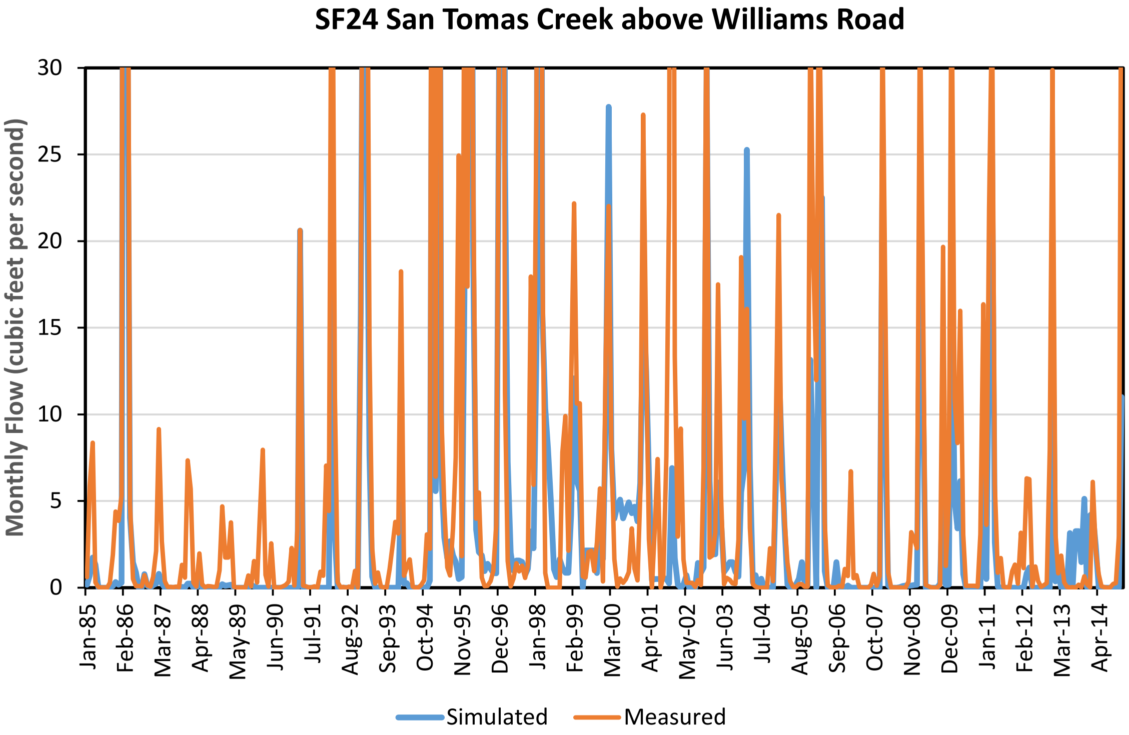

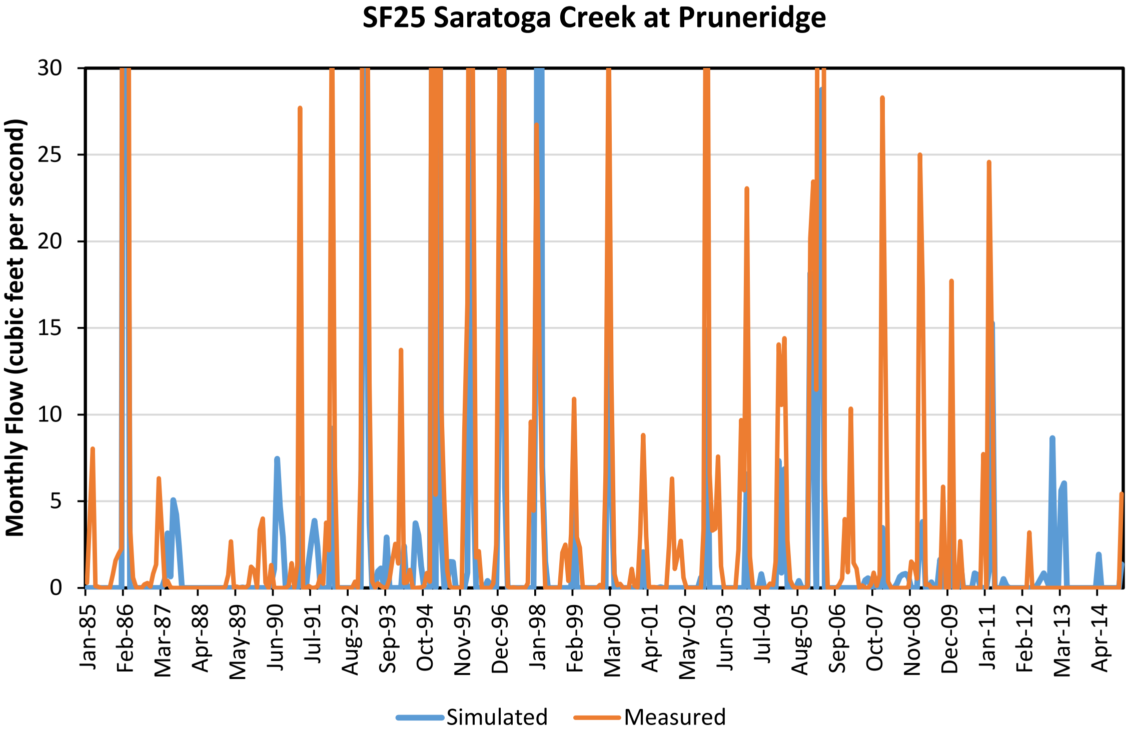

CFS - cubic feet per second

December 2017

TODD GROUNDWATER

Figure 4-16g
Simulated and Measured Streamflow Hydrographs

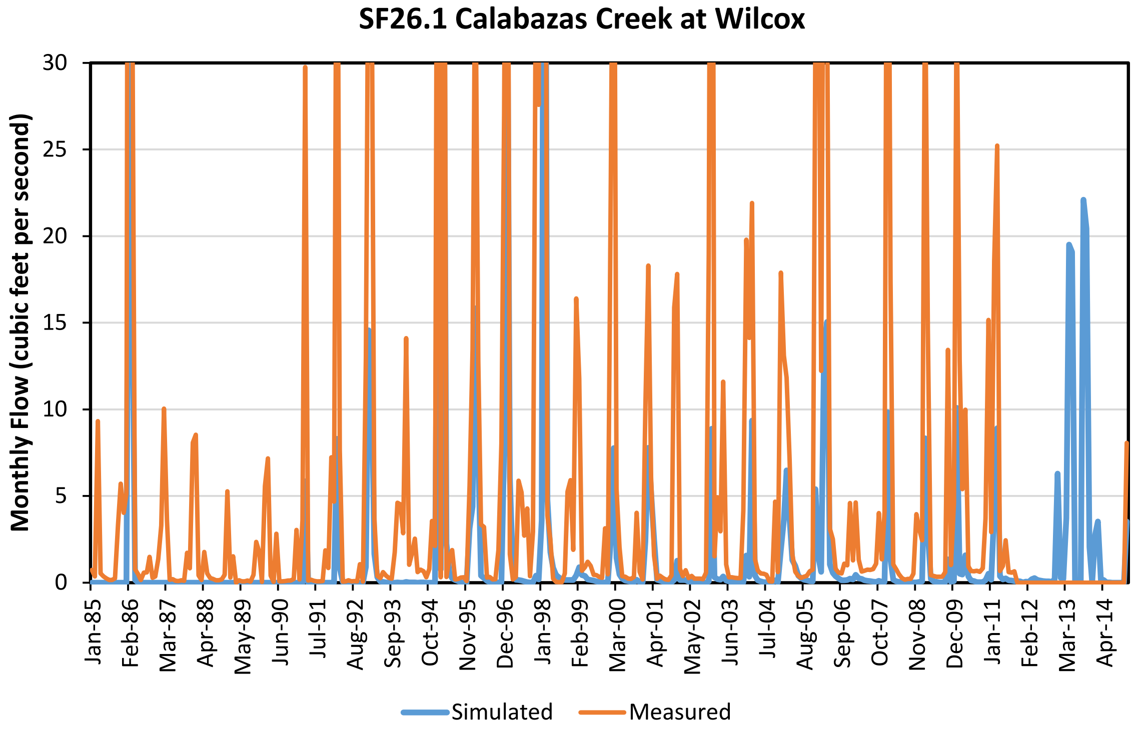

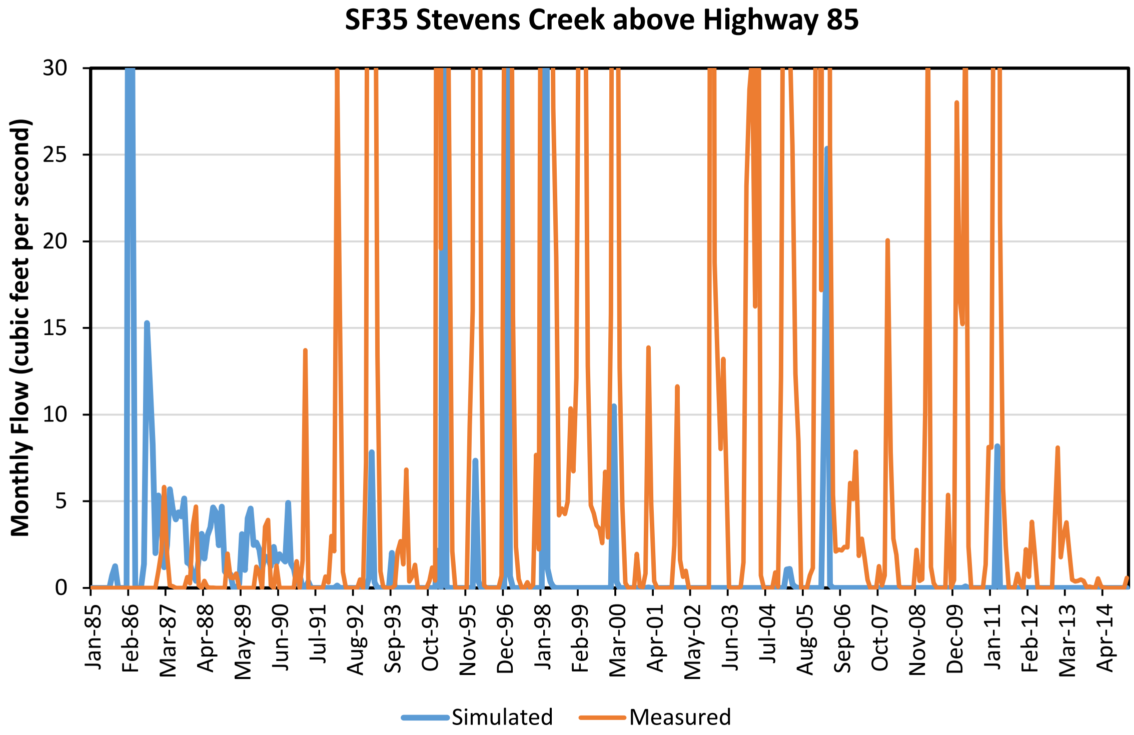

CFS - cubic feet per second

December 2017

TODD GROUNDWATER

Figure 4-16h
Simulated and Measured Streamflow Hydrographs

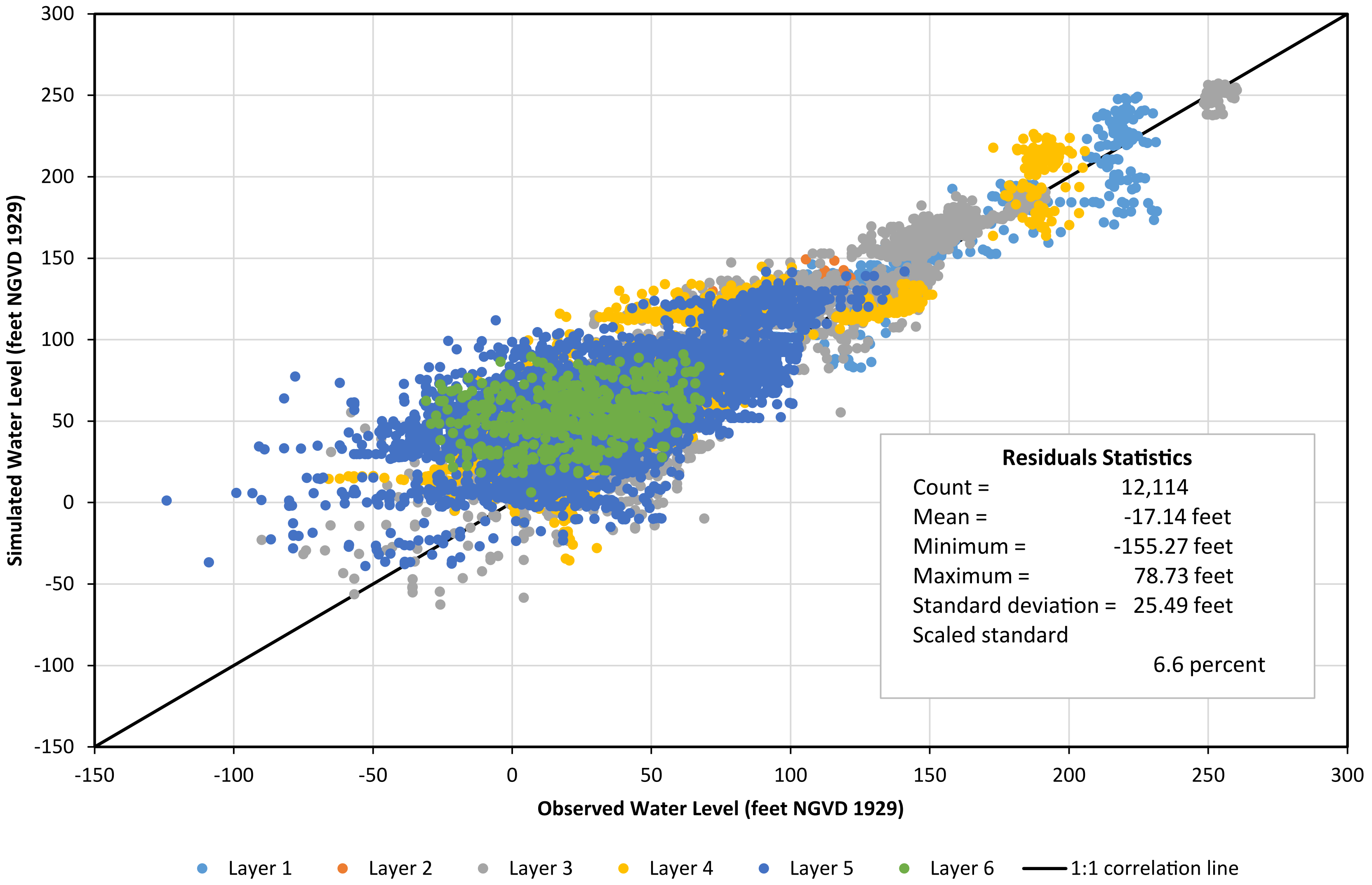

Residuals Statistics

Count =	12,114
Mean =	-17.14 feet
Minimum =	-155.27 feet
Maximum =	78.73 feet
Standard deviation =	25.49 feet
Scaled standard	6.6 percent

NGVD - National Geodetic Vertical Datum

December 2017

TODD GROUNDWATER

Figure 4-17
Scatterplot of Water Level Residuals

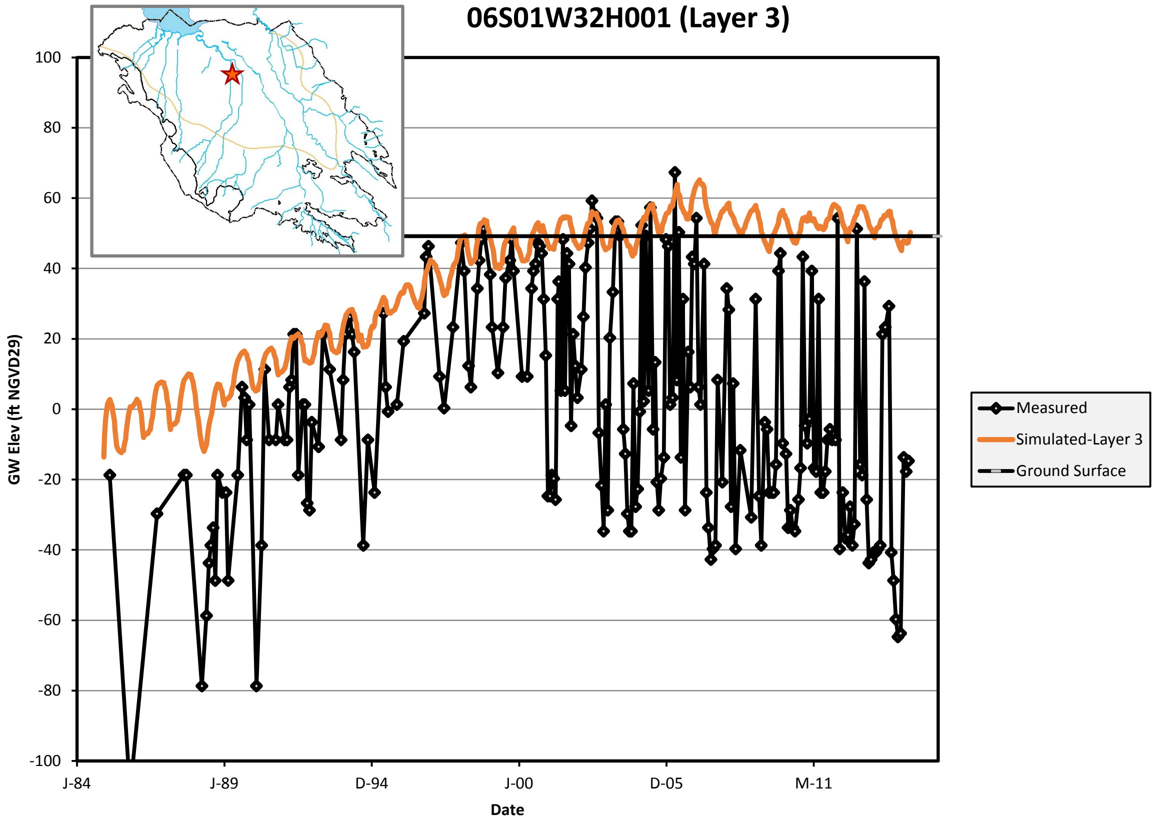

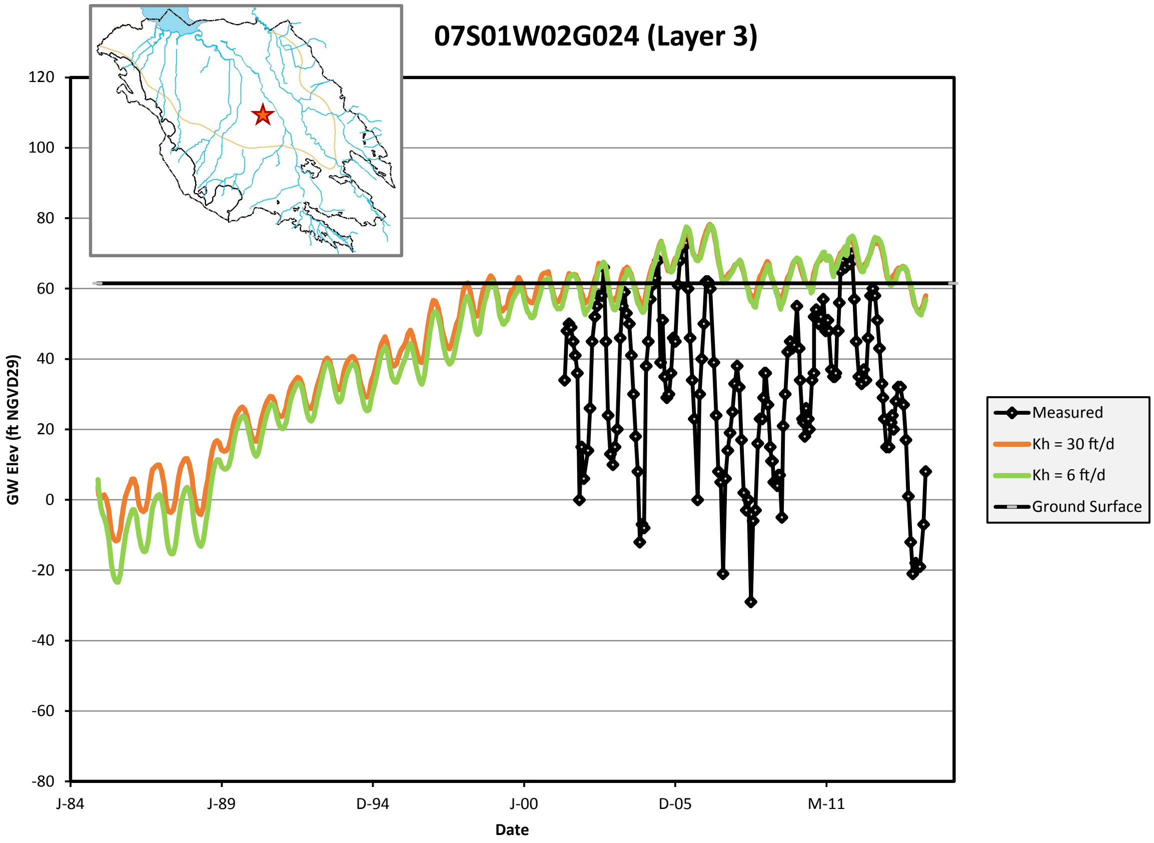

December 2017

TODD GROUNDWATER

Figure 4-18a
Sensitivity Test of the Central Low-Kh Zone

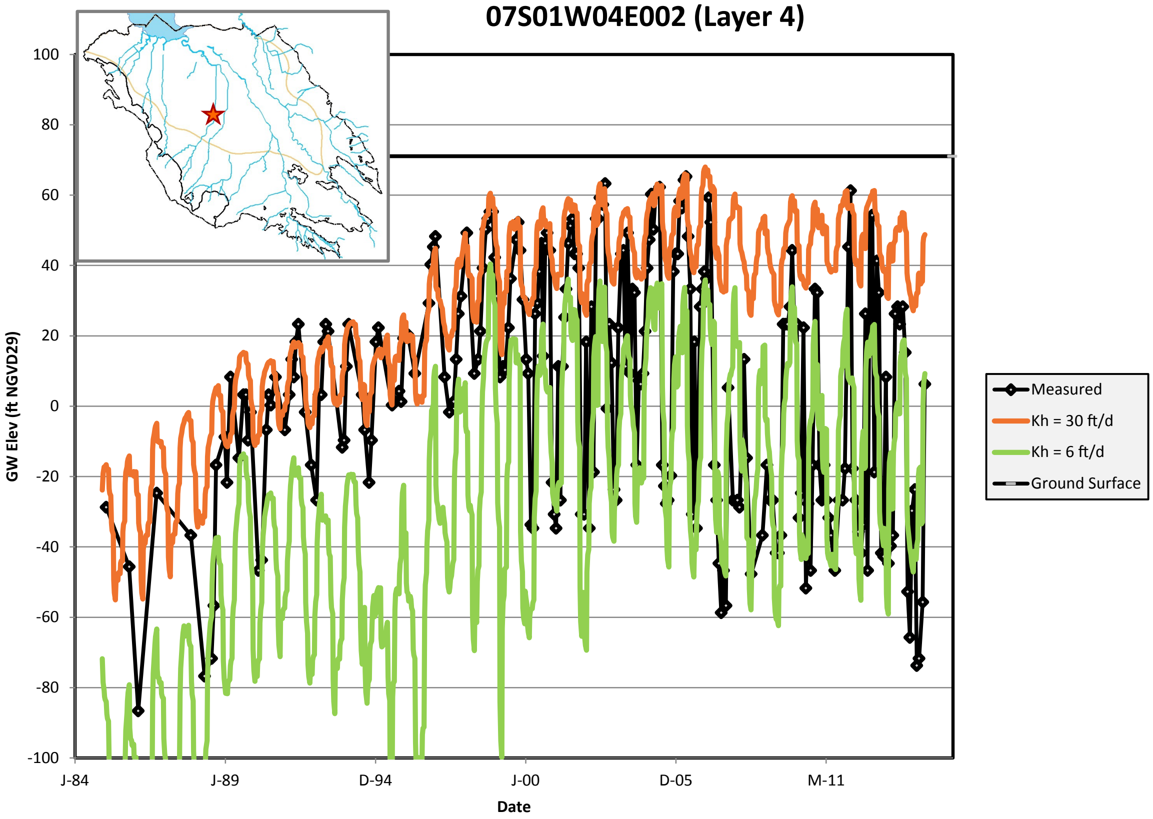

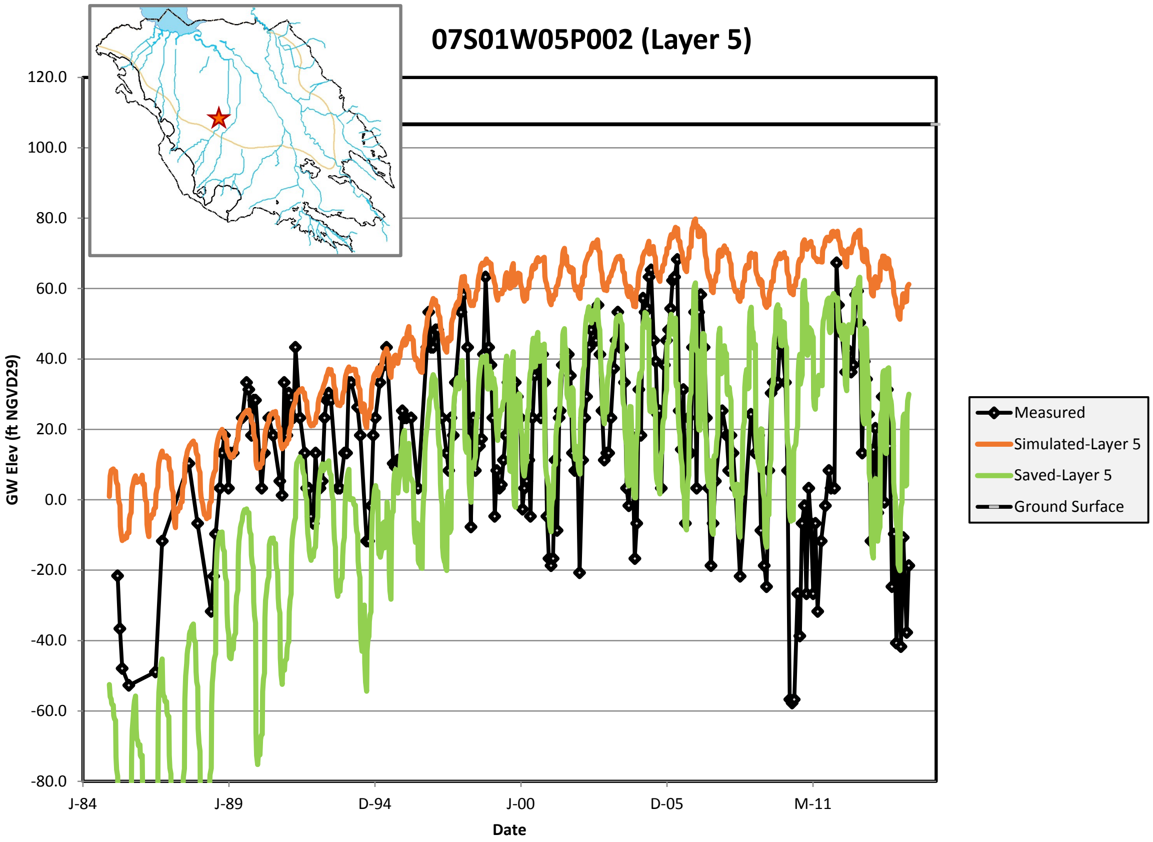

December 2017

TODD GROUNDWATER

Figure 4-18b
Sensitivity Test of the Central Low-Kh Zone

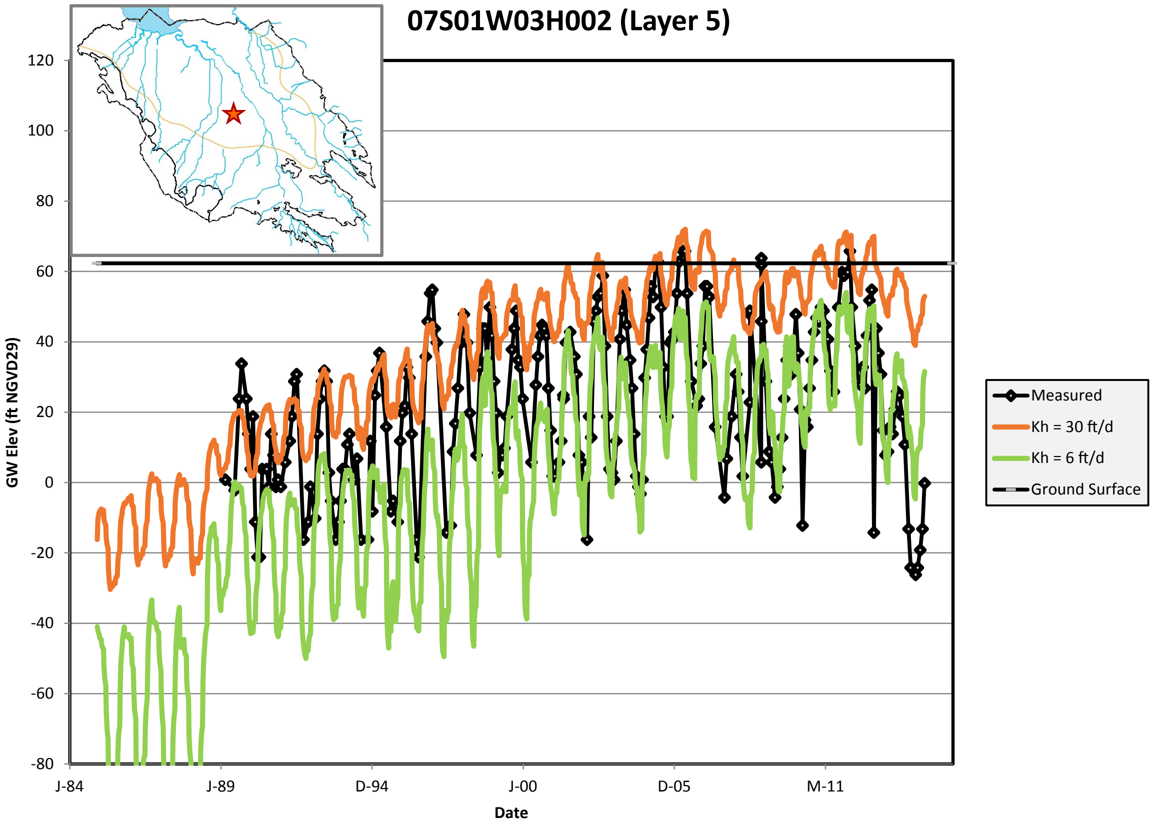

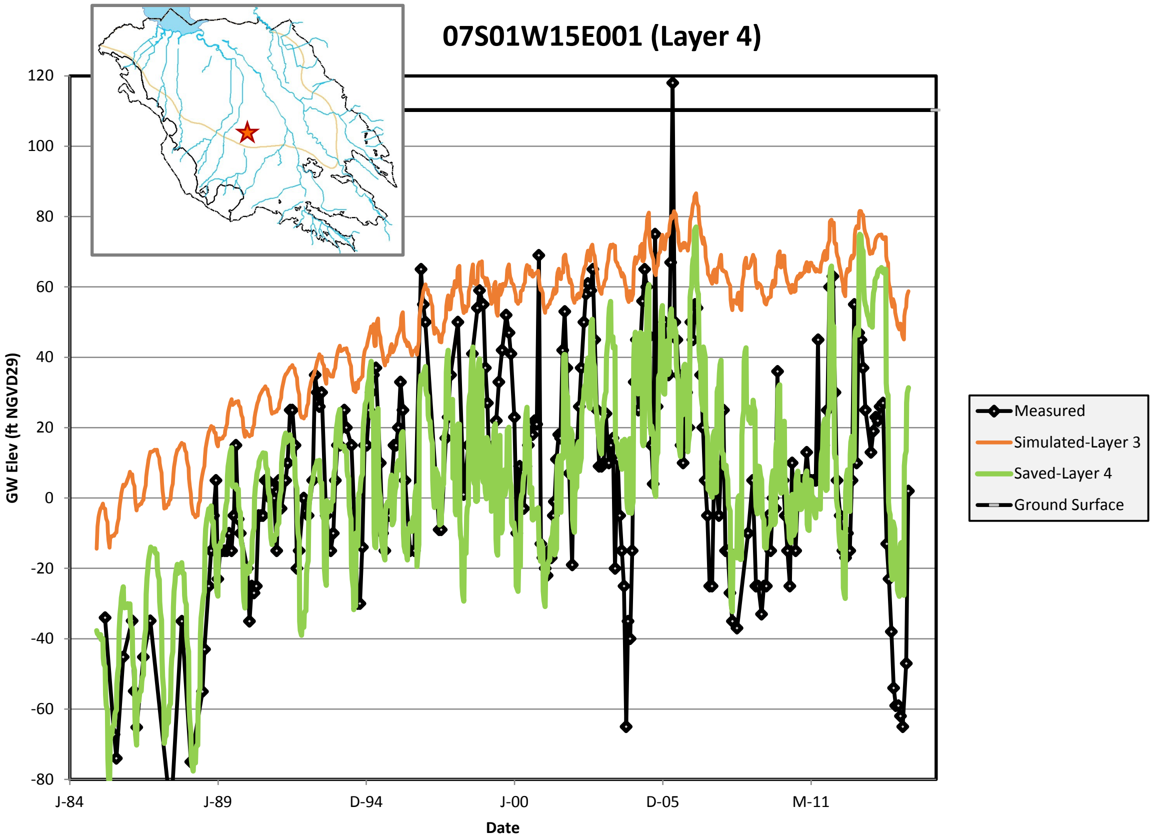

December 2017

TODD GROUNDWATER

Figure 4-18c
Sensitivity Test of the Central Low-Kh Zone

07S01W09Q001 (Layer 3)

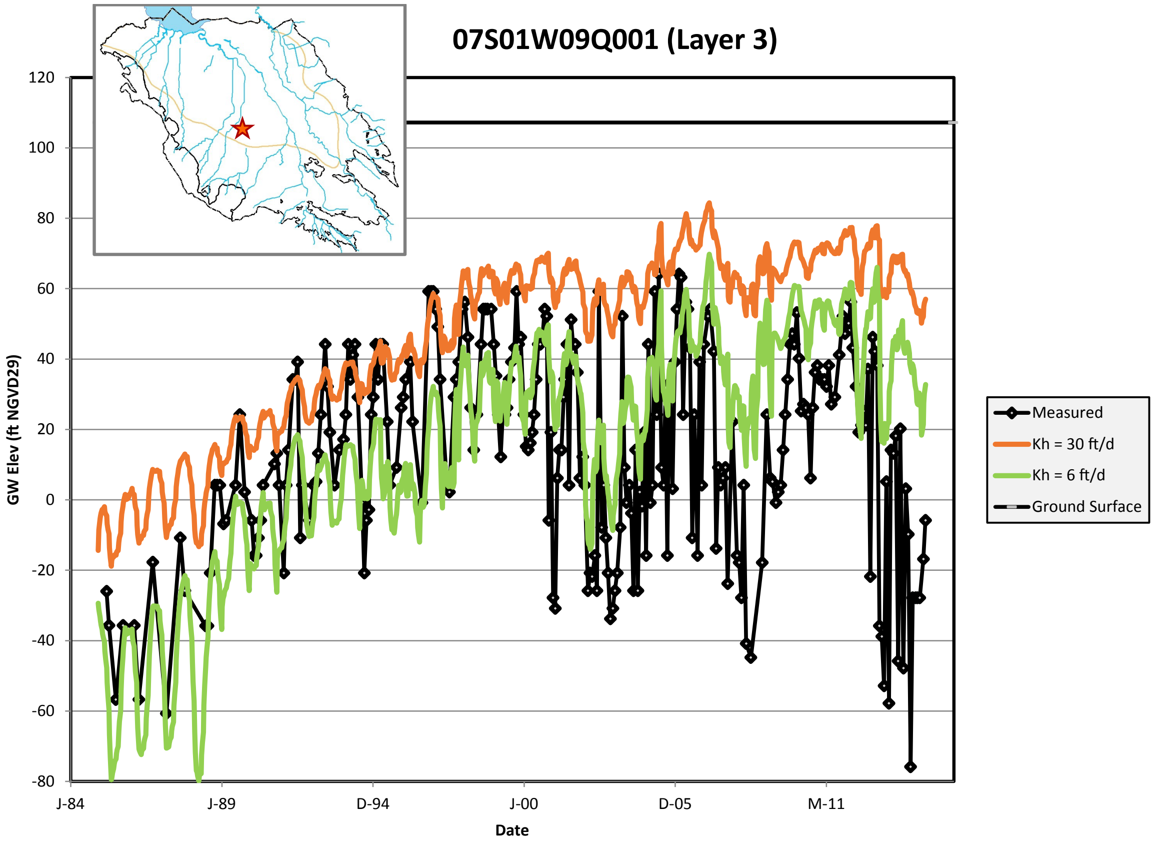

07S01W11D002 (Layer 5)

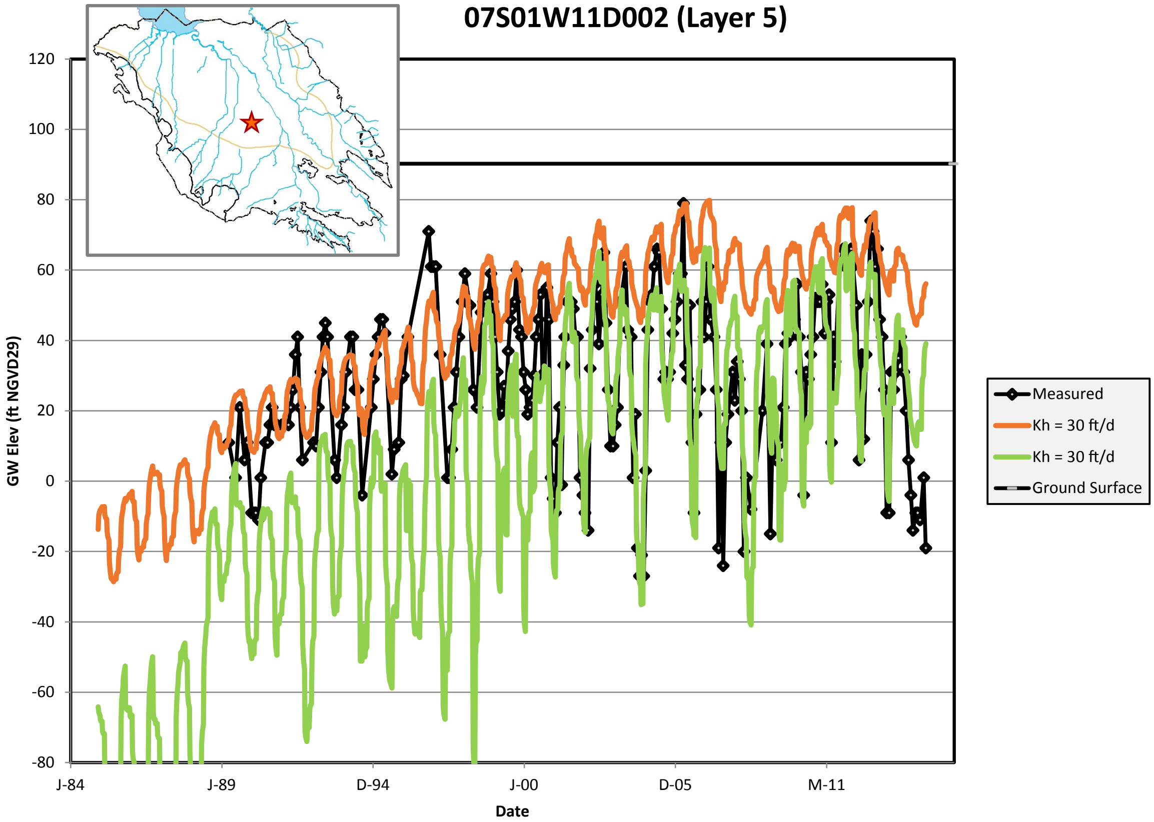

December 2017

TODD GROUNDWATER

Figure 4-18d
Sensitivity Test of the Central Low-Kh Zone

Sheets

Parallel 1

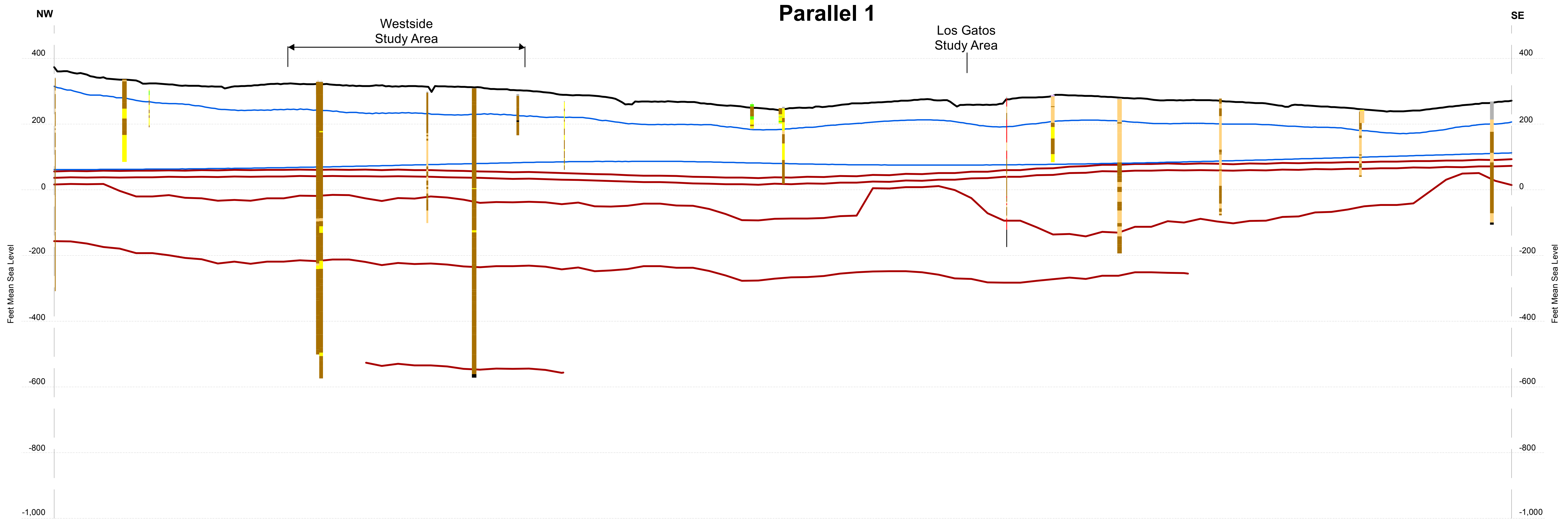

Parallel 2

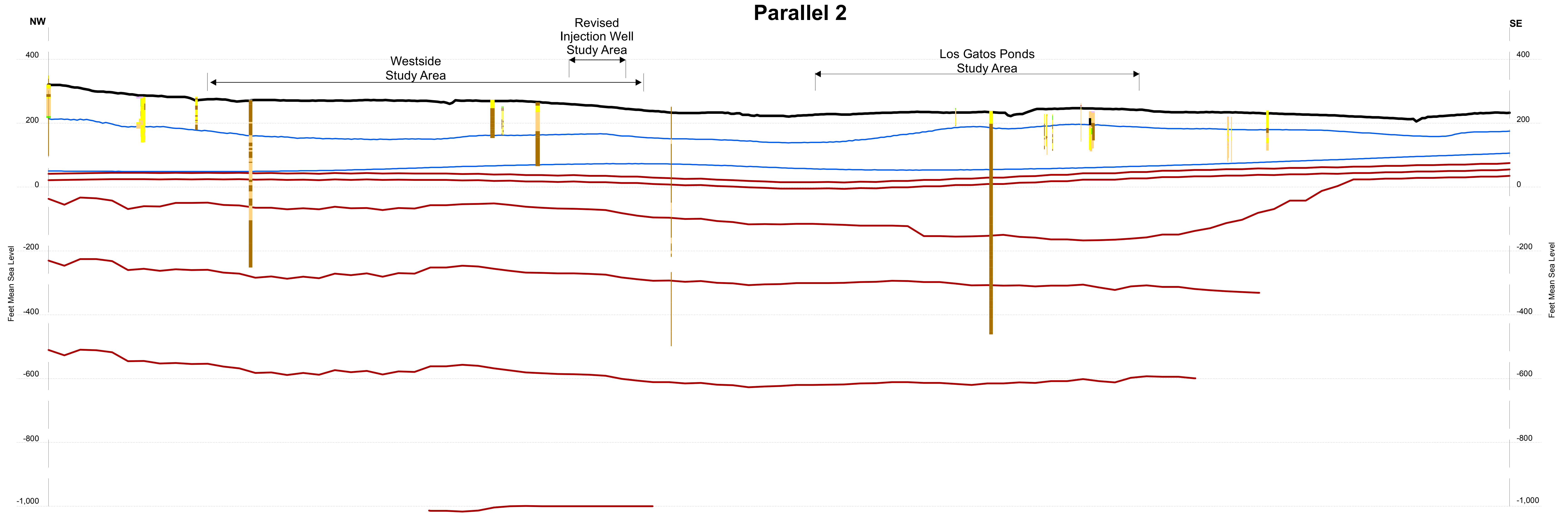

Parallel 3

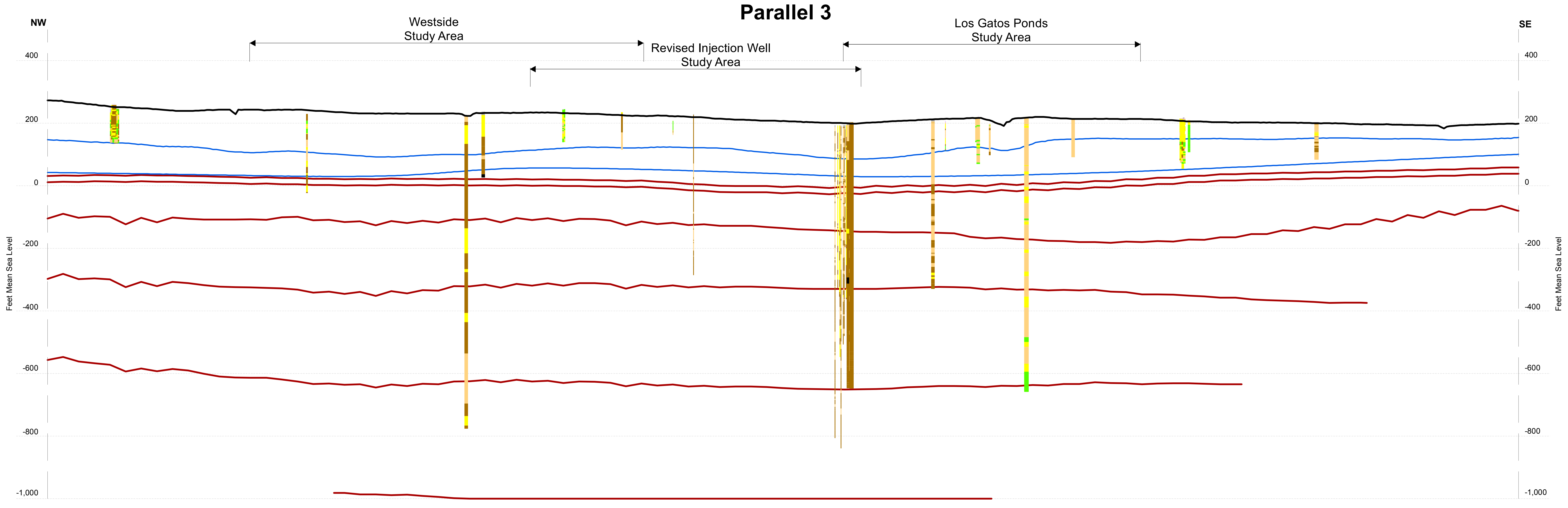

Parallel 4

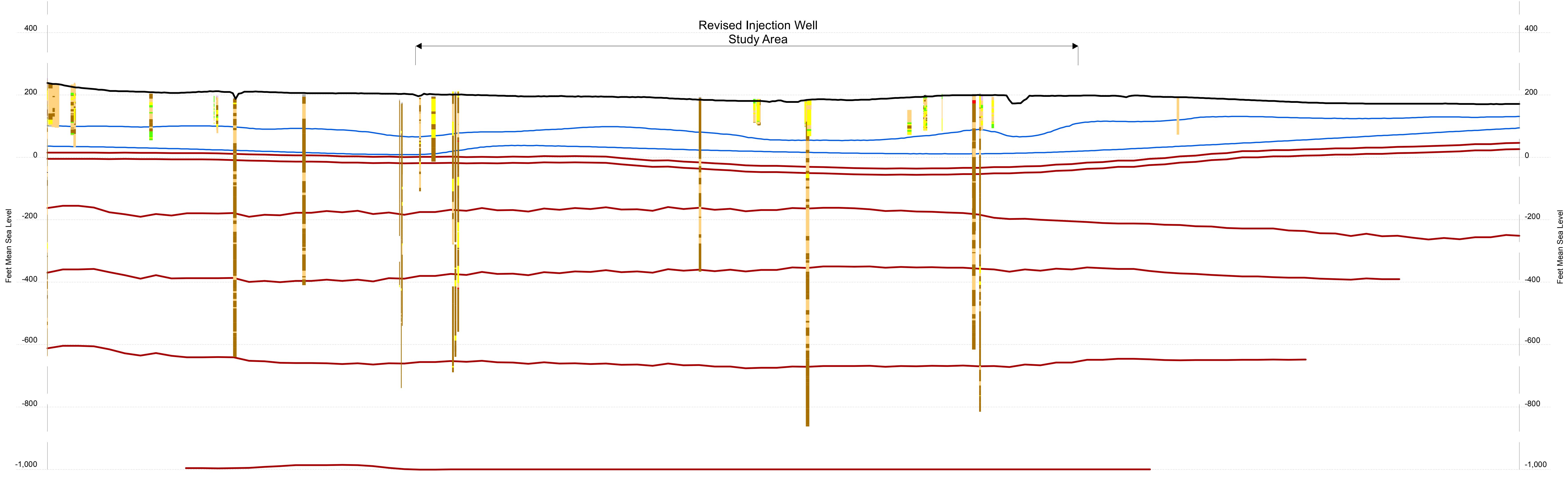

— Ground Surface
— High (1989) and Low (2012) Groundwater Elevations
— IMOD Model Layers

Lithology
- ▬ Topsoil
- ▬ Fill
- ▬ Boulders / Cobbles
- ▬ Gravel
- ▬ Sand
- ▬ Silt
- ▬ Clay
- ▬ Bedrock

Note:
The thickness of the lithology lines for wells and boreholes is a function of the distance of the point from the section line. The closer the point, the wider the line is shown on the section.

Wells and boreholes may start above or below ground surface in the section as a result of being projected onto the section line.

0 1,000 2,000
Scale in Feet
10 X Vertical Exaggeration

December 2017

TODD GROUNDWATER

Sheet 2-1
Sections
Parallel 1
through Parallel 4

Parallel 5

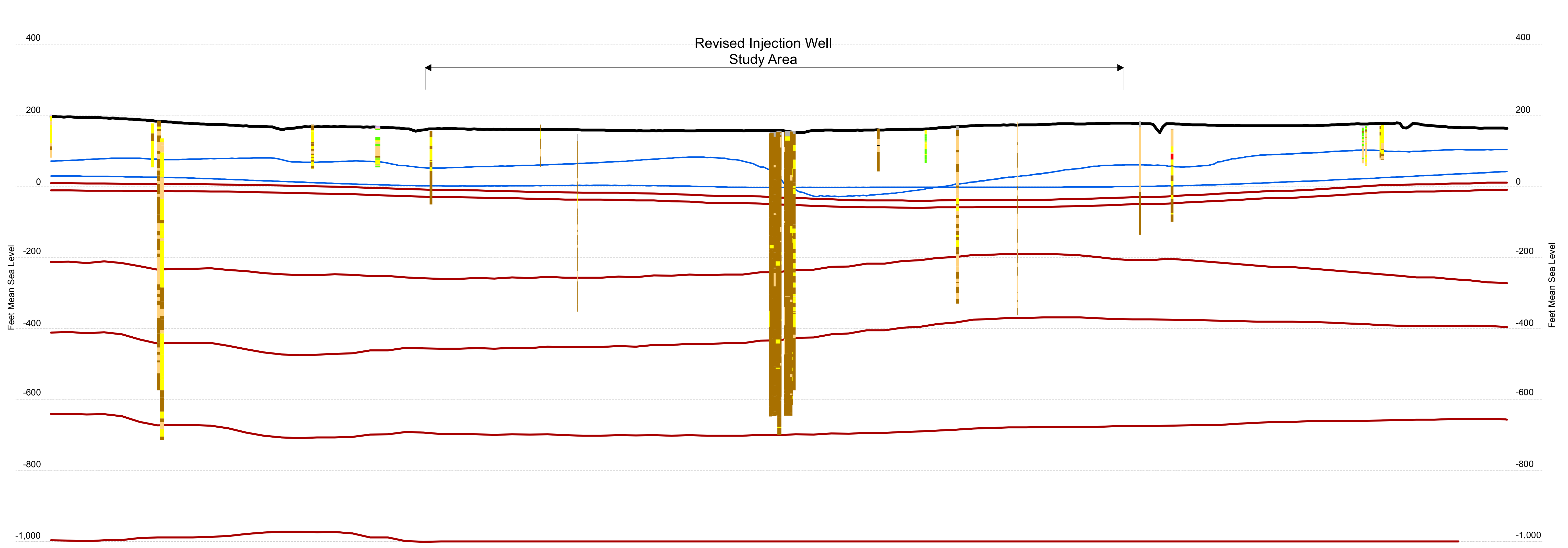

Parallel 6

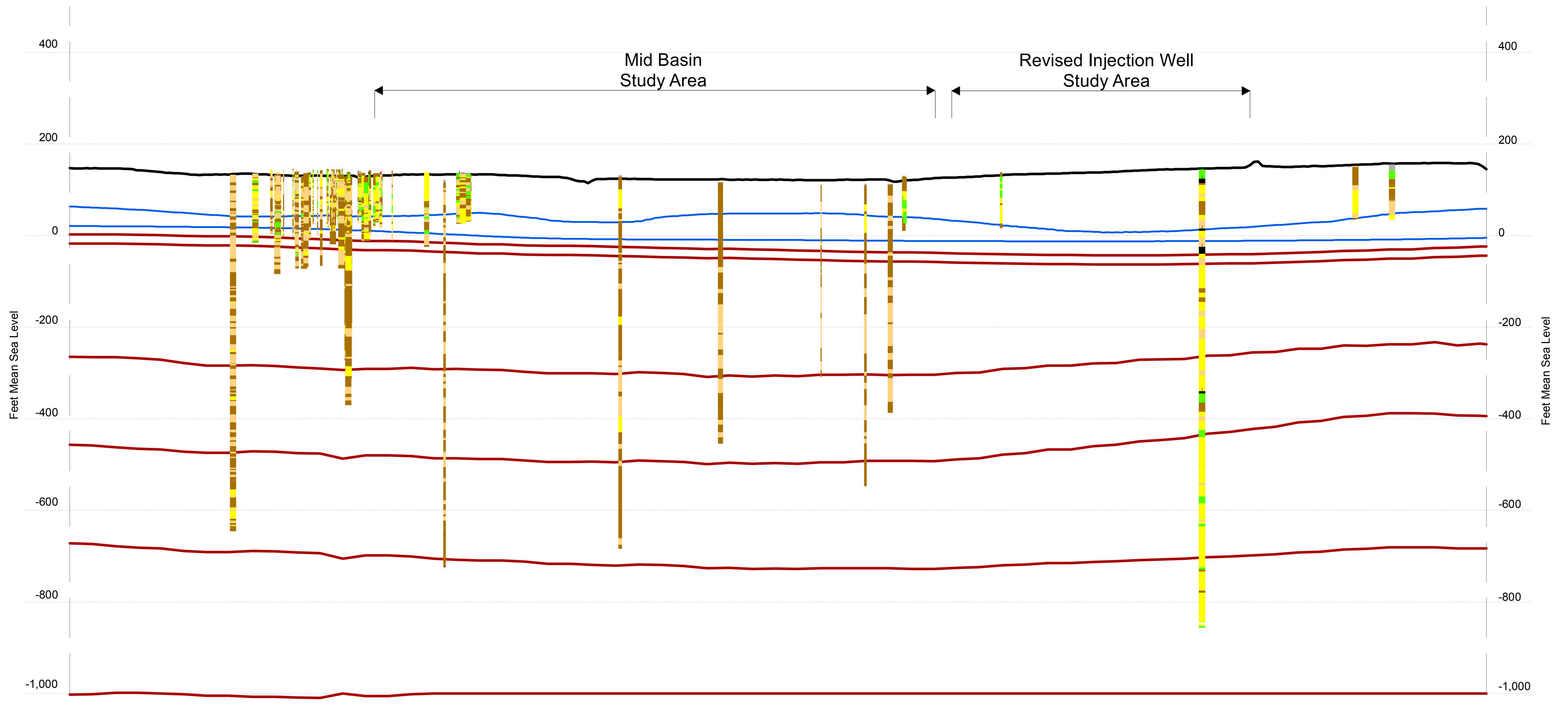

Parallel 7

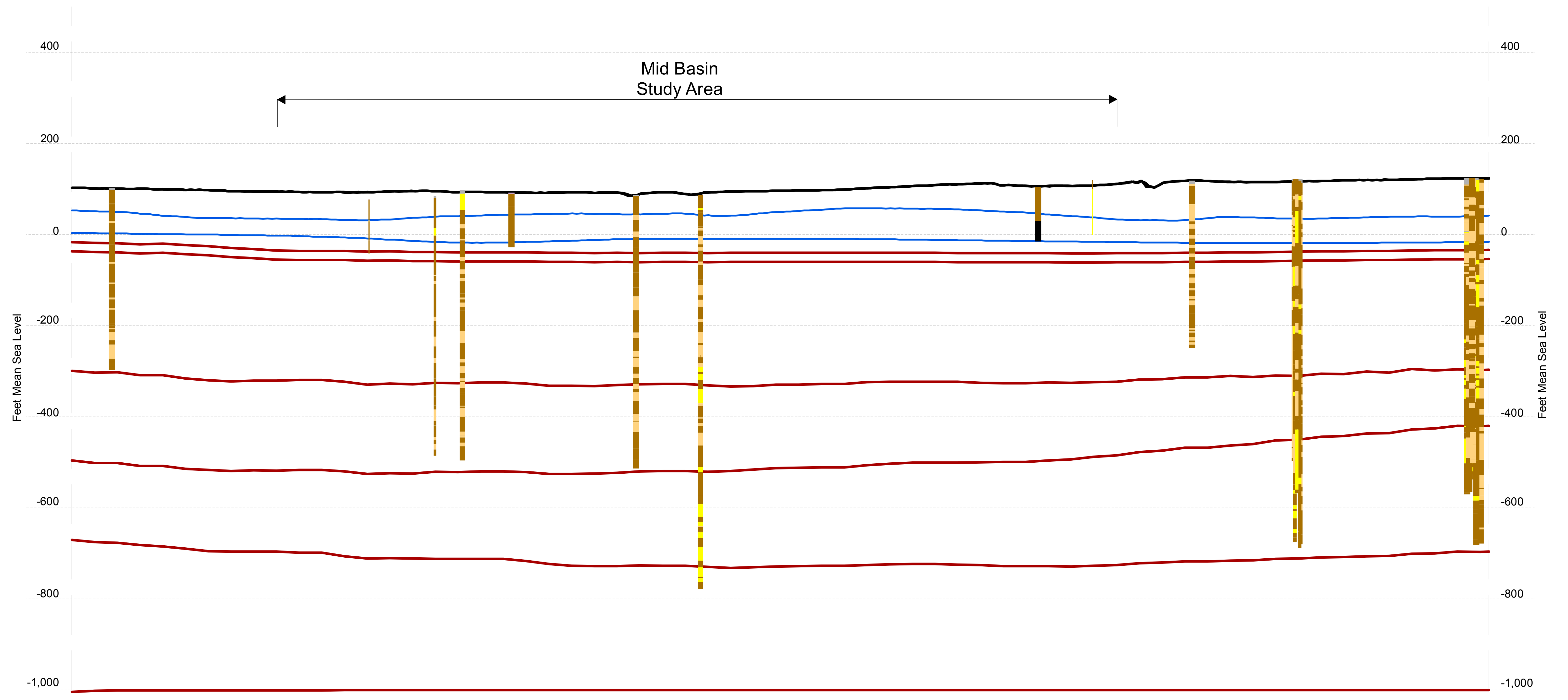

Parallel 8

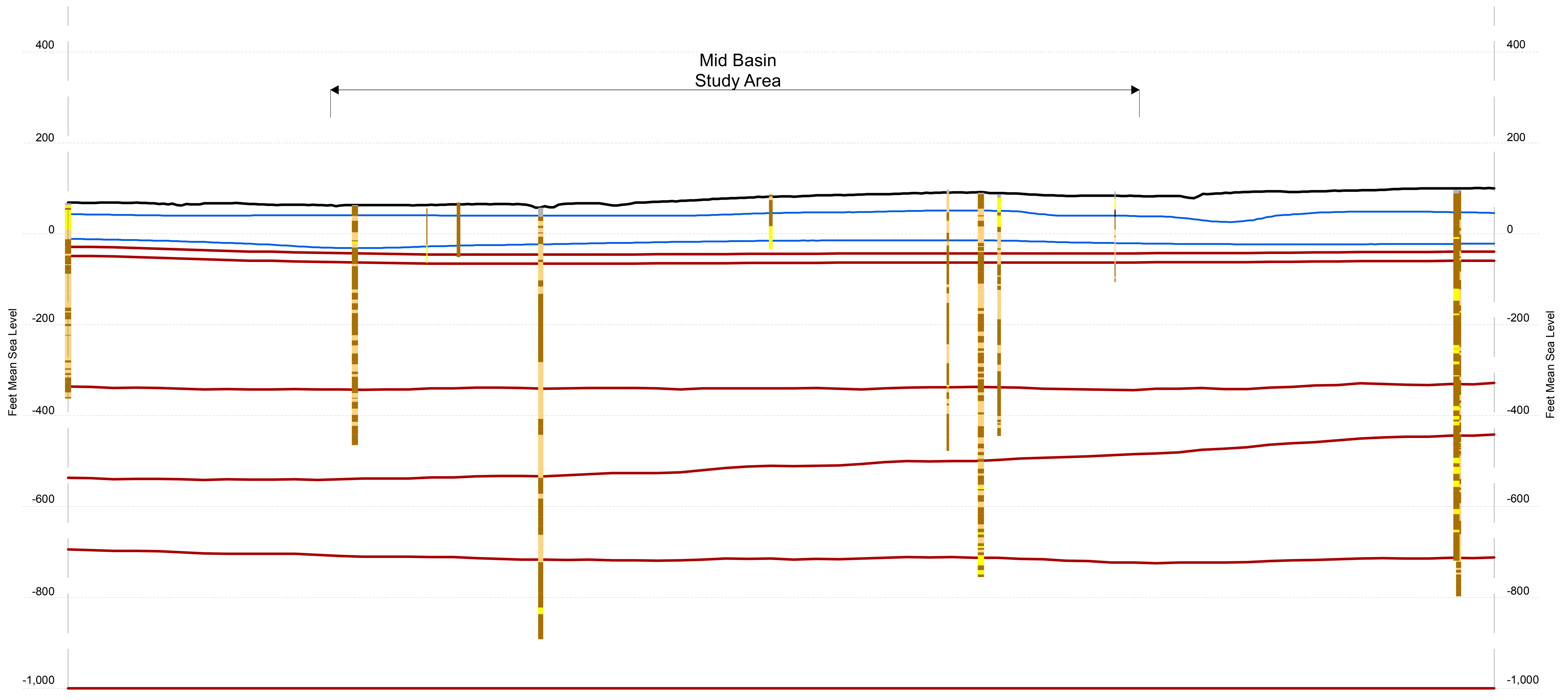

- Ground Surface
- High (1989) and Low (2012) Groundwater Elevations
- IMOD Model Layers

Lithology

- Topsoil
- Fill
- Boulders / Cobbles
- Gravel
- Sand
- Silt
- Clay
- Bedrock

Note:
The thickness of the lithology lines for wells and boreholes is a function of the distance of the point from the section line. The closer the point, the wider the line is shown on the section.

Wells and boreholes may start above or below ground surface in the section as a result of being projected onto the section line.

0 1,000 2,000
Scale in Feet

10 X Vertical Exaggeration

December 2017

TODD
GROUNDWATER

Sheet 2-2
Sections
Parallel 5
through Parallel 8

Path: T:\Projects\SCVWD IPR 37809\GIS\Maps\Figures\Conceptual Model Figures\Sheet 2-2 Sections Parallel 5 - 8.mxd

Parallel 9

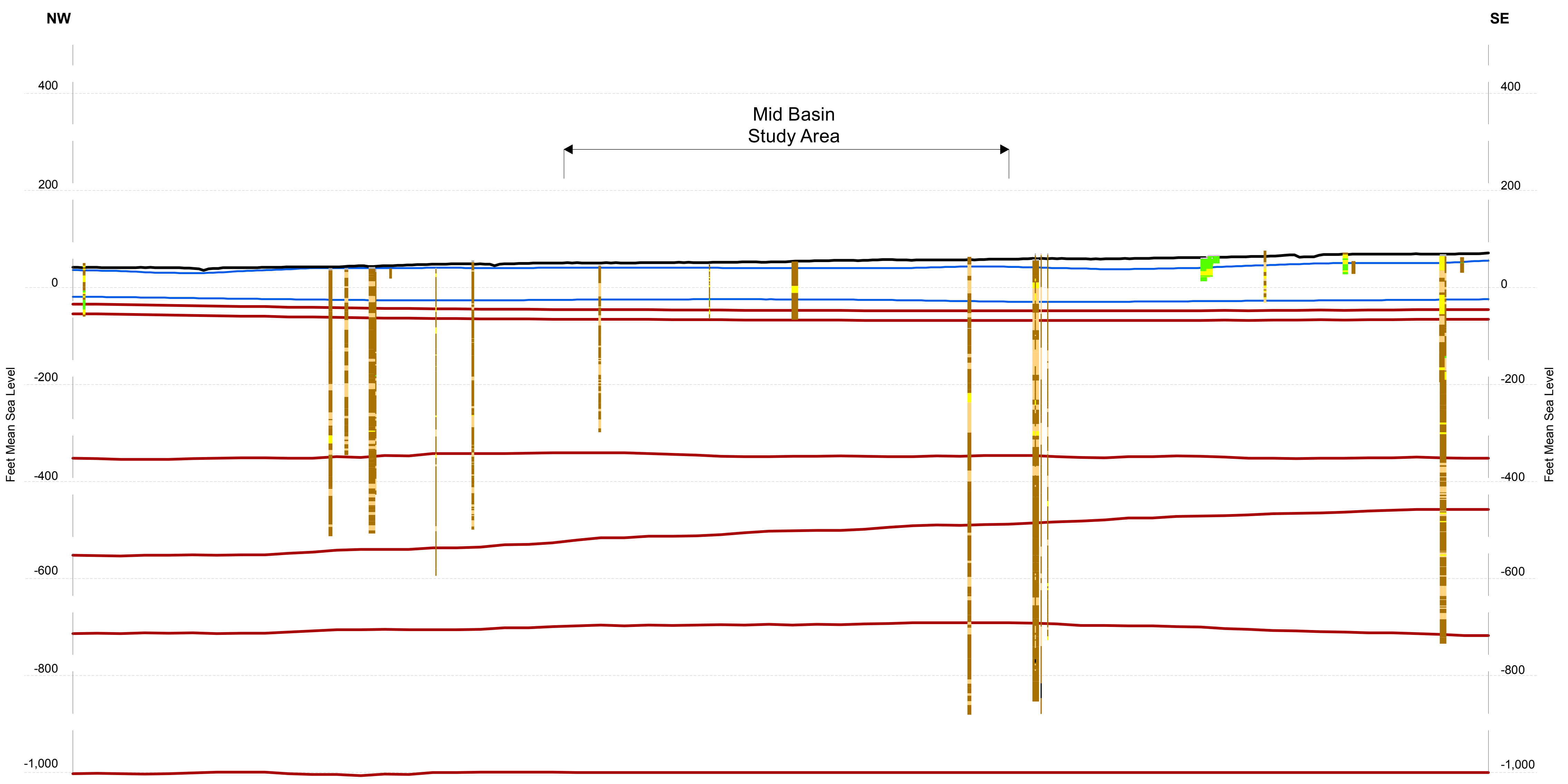

Parallel 10

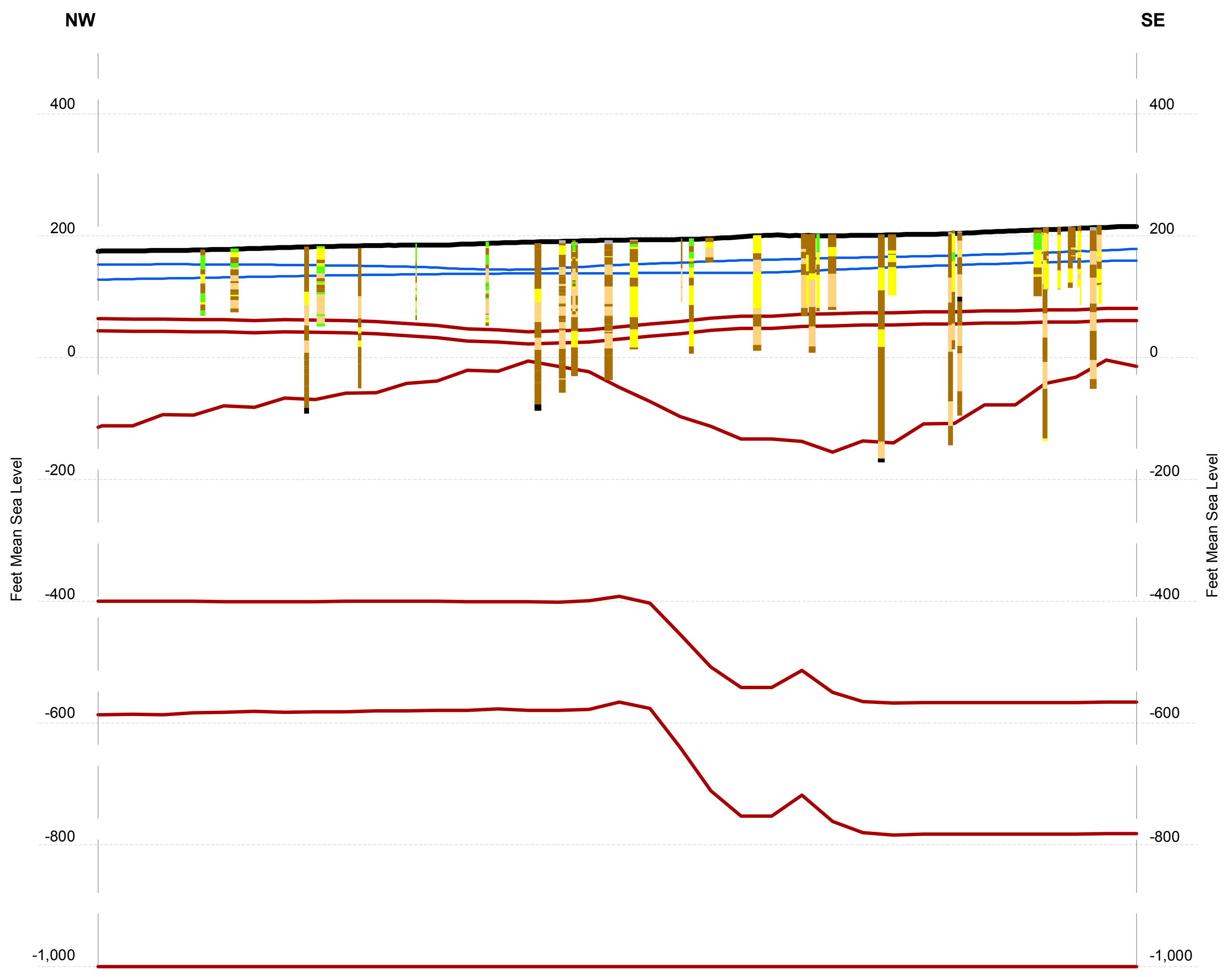

Parallel 11

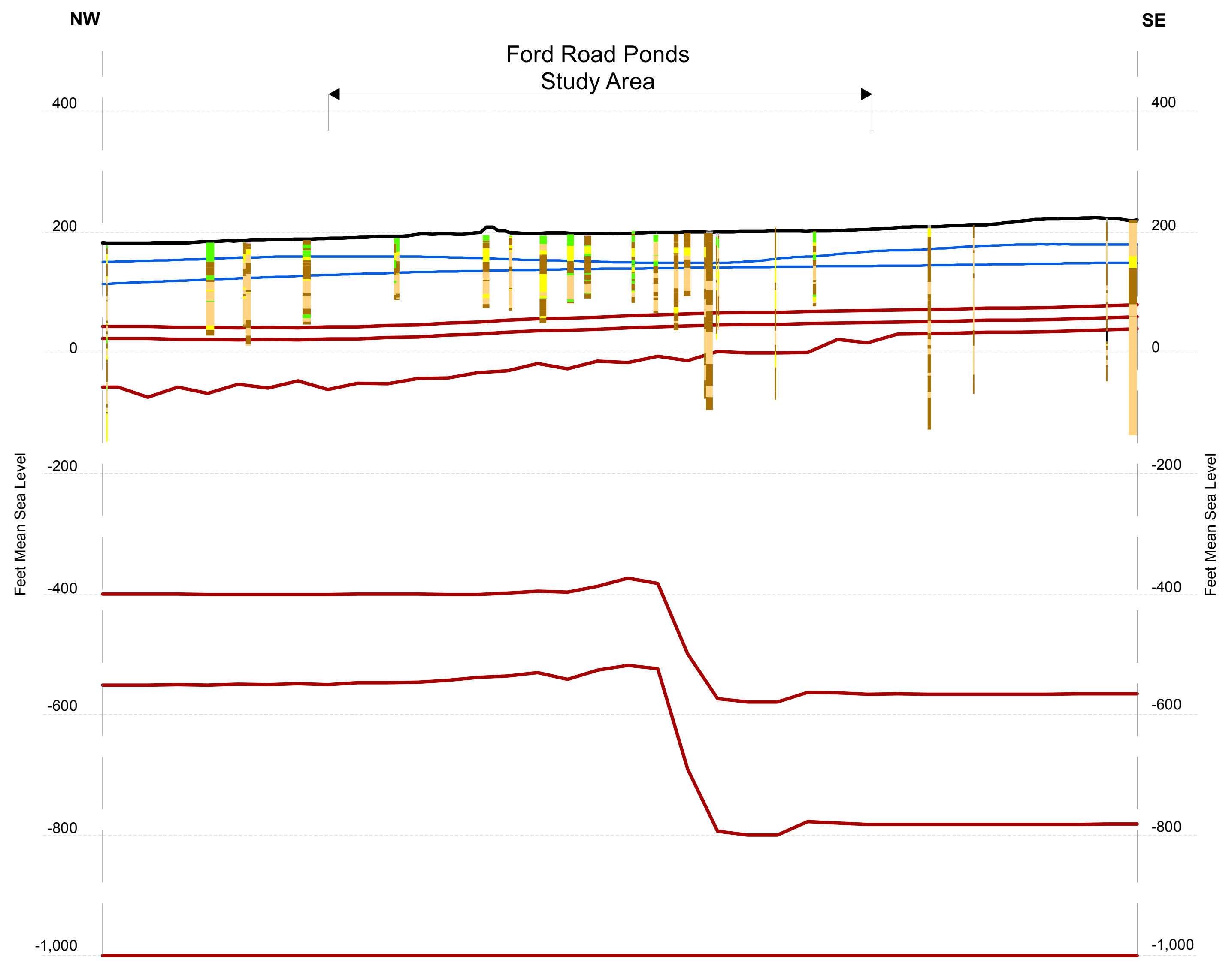

Parallel 12

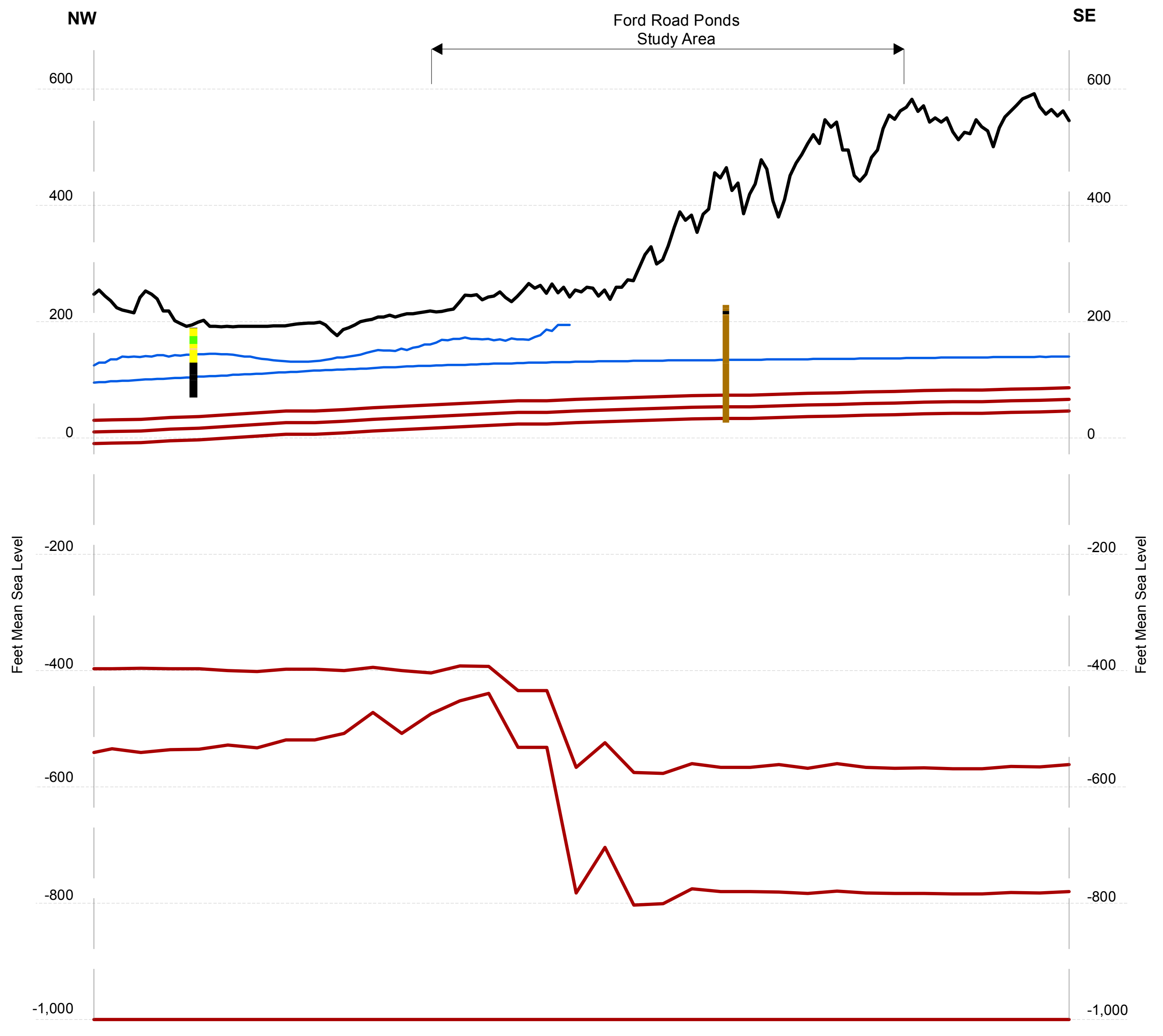

— Ground Surface
— High (1989) and Low (2012) Groundwater Elevations
— IMOD Model Layers

Lithology

- ▬ Topsoil
- ▬ Fill
- ▬ Boulders / Cobbles
- ▬ Gravel
- ▬ Sand
- ▬ Silt
- ▬ Clay
- ▬ Bedrock

Note:
The thickness of the lithology lines for wells and boreholes is a function of the distance of the point from the section line. The closer the point, the wider the line is shown on the section.

Wells and boreholes may start above or below ground surface in the section as a result of being projected onto the section line.

0 1,000 2,000
Scale in Feet

10 X Vertical Exaggeration

December 2017

TODD GROUNDWATER

Sheet 2-3
Sections
Parallel 9
through Parallel 12

Cross 1

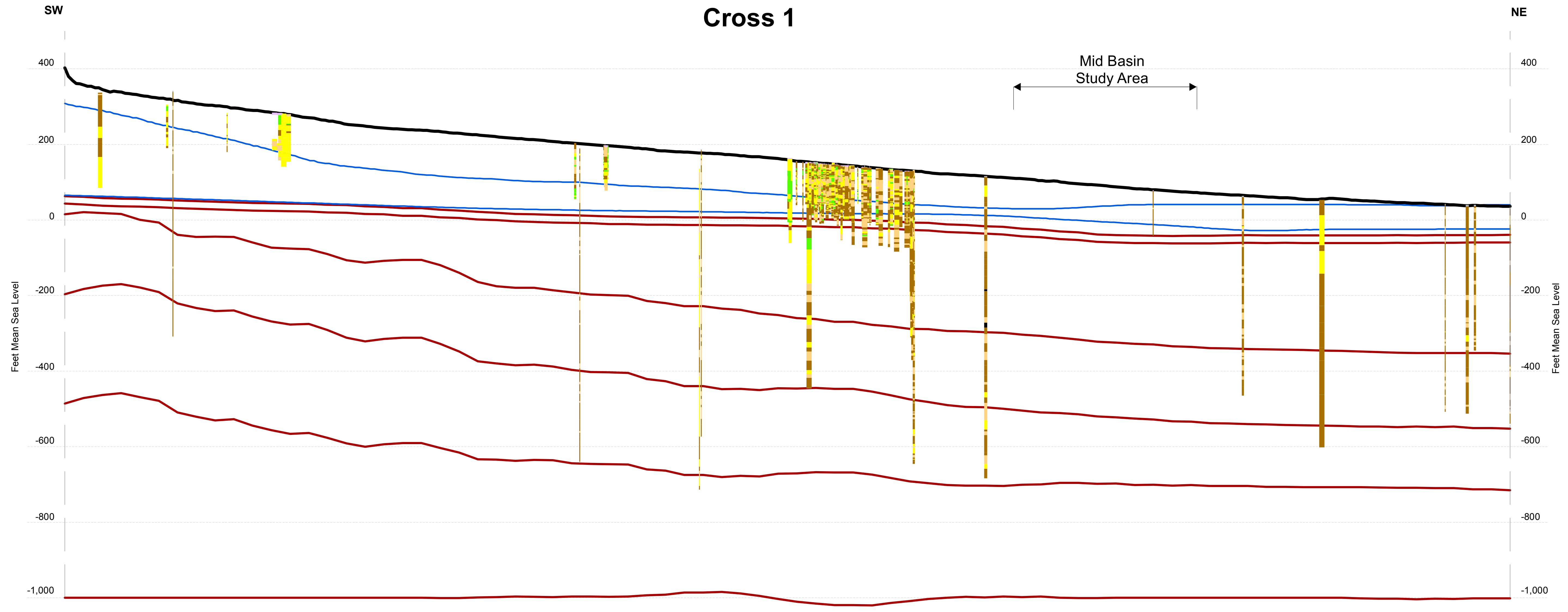

Cross 2

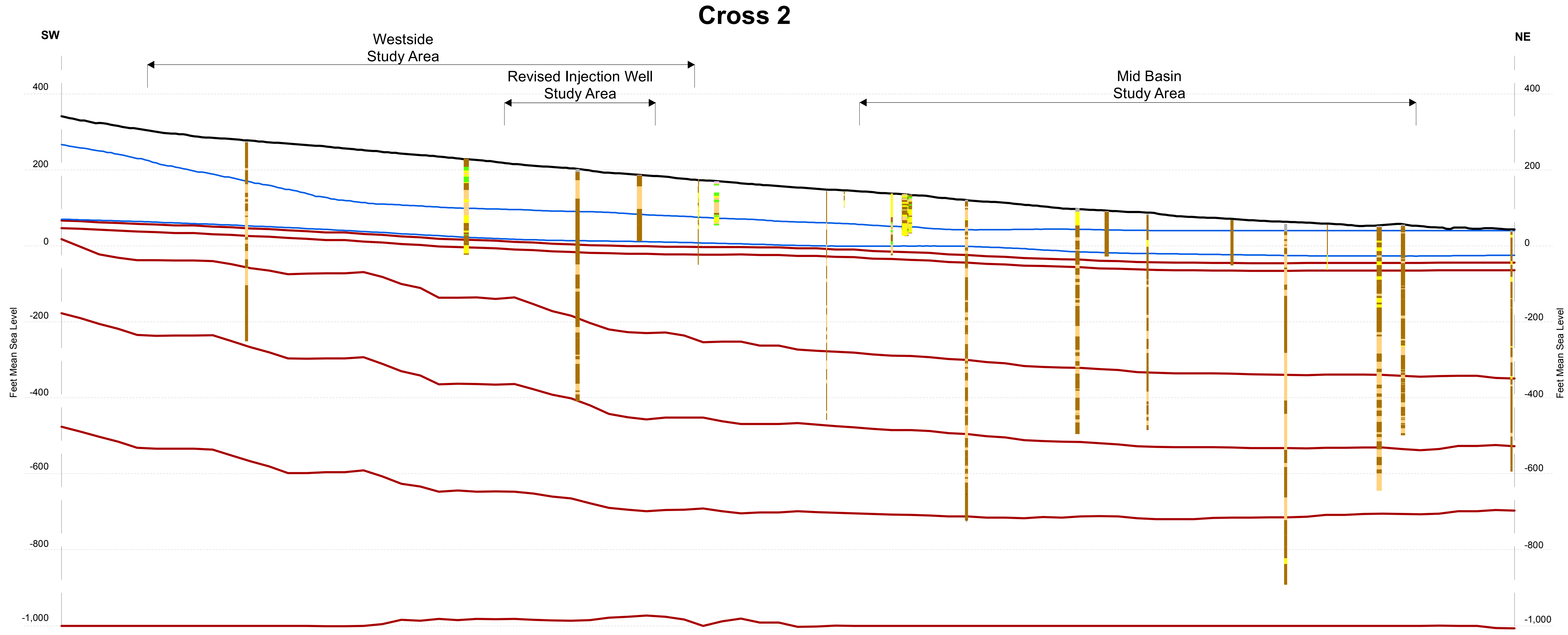

Cross 3

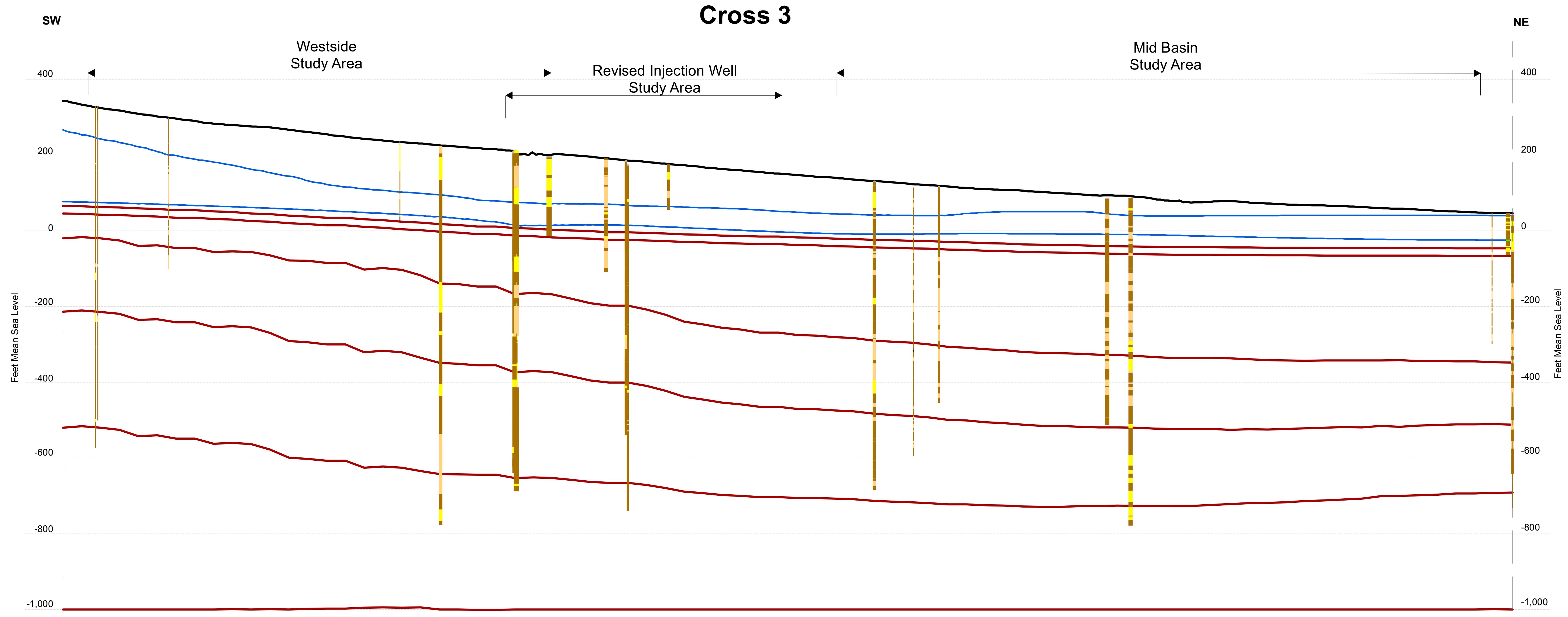

Cross 4

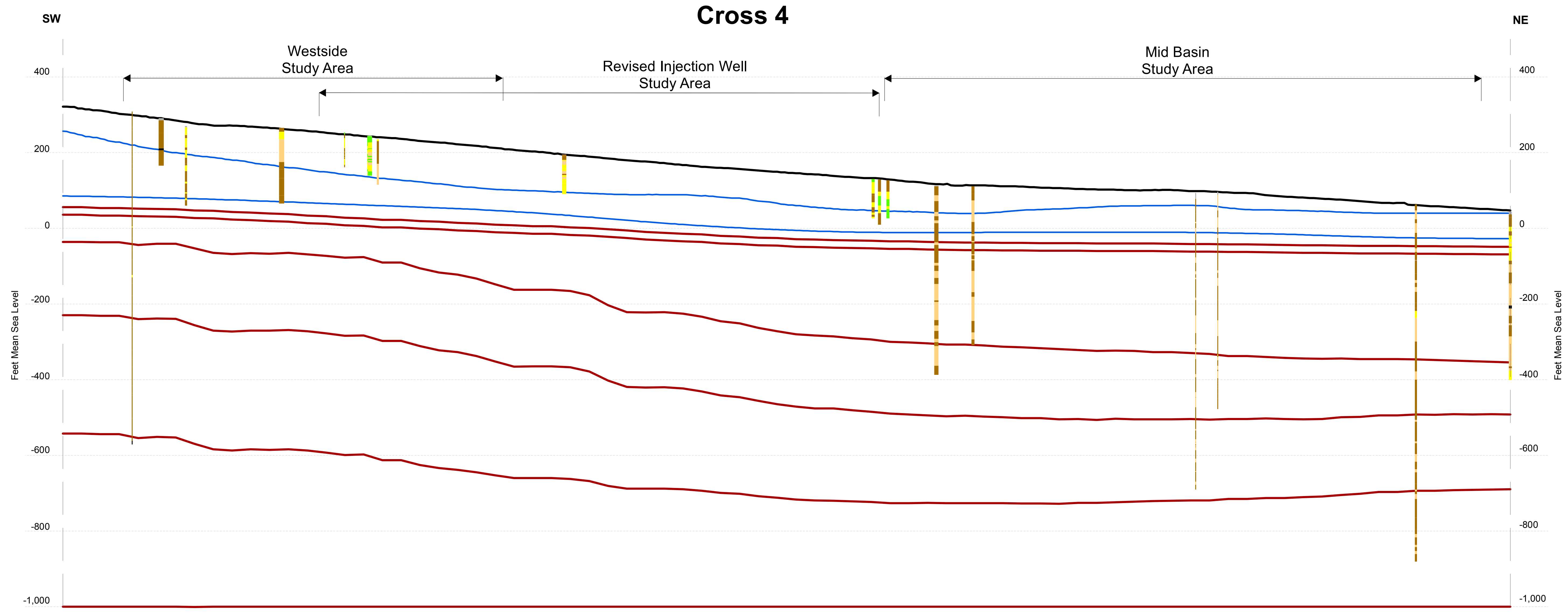

— Ground Surface
— High (1989) and Low (2012) Groundwater Elevations
— IMOD Model Layers

Lithology

- ▬ Topsoil
- ▬ Fill
- ▬ Boulders / Cobbles
- ▬ Gravel
- ▬ Sand
- ▬ Silt
- ▬ Clay
- ▬ Bedrock

Note:
The thickness of the lithology lines for wells and boreholes is a function of the distance of the point from the section line. The closer the point, the wider the line is shown on the section.

Wells and boreholes may start above or below ground surface in the section as a result of being projected onto the section line.

0 1,000 2,000
Scale in Feet

10 X Vertical Exaggeration

December 2017

TODD
GROUNDWATER

Sheet 2-4
Sections
Cross 1
through Cross 4

Cross 5

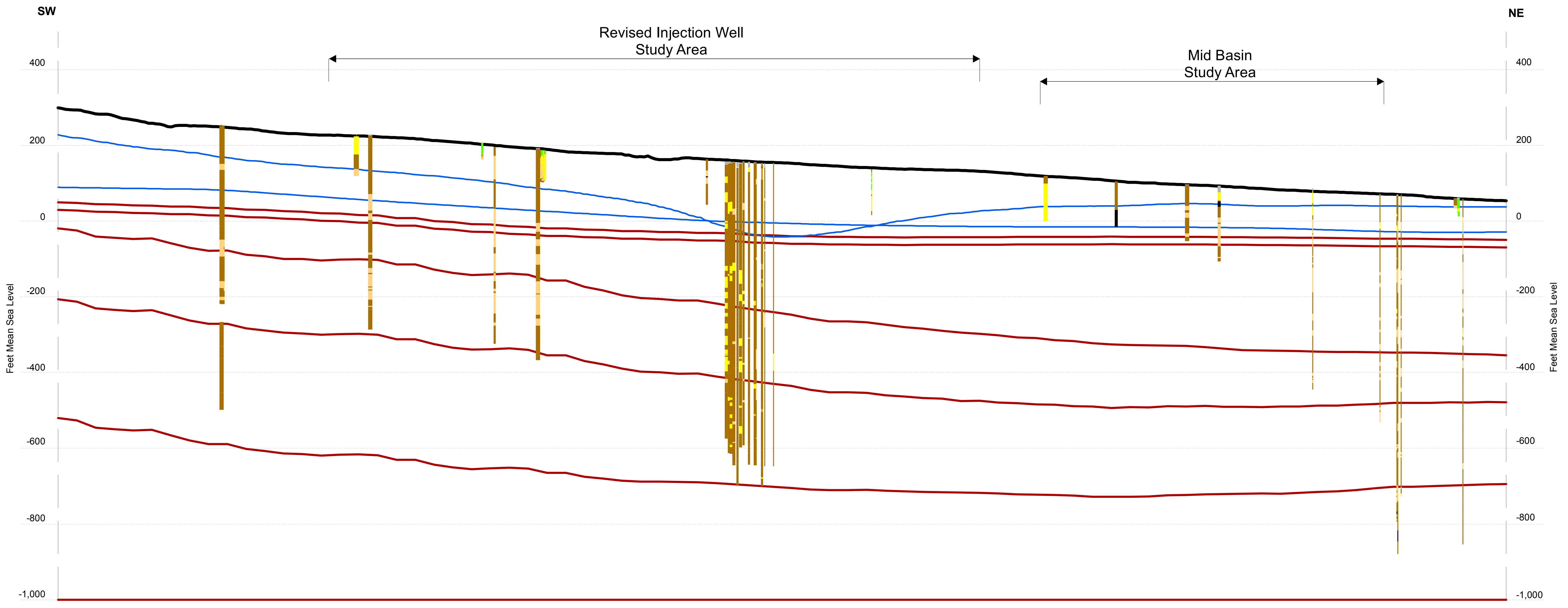

Cross 6

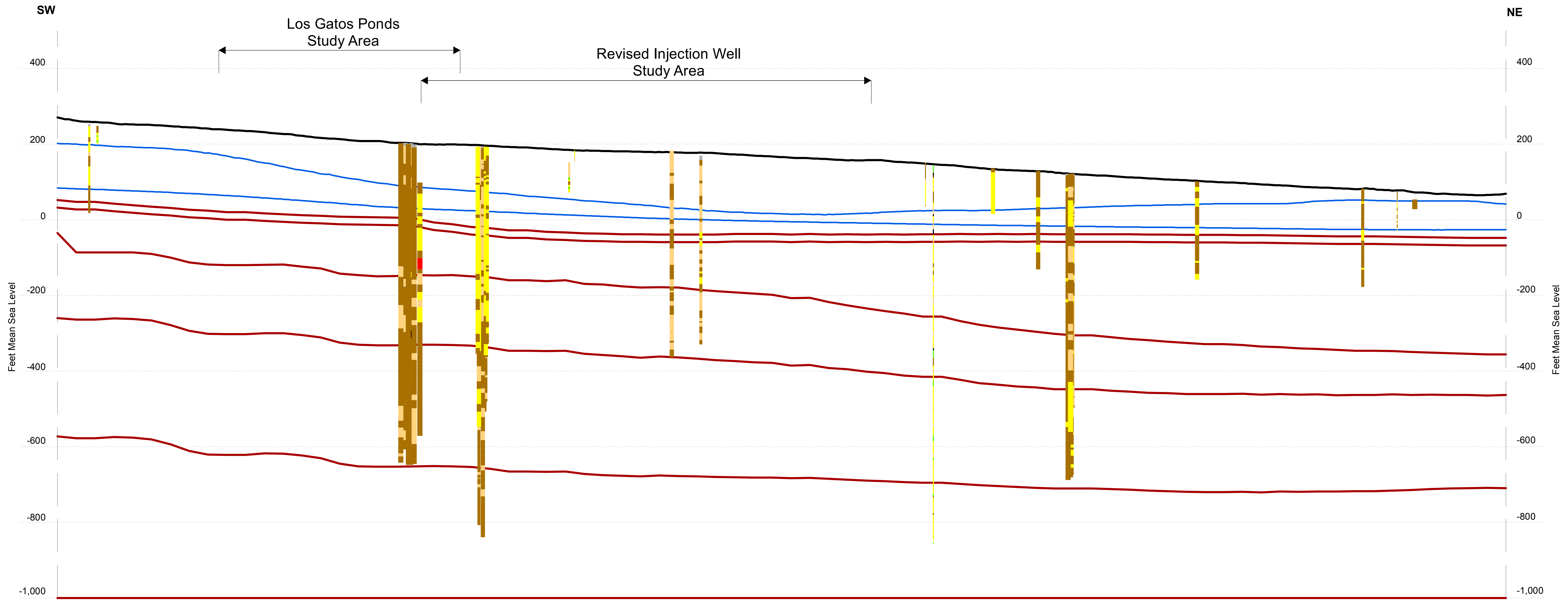

Cross 7

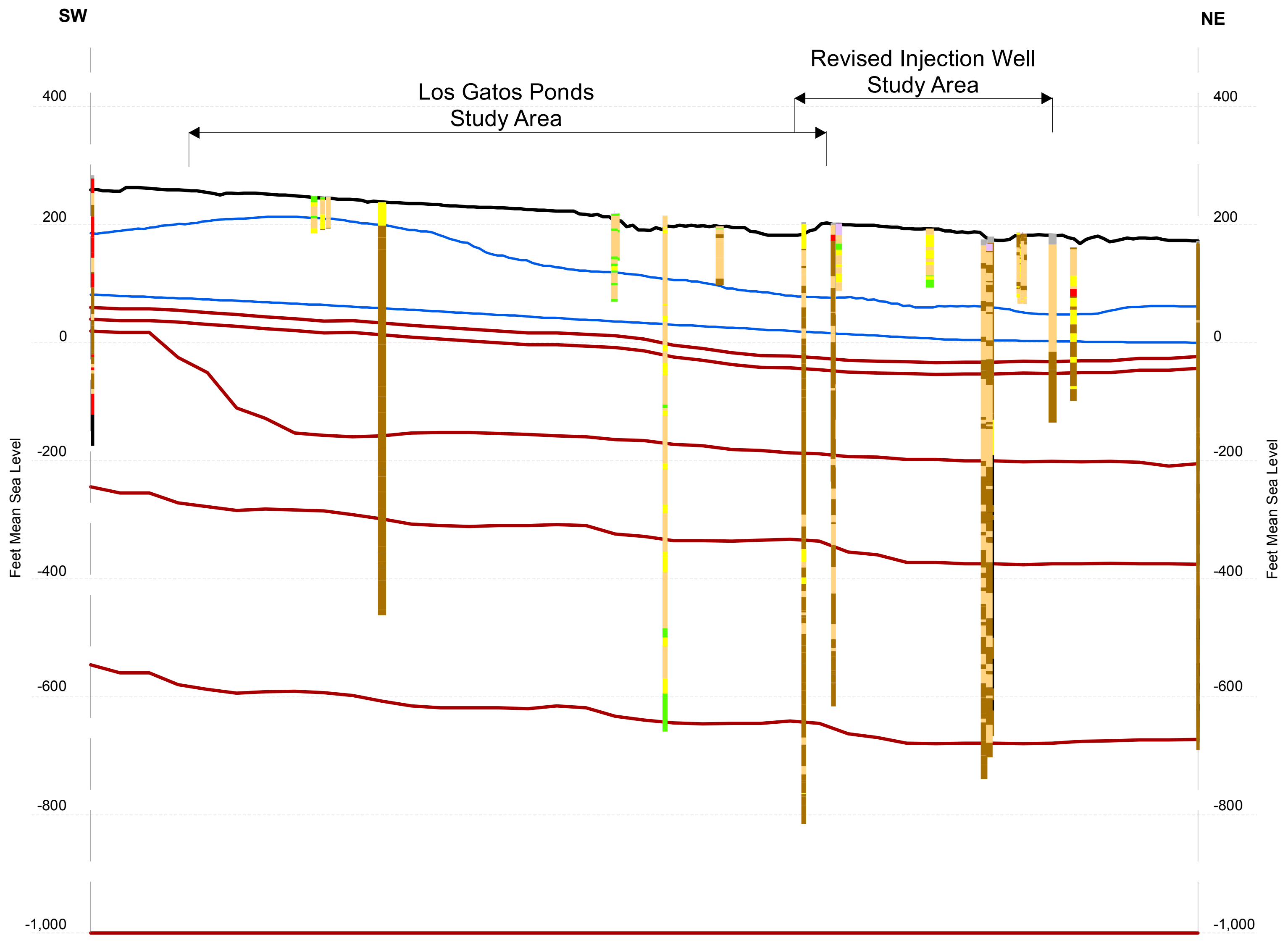

Cross 8

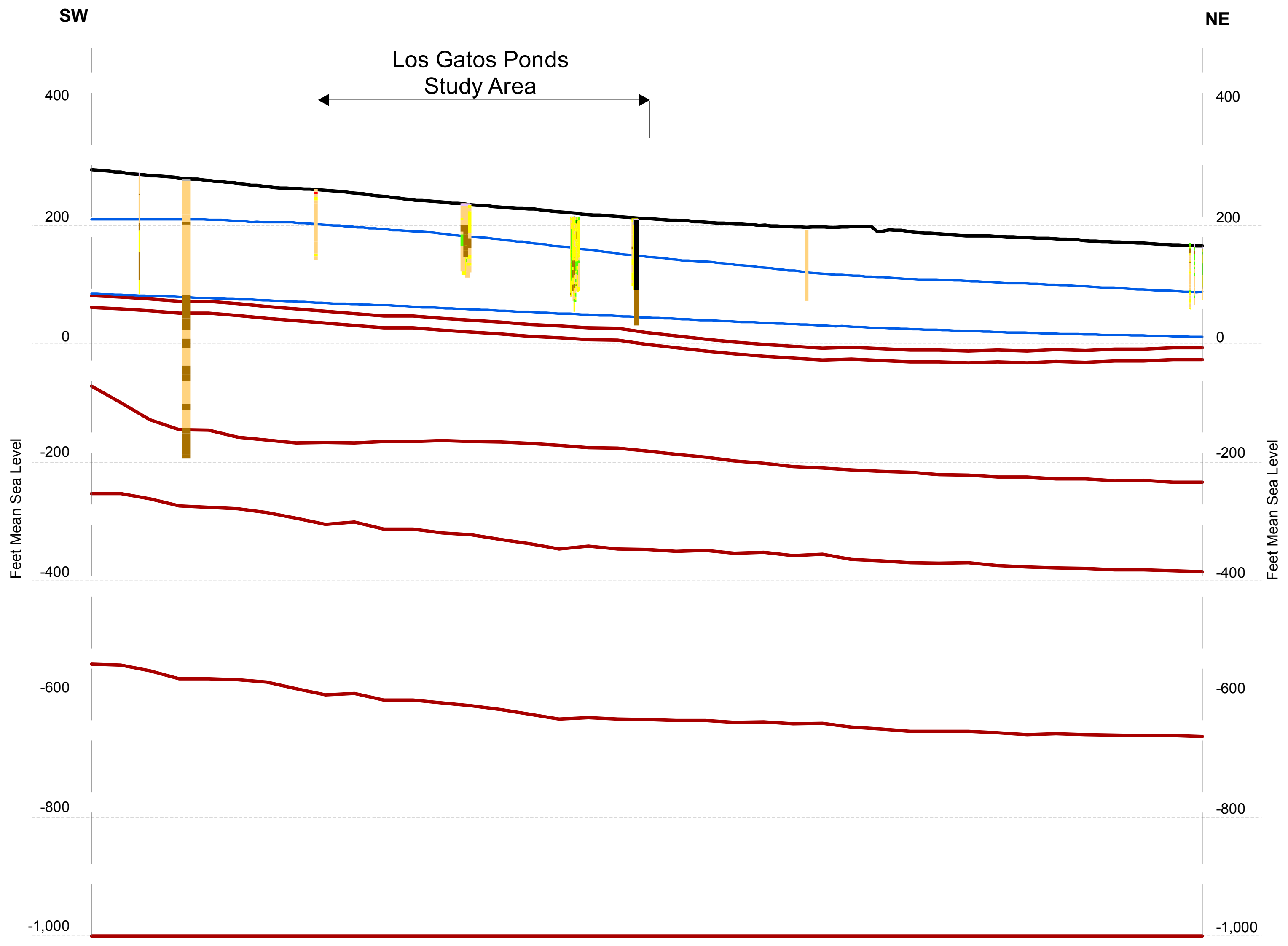

- ▬ Ground Surface
- ▬ High (1989) and Low (2012) Groundwater Elevations
- ▬ IMOD Model Layers

Lithology

- ▬ Topsoil
- ▬ Fill
- ▬ Boulders / Cobbles
- ▬ Gravel
- ▬ Sand
- ▬ Silt
- ▬ Clay
- ▬ Bedrock

Note:
The thickness of the lithology lines for wells and boreholes is a function of the distance of the point from the section line. The closer the point, the wider the line is shown on the section.

Wells and boreholes may start above or below ground surface in the section as a result of being projected onto the section line.

0 1,000 2,000
Scale in Feet

10 X Vertical Exaggeration

December 2017

TODD GROUNDWATER

Sheet 2-5
Sections
Cross 5
through Cross 9

Cross 9

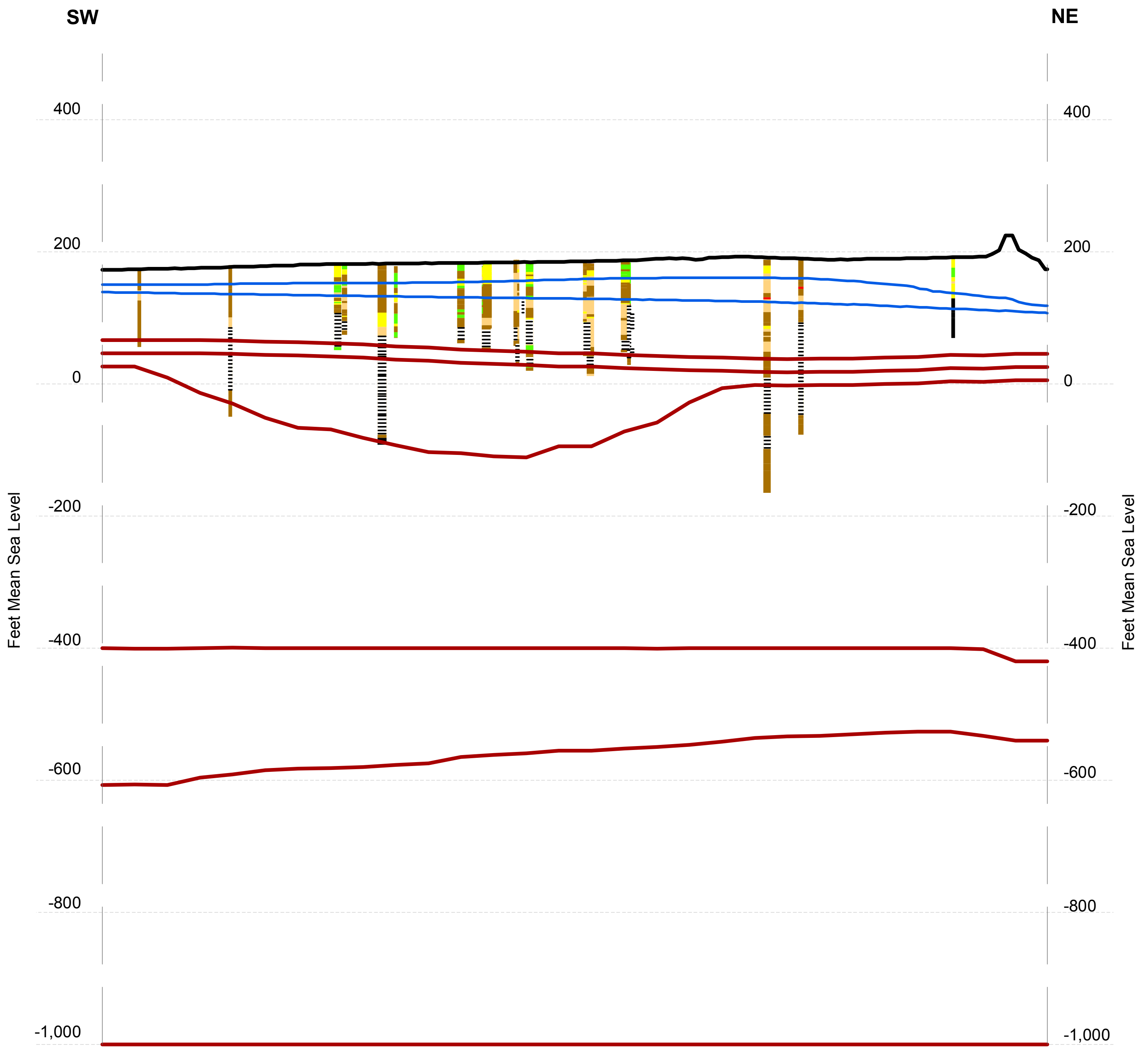

Cross 10

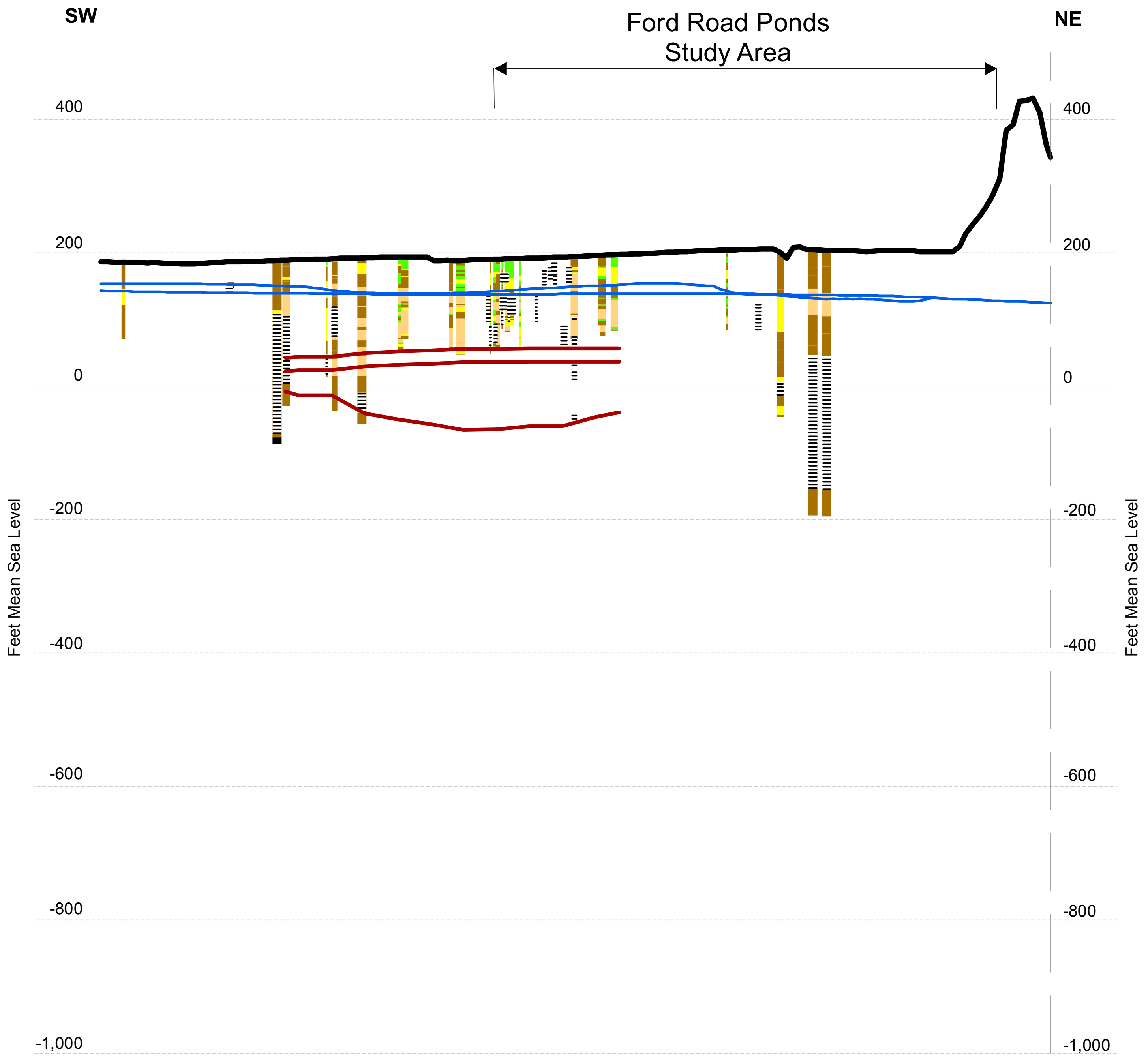

Cross 11

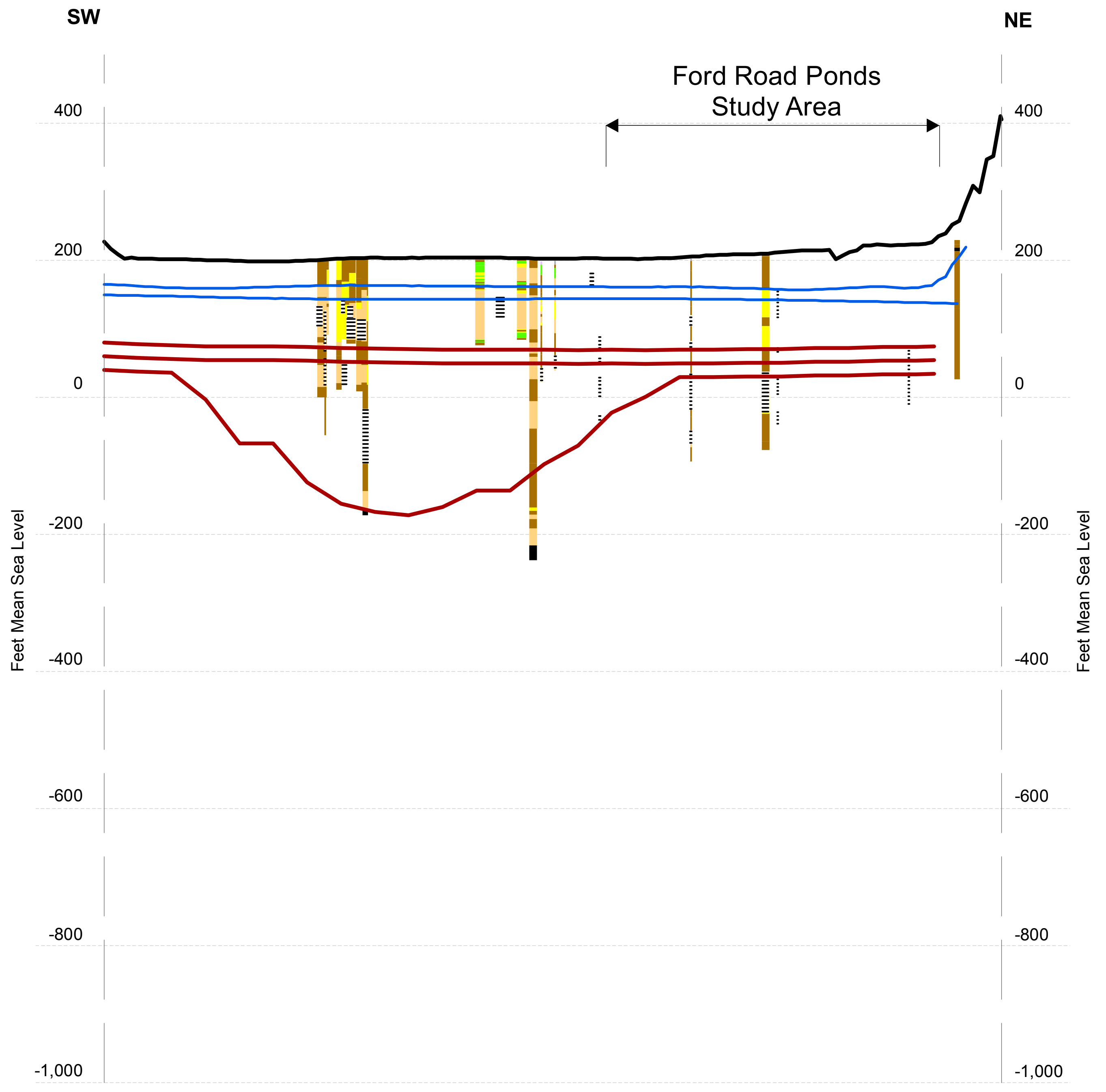

Cross 12

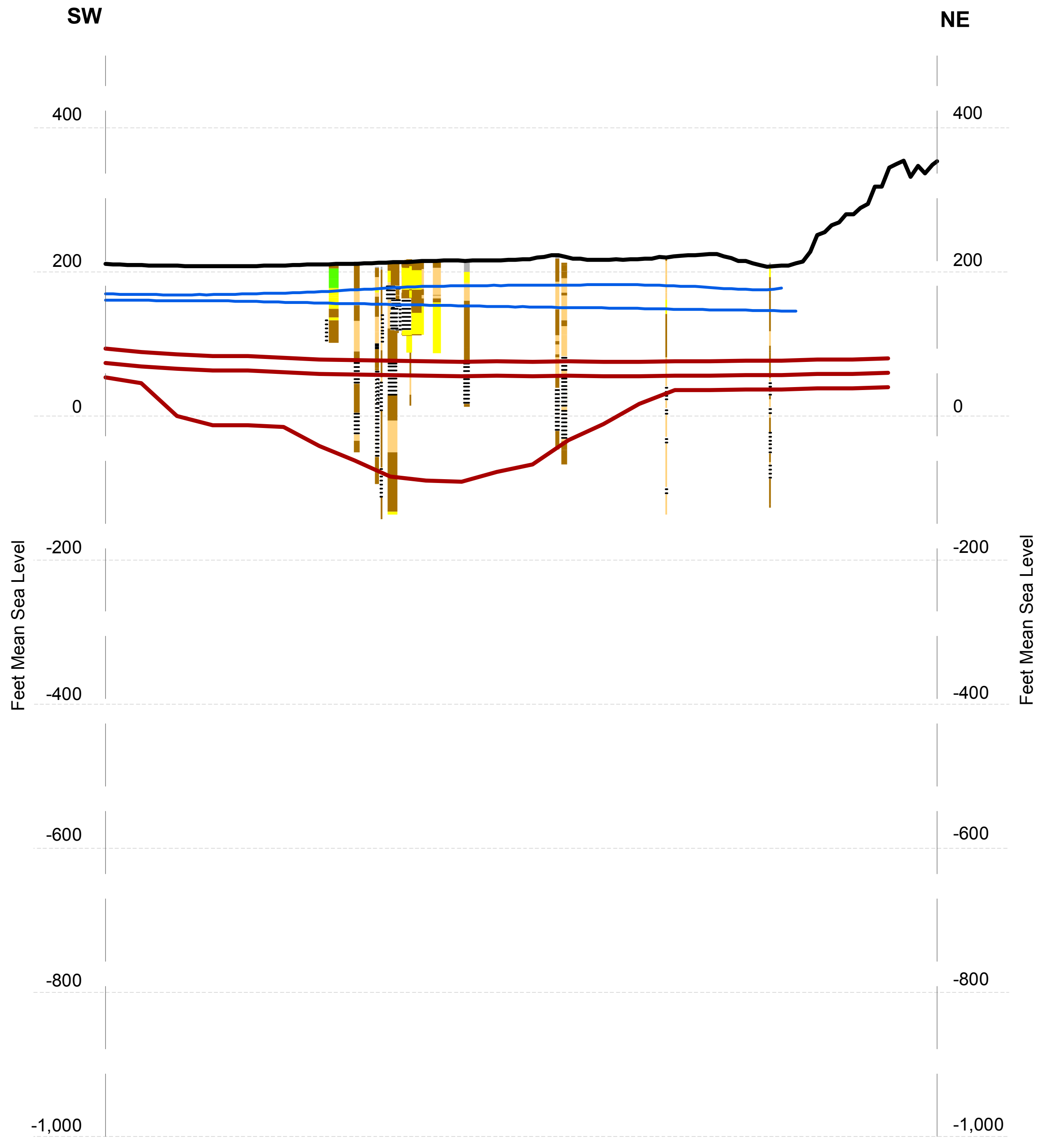

▬ Ground Surface
▬ High (1989) and Low (2012) Groundwater Elevations
▬ IMOD Model Layers

Lithology
▬ Topsoil
▬ Fill
▬ Boulders / Cobbles
▬ Gravel
▬ Sand
▬ Silt
▬ Clay
▬ Bedrock

Note:
The thickness of the lithology lines for wells and boreholes is a function of the distance of the point from the section line. The closer the point, the wider the line is shown on the section.

Wells and boreholes may start above or below ground surface in the section as a result of being projected onto the section line.

0 1,000 2,000
Scale in Feet

10 X Vertical Exaggeration

December 2017

TODD
GROUNDWATER

Sheet 2-5
Sections
Cross 5
through Cross 9

Path: T:\Projects\SCVWD IPR 37809\GIS\Maps\Figures\Conceptual Model Figures\Sheet 2-6 Sections Cross 9 - 12.mxd